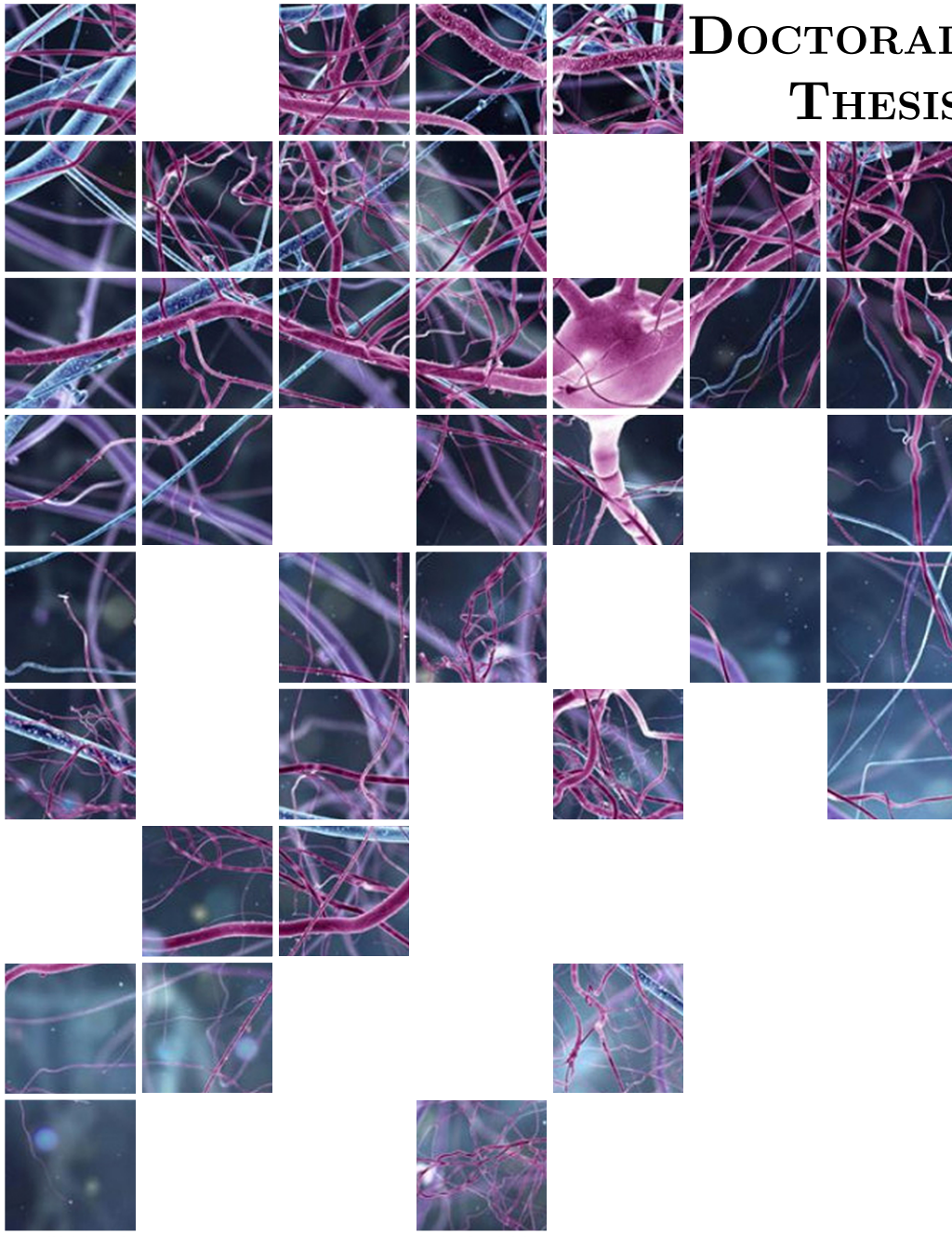

Doctoral Thesis

Characterization of the spontaneous EEG activity in the Alzheimer's disease continuum

From local activation to network organization

Saúl J. Ruiz-Gómez

Universidad de Valladolid

Doctoral Program of
Information and Telecommunication Technologies

Doctoral Thesis

Characterization of the spontaneous EEG activity in the Alzheimer's disease continuum: from local activation to network organization

Thesis presented by **D. Saúl José Ruiz-Gómez**
to apply for the *Ph.D. degree*
from the *University of Valladolid*

Directed by:
Dr. Carlos Gómez Peña
Dr. Roberto Hornero Sánchez

2021
Valladolid, Spain

"I think that even if you don't know who I am someday,
you'll still know that I love you."

Lisa Genova, neuroscientist

"Creo que, aunque no supieras quién soy,
seguirías sabiendo que te quiero."

Lisa Genova, neurocientífica

Defense

Título	Characterization of the spontaneous EEG activity in the Alzheimer's disease continuum: from local activation to network organization
Autor	D. Saúl José Ruiz-Gómez
Directores	Dr. D. Carlos Gómez Peña Dr. D. Roberto Hornero Sánchez
Departamento	Teoría de la Señal y Comunicaciones e Ingeniería Telemática

---

Tribunal

Presidente	Dr. D.
Vocales	Dr. D.
Secretario	Dr. D.

acuerda otorgarle la calificación de

En Valladolid, a de del

Universidad de Valladolid

Escuela Técnica Superior de Ingenieros de Telecomunicación
Dpto. de Teoría de la Señal y Comunicaciones e Ingeniería Telemática

Research Stay for the International Mention

City:	Tartu (Estonia)
Faculty:	Institute of Computer Science
Institution:	Computer Science of University of Tartu
Research group:	Computational Neuroscience Lab
Dates:	31/08/2020 – 01/12/2020
Duration:	92 days (3 months)
Supervisor:	Prof. Dr. Raúl Vicente Zafra

Agradecimientos

En primer lugar, me gustaría expresar mi más sincera gratitud a mis directores de Tesis, los Doctores Carlos Gómez y Roberto Hornero, por introducirme y guiarme durante estos años en esta aventura investigadora. Hace prácticamente ocho años desde el día en el que solicité la supervisión para realizar un trabajo fin de grado sobre análisis de registros electroencefalográficos. Tras muchos debates y muchas presentaciones de resultados junto con el Dr. Jesús Poza, aquí estamos para concluir este periodo. Muchas gracias por vuestro compromiso, vuestra paciencia y vuestros consejos durante estos años.

Este agradecimiento es extensivo al resto del Grupo de Ingeniería Biomédica (GIB), a María, Daniel, Gonzalo, Javier G., Alejandro, Víctor M., Fernando, Pablo, Verónica, Roberto, Eduardo, Adrián, Víctor R., Aarón, Jorge, Javier O., Víctor G. y Marcos. Además de formar un grupo de investigación cada día más potente, hemos formado un ambiente en el que es muy fácil trabajar. Y no sólo eso, también los '*happy meals*', las bromas, los partidos, las quedadas y los viajes han hecho esta etapa algo inolvidable. Para mí ha sido un placer ser el administrador del grupo de 'Bajas Esferas del GIB', espero con ansia el momento en el que me echéis del mismo. Será una buena señal de que todo ha salido bien.

También me gustaría agradecer al Dr. Raúl Vicente y al *Institute of Computer Science* de la Universidad de Tartu por acogerme en uno de los mejores centros de investigación de Europa. Sin duda, mi estancia en la ciudad de Tartu y en Estonia fue una experiencia inolvidable, donde crecí profesional y personalmente. A pesar de todas las limitaciones derivadas de la pandemia, gracias por hacerme sentir como en casa y pasar un tiempo increíble allí.

Sin embargo, el mayor de los agradecimientos se lo dedico a mi familia, mis padres y mi hermana, por el esfuerzo que han demostrado en educarme y ayudarme a crecer como persona. Poder sentir su orgullo por cada pequeño logro conseguido da las fuerzas necesarias para ir a por el siguiente.

De la misma forma, si hay una persona que tiene bastante culpa de que esté escribiendo estas líneas ahora mismo es ella, Alba. Desde que nos conocimos no me hizo falta mucho tiempo para saber que iba a ser alguien tan sumamente importante que marcaría un antes y un después en mi vida. Con ella he aprendido, he madurado y sólo espero que le haya merecido la pena llegar hasta aquí y esté tan orgullosa de lo que tenemos como lo estoy yo. Sin su ayuda este camino habría sido mucho más difícil, muchas gracias.

Abstract

The human brain has billions of neurons with long and branching extensions that enable them to form connections and communicate with each other. The changes in these networks throughout the life span are responsible for physiological brain aging. However, normal brain aging can be altered by some physiopathological processes, like those associated with dementia due to Alzheimer's disease (AD) and mild cognitive impairment (MCI). AD is a progressive neurodegenerative disorder that causes cognitive, behavioral and functional alterations interfering with the patients' ability to carry out the activities of daily living. MCI is usually considered a prodromal stage of AD in which individuals show evidences of AD brain changes and exhibit a memory impairment beyond what would be expected for their age, but do not fully accomplish the criteria for dementia diagnosis. Despite the high prevalence of these neurodegenerative processes, the current knowledge about them is still limited. During the last decades, several neuroimaging techniques have been used to detect brain changes associated with neurodegeneration. Among them, electroencephalography (EEG) stands out for its high temporal resolution, necessary to study the dynamical processes involved in complex brain systems. Additionally, it is widely used in clinical settings due to its low cost and portability.

In this context, the present Doctoral Thesis is focused on the characterization of the spontaneous EEG activity in the different stages of AD and MCI with the aim of gaining further insights into the neural substrates underlying their pathophysiology. For this purpose, two EEG databases have been studied, the former acquired in a clinical environment at the Río Hortega University Hospital and the latter acquired in a research environment as a result of a research project. Particularly, they have been investigated from three different levels of analysis depending on the way interactions are taken into account: (i) local activation; (ii) interaction between pair-wise electrodes; and (iii) network organization. Therefore, the contributions of the present Doctoral Thesis are canalized in these levels of

analysis.

In our first study, we developed and evaluated a three-way classification model with the aim of discriminating between AD patients, MCI subjects and healthy control (HC) subjects based on local activation features. Here, we take advantage of the complementary information provided by spectral measures and nonlinear methods to feed the classification model. These metrics also allowed us to investigate the changes in the EEG background activity in AD and MCI and study the abnormal brain changes associated with these neurodegenerative processes.

Secondly, two studies that analyze the interactions between pair-wise electrodes were carried out. The first one was focused on the comparison of two coupling metrics derived from nonlinear methods. Only a few studies have applied entropy-based coupling metrics to biological systems, but they have never been used for the EEG characterization in AD. In this context, Cross-Approximate Entropy and Cross-Sample Entropy, and their parameter configurations, were compared to determine which of them yields more information about the abnormal coupling patterns in AD and MCI. In the second study, a new model to build synthetic signals based on the combination of a real-head surface-model and a set of coupled Kuramoto oscillators was proposed to study the behavior of different functional connectivity metrics under the effect of simulated volume conduction. Particularly, we evaluated how they are affected by volume conduction and if they are able to detect real changes in synchronization. Furthermore, the brain alterations in the different stages of AD continuum were characterized using the metric less affected by the influences of volume conduction (Phase Lag Index), thus reducing this bias.

Lastly, we presented the design, development and evaluation of a new methodology to build multiplex network parameters based on the Canonical Correlation Analysis (CCA). CCA was used to determine the coefficients that maximize the correlation between electrode-level and source-level frequency-specific network parameters. In particular, we selected three parameters that are sufficiently representative and intuitive of the properties of the network and provide complementary information about how the brain network could work: strength, characteristic path length, and clustering coefficient. The behavior of the new CCA multiplex parameters was firstly studied using the synthetic signals generated with the Kuramoto model varying the level of connectivity. Then, the changes in the global brain network topology during the different stages of AD continuum were analyzed using these novel parameters.

The application of these methods following the three levels of analysis led us to the main findings of the present Doctoral Thesis: (i) the local changes in the EEG

background activity reflect a slowing of the EEG rhythms, a complexity loss, and a regularity increase, alterations that are related to the progression of AD; these changes were captured by a three-way classification model that showed a high diagnostic ability and culminated in a simplified clinical screening strategy for AD diagnosis (ii) a significant connectivity deficit in high frequency bands and a connectivity excess in low frequency bands were progressively found as the disease severity increases using entropy-based nonlinear metrics and Phase Lag Index; and (iii) the interpretation of the CCA multiplex parameters can be analogous to their frequency-specific counterparts and they revealed a loss of both integration and segregation in the multiplex brain networks as the disease progresses, making the AD networks more vulnerable as a consequence of the neurodegenerative process.

These findings provide further and reliable insights into the brain alterations, useful to gain better understanding into the AD pathophysiology in its different stages. Furthermore, the novel models and methodologies proposed in the present Doctoral Thesis provide new perspectives for the study of the spontaneous EEG at the different levels of analysis.

Acronyms

Aβ	Amyloid Beta
Acc	Accuracy
AD	Alzheimer's Disease
AD_{mil}	Mild Alzheimer's Disease
AD_{mod}	Moderate Alzheimer's Disease
AD_{sev}	Severe Alzheimer's Disease
AEC	Amplitude Envelope Correlation
AMI	Auto-Mutual Information
C	Clustering Coefficient
CAR	Common Average Reference
CCA	Canonical Correlation Analysis
ciPLV	Corrected Imaginary Phase Locking Value
Cross-ApEn	Cross-Approximate Entropy
Cross-SampEn	Cross-Sample Entropy
CSF	Cerebrospinal Fluid
CTM	Central Tendency Measure
CV	Cross-Validation
DT	Decision Tree
ECoG	Electrocorticography
EEG	Electroencephalography
FCBF	Fast Correlation-Based Filter
FDR	False Discovery Rate
FIR	Finite Impulse Response
fMRI	Functional Magnetic Resonance Imaging
FWER	Family-Wise Error Rate
FuzzyEn	Fuzzy Entropy
HC	Healthy Controls

HURH	Hospital Universitario Río Hortega
IAF	Individual Alpha Frequency
ICA	Independent Component Analysis
iCOH	Imaginary Part of Coherence
JCR	Journal Citation Reports
L	Characteristic Path Length
lagCOH	Lagged Coherence
LDA	Linear Discriminant Analysis
LOO	Leave One Out
LZC	Lempel-Ziv Complexity
MCI	Mild Cognitive Impairment
MEG	Magnetoencephalography
MF	Median Frequency
MLP	Multi-Layer Perceptron
MMSE	Mini-Mental State Examination
MSCOH	Magnitude Squared Coherence
NIH	National Institutes of Health
NINCDS-ADRDA	National Institute of Neurological and Communicative Diseases and Stroke and the Alzheimer's Disease and Related Disorders Association
NMF	Non-negative Matrix Factorization
NPV	Negative Predictive Value
PCA	Principal Component Analysis
PET	Positron Emission Tomography
PLI	Phase Lag Index
PLV	Phase Locking Value
PPV	Positive Predictive Value
PSD	Power Spectral Density
PSD_n	Normalized Power Spectral Density
QDA	Quadratic Discriminant Analysis
RP	Relative Power
s	Strength
SampEn	Sample Entropy
SD	Standard Deviation
SE	Spectral Entropy
Se	Sensitivity
SL	Synchronization Likelihood

sLORETA	Standardized Low Resolution Brain Electromagnetic Tomography
Sp	Specificity
SU	Symmetrical Uncertainty
SVM	Support Vector Machine
SW	Small-World
VHP	Visual Human Project®
WOS	Web Of Science

Contents

List of Figures

List of Tables

Chapter 1

Introduction

The current Doctoral Thesis focuses on characterizing brain activity using local activation measures, neural coupling methods and network parameters derived from Complex Network Theory to elucidate neural changes in dementia due to Alzheimer's disease (AD) and its prodromal form, mild cognitive impairment (MCI). For this purpose, we analyzed resting-state electroencephalographic (EEG) signals, acquired while subjects were awake with closed eyes. This research have led to the publication of four articles in journals indexed in the Journal Citation Reports (JCR) from the Web of Science^{TM}(WOS). Specifically, they were published between January 2018 and February 2021. As a consequence of the aforementioned scientific productivity, this Thesis is written as a compendium of publications.

The thematic consistency of the papers included in the Doctoral Thesis is justified in section 1.1. The general context of biomedical engineering and neural signal processing is briefly described in section 1.2. Sections 1.3 and 1.4 are devoted to the aetiology, diagnosis and treatment of AD and MCI, respectively. Section 1.5 is focused on explaining the basis of neural oscillations and their generation, taking into account the volume conduction problem and how it affects to different processing methods. Finally, the state of the art is described in section 1.6.

1.1 Compendium of publications: thematic consistency

One of the most remarkable developments in the history of clinical neurology was the invention of the electroencephalogram. Since this moment, in 1929, several efforts have been made to understand the relations between nearby and distant brain regions. However, even today, further research is needed to understand how cortical neuronal pools exchange information forming a complex neural network. In recent years, with the technical and computational advances, more sophisticated tools have been developed to record, analyze and model functional brain networks.

Typically, structural and functional organization of neural networks in brain disorders have been evaluated in three different levels of analysis depending on the way interactions are taken into account: (i) analysis of local activation patterns in individual sensors, (ii) analysis of interactions between pair-wise sensors using connectivity and synchronization metrics, and (iii) analysis of the functional organization of brain networks, applying novel parameters derived from complex network theory (Stam and van Straaten, 2012). In this context, the present Doctoral Thesis aims at analyzing the underlying neural changes following the aforementioned levels of analysis in the different stages of AD and its prodromal stage, MCI. This is the common thread shared by all the papers included in the present compendium of publications. The thematic consistency between the papers is illustrated in the Figure 1.1.

According to the chronological order, the first paper (Ruiz-Gómez et al., 2018a) was focused on the local activation level. In this publication, we studied the changes that dementia due to AD and MCI due to AD provoke in several spectral and nonlinear parameters. Then, a three-way classification approach was performed using different classifiers (e.g., Linear Discriminant Analysis, Quadratic Discriminant Analysis, and Multi-Layer Perceptron Artificial Neural Network) in order to propose a screening protocol of AD based on these features. The next two papers were focused on the analyses of interactions between sensors (Ruiz-Gómez et al., 2018b, 2019b). In particular, the second paper (Ruiz-Gómez et al., 2018b) was aimed at assessing the ability of two connectivity metrics derived from entropy measures (Cross-Approximate Entropy and Cross-Sample Entropy) to characterize the abnormal coupling patterns in AD and MCI and evaluate if these metrics be useful to discriminate them from healthy control (HC) subjects. In the third paper (Ruiz-Gómez et al., 2019b), the electrical activity of brain sources was simulated using the combination of a surface-based computational model and a set

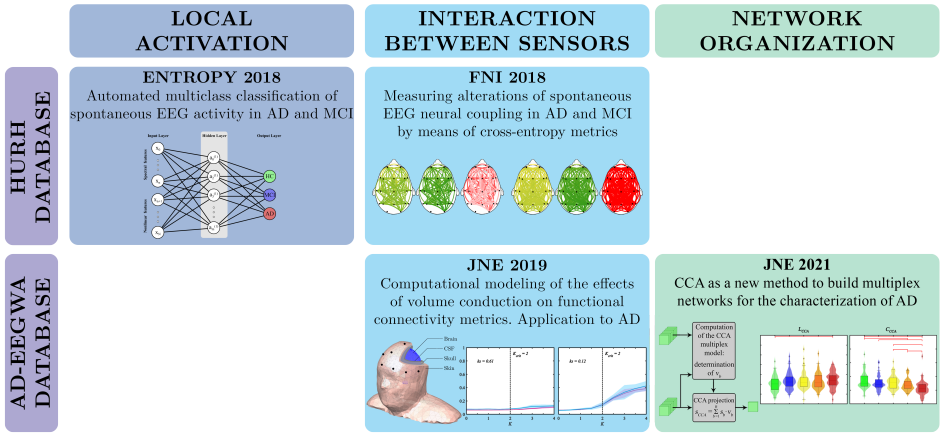

Figure 1.1: Schematic diagram of the main publications included in the compendium. HURH: Río Hortega University Hospital (HURH, Hospital Universitario Río Hortega), AD-EEGWA: 'Análisis y correlación entre el genoma completo y la actividad cerebral para la ayuda en el diagnóstico de la enfermedad de Alzheimer'. FNI: Frontiers in Neuroinformatics, JNE: Journal of Neural Engineering.

of coupled oscillators. Then, we analyzed how different functional connectivity metrics are affected by the spurious effects of volume conduction and if they were able to characterize the brain alterations during AD continuum. Lastly, the fourth paper (Ruiz-Gómez et al., 2021) was focused on the analysis of the changes in the functional organization of brain networks during AD continuum. Specifically, the aim of this study was two-fold: to propose a new method to build multiplex networks integrating information from conventional frequency-specific networks using canonical correlation analysis, and to characterize the multiplex network at the different stages of the AD continuum.

As the present Doctoral Thesis is organized as a compendium of publications, consulting each paper separately is essential for a comprehensive understanding of this document as a whole. The aforementioned manuscripts are available in the Appendix A. Furthermore, titles, authors, and abstracts of each paper, as well as the journals in which they were published are shown below:

Automated Multiclass Classification of Spontaneous EEG Activity in Alzheimer's Disease and Mild Cognitive Impairment (Ruiz-Gómez et al., 2018a).

Saúl J. Ruiz-Gómez, Carlos Gómez, Jesús Poza, Gonzalo C. Gutiérrez-Tobal, Miguel A. Tola-Arribas, Mónica Cano, and Roberto Hornero. *Entropy*, vol. 20 (1), 35, pp. 1-15, 2018. Impact factor in 2018: 2.419, Q2 in "PHYSICS, MULTIDISCIPLINARY" (JCR-WOS).

DOI: `https://doi.org/10.3390/e20010035`

Abstract: The discrimination of early Alzheimer's disease (AD) and its prodromal form (i.e., mild cognitive impairment, MCI) from cognitively healthy control (HC) subjects is crucial since the treatment is more effective in the first stages of the dementia. The aim of our study is to evaluate the usefulness of a methodology based on electroencephalography (EEG) to detect AD and MCI. EEG rhythms were recorded from 37 AD patients, 37 MCI subjects and 37 HC subjects. Artifact-free trials were analyzed by means of several spectral and nonlinear features: relative power in the conventional frequency bands, median frequency, individual alpha frequency, spectral entropy, Lempel–Ziv complexity, central tendency measure, sample entropy, fuzzy entropy, and auto-mutual information. Relevance and redundancy analyses were also conducted through the fast correlation-based filter (FCBF) to derive an optimal set of them. The selected features were used to train three different models aimed at classifying the trials: linear discriminant analysis (LDA), quadratic discriminant analysis (QDA) and multi-layer perceptron artificial neural network (MLP). Afterwards, each subject was automatically allocated in a particular group by applying a trial-based majority vote procedure. After feature extraction, the FCBF method selected the optimal set of features: individual alpha frequency, relative power at delta frequency band, and sample entropy. Using the aforementioned set of features, MLP showed the highest diagnostic performance in determining whether a subject is not healthy (sensitivity of 82.35% and positive predictive value of 84.85% for HC vs. all classification task) and whether a subject does not suffer from AD (specificity of 79.41% and negative predictive value of 84.38% for AD vs. all comparison). Our findings suggest that our methodology can help physicians to discriminate AD, MCI and HC.

Measuring Alterations of Spontaneous EEG Neural Coupling in Alzheimer's Disease and Mild Cognitive Impairment by Means of Cross-Entropy Metrics (Ruiz-Gómez et al., 2018b).

Saúl J. Ruiz-Gómez, Carlos Gómez, Jesús Poza, Mario Martínez-Zarzuela, Miguel A. Tola-Arribas, Mónica Cano, and Roberto Hornero. *Frontiers in Neuroinformatics*, vol. 12 (76), pp. 1-11, 2018. Impact factor in 2018: 2.680, Q1 in "MATHEMATICAL & COMPUTATIONAL BIOLOGY" (JCR-WOS).

DOI: `https://doi.org/10.3389/fninf.2018.00076`

Abstract: Alzheimer's Disease (AD) represents the most prevalent form of dementia and is considered a major health problem due to its high prevalence and its economic costs. An accurate characterization of the underlying neural dynamics in AD is crucial in order to adopt effective treatments. In this regard, mild cognitive impairment (MCI) is an important clinical entity, since it is a risk-state for developing dementia. In the present study, coupling patterns of 111 resting-state electroencephalography (EEG) recordings were analyzed. Specifically, we computed Cross-Approximate Entropy ($Cross-ApEn$) and Cross-Sample Entropy ($Cross-SampEn$) of 37 patients with dementia due to AD, 37 subjects with MCI, and 37 healthy control (HC) subjects. Our results showed that $Cross-SampEn$ outperformed $Cross-ApEn$, revealing higher number of significant connections among the three groups (Kruskal-Wallis test, FDR-corrected p-values<0.05). AD patients exhibited statistically significant lower similarity values at θ and β_1 frequency bands compared to HC. MCI is also characterized by a global decrease of similarity in all bands, being only significant at β_1. These differences shows that β band might play a significant role in the identification of early stages of AD. Our results suggest that $Cross-SampEn$ could increase the insight into brain dynamics at different AD stages. Consequently, it may contribute to develop early AD biomarkers, potentially useful as diagnostic information.

Computational modeling of the effects of EEG volume conduction on functional connectivity metrics. Application to Alzheimer's disease continuum (Ruiz-Gómez et al., 2019b).

Saúl J. Ruiz-Gómez, Roberto Hornero, Jesús Poza, Aarón Maturana-Candelas, Nádia Pinto, and Carlos Gómez. *Journal of Neural Engineering*, vol. 16 (6), pp. 066019, 2019. Impact factor in 2019: 4.141, Q1 in "ENGINEERING, BIOMEDICAL" (JCR-WOS).

DOI: https://doi.org/10.1088/1741-2552/ab4024

Abstract: Objective. The aim of this study was to evaluate the effect of electroencephalographic (EEG) volume conduction in different measures of functional connectivity and to characterize the EEG coupling alterations at the different stages of dementia due to Alzheimer's disease (AD). *Approach.* Magnitude squared coherence ($MSCOH$), imaginary part of coherence ($iCOH$), lagged coherence ($lagCOH$), amplitude envelope correlation (AEC), synchronization likelihood (SL), phase lag index (PLI), phase locking value (PLV), and corrected imaginary PLV ($ciPLV$) were applied to: (i) synthetic signals generated with a Kuramoto-based model of several coupled oscillators; and (ii) a resting-state EEG database of real recordings from 51 cognitively healthy controls, 51 mild cognitive impairment (MCI) subjects, 51 mild AD (AD_{mil}) patients, 50 moderate AD (AD_{mod}) patients, and 50 severe AD (AD_{sev}) patients. *Main results.* Our results using synthetic signals showed that PLI was the least affected parameter by spurious influences in a simulated volume conduction environment. Results using real EEG recordings showed that spontaneous activity of MCI patients is characterized by a significant coupling increase in the θ band. As dementia progresses, this increase in the θ band became more pronounced, and a significant widespread decrease in α band appeared at the last stage of dementia. *Significance.* Our results revealed that the estimation of functional EEG connectivity using PLI could reduce the bias introduced by the spurious influence of volume conduction, and it could increase the insight into the underlying brain dynamics at different stages of the AD continuum.

A new method to build multiplex networks using Canonical Correlation Analysis for the characterization of the Alzheimer's disease continuum (Ruiz-Gómez et al., 2021).

Saúl J. Ruiz-Gómez, Roberto Hornero, Jesús Poza, Eduardo Santamaría-Vázquez, Víctor Rodríguez-González, Aarón Maturana-Candelas, Carlos Gómez. *Journal of Neural Engineering*, vol. 18 (2), pp. 026002, 2021. Impact factor in 2019: 4.141, Q1 in "ENGINEERING, BIOMEDICAL" (JCR-WOS).

DOI: `https://doi.org/10.1088/1741-2552/abd82c`

Abstract: Objective. The aim of this study was to propose a new method to build multiplex networks integrating information from frequency-specific networks. Furthermore, we analyzed how these metrics are affected by variations of connectivity and their ability to characterize the brain alterations during Alzheimer's disease (AD) continuum. *Approach.* A new method based on canonical correlation analysis (CCA) was applied to: (i) synthetic signals generated with a Kuramoto-based model; and (ii) a resting-state EEG database formed by recordings from 51 cognitively healthy controls, 51 mild cognitive impairment subjects, 51 mild AD patients, 50 moderate AD patients, and 50 severe AD patients. *Main Results.* Our results using synthetic signals showed that the interpretation of the proposed CCA-based multiplex parameters (multiplex average node degree, multiplex characteristic path length and multiplex clustering coefficient) can be analogous to their frequency-specific counterparts, as they displayed similar behaviors in terms of average connectivity, integration, and segregation. Findings using real EEG recordings revealed that dementia due to AD is characterized by a significant increase in average connectivity, and by a loss of integration and segregation. *Significance.* We can conclude that CCA can be used to build multiplex networks based on neural data, integrating information from frequency-specific networks. Additionally, our results showed the usefulness of the proposed method to build and interpret multiplex networks. A loss of 'small-world' network properties as dementia due to AD progresses was also revealed, which indicates an increase of brain networks vulnerability in AD.

1.2 Context: neural signal processing and modeling

Biomedical engineering is defined as an interdisciplinary field that applies engineering principles to understand, model and modify biological systems, as well as design and manufacture tools that can monitor physiologic functions and assist in the diagnosis and treatment of patients (Bronzino and Peterson, 2014). Biomedical engineering bridges the gap between engineering and medicine, combining the identification and problem-solving of engineering with the medical issues and needs of our healthcare system using technology. The range of biomedical engineering activities is wide, including both experimental and theoretical research in clinical, industrial and academic environments (Bronzino and Peterson, 2014). In this context, biomedical signal processing has become one of the most relevant activities in this field.

The different physiologic systems in the human body (e.g. cardiovascular, endocrine, nervous, vision, auditory, gastrointestinal, and respiratory) produce a large number of biomedical signals that reflects their physiological underpinnings. However, the information of these raw signals is not directly interpretable, and a processing step is needed to interpret them. Biomedical signal processing aims at extracting features that characterize the physiological signals by applying mathematical and information theory methodologies (Bronzino and Peterson, 2014). Particularly, neural signal processing has become the key to increase the insight into the neural interactions in the human brain from an engineering perspective.

In this Doctoral Thesis, neural signal processing is applied to physiological signals derived from the brain. The study of these signals, acquired using the EEG, has allowed us to help in the characterization of dynamical neural alterations at the different stages of dementia due to AD and its prodromal stage, MCI. Additionally, a preliminary AD-MCI screening strategy based on local activation metrics was also proposed. However, the technical limitations of the EEG affect directly to the recorded signals, such as the volume conduction problem. This fact led us to build a computational model to simulate the volume conduction effects over the signals when they travel from the brain sources to the EEG electrodes. Finally, a novel method to build multiplex networks that overcome the limitations of the current methods was also propounded. Next sections provide a detailed overview about the different stages of AD, important to understand the characteristics of the disease under study in this Doctoral Thesis, and about the EEG, the technique used to register the electrical activity of the brain.

1.3 Dementia due to Alzheimer's disease

Dementia due to AD is a progressive neurodegenerative disease that causes cognitive, behavioral and functional alterations (Alzheimer's Association, 2020). Described more than 100 years ago by the German psychiatrist and neuropathologist Alois Alzheimer, AD now represents one of the biggest global public health problems in developed countries with aged population (Blennow et al., 2006). Current estimates suggest that 44 million people live with dementia worldwide, with AD representing the 60-80% of the cases of dementia (Lane et al., 2018). Furthermore, this number is predicted to double by 2030 and more than triple by 2050 (Alzheimer's Association, 2020).

During the progression of the disease, three phases can be distinguish: preclinical AD, MCI and AD (Jack et al., 2011). Furthermore, the AD phase can be further divided into mild, moderate and severe AD, depending on how the symptoms interfere with the patients' ability to carry out activities of the daily living (Alzheimer's Association, 2020). In the preclinical AD phase, individuals did not yet developed any typical AD symptom such as memory loss. They only present brain changes that indicate the earliest signs of AD, as abnormal levels of beta-amyloid and decreased metabolism of glucose (Bischof et al., 2016). However, their brains are able to compensate these changes, enabling them to continue to function normally (Alzheimer's Association, 2020). When individuals showed evidences of AD brain changes and exhibit a memory impairment beyond what would be expected for their age, but do not fully accomplish the criteria for dementia diagnosis, a new clinical entity appears: MCI (Petersen et al., 2018) (see section 1.4). In the earliest AD stage, known as mild AD, patients are able to drive and work, and may function independently but they show symptoms as reading problems. The next stage, moderate AD, is often the longest one. Moderate AD patients typically show increasingly difficulties communicating and performing activities of daily living. Finally, severe AD is the last stage of this disease, in which patients require a greater level of care as they eventually loose the ability of control movement and they become bed-bound (Alzheimer's Association, 2020).

1.3.1 Pathogenesis

AD is characterized, at macroscopic level, by at least moderate cortical atrophy in multimodal association cortices and limbic lobe structures and by enlarged sulcal spaces in the frontal and temporal cortices with atrophy of the gyri (Deture and Dickson, 2019). However, none of these macroscopic features is specific to AD, and

remains unaffected for clinically normal people that may have moderate cortical atrophy with white matter volume loss (Deture and Dickson, 2019).

At the microscopic level, the characteristic lesions in AD are the presence of extracellular senile plaques and intracellular neurofibrillary tangles. These lesions mostly occur in the medial temporal lobe structures and cortical areas of the brain, and derive in a degeneration of the neurons and synapses (Blennow et al., 2006).

1) **Senile plaques.** Amyloid plaques are formed by the extracellular accumulation of amyloid beta (Aβ) peptides that result from the abnormal processing of amyloid precursor protein and an imbalance in the production and clearance pathways (Deture and Dickson, 2019; Kumar et al., 2015). Amyloid deposit density is higher in the occipital and temporal lobes, cortical areas responsible for memory and learning (Cummings et al., 2003). However, there is evidence to suggest that the neurofibrillary tangles correlate better with cognitive impairment than senile amyloid plaques (Dickson et al., 1992).

2) **Neurofibrillary tangles.** They are composed of a pair of helical filaments of abnormally phosphorylated tau protein, which twist around each another forming periodic structures. Tau proteins are usually found in neurons cells and are responsible of modulating the stability of the axonal microtubules of the cytoskeleton, something essential for axonal transport. Furthermore, tau protein also becomes prone to aggregation into insoluble fibrils in tangles, further compromising neuronal function. Neurofibrillary tangles starts early in the disease process in neurons in the transentorhinal region, spreads to the hippocampus and amygdala, and later to the neocortical association areas in later stages of AD (Blennow et al., 2006).

In addition to these microscopic features, other pathologic changes are inevitably detected in AD. Granulovacuolar degeneration of pyramidal neurons in the hippocampus, inflammatory responses of microglial cells, and synaptic loss are such findings, but nonetheless they are not as well characterized in terms of clinical relevance (Aisen, 2002; Webber et al., 2005).

1.3.2 Diagnosis

A definite diagnosis of AD can be only made through necropsy, which is the microscopic analysis of the patient's brain after death. However, the medical history of the patient and different clinical, neurological, and psychiatric examinations

serves as the basis in the daily clinical practice. The Mini–Mental State Examination (MMSE) is the most widely used neurophysiological test to measure cognitive impairment, in both clinical and research settings. It was originally introduced by Folstein (Folstein et al., 1975) and consists of 30 questions that evaluate orientation, learning, attention, calculation, recall, repetition, comprehension, reading, writing and drawing a complex figure shown (Cummings et al., 2003). Although it is used to estimate the severity and progression of cognitive impairment, this test is not very sensitive to the abnormalities that appear in the early stages of AD.

The original criteria used for the clinical diagnosis of AD were published in 1984 by the National Institute of Neurological and Communicative Diseases and Stroke and the Alzheimer's Disease and Related Disorders Association (NINCDS-ADRDA) (McKhann et al., 1984). These criteria for probable AD largely depend on the exclusion of other dementias. According to the NINCDS-ADRDA criteria, AD cannot be diagnosed until the patient has cognitive signs severe enough to interference with social or occupational activities. It was not until 2011 when the clinical diagnostic criteria for AD were revised, and research guidelines for earlier stages of the disease were characterized to reflect a deeper understanding of the disorder. The National Institutes of Health (NIH) and the Alzheimer's Association workgroup led the development of the new guidelines. The main updates in these guidelines include: (i) the division of the AD spectrum in three stages (preclinical AD, MCI and AD); (ii) recognize that other aspects of cognition, such as word-finding ability or judgment, may become impaired before memory loss; (iii) reflect a better understanding of the distinctions and associations between AD and other dementias; and (iv) recognize the potential use of new biomarkers as indicators of underlying brain disease to diagnose AD (Jack et al., 2011; McKhann et al., 2011).

Some neuroimage methods have shown promising results as diagnostic tools for AD, including MRI measurements of medial temporal lobe atrophy, positron emission tomography imaging of glucose metabolism and Aβ deposits, and EEG biomarkers. At present, some of these imaging techniques, as well as biomarkers in blood and cerebrospinal fluid, are recommended in the consensus guidelines for AD diagnosis (Khoury and Ghossoub, 2019). However, some biomarkers cannot yet be routinely used in clinical diagnosis and track progression before further testing and validation.

1.3.3 Treatment

Despite the fact that there is no cure for AD, some therapies may help to alleviate the symptoms provoked by the disease, providing temporary improvement, reducing the rate of cognitive decline, and improving the quality of life of the patients. Research advances in the knowledge of neurotransmitter disturbances and molecular pathogenesis of AD have led to the development of therapies based on drugs with symptomatic effects, drugs with disease-modifying potential, and drug from epidemiological data in randomized trials (Blennow et al., 2006). Furthermore, non-pharmacological treatments represent complementary methods that should be tailored according to particular patients' conditions, such as compliance to treatment, AD severity, and available sanitary and professional resources (Cammisuli et al., 2016).

1) **Symptomatic treatments.** The aim of these therapies is to reduce the symptoms associated with AD, as well as reduce the rate of cognitive decline that occurs as AD progresses. The AD cholinergic hypothesis states that degeneration of cholinergic neurons causes disturbances in presynaptic cholinergic terminals in the hippocampus and neocortex (Terry and Buccafusco, 2003). Hence, one therapeutic approach is focused on inhibiting acetylcholinesterase and thus enhancing the cholinergic neurotransmission (Blennow et al., 2006). The most common acetylcholinesterase inhibitors, approved for clinical use in AD, are donepezil, rivastigmine, and galantamine. Additionally, AD is also characterized by increased glutamatergic activity that may impair neuronal function. In this regard, memantine is believed to protect neurons from glutamate-mediated excitotoxicity and show positive effects on cognitive and behavioural symptoms in AD patients (McShane et al., 2019).

   In the late stages of AD, different behavioural signs, such as aggression, psychomotor agitation, and psychosis (hallucinations and delusions), are very common. In this case, atypical antipsychotic drugs as risperidone and olanzapine has shown their efficacy reducing these symptoms (Brodaty et al., 2003; Street et al., 2000).

2) **Disease-modifying treatments.** The advances in the molecular AD pathogenesis have led to the development of different therapeutic strategies focused on inhibiting brain Aβ production and aggregation, and to increase Aβ clearance from the brain. These approaches include the use of secretase

modulators that reduce the brain concentration and production of Aβ. The generation of antibodies by Aβ immunotheraphy also induces the clearance of amyloid plaques by microglia. Finally, other small peptides can act as Aβ inhibitors, as they interfere with Aβ interactions and prevent the fibrillisation present in the senile plaques (Blennow et al., 2006).

3) **Epidemiology-based treatments.** The conclusions extracted in several epidemiological studies have served as the theoretical basis for different treatment approaches. Some of these studies suggest that some drugs have a protective effect against AD, such as anti-inflammatory agents, cholesterol-lowering drugs, estrogens or antioxidants. However, when these hypotheses have been investigated in randomized clinical trials, the beneficial effects of these treatments were not so clearly seen (Briggs et al., 2016).

4) **Non-pharmacological treatments.** The main non-pharmacological treatments include exercise and motor rehabilitation, cognitive rehabilitation, occupational therapy, psychological therapy, and new technologies, including virtual reality, gaming, and telemedicine (Cammisuli et al., 2016). Some studies showed statistically significant effects of these therapies on some outcomes, but their clinical significance is uncertain. Further randomized controlled trials with innovative designs are still needed to explore their efficacy in AD and dementia (Zucchella et al., 2018).

1.4 Mild cognitive impairment

MCI is usually considered a prodromal stage of AD in which individuals showed evidences of AD brain changes and exhibit a memory impairment beyond what would be expected for their age, but do not fully accomplish the criteria for dementia diagnosis (Petersen, 2016). Recent studies found that from 15% to 32% of MCI patients older than 65 had developed dementia after 2 and 5 years follow up (Petersen, 2016; Ward et al., 2013), whereas the conversion rate of healthy people is only 1–2% per year. This fact has made MCI to be considered a prodromal stage of AD. However, not every MCI subject progresses to AD or dementia, as some of them remain with stable MCI. Then, identifying those MCI subjects that are more likely to develop AD or other dementias is a major goal of current research.

Despite the common characteristic features, a more detailed classification into MCI subtypes can be carried out taking into account whether there is an impairment in memory (amnestic and nonamnestic MCI), and whether this is the only

one present or more cognitive domains are affected (single and multiple domain). Traditionally, amnestic MCI is the typical prodromal stage of dementia due to AD, but other phenotypes can also lead to this type of dementia, such aslogopenic aphasia or posterior cortical atrophy (Petersen, 2016).

1.4.1 Pathogenesis

In general, there is a large neuropathological heterogenicity between MCI subjects. However, the initial degenerative changes in MCI begin years before the symptoms. They range from the complete absence of AD-type pathology to findings that meet the criteria for AD diagnosis, such as the presence of senile plaques and neurofibrillary tangles. However, there are also other cases with neuropathological findings compatible with other types of dementias such as vascular or Lewy bodies (Jicha et al., 2006).

The initial degenerative MCI changes include modifications in the metabolism of the amyloid precursor protein that leads to Aβ peptide and the increased concentration of tau protein. Most studies show that patients with MCI have intermediate Aβ concentration between AD patients and HC subjects (Herukka et al., 2007). Furthermore, the elevation of tau concentration levels increases in people with MCI that progresses to dementia due to AD, compared with those who remain stable. Likewise, these concentrations are higher in patients with MCI compared to HC subjects, but lower if we compare them with AD patients (Herukka et al., 2007).

1.4.2 Diagnosis

An early diagnosis is crucial since treatments are more effective in the first stages of the dementia and could stop or delay the neurodegenerative process, despite that current therapies are not able to heal MCI or AD (Lin and Neumann, 2013). The aforementioned MCI heterogeneity makes very difficult for the clinician to distinguish whether a person's cognitive changes are due to normal aging or the onset of probable AD.

As for AD diagnosis, different techniques are usually used to diagnose MCI, such as the patient's history, clinical examinations, brain scans, neuroimaging techniques, etc. Similarly, the MCI clinical diagnosis is complemented with the evaluation of the cognitive capacity loss with the performance of neuropsychological tests, such as MMSE (Folstein et al., 1975). The interpretation of MMSE results could depend on age and educational level factors, but MCI patients with

cognitive deficits in two or more areas usually obtain a score lower than 24.

Actually, the most extended criteria for the diagnosis of MCI due to AD are those proposed by the National Institute on Aging and the Alzheimer's Association of the NIH in 2011 (Albert et al., 2011). They include core clinical criteria that could be used by healthcare providers, and research criteria based on advanced imaging techniques or cerebrospinal fluid analysis that could be used in clinical research settings, including clinical trials (Albert et al., 2011).

1) **Core clinical criteria for MCI diagnosis.** The main clinical MCI changes include: (i) a cognitive concern reflecting a change in cognition reported by patient, informant or clinician (i.e., historical or observed evidence of decline over time); (ii) an objective evidence of impairment in one or more cognitive domains, typically including memory (i.e., formal or bedside testing to establish level of cognitive function in multiple domains); (iii) the preservation of independence in functional abilities, despite they may take more time, be less efficient, and make more errors at performing such activities than in the past; and (iv) these cognitive changes should be sufficiently mild (i.e., no evidence of a significant impairment in social or occupational functioning) (Albert et al., 2011). To meet the core clinical criteria for MCI, it is also necessary to discard other brain diseases that could account for the decline in cognition (e.g., vascular, traumatic, medical causes of cognitive decline), provide evidence of longitudinal decline in cognition, and report history consistent with AD genetic factors.

2) **Research criteria incorporating biomarkers.** The use of biomarkers for helping MCI diagnosis could provide further insights into the underlying etiology of MCI and determine the likelihood of progression of MCI patients to dementia due to AD. They may be divided into several different classes: (i) biomarkers that directly reflect the Aβ deposition (i.e., Aβ42 levels in the Cerebrospinal Fluid (CSF) and positron emission tomography (PET) measures of fibrillar Aβ); (ii) biomarkers that reflect neuronal injury (i.e., tau and phosphorylated-tau concentration levels in the CSF, volumetric measures of hippocampal volume or medial temporal atrophy); and (iii) biomarkers associated with biochemical changes (i.e., inflammatory biomarkers, oxidative stress, and other markers of synaptic damage and neurodegeneration, such as cell death) (Albert et al., 2011).

1.4.3 Treatment

Due to the heterogeneity of MCI, the medical recommendations may vary and they should be more focused on the particular symptoms. Nowadays, no accepted professional guideline for the MCI treatment exists. The possible memory changes and thinking skills that would indicate patients worsening are regularly monitored by the physician.

The main objectives in the MCI treatment should be aimed at reducing the risk of progression to dementia, improving quality of life and avoiding functional deterioration. There are mainly two approaches for MCI treatment, pharmacological and non-pharmacological therapies.

1) **Pharmacological treatment.** They are aimed at reducing the symptoms associated with MCI and slow its progression to dementia. Despite the fact that no drugs have been currently approved for treating MCI, drugs that are also used in the treatment of AD, such as donepezil, rivastigmine, and galantamine, would help with MCI symptoms (Karakaya et al., 2013). Furthermore, MCI treatment often include medication for other illness the patient may have that increase the chances of developing dementia, such as heart problems, diabetes, strokes, or depression (Kelley, 2015).

2) **Non-pharmacological therapies.** The participation in different cognitive activities has been shown to decrease the risk of progression to dementia. These therapies include: (i) cognitive training of memory, attention, or problem solving; (ii) psychoeducational programs aimed to better understanding the disease and reducing anxiety symptoms; (iii) cognitive rehabilitation that allows living and accepting the deficits of the patient; and (iv) memory therapies that help to reduce depressive symptoms (Kelley, 2015).

1.5 Electroencephalography

Several neuroimaging techniques have been used to detect brain changes associated with the AD neurodegeneration. Figure 1.2 shows the most popular ones, distributed in function of their temporal and spatial resolutions, and their degree of invasiveness. In order to study the real-time dynamical processes involved in complex brain systems, techniques with high temporal resolution are required (Cohen, 2014). Additionally, the low cost, the portability, and the widespread use in clinical settings makes the EEG one of the most important techniques to

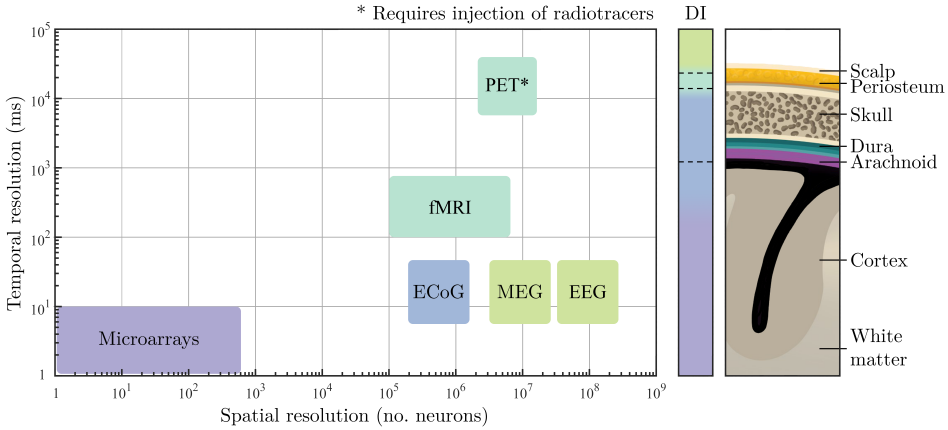

Figure 1.2: Temporal and spatial resolution of different brain activity measurement techniques. Degree of invasiveness (DI) is also represented as a color gradient, according to the brain layers (right). ECoG: electrocorticography, MEG: magnetoencephalography, EEG: electroencephalography, fMRI: functional magnetic resonance imaging, PET: positron emission tomography.

measure the brain activity. EEG measures non-invasively the electrical activity generated by pyramidal neurons in the cerebral cortex working together in large and synchronized pools. The coordinated firing of millions of neurons produces an electrical field strong enough to be recorded from electrodes placed over the scalp after going through the different brain tissues (Nunez and Srinivasan, 2009).

These electrical fields are measured as electric potential differences between the electrodes, also known as EEG channels, and a reference. The reference electrode can be located in a ground far enough from brain sources (e.g. at the ear, mastoid, or neck), or a specific EEG channel can be used as online reference. However, some recording equipments are able to use the common average reference (CAR) method, using the average of all EEG channels as the reference. This configuration minimizes uncorrelated sources of signal and noise through averaging, while eliminating sources of noise that are common to all sites. The EEG channels are located to maximize the covered area of the scalp following the specifications of different standards, such as International Systems 10–20 or 10–10. These standards establish landmarks following proportional distances of 10% and 20% between the nasion and the inion and between preauricural points (Klem et al., 1999). In the present Doctoral Thesis, 19 EEG electrodes following the standard 10–20 have been used, with CAR as reference. The specific position of each recorded EEG channel is depicted in the Figure 1.3.

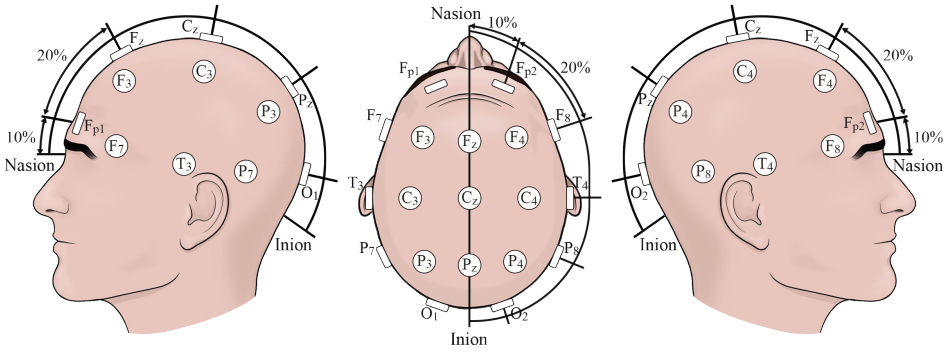

Figure 1.3: Schematic views of the standard International System 10–20 montage for EEG recordings: (A) left lateral, (B) top, and (C) right lateral. This standard uses proportional distances of 10% and 20% between the nasion and the inion and between preauricural points for locating the landmarks.

1.5.1 Neural oscillations

The high sampling rate of the EEG equipments (commonly over 200 Hz) provides a suitable temporal resolution to capture real-time electric variations in the cerebral cortex produced by different neurological processes.

As EEG is only sensitive to the coordinated activity of neuronal pools, it is often interpreted a rhythmic activity that reflects neuronal oscillations (Nunez and Srinivasan, 2009). Particularly, the oscillations that are thought to be associated with different cognitive processes are comprised in a frequency range between 1 and 70 Hz (Cohen, 2014). As Figure 1.4 displays, typical EEG analyses divide these oscillations into the following frequency bands:

1) **Delta (δ, 1–4 Hz).** The slowest neural rhythms are characterized by high-amplitude waves. They are usually seen in the occipital electrodes of awake babies and in frontal regions of adults during deep sleep. Some delta activity is also normal in elderly people older than 60 years at the onset of drowsiness. However, an excessive and generalized delta activity is abnormal and could indicate structural brain lesions and various types of encephalopathies (Tatum et al., 2014).

2) **Theta (θ, 4–8 Hz).** Theta frequencies are found in frontal or frontocentral regions in young adults. However, intermittent bursts of generalized theta activity are often abnormal, and could be associated with mild diffuse encephalopathy and noncommunicating hydrocephalus (Tatum et al., 2014).

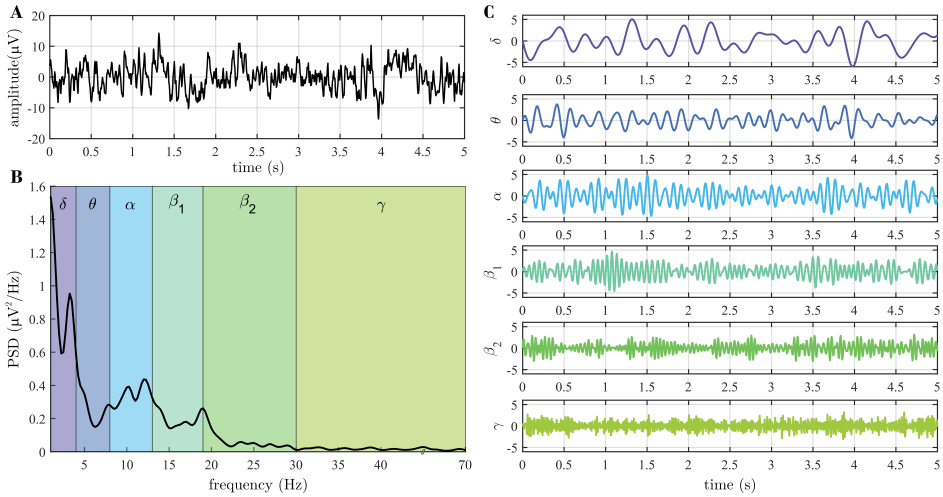

Figure 1.4: Neuronal oscillations of electroencephalographic (EEG) signals of a healthy awake subject with eyes closed. (A) EEG segment of 5 seconds from channel Pz; (B) power spectral density (PSD) of the EEG signal; (C) decomposition of the EEG segment in the six main bands: δ (1–4 Hz), θ (4–8 Hz), α (8–13 Hz), β_1 (13–19 Hz), β_2 (19–30 Hz) and γ (30–70 Hz).

3) **Alpha (α, 8–13 Hz).** Alpha waves are the most predominant normal adult rhythms in occipital and parietal regions during relaxed wakefulness. Their amplitude is closely related with eyes conditions, being increased immediately after eye closing, and attenuated in eye opening or mental exertion (Tatum et al., 2014).

4) **Beta (β, 13–30 Hz).** Predominant in precentral and frontal regions, beta activity is commonly increased due to anxiety, mental activation, drowsiness and light sleep. The consumption of different anxiolytics, such as benzodiazepines, barbiturates, and chloral hydrate, is often associated with an excessive activity in this band (Tatum et al., 2014). Conventionally, beta EEG rhythms are divided into two frequency sub-bands, β_1 (13–19 Hz) and β_2 (19–30 Hz).

5) **Gamma (γ, 30–70 Hz).** The highest neuronal rhythms are thought to be associated with basic sensory and high cognitive processing. Gamma-band activity is also associated with the interactions between excitatory and inhibitory neurotransmitter concentrations, as well as specific hippocampal memory deficits (Fuchs et al., 2007).

1.5.2 Volume conduction

The spatial resolution of the EEG is limited by the number of electrodes placed in the scalp. Furthermore, the electrical signals generated by synchronized neuronal pools have to travel across different surfaces in the head until they are recorded at the scalp electrodes, as shown in Figure 1.5. During this journey, signals suffer from attenuation, expansion, and noise contamination. These effects cause the volume conduction problem, which is mainly characterized by two phenomena: common sources effect and field spread. The former is due to the fact that nearby electrodes are very likely to pick up the electrical activity from the same brain sources, even if they are independent (Schoffelen and Gross, 2009; Stam et al., 2007). The field spread is the effect of the spread of the electromagnetic waves when traveling from a cerebral tissue to the next one, as a consequence of their different tissue conductivities. Both effects are illustrated in the Figure 1.5.

These EEG inherent effects cause that there is no unique solution when estimating the active neuronal sources in the brain from the time series recorded on the scalp. Furthermore, in order to achieve a correct interpretation of coupling results, it is important to employ connectivity metrics able to estimate real brain interactions, not yielding significant values between independent sources and minimizing the effect of volume conduction effects.

1.6 State of the art

The main contributions of this Doctoral Thesis are related with the characterization of the EEG brain alterations in AD and MCI from three different levels of analysis: local activation, interaction between pair-wise sensors, and network organization. Therefore, the next subsections reflect a comprehensive state of the art revision of this topic in these levels.

1.6.1 Local activation

The brain changes that AD and MCI elicit in EEG activity have been traditionally analyzed using simple signal processing methods, such as local activation measures.

On one hand, the spectral analyses in specific frequency bands have reflected a progressive slow-down of the EEG activity in AD and MCI. Particularly, they are associated with an increase of power in low frequencies (δ and θ) and a decrease of power in higher frequencies (α and β), revealed by both the absolute power and the relative power (RP) in each band (Babiloni et al., 2017; Farina et al.,

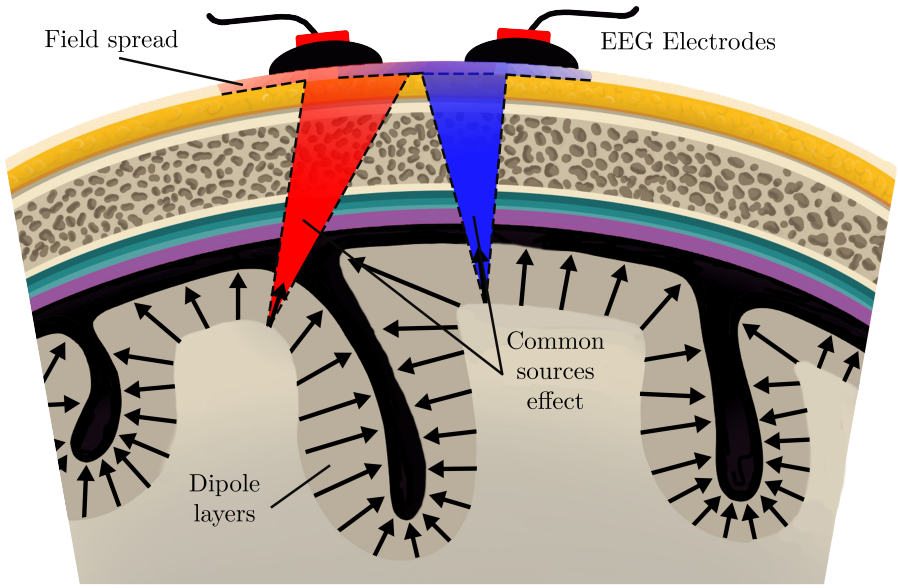

Figure 1.5: Anatomical illustration of the different head surfaces. Pyramidal cells are depicted as dipole layers. EEG is more sensitive to dipoles perpendicular to the electrode and insensitive for such dipoles that cancel themselves. Common sources effect and field spread phenomena are also depicted.

2020; Liu et al., 2016; Musaeus et al., 2018; Poil et al., 2013; Roh et al., 2011). This trend is also revealed by a decrease in the median frequency (MF) values (Gaubert et al., 2019; Hatz et al., 2015; Kang et al., 2015) and a decrease in spectral entropy (SE) values (Coronel et al., 2017; Gaubert et al., 2019) for AD patients compared with HC subjects. These changes can be associated with different brain alterations. The slowing of neural oscillations in AD could be consequence of the loss of neurotransmitter acetylcholine, since the cholinergic system modulates spontaneous cortical activity at low frequencies (Osipova et al., 2003). Table 1.1 shows a summary of the results obtained in previous studies using spectral metrics.

On the other hand, nonlinear analysis techniques have also been widely used in order to provide complementary information to spectral measures. Previous EEG studies reported a loss of complexity and irregularity associated with early AD and MCI using different nonlinear metrics, such as Lempel-Ziv complexity (LZC) (Abásolo et al., 2006; Liu et al., 2016; McBride et al., 2014), multiscale entropy (MSE) Escudero et al. (2006), auto-mutual information (AMI) (Abásolo et al., 2008), sample entropy (SampEn) (Kang et al., 2015; McBride et al., 2014), and

Table 1.1: Summary of the results obtained in previous local activation studies using spectral metrics.

Study	Data set	Methods	Results
Roh et al. (2011)	41 AD, 38 MCI, and 39 HC subjects	RP	Increases in RP(δ) and RP(θ), and decreases in RP(α) and RP(β_2) bands, higher for AD patients and moderate for MCI subjects
Poil et al. (2013)	22 stable MCI and 8 progressing to AD	RP	Significant decreases in RP(α) for the subjects that progress to AD in comparison with stable MCI subjects
Kang et al. (2015)	17 AD and 24 HC subjects	MF	AD patients showed significantly lower MF values than HC subjects
Hatz et al. (2015)	26 AD, 9 MCI, 26 HC subjects	MF	Higher MF values for HC and MCI subjects compared with AD patients
Liu et al. (2016)	24 AD and 24 HC subjects	RP	A significant increase in RP(θ) and a significant decrease in RP(α) for AD patients
Babiloni et al. (2017)	42 AD and 40 HC subjects	RP IAF	Increases in RP(δ), and decreases in RP(α) and IAF for AD patients
Coronel et al. (2017)	79 AD patients	SE	Reductions in SE values as the MMSE score decreased
Musaeus et al. (2018)	117 AD, 117 MCI, and 138 HC subjects	RP, P	Increases in the RP(θ) and P(θ), and decreases in RP(β_1), P(β_1), and P(β_2) as the disease severity increases
Gaubert et al. (2019)	139 preclinical AD and 175 HC subjects	MF, SE	After exceeding a certain level of amyloid load, MF and SE values decreased markedly
Farina et al. (2020)	102 AD, 121 MCI, and 138 HC subjects	RP	Significant increases in the RP(δ) and RP(θ) for AD patients, but only significant increases in RP(θ) for MCI patients compared with HC subjects

RP: Relative Power; MF: Median Frequency; IAF: Individual Alpha Frequency; SE: Spectral Entropy; P: Absolute Power.

fuzzy entropy (FuzzyEn) (Cao et al., 2015; Simons et al., 2018). These decreases of EEG complexity and variability can be related to the loss of neurons or synapses (Jeong et al., 2001) and to alterations in information processing at the cerebral cortex (Baraniuk et al., 2001). Despite the fact that the slowing in the EEG acivity and the loss of complexity can be explained as a consequence of different brain alterations, they could be strongly correlated as suggested in Dauwels et al. (2011). A summary of the results obtained in previous studies using nonlinear metrics are shown in Table 1.2.

Table 1.2: Summary of the results obtained in previous local activation studies using nonlinear metrics.

Study	Data set	Methods	Results
Abásolo et al. (2006)	11 AD and 11 HC subjects	LZC, CTM	Significant complexity decrease (lower LZC values) and no significant variability decrease (higher CTM values) for AD patients
Escudero et al. (2006)	11 AD and 11 HC subjects	MSE	EEG background activity is less complex in AD patients than in HC subjects
Abásolo et al. (2008)	11 AD and 11 HC subjects	AMI	AMI decreased more slowly with time delays in AD patients than in controls, suggesting more regular time series for AD patients
McBride et al. (2014)	17 AD, 16 MCI, and 15 HC subjects	LZC, SampEn	Complexity and irregularity decrease revealed by lower LZC and SampEn values for AD patients
Kang et al. (2015)	17 AD and 24 HC subjects	SampEn	AD patients showed significantly lower SampEn values than HC subjects
Cao et al. (2015)	20 AD and 20 HC subjects	FuzzyEn	FuzzyEn values of AD are significantly decreased in α frequency band
Liu et al. (2016)	24 AD and 24 HC subjects	LZC	AD patients showed lower LZC values, revealing a complexity decrease in all frequency bands (only significant in α)
Simons et al. (2018)	11 AD and 11 HC subjects	FuzzyEn	AD patients showed significantly lower FuzzyEn values for AD patients in comparison with HC subjects

LZC: Lempel-Ziv Complexity; CTM: Central Tendency Measure; MSE: Multiscale Entropy; AMI: Auto-Mutual Information; SampEn: Sample Entropy; FuzzyEn: Fuzzy Entropy.

1.6.2 Interactions between sensors

In order to obtain a better understanding of the organization and functioning of the brain, it has been studied as a functional network analyzing the interactions between sensors, since local activation parameters are no longer sufficient for a full characterization of brain dynamics (Stam and van Straaten, 2012).

Coupling between EEG electrodes have been traditionally quantified with linear methods, such as coherency and spectral estimations (Moretti et al., 2008; Tóth et al., 2014). Particularly, previous studies reported widespread connectivity increases in AD and MCI patients compared to HC subjects at lower frequency bands. These increases in AD were statistically significant at δ (Mammone et al., 2017; Moretti et al., 2008) and θ (Briels et al., 2020; Canuet et al., 2012; Hatz et al., 2015; Mammone et al., 2017). Contradictory results were reported for MCI

Table 1.3: Summary of the results obtained in previous local activation studies using coupling metrics.

Study	Data set	Methods	Results
Pijnenburg et al. (2004)	14 AD, 11 MCI, and 14 HC subjects	SL	SL was significantly decreased in the upper α (10–12) and β bands in AD and MCI
Moretti et al. (2008)	85 MCI and 30 HC subjects	MSCOH	The MCI subjects showed increases of interhemispheric MSCOH values in δ and θ bands
Canuet et al. (2012)	125 AD and 60 HC subjects	LPS	Decreased connectivity patterns in AD at α_2 (10-13 Hz), and widespread increases in θ band
Tóth et al. (2014)	9 MCI and 14 HC subjects	PLI	Significant decreases of PLI in δ and θ were present in MCI patients
Hatz et al. (2015)	26 AD, 9 MCI, 26 HC subjects	PLI	PLI was higher in the AD group than in the MCI-stable and HC groups in the θ band
Engels et al. (2015)	318 AD and 133 HC subjects	PLI	AD patients showed widespread PLI decreases in the α band compared with HC subjects
Gómez et al. (2016)	37 and 20 HC subjects	Cross-SampEn	Cross-SampEn values were lower in the AD group for all the interactions between EEG channels
Mammone et al. (2017)	7 AD and 8 MCI subjects	PDI, MSCOH	Increased connectivity in δ and θ bands for AD patients compared with MCI subjects
Briels et al. (2020)	214 AD, 197 HC subjects; 196 AD and 202 HC subjects	AEC, MSCOH, PLI, PLV	Widespread decreases of AEC in α and β bands for AD patients. Decrease of MSCOH and PLV values in α band for AD patients. Global increase in PLI and wPLI values at θ frequency band in AD subjects compared to SCD subjects

SL: Synchronizaation Likelihood; MSCOH; Magnitude Squared Coherence; LPS: Lagged Phase Synchronizataion; PLI: Phase Lag Index; Cross-SampEn: Cross Sample Entropy; PDI: Permutation Disalignment Index; AEC: Amplitude Envelope Correlation; PLV: Phase Locking Value.

patients. Increases of interhemispheric connectivity values in δ and θ were obtained (Moretti et al., 2008). However, significant decreases of connectivity within and between regions in these frequency bands were also reported for MCI patients (Tóth et al., 2014). In the case of higher frequency bands, connectivity decreases at the α and β bands were obtained for AD and MCI patients compared to HC subjects using different coupling metrics (Briels et al., 2020; Engels et al., 2015; Pijnenburg et al., 2004). Furthermore, Canuet et al. (2012) found that source connectivity patterns between different regions of interest in AD patients were characterized by a reduction of synchronization in α_2 band (10-13 Hz), involving mainly temporal and frontal connections. Nevertheless, these methods are not

suitable for characterizing nonstationary signals and the alterations found depend on the particular coupling parameter. In this regard, entropy-based measures are very well-suited to analyze short and noisy one-dimensional time series and their multidimensional versions are a good option for the analysis of multiple signals recorded from many electrodes. Only a few studies have applied these metrics to biological systems (Licinio et al., 1998; Martínez-Zarzuela et al., 2013; Pincus and Singer, 1996), but none of them has analyzed the spontaneous EEG activity. Only our preliminary study analyzed the broadband spontaneous EEG activity in AD by means of nonlinear metrics, revealing a higher degree of similarity between channels in AD patients than in HC subjects (Gómez et al., 2016). Table 1.3 shows a summary of the connectivity results obtained in previous studies.

However, these results may be biased due to volume conduction effects due to fact that some of the employed coupling metrics could obtain spurious connectivity estimations between independent sources.

1.6.3 Network organization

A graph constructed from connectivity results can be viewed as an abstract representation of the cerebral activity. Therefore, the organization of these brain networks can be quantified using parameters derived from complex network theory.

Generally, AD is mainly associated with a loss in local information processing (revealed by decreases in integration) and a gain in global information processing (revealed by increases in segregation) in the conventional frequency bands (Afshari and Jalili, 2017; de Haan et al., 2009; Stam et al., 2009). However, previous studies reported contradictory results depending on the frequency band under analysis, and inconsistent results between them when studying the same frequency band. With regard to the contradictory results depending on the frequency band under analysis, significant clustering coefficient decreases were obtained in α band, while increases in θ were also reported in the same study (Stam et al., 2009). The opposite trend was reported for the characteristic path length, with significant increases in α and decreases in θ (Stam et al., 2009). Regarding the inconsistent results between studies, some works did not find significant differences between AD and control subjects (Lo et al., 2010; Sanz-Arigita et al., 2010), others found significant decreases in AD (Stam et al., 2009; Tijms et al., 2013) and other studies also found an increased clustering in AD (He et al., 2008; Yao et al., 2010; Zhao et al., 2012). This issue also happens with the characteristic path length, as higher

Table 1.4: Summary of the results obtained in previous local activation studies using graph parameters derived from complex network theory.

Study	Data set	Methods	Results
Stam et al. (2009)	18 AD and 18 HC subjects	L, C, and normalized L and C	C values were lower and L values were higher for AD patients in the lower α band (8-10 Hz). Its normalized values obtained using 50 surrogate random networks were both decreased for AD patients
de Haan et al. (2009)	20 AD and 23 HC subjects	L, C, and normalized L and C	Normalized C values were lower in α and β bands and normalized L values were lower in α and γ bands compared to HC subjects
Lo et al. (2010)	25 AD and 30 HC subjects	L, C, E_{global} and E_{local}	AD patients had significantly increased L and E_{global} implying the dysconnectivity and topological disorganization of their networks
Sanz-Arigita et al. (2010)	18 AD and 21 HC subjects	L and C	L in AD networks is closer to the theoretical values of random networks than HC networks, while no significant differences were found in C
Yao et al. (2010)	91 AD, 113 MCI and 98 HC subjects	Normalized L and C	Higher normalized C and L values in AD. MCI networks exhibited intermediate values
Zhao et al. (2012)	33 AD and 20 HC subjects	L, C, E_{global} and E_{local}	Significant increased L, C and E_{local} values, but significant decreased E_{global} in AD patients compared with HC subjects
Tijms et al. (2013)	38 AD and 38 HC subjects	SW and normalized L and C	AD networks were characterized by a more random topology as indicated by a decrease in SW, normalized L and normalized C
Miraglia et al. (2016)	30 AD, 30 MCI, and 30 HC subjects	SW	AD brain networks are characterized by higher SW in α band and lower SW in β_2 and γ bands. MCI SW values are midway between AD and HC
Afshari and Jalili (2017)	25 AD and 26 HC subjects	E_{global} and E_{local}	AD networks showed decreased E_{global} in α and β bands. AD patients had significantly higher E_{local} values in α and β
Vecchio et al. (2017)	110 AD and 34 HC subjects	L, C, and SW	HC showed higher SW values than AD in the δ, θ, and β bands, while the opposite was found in the α band

L: characteristic path length; C: clustering coefficient; E_{global}: global efficiency; E_{local}: local efficiency; SW: small-world.

values as the disease progresses were reported (He et al., 2008; Lo et al., 2010; Yao et al., 2010; Zhao et al., 2012), but also lower values (Sanz-Arigita et al., 2010; Tijms et al., 2013).

In the case of the small-world (SW) characteristics of the network, HC showed higher SW values than AD in δ, θ, β and γ frequency bands, while the opposite was found in the α band (Miraglia et al., 2016; Vecchio et al., 2017). Furthermore, MCI subjects showed midway SW values between AD and HC subjects (Miraglia et al., 2016). All these results tangle the possible clinical interpretations and makes it difficult to extract conclusions about the changes in the global brain network provoked by the AD neurodegeneration process. Then, an approach that considers the information of all layers together could capture the relevant information of the whole brain network. This is the reason why multiplex network approaches have focused a great attention in recent years. A summary of the results obtained in previous studies using graph parameters are shown in Table 1.4.

Multiplex network theory has been applied in EEG studies, where each frequency-specific network corresponds to a layer. However, the links between these layers are often not available. To avoid this issue, different methods have been used to build multiplex networks: from a simple parameter sum across all frequency-specific layers to more complex approaches (Boccaletti et al., 2014; Kabbara et al., 2018; Yu et al., 2017). Then, the comparison between multiplex networks and the estimation of multiplex parameters could be biased if the way of assigning weights to inter-layer links are different across studies (Stam, 2014). Furthermore, these approaches could compensate opposite trends between groups as a consequence of how they determine the link weights between the frequency-specific layers, and blur the differences between them.

Chapter 2

Hypothesis and objectives

During the last decades, the neural mechanisms associated with neurodegeneration and cognitive decline of the brain have focused a great research attention. However, the neurophysiological substrates that underlie the biological lesions in MCI and dementia due to AD have not yet been completely understood. Therefore, the proposal of this Doctoral Thesis is focused on characterizing these brain changes during the different stages of the AD continuum.

The main hypothesis of the present Doctoral Thesis, and the particular hypotheses that have motivated each study, are described in section 2.1. On the other hand, the main and specific objectives are described in section 2.2.

2.1 Hypotheses

In the last decades, growing efforts have been made to understand the underlying brain dynamics associated with the neurodegeneration processes provoked by MCI and AD. The human brain is comprised by billions of interconnected neurons forming an extremely complex network. The synchronous activity generated by synchronized firing of cortical neuronal pools gathers information on the intricate dynamical brain processes. In this context, the proposed approaches following three levels of analysis provide an adequate framework to characterize this alterations in information processing between distant brain regions. Furthermore, high temporal resolution techniques, such as the EEG, enables the direct characterization of spontaneous cortical oscillatory activity and potentially brain dynamics. Therefore, the analyses of the neural EEG spontaneous activity at different levels could be useful for understanding the altered brain dynamics underlying the

neurodegenerative processes in the different stages of the AD continuum.

In order to obtain a more complete characterization of human neural networks in AD and MCI, EEG data were examined from three different levels of analysis on the way in which interactions are taken into account: (i) analysis of local activation patterns in individual sensors; (ii) analysis of interactions between sensors using connectivity and synchronization metrics; and (iii) analysis of the functional organization of brain networks, applying novel parameters derived from complex network theory.

The application of different frequency (spectral measures) and time domain (nonlinear measures) methods to the EEG activity in individual sensors has led to observe two major effects in AD and MCI: slowing of the EEG and reduced complexity of the EEG signals. Therefore, in Ruiz-Gómez et al. (2018a), we hypothesized that *a methodology based on the combination of spectral and nonlinear features can be a useful tool to help in AD and MCI diagnosis.*

However, local activation studies are no longer sufficient for a full characterization of AD brain dynamics. This is why many EEG studies have focused on the analysis of interactions between sensors. Most of their results using functional connectivity metrics support the well-established hypothesis of AD as a 'disconnection syndrome'. Only a few studies have applied nonlinear methods, such as cross-entropy metrics, to biological systems with the aim of estimating the synchronization patterns of EEG signals. Hence, in Ruiz-Gómez et al. (2018b), we hypothesized that *cross-entropy metrics are able to characterize the disrupted coupling EEG patterns between distant brain regions in MCI and AD.*

However, the aforementioned results using functional connectivity metrics may be biased due to volume conduction effects as these metrics could reflect spurious coupling values between independent brain sources. Therefore, in the third publication (Ruiz-Gómez et al., 2019b), we hypothesized that *diverse functional connectivity measures are differently affected by volume conduction effects and it could bias the results.*

Based on coupling results, graphs can be constructed as an abstract representation of the cerebral activity. These representations have been quantified using parameters derived from Complex Network Theory and provide insights into the specific organization of the brain. Particularly, AD continuum is mainly associated with a progressive decrease of global information processing and a progressive increase of local information processing. However, previous studies did not report consistent results. They showed contradictory results depending on the frequency band under analysis, and they also reported inconsistent results between them

when studying the same frequency band. This tangles the possible clinical interpretations about the alterations that AD neurodegeneration elicits in the global brain network. Hence, we hypothesized that *a multiplex approach that analyzes together all the frequency bands could capture relevant information of the whole brain network* in Ruiz-Gómez et al. (2021).

These hypotheses form the main core of the present Doctoral Thesis, which can converge into the following global hypothesis:

> "*The use of concepts from three different level of analysis applied to the spontaneous EEG could provide a meaningful framework for discriminating the different stages of AD continuum and characterizing the alterations in the brain dynamics during the neurodegenerative process.*"

2.2 Objectives

The general goal of the present Doctoral Thesis is to study, design and apply biomedical signal processing methodologies to the EEG data with the aim of characterizing and discriminating the neural substrates altered during the AD continuum. These data were examined from three levels of analysis: local activation, connectivity between pair-wise sensors, and network organization. In order to achieve the main objective, the following specific objectives arise:

I. To review the bibliography and state-of-the-art related to biomedical signal processing methodologies useful to characterize EEG data. In particular, putting special emphasis in local activation measures, coupling metrics and the effect of volume conduction over them, and graph theory methods, in order to comprehensively characterize neural brain dynamics.

II. To build a database and expand the already existing one. Both databases are formed by EEG recordings, socio-demographic data and clinical variables from patients in the different stages of AD continuum, including MCI patients, and healthy controls.

III. To implement the more suitable methods to reduce the noise impact on the EEG signals, to obtain local, coupling and network measures that characterize the brain dynamics during the neurodegeneration process, and to model the volume conduction effects in the EEG signals.

IV. To evaluate the diagnostic performances of the selected methods and their ability to characterize the brain changes in the different stages of AD continuum.

V. To compare and discuss the obtained results with the aim of extracting the appropriate conclusions. This objective includes the comparison with the state-of-the-art EEG studies of MCI and AD.

VI. To disseminate the main results and conclusions of the research in JCR indexed journals, as well as in international and national conferences.

Chapter 3

Subjects and signals

In this compendium of publications, two different databases were used, as a new database was registered throughout during the development of the Doctoral Thesis. Firstly, section 3.1 describes the socio-demographic and clinical data of the subjects included in each study. The EEG acquisition, including the description of the EEG equipment, electrode locations and sampling rate, is included in section 3.2. Finally, section 3.3 describes the followed pre-processing procedure.

3.1 Subjects

Two different databases were analyzed in this Doctoral Thesis: (i) the former is composed by a total of 111 EEG recordings acquired in a clinical environment at the Río Hortega University Hospital (HURH, Hospital Universitario Río Hortega), and (ii) the latter consists of 253 EEG recordings acquired in a research environment as a result of the POCTEP 2014-2020 project 'Análisis y correlación entre el genoma completo y la actividad cerebral para la ayuda en el diagnóstico de la enfermedad de Alzheimer' (AD-EEGWA). See Table 3.1 and Table 3.2 for the socio-demographic and clinical data of the subjects included in each dataset.

All subjects and caregivers gave their written informed consent to be included in each study in accordance with the Declaration of Helsinki. All studies were carried out in accordance with the recommendations of the Code of Ethics of the World Medical Association and the protocols were approved by the Ethics Committee of the HURH (Valladolid, Spain) and by the Ethics Committee of Porto University (Porto, Portugal).

Table 3.1: Socio-demographic and clinical data of the Río Hortega University Hospital database.

	HC subjects	**MCI patients**	**AD patients**
Number of subjects	37	37	37
Age (years) (mean ± SD[1])	76.3 ± 3.5	76.0 ± 7.3	79.8 ± 6.0
Sex (Male : Female)	12 : 25	16 : 21	12 : 25
MMSE[2] (mean ± SD[1])	28.9 ± 1.3	27.3 ± 1.9	21.2 ± 3.3

[1]SD: standard deviation. [2]MMSE: Mini Mental State Examination score.
MCI: mild cognitive impairment patients; AD: Alzheimer's disease patients.

Table 3.2: Socio-demographic and clinical data of the AD-EEGWA database.

	HC subjects	**MCI patients**	**AD_{mil} patients**	**AD_{mod} patients**	**AD_{sev} patients**
Number of subjects	51	51	51	50	50
Age (years) (mean ± SD[1])	80.1 ± 7.1	85.5 ± 7.2	80.7 ± 7.0	81.3 ± 8.0	80.0 ± 7.8
Sex (Male : Female)	26 : 25	15 : 36	21 : 30	7 : 43	7 : 43
MMSE[2] (mean ± SD[1])	28.8 ± 1.1	23.3 ± 2.8	22.5 ± 2.3	13.6 ± 2.8	2.42 ± 3.7

[1]SD: standard deviation. [2]MMSE: Mini Mental State Examination score.
MCI: mild cognitive impairment patients; AD_{mil}: mild Alzheimer's disease patients; AD_{mod}: moderate Alzheimer's disease patients; AD_{sev}: severe Alzheimer's disease patients.

3.2 EEG acquisition protocol

The EEG acquisition was very similar for both databases. For each subject, five minutes of spontaneous EEG activity were recorded using a 19-channel system at the electrodes Fp1, Fp2, Fz, F3, F4, F7, F8, Cz, C3, C4, T3, T4, T5, T6, Pz, P3, P4, O1, and O2 following the International System 10–20 (see Figure 1.3). Subjects were asked to stay in a relaxed state, awake, and with closed eyes during EEG acquisition. Drowsiness episodes, eye-movement related artifacts and muscle activity were identified and marked during the course of the EEG recordings.

Depending of the database, the EEG acquisition equipment and the sampling rate vary. HURH recordings were acquired with a XLTEK® (Natus Medical, Pleasanton, CA, USA) at a sampling rate of 200 Hz, whereas AD-EEGWA database was recorded using a Nihon Kohden Neurofax JE-921A (Nihon Kohden, Tokio, Japan) at a sampling rate of 500 Hz. In both cases, signals were re-referenced by means of common average referencing (CAR). After the EEG acquisition, a pre-processing stage must be performed to remove artifacts and reduce undesirable noise.

3.3 EEG pre-processing

In order to minimize the presence of noise and artifacts, signals were pre-processed following a three-steps procedure:

1) **Frequency filtering.** Signals were digitally filtered between 0.4 and 98 Hz using a Hamming window bandpass finite impulse response (FIR) filter (filter order 2000, forward and backward filtering) to limit their spectral content. Then, the power line frequency interference (50 Hz) was removed using a band-stop digital filter (Hamming window, filter order 2000, forward and backward filtering).

2) **Independent Component Analysis (ICA).** In order to minimize the presence of oculographic, cardiographic, and myographic artifacts, ICA components associated with these artifacts were discared by visual inspection. Mathematically, ICA can be viewed as a linear decomposition that is based on minimizing the mutual information between the data projections or maximizing their joint entropy (Delorme and Makeig, 2004). Furthermore, it seeks to find components that are mutually independent, meaning that the cross-correlations between components, as well as all the higher order moments of the signals, are zero (Makeig et al., 1997). Performing ICA decomposition is most appropriate when sources are linearly mixed in the recorded signals. These assumptions are met for the EEG activity recorded in the scalp, as the EEG electrodes capture several brain sources as a consequence of volume conduction effects (Delorme and Makeig, 2004).

3) **Artifact-free epoch selection.** After ICA reconstruction, a band-pass digital filter was applied to limit the spectral content to the frequency band of interest between 1 and 70 Hz (Hamming window, filter order 2000, forward and backward filtering). Then, EEG data were divided into no overlapping 5 seconds length epochs. Finally, two experienced technicians selected the artifact-free epochs that were considered for further analysis.

Chapter 4

Methods

This chapter describes briefly the different methods that have been applied in this Doctoral Thesis. However, the detailed explanation of the employed methods can be found in the papers of the compendium (see Appendix A). In this Thesis, a new method to model synthetic signals to study some of the EEG characteristics has been proposed (section 4.1). Then, the characterization of the brain alterations during AD continuum has been addressed from three levels of analysis: local activation (section 4.2), similarity or connectivity between pair-wise sensors (section 4.3), and network organization (section 4.4). Finally, the description of the applied statistical analyses and classification methods is provided in sections 4.5 and 4.6, respectively.

4.1 Synthetic EEG signals

In this Doctoral Thesis, a new method to build synthetic EEG signals was proposed (Ruiz-Gómez et al., 2019b). For this purpose, we used the combination of a real-head surface-model built from information of the Visible Human Project® (VHP) dataset, and a set of coupled oscillators forming a Kuramoto model, which models the artificial sources inside the brain surface.

4.1.1 Real-head surface-model

The VHP is an open-source dataset that contains a large amount of magnetic resonance images, computed tomographies, and anatomical cryosection images. This dataset was designed for the study of human anatomy, for testing medical

imaging algorithms, and for building three-dimensional representations of both males and females bodies (U.S. National Library of Medicine, 2018). Particularly, the result of these 3D-computational models is the description of each individual tissue as a triangular surface mesh.

In our particular case, we used a previously created model built using anatomical cryosection images from a patient, described in Makarov et al. (2016) and also available online at https://www.wiley.com/legacy/wileychi/makarov/matlab.html. Particularly, this model has already been used in different studies to study the propagation of electromagnetic fields through the human head and transcranial direct current stimulation (Elloian et al., 2014; Noetscher et al., 2014). The brain, the CSF, the skull, and the skin were identified and hand-segmented using ITK-Snap (Yushkevich et al., 2006).

In Ruiz-Gómez et al. (2019b), we simulated the electromagnetic waves propagation from sources to electrodes, taking into account their attenuation. This attenuation defines the rate of amplitude loss of an electromagnetic wave defined by the parameter α (electrical attenuation). For each of the aforementioned modeled tissues, α was assigned according to a previous study (Gosselin et al., 2014): $\alpha_{brain} = 6.8$, $\alpha_{CSF} = 0.1$, $\alpha_{skull} = 54.55$, and $\alpha_{skin} = 21.158$.

Once the model was created, the electrical activity of the brain sources was simulated using a set of coupled oscillators forming a Kuramoto model.

4.1.2 Kuramoto model

The original model proposed by Kuramoto described the phase dynamics of a set of coupled oscillators. Specifically, all of the N oscillators that form the set are equally weighted and purely sinusoidal. The phase dynamics of each oscillator is described by the following differential equation (Kuramoto, 1975):

$$\frac{d\theta_i}{dt} = \omega_i + \frac{K}{N}\sum_{j=1}^{N}\sin(\omega_j - \omega_i), \tag{4.1}$$

where θ_i represents the phase of the i-th oscillator, whose natural frequency is ω_i, and K is the global coupling strength between all oscillators. This equation reflects that the phase evolution of each oscillator is determined by its natural frequency, ω_i, and the average influence of all other oscillators.

The distribution of the natural frequencies of each oscillator $g(\omega)$ are distributed according to some unimodal and symmetric probability distribution $g(\omega)$.

That is, the distribution should fulfill that $g(\omega) = g(-\omega)$ for all ω. Typically, Lorentzian distributions centered around ω_0 and with width γ are used to determine these natural frequencies (Strogatz, 2000):

$$g(\omega) = \frac{\gamma}{\pi[\gamma^2 + (\omega - \omega_0)^2]}. \tag{4.2}$$

The global level of synchronization between the N oscillators that compose the system over time, $r(t)$, is defined as:

$$r(t) = \frac{1}{N} \sum_{j=1}^{N} e^{j\theta_i(t)}. \tag{4.3}$$

In order to obtain the state of each oscillator over time, the model is integrated numerically varying the global coupling K. In this context, two different scenarios appear. On one hand, for simulations with K less than a certain threshold K_{crit}, $r(t)$ evolves towards zero. In this case, the oscillators act as if they were unsynchronized. On the other hand, when K exceeds K_{crit}, $r(t)$ grows exponentially. This means that a single cluster of synchronized oscillators emerges (Strogatz, 2000). In the case that the natural frequencies are taken from a Lorentzian distribution, the critical value K_{crit} is only determined by the distribution width and is given by $K_{crit} = 2\gamma$ (Stam et al., 2007).

Particularly, the state of each oscillator was obtained integrating numerically the equation 4.1 using the Runge-Kutta method of order 4 (Stam et al., 2007). Then, the state of the i-th oscillator, which was obtained from the frequency ω_0, at time t is given by:

$$O_{i,\omega_0}(t) = A_{\omega_0} \sin \theta_i(t), \tag{4.4}$$

where A_{ω_0} was a constant amplitude for all the oscillators obtained with the same ω_0, but frequency-dependent. The resulting time series represent the electrical activity of the brain sources.

4.1.3 Simulation of the synthetic EEG signals

Many different parameters of the previously described Kuramoto model should be set for to obtain the synthetic EEG signals that represent the electrical activity of the brain sources.

1) **Central frequencies of each oscillator.** The natural frequencies ω_0 were established by evaluating the EEG band of interest between 1 and 70 Hz

into spectral bands of 1 Hz wide. Hence, $f_0 \in [1.5, 69.5]$ Hz (step=1 Hz) and $\omega_0 = 2\pi f$.

2) **Total number of oscillators.** For each frequency band, $N = 200$ oscillators randomly placed inside the brain mesh were simulated, each one representing an active cerebral source. Despite the fact that an infinite number of oscillators is needed to extract analytical results, it has been demonstrated that a limited number of them can be used to explain empirical results (Kiss et al., 2002). Also, this number of brain sources allowed every synthetic electrode to have a closest brain source with a low computational cost.

3) **Specific oscillation frequencies.** Specific oscillation frequencies were determined by a Lorentzian distribution of central frequency ω_0 and width $\gamma = 1$ (Ahmadi et al., 2019; Ruiz-Gómez et al., 2019b; Stam et al., 2007).

4) **Numerical integration.** The time step to carry out the numerical integration used to obtain the state of the oscillators was set to 2 ms (corresponding to a sample frequency of 500 Hz). This value was selected according to the sample frequency of the real EEG recordings of the AD-EEGWA database.

5) **Amplitude of the oscillators.** The amplitude values, A_{ω_0}, were determined as the squared root of the relative power in each 1-Hz frequency band centered at ω_0. For this purpose, only the real EEG recordings of the AD-EEGWA database was taken into account.

Finally, in order to analyze the effect of EEG volume conduction, we simulated two different scenarios: (i) an ideal volume conduction-free case in which each source is only registered by the closest EEG electrode, and (ii) the real-case with volume conduction, where each source activity is registered by all simulated EEG electrodes (Ruiz-Gómez et al., 2019b).

4.2 Local activation

After the pre-processing stage, artifact-free epochs were firstly analyzed by means of metrics that are focused on determining the level of activation of individual neuronal groups (Ruiz-Gómez et al., 2018a). Two different types of parameters can be distinguish from the point of view of how the information is extracted: spectral and nonlinear features.

4.2.1 Spectral features

In order to characterize the EEG activity based on the analysis of their spectral content, the following spectral parameters have been calculated from the normalized power spectral density (PSD_n): relative power (RP), median frequency (MF), individual alpha frequency (IAF), and spectral entropy (SE).

1) **Relative power.** RP represents the relative contribution of different frequency components to the global power spectrum (Rodriguez et al., 1999). It is obtained by summing the contributions of the spectral components that comprise each frequency band:

$$\mathrm{RP}(f_1, f_2) = \sum_{f_1}^{f_2} \mathrm{PSD_n}(f), \tag{4.5}$$

where f_1 and f_2 are cut-off frequencies of each frequency band.

2) **Median frequency.** MF is defined as the frequency that comprises the half of the PSD_n power. Mathematically, it can be defined as:

$$\sum_{1\ \mathrm{Hz}}^{\mathrm{MF}} \mathrm{PSD_n}(f) = 0.5 \sum_{1\ \mathrm{Hz}}^{70\ \mathrm{Hz}} \mathrm{PSD_n}(f), \tag{4.6}$$

as the EEG band of interest taken into account is between 1 and 70 Hz.

3) **Individual alpha frequency.** IAF estimation is based on the calculation of the MF in the extended alpha band (4–15 Hz). Then, it is defined as (Moretti et al., 2004):

$$\sum_{4\ \mathrm{Hz}}^{\mathrm{IAF}} \mathrm{PSD_n}(f) = 0.5 \sum_{4\ \mathrm{Hz}}^{15\ \mathrm{Hz}} \mathrm{PSD_n}(f), \tag{4.7}$$

4) **Spectral entropy.** SE is a disorder quantifier whose original meaning implies uncertainty of information in terms of disorder, discrepancy and diversity. Its definition is based on a probability distribution and provides an estimation of the signal irregularity in terms of the flatness of the power spectrum (Powell and Percival, 1979). Narrow power spectrum signals with only a few spectral components (e.g., a highly predictable signal like a sum of sinusoids) yield a low SE value, while uniform power spectrum signals with a broad spectral content (e.g., a highly irregular signal like white noise)

provide a high entropy value. The equation for computing SE is:

$$\mathrm{SE} = -\sum_{1\ \mathrm{Hz}}^{70\ \mathrm{Hz}} \mathrm{PSD_n}(f) \cdot \log[\mathrm{PSD_n}(f)], \tag{4.8}$$

4.2.2 Nonlinear features

In order to complement the spectral analysis an provide complementary information, five global nonlinear methods were also calculated: Lempel–Ziv complexity (LZC), central tendency measure (CTM), sample entropy (SampEn), fuzzy entropy (FuzzyEn), and auto-mutual information (AMI).

1) **Lempel–Ziv complexity (LZC).** LZC estimates the complexity of a finite sequence of symbols, with higher LZC values for more complex time series (Lempel and Ziv, 1976). It is computed as the normalized number of subsequences of consecutive characters, after the transformation of the original time series, $\mathrm{x}[n]$, into a finite symbol string, $\mathrm{s}[n]$. Usually, a binary transformation using the median of the signal, $\tilde{\mathrm{x}}$, as threshold is carried out:

$$\mathrm{s}[n] = \begin{cases} 1 & \text{if } \mathrm{x}[n] < \tilde{\mathrm{x}} \\ 0 & \text{if } \mathrm{x}[n] \geq \tilde{\mathrm{x}} \end{cases} \tag{4.9}$$

Then, $\mathrm{s}[n]$ is scanned from left to right and a complexity counter $\mathrm{c}(n)$ is increased every time a new subsequence of consecutive characters is found. In order to make this value independent from the length of the time series, LZC values are normalized between 0 and 1:

$$\mathrm{C}(n) = \frac{c(n)}{b(n)}, \tag{4.10}$$

with $\mathrm{b}(n)$ defined as:

$$\mathrm{b}(n) = \lim_{n\to\infty} \mathrm{c}(n) \equiv \frac{n}{\log_\alpha(n)} \tag{4.11}$$

and $\alpha = 2$ since the number of symbols is 2.

2) **Central tendency measure (CTM).** CTM quantifies the degree of variability of a given time series. It is calculated as the proportion of points that fall within a circular region of radius ρ using the first-order differences of the

data as basis (Cohen et al., 1996):

$$\mathrm{CTM} = \frac{1}{N-2}\sum_{n=1}^{n-2}\delta[n], \tag{4.12}$$

where

$$\delta[n] = \begin{cases} 1 & \text{if } \{(\mathrm{x}[n+2]-\mathrm{x}[n+1])^2 + (\mathrm{x}[n+1]-x[n])^2\}^{\frac{1}{2}} \leq \rho \\ 0 & \text{otherwise.} \end{cases} \tag{4.13}$$

where N is the size of the time series. CTM ranges between 0 and 1, with higher values corresponding to less variable time series. The value of the radius ρ must be determined experimentally, depending on the characteristics of the data (Cohen et al., 1996).

3) Sample entropy (SampEn). SampEn is an embedding entropy used to quantify the irregularity. It takes always either zero or positive values, with higher values associated with more irregular time series. It is defined as the negative natural logarithm of the conditional probability that two sequences similar for a determined number of points remain similar at the next point, within a tolerance, excluding self-matches (Richman and Moorman, 2000):

$$\mathrm{SampEn}(m, r, N) = \lim_{N\to\infty} -\ln\left(\frac{A^m(r,N)}{B^m(r,N)}\right), \tag{4.14}$$

where r is the tolerance, N the signal length, and $A^m(r,N)$ and $B^m(r,N)$ denote the probabilities of matching for templates of $m+1$ and m points, respectively. A match between two templates of length m, $x_m(i)$ and $x_m(j)$, occurs when $d[x_m(i), x_m(j)] < R$, where $d[\cdot]$ denotes the Chebyshev distance and the tolerance value R is usually dependent of the standard deviation of x (i.e. $R = r \cdot \sigma_x$) (Richman and Moorman, 2000).

$$\mathrm{SampEn}(m, r, N) = -\ln\left(\frac{N-m+1}{N-m-1}\cdot\frac{A}{B}\right), \tag{4.15}$$

where A and B denote the number of templates of lengths $m+1$ and m that matches for each different combination of i and j (given $i \neq j$), respectively. This estimator is unbiased due to the normalization. However, its variance decreases when the length of the signal increases.

4) Fuzzy entropy (FuzzyEn). FuzzyEn measures the time series irregularity

providing information about how a signal fluctuates with time. This information is obtained evaluating the conditional probability of two vectors that are similar for m points remain similar for the next $m+1$ points. Similarly to SampEn, higher FuzzyEn values indicate more irregular time series. However, in the case of FuzzyEn, the vectors similarity only depends on their shapes rather than their absolute coordinates, as it removes the baseline in the construction of m-dimensional vectors (Chen et al., 2007). Mathematically, FuzzyEn is defined as the negative natural logarithm of the deviation of the function ϕ when is calculated from a m-length sequence from this function when is calculated with a dimension $m+1$ (Chen et al., 2007):

$$\text{FuzzyEn}(m, r, N) = \ln \phi^m(n, r) - \ln \phi^{m+1}(n, r), \tag{4.16}$$

with ϕ^m defined as:

$$\phi^m(n, r) = \frac{1}{N-m} \sum_{i=1}^{N-m} \left(\frac{1}{N-m+1} \sum_{j=1, j\neq i}^{N-m} D_{ij}^m \right), \tag{4.17}$$

where D_{ij}^m is the similarity degree calculated through a fuzzy function as $D_{ij}^m = \exp[-(d_{ij})^n / r]$. d_{ij} is the distance between each two vectors of length m, computed as the maximum absolute difference of their corresponding scalar components.

5) **Auto-mutual information (AMI).** AMI estimates the regularity of the time series as the degree to which a time-delayed version of a signal can be predicted from the original one. Its values are normalized and higher values are associated with more predictable time series, thus more regular. The definition of AMI between one time series $x[n]$ and its time-delayed version $x[n+k]$ is (Fraser and Swinney, 1986):

$$AMI = \sum_{x[n], x[n+k]} P_{XX_k}[x[n], x[n+k]] \cdot \log_2 \frac{P_{XX_k}[x[n], x[n+k]]}{P_X[x[n]] \cdot P_{X_k}[x[n+k]]} \tag{4.18}$$

where $P_{X_k}[x[n]]$ is the probability density for the measurement $x[n]$, while $P_{XX_k}[x[n], x[n+k]]$ is the joint probability density for the measurements of $x[n]$ and $x[n+k]$. respectively. In the present Doctoral Thesis, we have estimated these probabilities from histograms.

4.3 Connectivity

The second level of analysis is focused on the study of the similarity or connectivity between pair-wise sensors. For this purpose, the behavior of two different types of coupling measures have been studied: functional connectivity metrics (Ruiz-Gómez et al., 2019b) and coupling metrics derived from nonlinear methods (Ruiz-Gómez et al., 2018b).

4.3.1 Functional connectivity metrics

Different functional coupling metrics have been used to estimate the connectivity between each pair of electrodes: magnitude squared coherence (MSCOH), imaginary part of coherence (iCOH), lagged coherence (lagCOH), amplitude envelope correlation (AEC), synchronization likelihood (SL), phase lag index (PLI), phase locking value (PLV), and corrected imaginary PLV (ciPLV). These metrics provide distinct and complementary information as a consequence of their inference processes. This fact led us to study their ability to capture real changes in synchronization and analyze how are they affected by the spurious effects of volume conduction in Ruiz-Gómez et al. (2019b).

1) **Magnitude squared coherence (MSCOH).** MSCOH is a widely used measure that estimates the similarities in the frequency content of two signals. It combines both amplitude and phase synchrony information extracted from the normalized cross-spectral density distributions. For two time series X and Y (obtained from two different EEG channels), it is defined as (Roach and Mathalon, 2008):

$$\mathrm{MSCOH}_{X,Y} = |\mathrm{COH}_{X,Y}|^2 = \frac{|S_{XY}|^2}{P_X P_Y}, \tag{4.19}$$

where $\mathrm{COH}_{X,Y}$ is the complex value of coherence between X and Y, S_{XY} is the cross-spectrum of X and Y, and P_X and P_Y are the power spectral density of X and Y respectively.

2) **Imaginary part of coherence (iCOH).** iCOH is the result of the projection of $\mathrm{COH}_{X,Y}$ into the imaginary axis. Its main advantage is that it excludes instantaneous interactions, which are known to be related to volume conduction effects (Nolte et al., 2004). Its mathematical formulation reads:

$$\mathrm{iCOH}_{X,Y} = \Im\{\mathrm{COH}_{X,Y}\}, \tag{4.20}$$

where $\Im\{\cdot\}$ represents the imaginary part.

3) **Lagged coherence (lagCOH).** lagCOH was proposed by Pascual-Marqui et al. (2011) to estimate connectivity between different brain regions removing the instantaneous contribution. This lagged component is minimally affected by volume conduction effects, thus containing almost pure physiological information. It is defined as (Pascual-Marqui et al., 2011):

$$\text{lagCOH}_{X,Y} = \frac{[\Im\{S_{X,Y}\}]^2}{S_X S_Y - \Re\{S_{XY}\}^2}, \tag{4.21}$$

where $\Re\{\cdot\}$ represents the real part.

4) **Amplitude envelope correlation (AEC).** AEC estimates the correlation of two times series based on their amplitudes. The procedure to compute the AEC consists in three steps and is performed for each EEG trial separately. Firstly, time series for each EEG channel are orthogonalized with the aim of reducing the source leakage and volume conduction effects (O'Neill et al., 2018). Then, their power envelopes are computed as the magnitude of the analytic signal using the Hilbert transform. Finally, AEC is calculated as the Pearson correlation between the *log*-transformed power envelopes (Brookes et al., 2014).

5) **Synchronization likelihood (SL).** SL is a measure of generalized synchronization that detects nonlinear and linear dependencies between two signals. Conceptually, the likelihood that if a system which is at the same state at two different times, another system will also be in the same state at these two times describes how strongly a channel is synchronized to all the other channels. The detailed procedure to compute SL can be found in Stam and Van Dijk (2002).

6) **Phase lag index (PLI).** PLI was also proposed by Stam et al. (2007) with the aim of overcoming the SL limitations. It quantifies the asymmetry of the phase difference distributions of two time series being insensitive to shared signals at zero phase lag. PLI ranges between 0 and 1, where a value of 0 indicates either no coupling or coupling with a phase difference centered around 0 module π, and a value of 1 indicates perfect phase locking at a value of phase difference different from 0 module π. Then, the stronger the nonzero phase locking is, the larger the PLI will be. The mathematical equation to

compute PLI reads as follows (Stam et al., 2007):

$$\mathrm{PLI}_{X,Y} = |\langle sign\sin(\Delta\phi_{X,Y})\rangle|, \tag{4.22}$$

where $\langle\cdot\rangle$ indicates the expectation operator and $\Delta\phi_{X,Y}$ is the phase difference or relative phase between signals X and Y.

7) **Phase locking value (PLV).** PLV is a time-dependent connectivity measure that looks for latencies at which the phase difference between the signals varies little across trials (Lachaux et al., 1999). For resting-state data, it is defined as (Mormann et al., 2000):

$$\mathrm{PLV}_{X,Y}(t) = \frac{1}{T}|\sum_{t=1}^{T} e^{-i(\phi_X(t)-\phi_Y(t))}|, \tag{4.23}$$

where T is the data length and ϕ is the instantaneous phase of the signals X and Y at time t.

8) **Corrected imaginary phase locking value (ciPLV).** ciPLV was proposed by Bruña et al. (2018) to remove the contribution of the zero phase differences of PLV. The correction procedure is similar to the one followed to obtain lagCOH. Thus, this measure is also insensitive to zero-lag effects. It is defined as (Bruña et al., 2018):

$$\mathrm{ciPLV}_{X,Y}(t) = \frac{\frac{1}{T}\Im\{e^{-i(\phi_X(t)-\phi_Y(t))}\}}{\sqrt{1-(\frac{1}{T}\Re\{e^{-i(\phi_X(t)-\phi_Y(t))}\})^2}} \tag{4.24}$$

4.3.2 Coupling metrics derived from nonlinear methods

The application of nonlinear methods to two time series rather than an individual signal led to obtain coupling metrics, such as those used in this compendium: Cross-Approximate entropy (Cross-ApEn) and Cross-Sample entropy (Cross-SampEn). No previous study has analyzed the spontaneous EEG activity by means of entropy-based metrics, except our preliminary study (Gómez et al., 2016). This fact led us to study the ability of these metrics to characterize the abnormal coupling patterns in AD and MCI, and to evaluate if they are useful to discriminate them from HC subjects in Ruiz-Gómez et al. (2018b).

1) **Cross-Approximate entropy (Cross-ApEn).** The Cross-ApEn algorithm is the application of Approximate entropy algorithm to two simulta-

neously recorded signals. Cross-ApEn quantifies the statistical dissimilarity between them by determining the frequency in which m-length patterns in the first time sequence are similar to reference m-length patterns in the second time sequence within a determinate tolerance r. Mathematically, Cross-ApEn between two normalized time series u and v is defined as (Pincus, 2000):

$$\text{Cross–ApEn}(m, r, N) = \phi^m(r)(v||u) - \phi^{m+1}(r)(v||u), \tag{4.25}$$

with

$$\phi^m(r)(v||u) = \frac{1}{N-m+1} \sum_{i=1}^{N-m+1} \ln \frac{N_i^m(r)}{N-m+1} \tag{4.26}$$

$$\phi^{m+1}(r)(v||u) = \frac{1}{N-m+1} \sum_{i=1}^{N-m+1} \ln \frac{N_i^{m+1}(r)}{N-m+1} \tag{4.27}$$

where $N_i^m(r)$ is the number of times of j so that the distance between m-length patterns $x_m(i)$ and $y_m(j)$, extracted from u and v respectively, is smaller or equal to r with $i \neq j$. Similarly, $N_i^{m+1}(r)$ is the number of times of j so that the distance between patterns $x_{m+1}(i)$ and $y_{m+1}(i)$ of $m+1$ consecutive points, extracted from u and v respectively, is smaller or equal to r with $i \neq j$.

The values of Cross-ApEn could be non-defined, if the were no similar patterns between the two sequences within the selected tolerance. This limitation led to propose different correction strategies that assign non-zero values in absence of matches: *bias 0* and *bias max* (Richman and Moorman, 2000).

2) Cross-Sample entropy (Cross-SampEn). Cross-SampEn was proposed to overcome these drawbacks and is always defined and remains consistent for conditions where Cross-ApEn does not. Its algorithm is the extension of SampEn for to two time series, rather than an individual signal. The Cross-SampEn between two normalized time series u and v is (Richman and Moorman, 2000):

$$\text{Cross–SampEn}(m, r, N) = -\ln \left[\frac{A^m(r)(v||u)}{B^m(r)(v||u)} \right], \tag{4.28}$$

with

$$A^m(r)(v||u) = \frac{1}{N-m} \sum_{i=1}^{N-m} \ln \frac{a_i^m(r)}{N-m} \tag{4.29}$$

$$B^m(r)(v||u) = \frac{1}{N-m} \sum_{i=1}^{N-m} \ln \frac{b_i^m(r)}{N-m} \tag{4.30}$$

where $a_i^m(r)$ and $b_i^m(r)$ are the number of times of j so that the distance between patterns of $m+1$ consecutive points $x_{m+1}(i)$ and $y_{m+1}(i)$ and between m-length patterns $x_m(i)$ and $y_m(j)$ is smaller or equal to r with $i \neq j$, respectively. Analogously, $x_{m+1}(i)$ and $x_m(i)$ are extracted from u, whereas $y_{m+1}(i)$ and $y_{m+1}(i)$ are extracted from v.

4.4 Network organization

After the computation of each connectivity metric between all the pair-wise electrode combinations, adjacency matrices can be obtained. These matrices contain the values of the graph connection weight between the nodes i and j, represented as w_{ij}. In the case of using functional connectivity metrics to estimate the coupling, weights are ranged between 0 and 1, where 0 implies an absence of synchronization and 1 is obtained for two completely synchronized signals. Note that we used the full weighted connectivity matrix for the calculation of the graph parameters, since applying an arbitrary threshold to the connectivity matrix could introduce a bias.

4.4.1 Graph parameters

A large variety of graph measures have been proposed to study how the brain network could work, but they are strongly correlated (Rubinov and Sporns, 2010).

In this Doctoral Thesis, we have used three complementary graph measures that are sufficiently representative and intuitive of the properties of the network, with a low computational cost. Specifically, we have studied the connectivity strength, the network integration, and the network segregation.

1) **Global strength (s).** s is the most commonly used measure of density and represents the total 'wiring cost' of the network. It was computed as the mean average of the link weights:

$$\mathrm{s} = \frac{1}{N} \sum_{i \in N} s_i = \frac{1}{N} \sum_{i \in N} \sum_{j \in N} w_{ij}, \tag{4.31}$$

where w_{ij} is the connection weight between nodes i and j and N is the total number of nodes.

2) **Characteristic path length (L).** L is the most commonly used measure of functional integration. The information can be easily transferred across a highly integrated network, whereas a low integrated network presents more difficulties to combine specialized information from the different regions. Anatomically, these sequences of nodes and links that can be seen as potential routes of information flow paths between different brain regions. Specifically, L is defined as the average shortest path length between all pairs of nodes in the network (Rubinov and Sporns, 2010):

$$\mathrm{L} = \frac{1}{N} \sum_{i \in N} \frac{\sum_{j \in N, j \neq i} l_{ij}}{N-1}, \tag{4.32}$$

where l_{ij} is the shortest path length (distance) between nodes i and j.

3) **Clustering coefficient (C).** C is a simple segregation metric based on the number of triangles in the network. Network segregation quantifies the presence of brain information processing hubs, formed by densely interconnected brain regions. Mathematically, C represents the fraction of a node's neighbors that are also neighbors of each other and reflects the prevalence of clustered connectivity around individual nodes (Rubinov and Sporns, 2010):

$$\mathrm{C} = \frac{1}{N} \sum_{i \in N} \frac{2t_i}{s_i(s_i - 1)}, \tag{4.33}$$

where t_i is the geometric mean of triangles around node i and s_i is the strength of a node i.

Since connectivity results are frequency dependent, one value for every network parameter was obtained for each of the conventional EEG frequency bands.

4.4.2 Multiplex networks

Multiplex network theory has been applied in different real-world multiplex networks, such as social systems (Battiston et al., 2014) and interconnected hyperlink networks (De Domenico et al., 2016). In the case of EEG-based multiplex networks, each layer contains the information of frequency-specific networks (typically: delta, theta, alpha, beta-1, beta-2, and gamma). These layers are interconnected by inter-layer links, which connect the same set of electrodes across layers. Nevertheless, these link weights are often not available and different methods have been used to build the multiplex networks: from a simple parameter sum across

all frequency-specific layers to more complex approaches (Battiston et al., 2014; Boccaletti et al., 2014; Yu et al., 2017), such as using a quality function to determine the value of the link weights across the different layers (Kabbara et al., 2018). However, these methods present some limitations. Firstly, the estimation of multiplex parameters and the comparison between multiplex networks could be biased if the link weights are different across studies (Stam, 2014). Secondly, these approaches could compensate opposite trends between groups for the analyzed frequency bands and blur the differences between groups.

In Ruiz-Gómez et al. (2021), we propose to use the basis vectors obtained with canonical correlation analysis (CCA) to obtain multiplex network parameters reducing the frequency band dimensionality.

In order to compute CCA, two datasets of multidimensional variables are need. In our case, electrode and source-level network parameters in every frequency band formed these datasets. Mathematically, $X, Y \in \Re^{B \times N}$ where N is the number of observations and $B = 6$ corresponds to the six conventional EEG frequency bands. Once CCA was applied, the basis vectors $w, v \in \Re^{B \times 1}$ were obtained using only the subjects of a reference group. Finally, we computed the novel CCA multiplex parameters for the rest of the groups as the projection of their results onto these hyperplanes, which is equivalent to compute the linear combination of the frequency-dependent results multiplied by the basis vectors.

In terms of notation, our new CCA multiplex parameters are defined as $\mathrm{s_{CCA}}$, $\mathrm{L_{CCA}}$, and $\mathrm{C_{CCA}}$, corresponding to those obtained from the classical measures in each frequency band s, L, and C, respectively.

Mathematically, they are defined as:

$$\mathrm{s_{CCA}} = \sum_{b=1}^{B} \mathrm{s}_b \cdot v_b, \tag{4.34}$$

$$\mathrm{L_{CCA}} = \sum_{b=1}^{B} \mathrm{L}_b \cdot v_b, \tag{4.35}$$

$$\mathrm{C_{CCA}} = \sum_{b=1}^{B} \mathrm{C}_b \cdot v_b, \tag{4.36}$$

where s_b, L_b, and C_b are the values of s, L and C in the b-th frequency band, and v_b is the b-th value of the basis vectors obtained with CCA using only the subjects of the reference group.

4.5 Statistical analyses

In order to characterize the brain changes provoked by the neurodegenerative processes in the different stages of AD continuum, different statistical hypothesis tests were used. Before their application, data normality and homoscedasticity were assessed using the Shapiro-Wilk test and the Levene's test, respectively. As our data did not meet the normality and homoscedasticity assumptions, statistical differences were evaluated with non-parametric tests.

4.5.1 Hypothesis testing

Hypothesis testing is a statistical method that used experimental data to make quantitative decisions. Statistical tests evaluate whether there is enough evidence to reject the null hypothesis H_0. The returned p-value indicates the probability of obtaining a value as extreme or more extreme than the values obtained from the H_0 distribution, assuming that H_0 is true. The typical level of significance (α) to reject H_0 is usually set to 0.05. Thus, if p-value $< \alpha$, it is considered that there are statistically significant differences in the data (Narsky and Porter, 2013).

As the studies included in this compendium of publications were focused on comparing different groups of the AD continuum, our data were independent. Therefore, statistical differences between two severity groups were evaluated with the Mann-Whitney U-test, whereas the Kruskal-Wallis test was used for comparison between three or more groups.

4.5.2 Multiple testing correction

When a high number N of independent test are applied (e.g. when comparing the connectivity values for each pairwise electrodes of different severity groups), the probability of obtaining a false positive (type I error) by chance drastically increases to $1-(1-\alpha)^N$. This fact is known as *multiple comparisons problem*, and requires to establish a stricter α value or to adjust the p-values to compensate the inferences being made (Narsky and Porter, 2013).

The family-wise error rate (FWER) controlling procedures (e.g., Bonferroni, Šidák, Holm-Bonferroni) correct the probability of making at least one type I error by chance. On the other hand, the false discovery rate (FDR) controlling procedures (e.g., Benjamini-Hochberg, Benjamini-Yekutieli, Storey q-values) are designed to control the expected proportion of proportion of type I errors among the tests that have already been considered significant (Farcomeni, 2008). In this

Doctoral Thesis, the procedure of Benjamini-Hochberg was applied to correct the obtained p-values (Benjamini and Hochberg, 1995).

4.6 Classification analyses

In order to evaluate the diagnostic ability of the proposed methods, a feature classification step is needed. However, the characterization of the EEG may lead to the extraction of several features that provide similar information about the brain dynamics in the different stages of AD and MCI. Consequently, a feature selection stage was also included in our studies with the aim of removing redundant features.

4.6.1 Feature selection

Two different methods were used to derive an optimal set of features: stepwise multilinear regression with a conditional forward selection and fast correlation based filter (FCBF).

1) **Stepwise multilinear regression.** It is an iterative process that starts adding to the optimal set of variables those that meet a set significance criterion step-by-step (Guyon and Elisseeff, 2003). There are three types of stepwise regression: backward elimination, forward selection, and bidirectional elimination.

   Particularly, we used the backward elimination method in Ruiz-Gómez et al. (2019b). This procedure is an iterative process through which we start with all input variables and eliminate those that do not meet a set significance criterion step-by-step:

   (a) Firstly, we set an arbitrary significance level (alpha). Common values are in the range 0.05 and 0.25, depending in how restrictive it is to include variables in the model.

   (b) Secondly, we perform multiple linear regression with all the features and obtain the coefficients for each variable.

   (c) Thirdly, we find the feature with the highest p-value.

   (d) Finally, we check if p-value $>$ alpha. If yes, we remove the variable and proceed back to the second step; if no, we have reached the end of backward elimination.

2) Fast correlation based filter (FCBF). It is based on symmetrical uncertainty (SU) to remove the less relevant features that share more information with the other ones than with the group-membership variable (Yu and Liu, 2004). Particularly, this method consists of two steps: relevance analysis and redundancy analysis.

(a) In the first step, the relevance of the features is evaluated computing the SU between each feature X_i and the group membership Y:

$$SU(X_i, Y) = 2\left[\frac{H(X_i) - H(X_i|Y)}{H(X_i) + H(Y)}\right], \quad i = 1, 2, ..., I \quad (4.37)$$

where $H(\cdot)$ is the well-known Shannon's entropy, $H(X_i|Y)$ is the Shannon's entropy of X_i conditioned on Y, and I is the total number of features. SU values are normalized between 0 and 1. A value of SU = 1 indicates that it is possible to completely predict one feature when knowing other one. On the other hand, a value of SU = 0 indicates that the two variables are independent. Then, a ranking of features is done based on their relevance since the higher the value of SU is, the more relevant the feature is.

(b) The second step is focused on discarding redundant features that share more information with other features than with the target group. This redundant analysis is performed evaluating the SU values between each pair of features $SU(X_i, X_j)$, sequentially estimated beginning from the first-ranked ones. If X_i shares more information with X_j than with the corresponding group Y, $SU(X_i, X_j) \geq SU(X_i, Y)$ (with X_i being more highly ranked than X_j), the feature j is discarded due to redundancy and it is not considered in subsequent comparisons. The optimal features are those not discarded when the algorithm ends.

In the present Doctoral Thesis, FCBF was used to derive the optimal sets of non-redundant features in Ruiz-Gómez et al. (2018a) and in Ruiz-Gómez et al. (2018b).

4.6.2 Feature classification

The described diagnosis problem corresponds to a pattern classification task, which concerns the automated recognition of regularities in data (Bishop, 2006). Differ-

ent machine learning techniques have been proposed to tackle these classification tasks, but only supervised learning techniques are in the scope of the present Doctoral Thesis. These methods employ a discriminant function inferred from training examples to classify new test examples into different classes. Bayesian decision theory is used to establish the rule to make such a decision to minimize the probability of misclassification. Among the different supervised learning techniques, linear discriminant analysis (LDA), quadratic discriminant analysis (QDA), support vector machines (SVM), decision trees (DT), and multi-layer perceptron artificial (MLP) neural networks were used in this Doctoral Thesis. Particularly, LDA was used in the first three publications (Ruiz-Gómez et al., 2018a,b, 2019b), QDA was applied in both Ruiz-Gómez et al. (2018a) and Ruiz-Gómez et al. (2018b), SVM and DT were used in the second study (Ruiz-Gómez et al., 2018b), and MLP was only applied in Ruiz-Gómez et al. (2018a).

1) **Linear discriminant analysis (LDA).** LDA is a method that finds a linear combination of features which defines a hyperplane that separates two or more classes. The data is projected to a lower dimension as $y(\boldsymbol{X}) = \boldsymbol{w}^T \boldsymbol{X}$, where $\boldsymbol{X} \in \mathbb{R}^{n,m}$, n is the number of features, m represents the observations, and $\boldsymbol{w}$ is the weight vector (Bishop, 2006). These projection will try to maximize the distance of the mean of both classes, and simultaneously minimize the variance of each class, without making any assumption about the distribution of the data.

   For a multi-class classification problem like the one that concerns us (AD, MCI and HC), the decision rule is based on finding the class, among the different k classes, which maximizes the discriminant function assuming that the conditional density function of each class follows a multivariate normal distribution with identical covariance matrices for all classes (Friedman, 1989):

$$\hat{C}(x) = \underset{k}{\operatorname{argmax}}\, \delta_k(x), \tag{4.38}$$

   with

$$\delta_k(x) = \mu_k^T \Sigma^{-1} x - \frac{1}{2} \mu_k^T \Sigma^{-1} x \mu_k + \log(\pi_k) \tag{4.39}$$

   where μ_k is the mean vector for class k, Σ is the covariance matrix (the same for all classes), and π_k is the prior probability, computed as the initial proportion of vectors that belongs to class k.

2) **Quadratic discriminant analysis (QDA).** QDA is a variant of LDA in which an individual covariance matrix is estimated for every class of observa-

tions. QDA is particularly useful if there is prior knowledge that individual classes exhibit distinct covariances. In order to predict the classes of new data, the QDA models find the class with the smallest misclassification by establishing a quadratic decision boundary between classes in the feature space, instead the linear decision threshold of LDA (Bishop, 2006). Hence, the classification rule is based on finding the class, among the different k classes, which maximizes the quadratic discriminant function:

$$\hat{C}(x) = \underset{k}{\operatorname{argmax}}\, \delta_k(x), \tag{4.40}$$

with

$$\delta_k(x) = -\frac{1}{2}\log(|\Sigma_k|) - \frac{1}{2}(x-\mu_k)^T\Sigma_k^{-1}(x-\mu_k) + \log(\pi_k) \tag{4.41}$$

where μ_k is the mean vector for class k, Σ_K is the covariance matrix for class k, $|\cdot|$ is the determinant of matrix, and π_k is the prior probability of class k.

QDA tends to fit the data better than LDA, but it has more parameters to estimate, as the covariance matrix should be estimated for every class separately (Bishop, 2006). If there are many classes and not so many sample points, this can be a problem.

3) Support vector machines (SVM). SVM is a binary classifier that determines the optimal hyperplane boundary in a transformed high-dimensional to maximize separation. The weight vector w is obtained by solving an optimization problem based on Lagrange multipliers η^n, expressed as follows (Vapnik, 1999):

$$w = \sum_{n\in S} \eta^n t^n \varphi(x^n), \tag{4.42}$$

where t^n is the target or desired output and $\varphi(\cdot)$ maps training vectors into the higher dimensional space. The output of the SVM classifier is expressed in terms of these support vectors as follows (Vapnik, 1999):

$$y = \sum_{n\in S} \eta^n t^n K(x^n, x) + w_0, \tag{4.43}$$

where S is a subset of the indices $\{1, ..., N\}$ corresponding to the support vector and $K(\cdot,\cdot)$ represents the inner product kernel function in the transformed space. Particularly, in Ruiz-Gómez et al. (2018b), a polynomial ker-

nel is used. This kernel represents the similarity of vectors in a feature space over polynomials of the original variables, allowing learning of non-linear models (Goldberg and Elhadad, 2008).

4) **Decision trees (DT).** DT algorithms are non-parametric methods which rely on a recursive binary partitioning of the input space to make predictions on data (Bishop, 2006). Each of these divisions is made according to one single variable. However, specific strategies to grow the tree and to stop adding nodes to the tree are needed. In this regard, objective criteria such as the *Gini* index and pruning process are used to determine the optimal tree for each particular classification problem (Bishop, 2006). Once the tree is built, for any new input, the region it falls into is determined by starting at the top of the tree (root node) and following a path down to a specific leaf node according to the decision criteria at each node (Bishop, 2006).

5) **Multi-layer perceptron (MLP).** MLP is an artificial neural network inspired by the functioning of the human brain. It maps an input vector onto a set of output variables using a nonlinear function controlled by a vector of adjustable parameters. The architecture of a MLP network consists of three or more interconnected layers (input layer, hidden layers, and output layer), which are composed of simple neuron units known as *perceptrons* (Bishop, 2006). Each unit is characterized by an activation function $g()$ and the connections between them are associated with adaptive weights (w_{ij}).

In a multi-class classification task, the same number of output neurons and classes is needed. For each output neuron, the trained MLP model provides the posterior probability of belonging to each class. In the case of a single hidden layer, a configuration known to be capable of providing a universal function approximation (Hornik, 1991), y_i can be expressed as:

$$y_i(\mathbf{x}, \mathbf{w}) = \sum_{k=1}^{N_H} \left[w_{ij}\, g \left(\sum_{j=1}^{J} (w_{jk} x_j + b_k) \right) + b_i \right] \tag{4.44}$$

where $\mathbf{w}$ is a vector with all the adaptive paramenters (weights and bias), w_{ij} is the weight connecting hidden units with the output unit i, b_i is the bias associated with the output unit i, w_{jk} is the weight connecting the input unit j with the hidden unit k, and b_k is its associated bias. The number of neurons in the hidden layer, N_H, is a design parameter that should be optimized. The number of units in the input layer, J, is usually the number

features used to fed it.

With the aim of finding appropriate weights to connect neurons each other, MLP utilizes backpropagation in conjunction with an optimization method, such as gradient descent. Backpropagation is based on the definition of a suitable error function, which is minimized by updating the weights in the network, and gradient descent is used to minimize overfitting and achieve good generalization (Bishop, 2006).

4.6.3 Diagnostic ability statistics

The diagnostic ability of a test model can be expressed by several statistics. Their definitions rely on the number of subjects rightly and wrongly classified. In this compendium of publications, the following statistic were used (Flemons and Littner, 2003):

1) **Sensitivity (Se).** Proportion of patients that are correctly identified in binary classification tasks (i.e. the proportion of AD patients that are correctly identified by the test model) (Yershalmy, 1947).

2) **Specificity (Sp).** Proportion of subjects without the disease that are correctly identified in binary classification tasks (i.e. the proportion of HC that are correctly identified by the test model) (Yershalmy, 1947).

3) **Accuracy (Acc).** Proportion of overall subjects rightly classified. This definition is also valid for multiclass tasks.

4) **Predictive values.** Proportion of subjects rightly classified for a certain class, among all the subjects that the test model has assigned to that class. For binary classification tasks, positive and negative predictive values (PPV and NPV, respectively) are the most common (Heston, 2011).

5) **Cohen's kappa (τ).** Measure of agreement between predicted and observed classes, which does not consider the agreement that occurs by chance (Cohen, 1960). Its value ranges between -1 and 1, with $\tau = -1$ corresponding to total disagreement, $\tau = 0$ representing that the agreement is due to chance, and $\tau = 1$ meaning a perfect agreement between the observed and predicted classes (Cohen, 1960).

4.6.4 Model validation

Several methods have been used in order to evaluate the generalization capability of a model to an independent dataset. They are usually chosen according to the sample size and the degrees of freedom of each specific problem. Particularly, when the number of samples in the database is limited (small and medium-size number of samples), with no model free parameters to be adjusted, cross-validation (CV) was used. On the other hand, for the biggest databases, when some parameters need to be adjusted, a hold-out approach is usually used.

1) **Hold out.** In a hold out approach, the entire data sample is divided into a training set, for model fitting, and an independent test set, for estimating the model performance (Bishop, 2006; Witten et al., 2016). The main limitation of this validation procedure is that it implies excluding a significant amount of data from the model fitting process, which may derive in less generalizable models if the training set is not enough representative (Witten et al., 2016). Hence, hold out is only recommended for bigger databases. In our first two studies (Ruiz-Gómez et al., 2018a,b), our database was randomly divided into training and test sets. The training set was used to train the classification models and parameter fitting, while the test set was used to evaluate the discrimination ability of the models.

2) **Cross validation.** The CV algorithm split the database into equal partitions, called *folds*. Then, one of these folds is used sequentially for testing the model trained with the remainder dataset. In each iteration, a diagnostic ability statistic (e.g., accuracy) is obtained for each fold, as every fold has been used for testing exactly once. Therefore, the average of these statistics provides an adequate estimation of the generalization ability of the model (Witten et al., 2016). This technique is usually used keeping one sample for testing, resulting in a leave one subject out (LOO) CV procedure. This LOO CV procedure was followed in Ruiz-Gómez et al. (2019b) to evaluate the clinical performance of our proposal.

Chapter 5

Results

This chapter summarizes the most relevant results obtained during the development of the present Doctoral Thesis. They have been organized according to the hypotheses described in section 2.1, which have a direct relation with the papers included in the compendium of publications (see appendix A).

5.1 Automated multiclass classification of MCI and AD

The automatic discrimination between AD patients, MCI patients, and HC subjects was assessed using a methodology based on resting-state EEG and several spectral and nonlinear features (Ruiz-Gómez et al., 2018a). In this study, the HURH database was randomly divided into training and test set. The training set was used to select the optimal value of the different input parameters of each feature, to derive the optimal set of features, and to train the classification models. Finally, the test set was only used to evaluate the diagnostic ability of these models.

Table 5.1 shows the grand-averaged results for each feature and each severity group. On one hand, our spectral results suggested that AD and MCI elicit a slowing of spontaneous EEG activity. Particularly, RP values were higher for AD patients in low frequency bands (θ) and lower in high frequency bands (β_1, β_2 and γ) compared to MCI patients and HC subjects. This increase of slow rhythms was also observed by means of MF and IAF, as they were lower for AD patients than for HC subjects. Regarding the nonlinear parameters, lower LZC, SampEn,

Table 5.1: Grand-average results (displayed as median [interquartile range]) for each feature and each severity group. The selected features that formed the FCBF optimal set are highlighted in bold.

	Feature	HC subjects	MCI patients	AD patients
Spectral	**RP(δ)**	**0.227 [0.179, 0.277]**	**0.164 [0.102, 0.221]**	**0.158 [0.103, 0.229]**
	RP(θ)	0.111 [0.083, 0.131]	0.122 [0.087, 0.155]	0.143 [0.103, 0.188]
	RP(α)	0.243 [0.174, 0.291]	0.317 [0.224, 0.544]	0.279 [0.192, 0.447]
	RP(β_1)	0.128 [0.101, 0.155]	0.101 [0.081, 0.160]	0.101 [0.073, 0.141]
	RP(β_2)	0.111 [0.084, 0.138]	0.105 [0.048, 0.135]	0.091 [0.060, 0.119]
	RP(γ)	0.097 [0.074, 0.168]	0.087 [0.037, 0.145]	0.089 [0.047, 0.141]
	MF	10.584 [9.690, 11.900]	10.467 [8.639, 12.285]	9.971 [9.030, 10.997]
	IAF	**9.502 [8.751, 9.996]**	**9.404 [8.519, 9.972]**	**8.811 [8.510, 9.474]**
	SE	0.813 [0.760, 0.822]	0.796 [0.695, 0.816]	0.782 [0.733, 0.809]
Nonlinear	LZC	0.684 [0.6331, 0.7360]	0.667 [0.551, 0.731]	0.663 [0.589, 0.713]
	CTM[1]	0.101 [0.076, 0.129]	0.111 [0.086, 0.165]	0.116 [0.077, 0.183]
	SampEn[1]	**1.366 [1.288, 1.540]**	**1.312 [1.103, 1.489]**	**1.274 [1.034, 1.489]**
	FuzzyEn[1]	0.532 [0.466, 0.624]	0.514 [0.395, 0.618]	0.508 [0.427, 0.584]
	AMI	-0.149 [-0.184,-0.130]	-0.149 [-0.175,-0.124]	-0.145 [-0.164,-0.128]

[1]These results were obtained using the optimal parameters for each feature: $r = 0.075$ for CTM; $m = 1$ and $r = 0.1 \cdot SD$ for SampEn; and $m = 1$, $r = 0.1 \cdot SD$, and $n = 3$ for FuzzyEn (SD: standard deviation).

FuzzyEn and higher AMI values for AD patients than for HC subjects were found. Additionally, CTM values were higher in AD patients and lower in HC subjects. For all metrics, MCI subjects showed intermediate values between AD and HC. These results suggest less complex and irregular EEG signals as the disease severity progresses.

Then, three different diagnostic models were trained taking into account only the optimal features derived from FCBF, which were two spectral measures (RP(δ) and IAF) and a nonlinear one (SampEn). The MLP hyperparameters were optimized following a cross-validation procedure, leaving all trials for each subject out in every iteration. The optimal values were 11 neurons in the hidden layer and a regularization parameter of 45 (Ruiz-Gómez et al., 2018a).

The diagnostic ability of the different models was evaluated using only the test set, and each subject was automatically allocated in a particular group by applying a trial-based majority vote procedure. The confusion matrices of each model are displayed in Table 5.2. From these matrices, the overall accuracy in the three-class classification task can be obtained. MLP showed the highest accuracy (62.75%), whereas QDA and LDA showed slightly lower values (60.78% and 58.82%, respectively). Other performance statistics can be also obtained, as those relative to the HC subjects vs. all comparison and AD patients vs. all comparison, summarized in Table 5.3. MLP also showed the highest diagnostic performance when

Table 5.2: Confusion matrices of each model using the test set: subjects' classification applying a trial-based majority vote procedure.

	LDA			QDA			MLP		
Actual/Estimated	**HC**	**MCI**	**AD**	**HC**	**MCI**	**AD**	**HC**	**MCI**	**AD**
HC	11	4	2	13	3	1	12	3	2
MCI	4	7	6	4	7	6	4	8	5
AD	2	3	12	3	3	11	2	3	12

Table 5.3: Diagnostic performance for HC vs. all and AD vs. all, derived from confusion matrices.

	HC vs. All			AD vs. All		
	LDA	**QDA**	**MLP**	**LDA**	**QDA**	**MLP**
Se (%)	82.35	79.41	82.35	70.59	64.71	70.59
Sp (%)	64.71	76.47	70.59	76.47	79.41	79.41
Acc (%)	76.47	78.43	78.43	74.51	74.51	76.47
PPV (%)	82.35	87.10	84.85	60.00	61.11	63.16
NPV (%)	64.71	65.00	66.67	83.87	81.82	84.38

determining whether a subject is not healthy (Sensitivity of 82.35% and Positive Predictive Value of 84.85% in the HC vs. all classification tasks). Furthermore, MLP also showed the highest diagnostic capability when determining whether a subject does not suffer from AD (Specificity of 79.41% and Negative Predictive Value of 84.38% in the AD vs. all comparison). LDA and QDA showed similar tendencies although reaching lower diagnostic performances than MLP.

Taken together, the differences in the spontaneous EEG activity of AD and MCI characterized by means of spectral and nonlinear features, and also their complementarity, have allow us to obtain different three-class models with a high diagnostic ability.

5.2 Coupling alterations using cross-entropy metrics in AD and MCI

The usefulness of two coupling metrics derived from non-linear methods for discriminating between AD and MCI patients from cognitively HC subjects was studied in Ruiz-Gómez et al. (2018b). Additionally, the most adequate metric for characterizing the EEG patterns in AD and MCI among the analyzed cross-entropy metrics (Cross-ApEn and Cross-SampEn) and its optimal parameter configuration were determined. Note that in this study, the training and test distribution was the same as in our previously study (Ruiz-Gómez et al., 2018a).

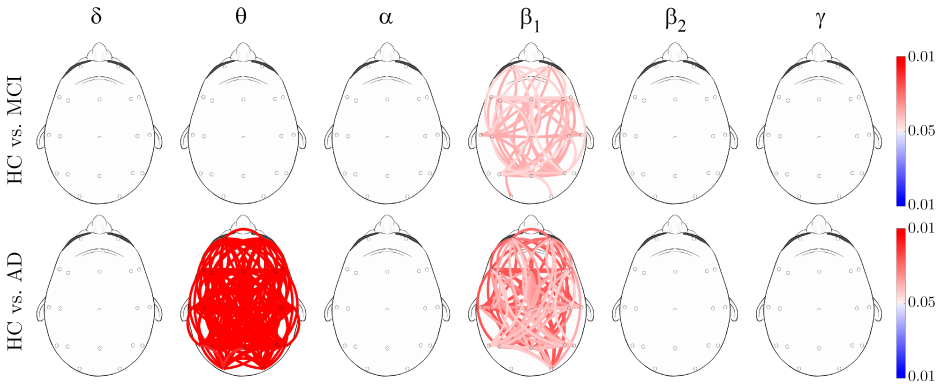

Figure 5.1: Cross-SampEn (m=1 and r=0.2) results for each classical EEG-frequency band. Connections between electrodes were only displayed when statistically significant within group differences were obtained (Mann-Whitney U-test, FDR-corrected p-values < 0.05). Red color tones indicate statistically significant connectivity increases in patients compared to controls, whereas blue color tones denote significant decreases. Figure adapted from Ruiz-Gómez et al. (2018b).

The optimal configuration for the metrics was selected evaluating all the typical combinations of m and r parameters as the configuration that exhibits the higher number of significant connections using only the training set. The total number of significant connections between the three groups (FDR-corrected p-values $<$ 0.05, Kruskal-Wallis test) for each parameters combinations was obtained. The combination of Cross-SampEn with m=1 and r=0.2 showed the largest number of significant connections. Then, the characterization of the coupling patterns for both comparisons was performed using this optimal parameter configuration and is depicted in figure 5.1. Our Cross-SampEn results showed that EEG activity in MCI patients is characterized by an overall similarity decrease in β_1 band, whereas AD patients present significant higher Cross-SampEn values in θ and β_1 frequency bands.

In order to evaluate the diagnostic ability of this metric, interpreting each connection between two electrodes in every frequency band as a feature, three different classifiers were trained: QDA, SVM, and DT. Before it, FCBF was applied for the binary classifications tasks to derive the two optimal sets (one for the HC vs. MCI comparisons, and the other for the and HC vs. AD comparison), which can be seen in Table 5.4. The diagnostic performances of the different models for both comparisons using the optimal FCBF sets of features can be seen in Table 5.5. Higher diagnostic results were found with SVM and DT (Acc = 73.53%) compared with QDA (Acc = 67.65%) for the case of the HC vs. MCI classification task.

Table 5.4: Optimal FCBF sets of features for HC vs. MCI and HC vs. AD comparisons. Each connection between two electrodes in every frequency band, estimated using Cross-SampEn with m=1 and r=0.2, was interpreted as a feature.

Comparison	Selected features			
HC vs. MCI	Fz-F4 in δ	Cz-C3 in θ	C4-Fp2 in α	P3-Fz in β_1
HC vs. AD	F7-Fp2 in δ	Fp1-C3 in θ	T3-T5 in θ	C3-Pz in γ

Table 5.5: Diagnostic performance for HC vs. MCI and HC vs. AD comparisons using the optimal FCBF sets of features. Each connection between two electrodes in every frequency band, estimated using Cross-SampEn with m=1 and r=0.2, was interpreted as a feature.

	HC vs. MCI			HC vs. AD		
	QDA	**SVM**	**DT**	**QDA**	**SVM**	**DT**
Se (%)	52.95	58.82	58.82	76.47	70.59	70.59
Sp (%)	82.35	88.24	88.24	76.47	94.12	94.12
Acc (%)	67.65	73.53	73.53	76.47	82.35	82.35
PPV (%)	75.00	83.33	83.33	76.47	92.31	92.31
NPV (%)	63.64	68.18	68.18	76.47	76.19	76.19

Also SVM and DT reached higher diagnostic performance for the HC vs. AD comparison (Acc = 82.35%) compared with QDA (Acc = 76.47%). Furthermore, both SVM and DT models present a good diagnostic capability for discriminating when a subject does not suffer AD (Sp = 94.12% and NPV = 76.19%) and MCI (Sp = 88.24% and NPV = 68.18%).

5.3 Modeling EEG volume conduction on functional connectivity metrics

Previous findings using functional connectivity metrics support the well-established hypothesis of AD as a 'disconnection syndrome' (D'Amelio and Rossini, 2012; Engels et al., 2015; Tóth et al., 2014), but all these results may be biased due to EEG volume conduction effects as these metrics could reflect spurious coupling values between independent brain sources. This hypothesis led us to create a synthetic model to evaluate how diverse functional connectivity measures are affected by volume conduction. Furthermore, we used the less affected metric to characterize the brain changes during the different stages of AD continuum (Ruiz-Gómez et al., 2019b).

Firstly, we generated a set of synthetic signals using the combination of the real-head surface-model built from information of the VHP dataset and a set of coupled

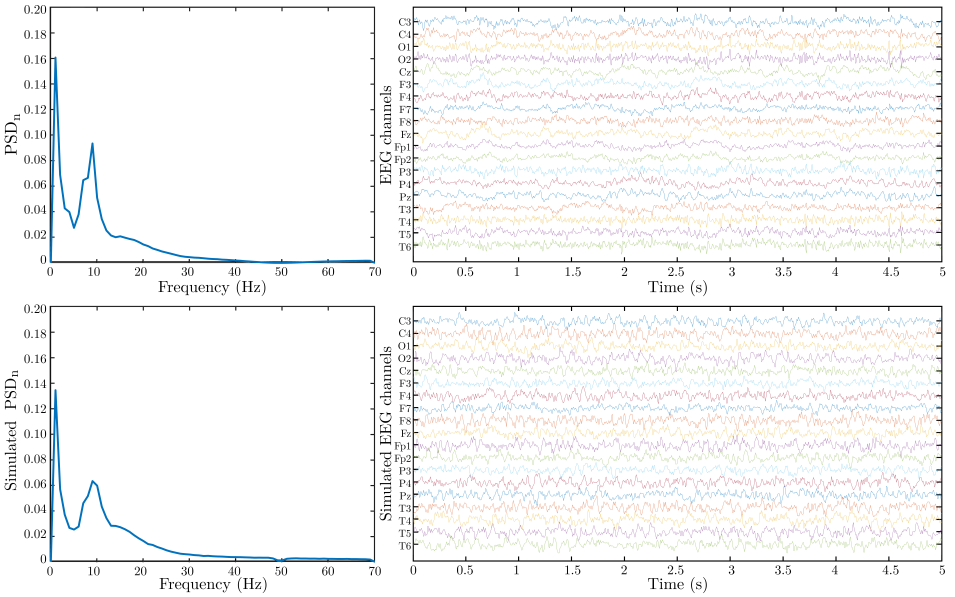

Figure 5.2: PSD_n function grand-averaged over all trials and channels (left panels), and two random 5 s EEG epochs from all EEG channels (right panels): (top) HC subject, and (bottom) synthetic signal obtained with the Kuramoto model in the simulated scenario with volume conduction. Figure from Ruiz-Gómez et al. (2019b).

oscillators forming a Kuramoto model. Then, we performed a qualitative analysis of the generated synthetic signals comparing them with the real EEG signals in both frequency and time domains. Figure 5.2 shows that the grand-averaged PSD_n across trials and channels for a real HC subject and the grand-averaged PSD_n across trials and simulated channels for a synthetic signal generated with the Kuramoto model are very similar. This similarity between real and synthetic signals is also supported by two randomly selected 5-s EEG epochs, as figure 5.2 also shows.

Then, with the aim of determining the coupling metric that is less affected by volume conduction, eight functional connectivity metrics were calculated from the time series generated with the Kuramoto model as a function of coupling strength K for both scenarios (with and without volume conduction). An ideal metric not affected by volume conduction is expected to show values close to 0 when oscillators are not coupled ($K < K_{crit}$) and then start to increase progressively as K grows. Furthermore, an ideal metric will obtain very similar curves for both simulated volume conduction scenarios, reflected by values of the two-sample Kolmogorov–Smirnov statistic (ks) close to 0. This behavior is showed in figure 5.3

(top-left graph).

Results obtained for the analyzed functional connectivity metrics are summarized in figure 5.3. These simulations showed that the analyzed metrics are sensitive to increases in the coupling strength for $K > K_{crit}$. For K values lower than K_{crit}, iCOH, lagCOH, AEC, PLI and ciPLV showed low values of connectivity in both simulated scenarios. However, MSCOH showed values over 0.2 in the volume conduction-free scenario and values around 0.35 under volume conduction conditions, when the expected values should be around 0 in both cases. For K higher than K_{crit}, all metrics reflected the coupling strength increases. MSCOH, SL, and PLV overestimated connectivity and were very affected by spurious influences of volume conduction, while PLI, AEC, and ciPLV were weakly influenced by the simulated volume conduction and underestimated the real coupling level. Quantitatively, the two-sample Kolmogorov-Smirnov test revealed that PLI was the metric least affected by the spurious influence of volume conduction ($ks = 0.12$), although none of the analyzed metrics are immune to it. For these reasons, the subsequent analysis with the real EEG recordings was performed using only PLI.

Finally, the EEG coupling patterns were obtained for each of the five groups of the AD-EEGWA database. The characterization of the different AD stages was assessed comparing HC subjects with each stage of dementia. Differences between groups obtained for each frequency band are presented in figure 5.4. After the FDR correction procedure, our PLI results showed that EEG activity in MCI subjects is characterized by statistically significant connectivity increases in the θ band when compared to HC subjects, especially for long-distance interhemispheric connections. PLI increases in θ band were also found for the comparison between HC subjects and $\mathrm{AD_{mil}}$. Furthermore, some connections in the β_2 band showed significant connectivity decreases for the HC subjects vs. $\mathrm{AD_{mil}}$ comparison. The aforementioned trend of coupling increases in the θ frequency band as the disease progresses continued, reaching its maximum number of significant differences for $\mathrm{AD_{mod}}$ patients compared with HC subjects. Additionally, our results revealed that $\mathrm{AD_{sev}}$ spontaneous EEG activity is characterized not only by widespread significant increases of PLI values in θ band, but also by an overall decrease of connectivity in α band. Finally, only a few connections showed statistically significant decreases in connectivity in β_2 band for the comparison between $\mathrm{AD_{sev}}$ patients and HC subjects.

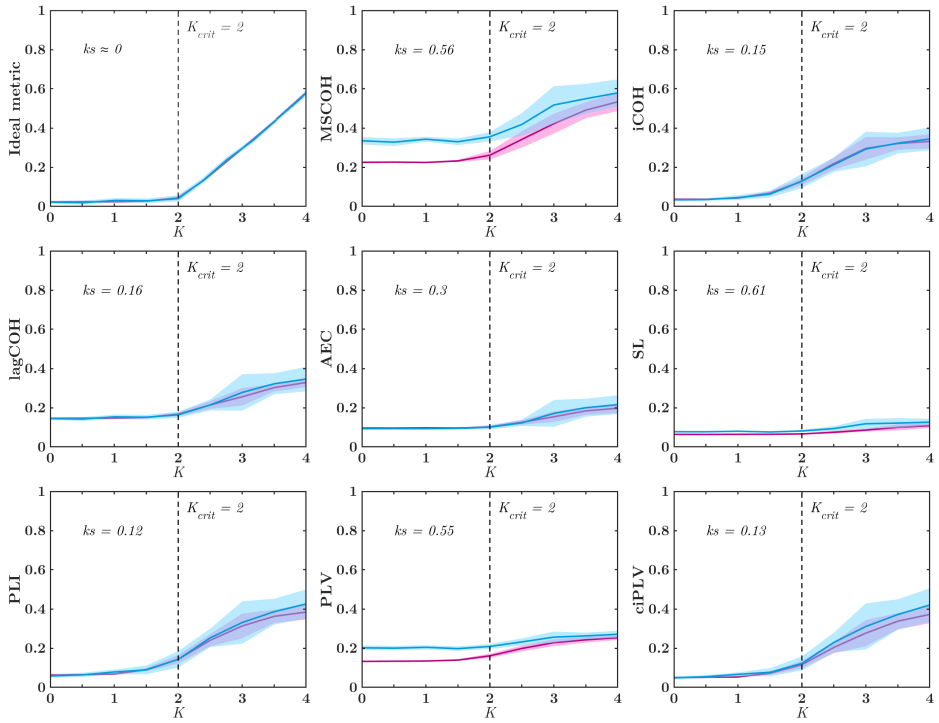

Figure 5.3: Expected graph for an ideal metric not affected by volume conduction effects. MSCOH, iCOH, lagCOH, AEC, SL, PLI, PLV, and ciPLV values as a function of global coupling intensity (K) for: ideal volume conduction-free (red), and real-case with volume conduction (blue) scenarios. The solid lines indicate the average values and the shaded areas represent the standard deviation of the 300 simulated epochs. Two-sample Kolmogorov-Smirnov test values (ks statistic) are specified for each metric. Figure adapted from Ruiz-Gómez et al. (2019b).

5.4 Novel method to build multiplex networks using CCA

In Ruiz-Gómez et al. (2021), we proposed a new multiplex approach that analyzes all frequency-dependent layers together capturing the relevant information of the whole brain network. This approach would facilitate the possible clinical interpretations about the alterations that AD neurodegeneration elicits from a global perspective of the brain. In order to construct the brain networks, adjacency matrices were computed using PLI. Our previous work using synthetic signals (Ruiz-Gómez et al., 2019b) demonstrated that PLI can detect real changes in synchronization and it was less affected by the volume conduction problem than

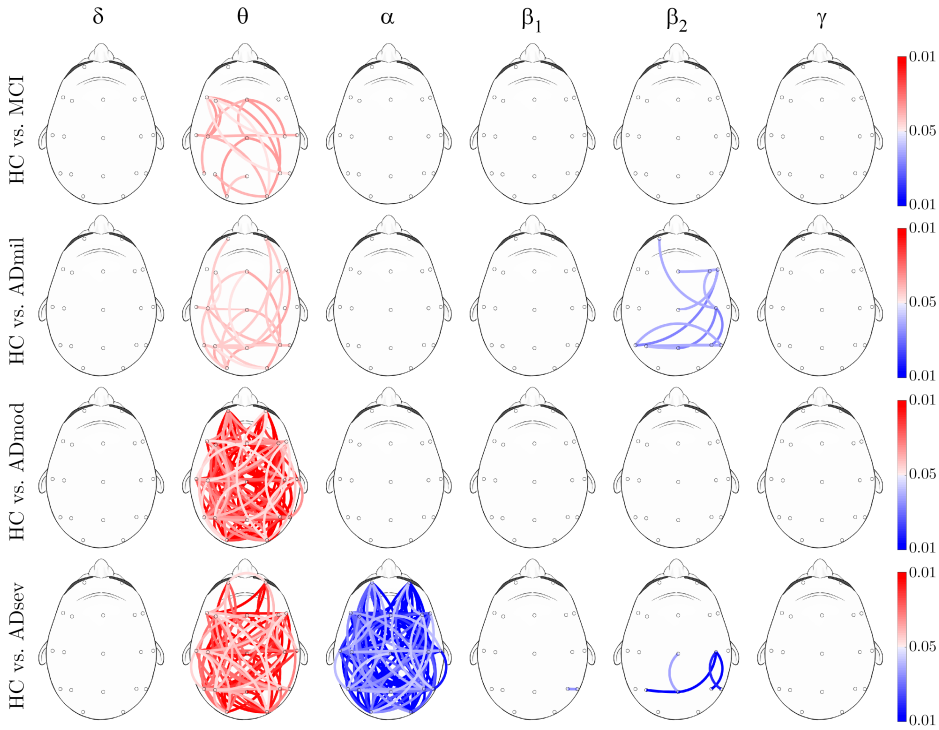

Figure 5.4: PLI results for each classical EEG-frequency band. Connections between electrodes were only displayed when statistically significant within group differences were obtained (Mann-Whitney U-test, FDR-corrected p-values < 0.05). Red color tones indicate statistically significant connectivity increases in patients compared to controls, whereas blue color tones denote significant decreases. Figure from (Ruiz-Gómez et al., 2019b).

the other analyzed measures.

The synthetic signals generated with the Kuramoto model were used to study the behavior of the new CCA multiplex parameters depending on the level of connectivity. It is divided into the following steps: (i) estimation of connectivity between pair-wise nodes at the electrode-level and source-level synthetic signals using PLI; (ii) computation of frequency-specific network parameters (s, L, and C); (iii) Computation of the multiplex model based on CCA: determination of the basis vector (v_b) that defines the reference hyperplane using the less connected signals ($K = 2$); and (iv) CCA projection: projection of the results onto these hyperplanes computing the linear combination of the frequency-dependent results multiplied by the reference basis vectors.

In the case of the real EEG recordings, the procedure is analogous to the one

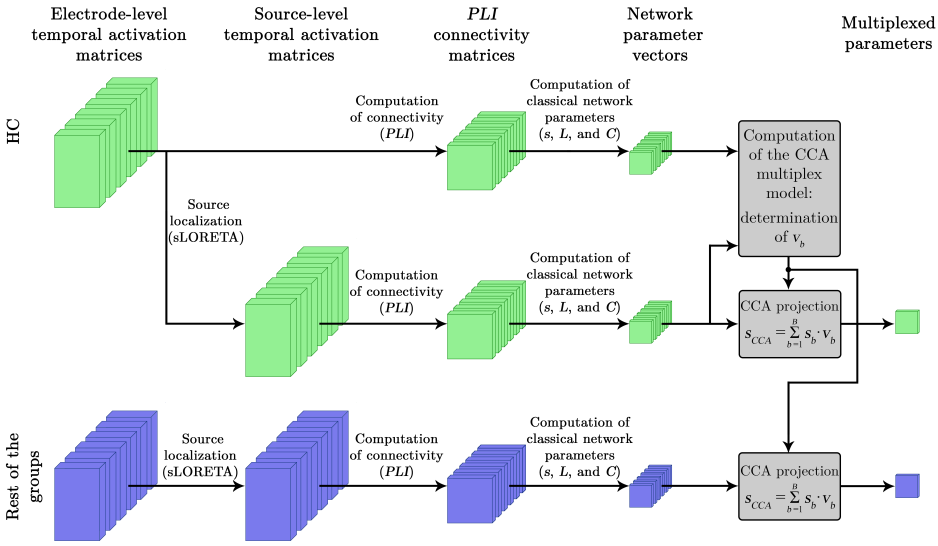

Figure 5.5: Block diagram of the used methodology with the real EEG signals. Figure adapted from Ruiz-Gómez et al. (2021).

described previously for the synthetic signals. However, a previous step is needed. In order to obtain the EEG signals in the source level, a reconstruction procedure from the real EEG recordings at the electrode level was used. The reconstruction method was standardized low resolution brain electromagnetic tomography (sLORETA), available in Brainstorm (http://neuroimage.usc.edu/brainstorm) (Tadel et al., 2011). sLORETA is based on a model of lineal distributed sources and provides a solution maximizing the correlation between neighboring sources, assuming that nearby neurons are synchronized (Pascual-Marqui, 2002). In addition, sLORETA reduces the errors on the estimated source activity applying some physiological restrictions. sLORETA provides high-dimensionality source-level signals, which were projected in 68 ROIs using the Desikan-Killiany atlas (Desikan et al., 2006). Furthermore, CCA hyperplanes were determined using the HC signals and then, the results from the rest of the groups were projected onto these hyperplanes. Figure 5.5 represents the followed procedure for the real EEG signals.

It is noteworthy that, in both cases, we only analyzed the source-level results. The main advantages of analyzing source-reconstructed networks are: (i) they are comparable regardless of the EEG recording system configuration if the same atlas is used (in this study, we used the Desikan-Killiany atlas); and (ii) source-level results will allow us to analyze and compare new groups that could have

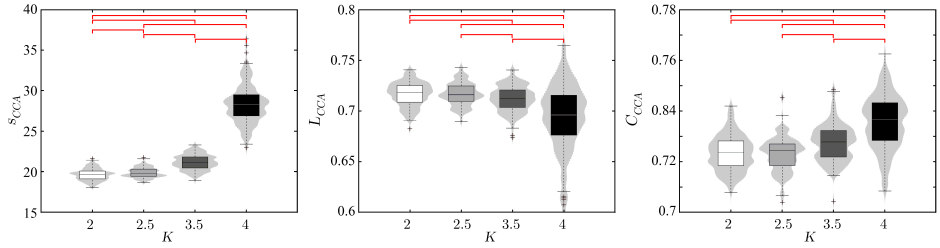

Figure 5.6: s_{CCA}, L_{CCA}, and C_{CCA} value distributions obtained using synthetic signals as a function of the Kuramoto model global coupling intensity (K). Statistically significant pairwise differences are marked with red brackets (p-values < 0.05, Mann-Whitney U-test). Figure from Ruiz-Gómez et al. (2021).

been recorded with different EEG configurations, or even using MEG, with the HC group used in this study.

The distributions for s_{CCA}, L_{CCA}, and C_{CCA} results using synthetic signals are shown in figure 5.6. s_{CCA} results revealed an increasing trend as connectivity increases, with larger differences between consecutive groups as the Kuramoto global coupling parameter (K) increases. In classical analysis, s becomes higher as connectivity increases and networks are more connected. L_{CCA} followed the opposite trend, as L_{CCA} results were smaller for higher values of global coupling. The expected behavior is to obtain lower values of L as connectivity increases, because it will lead to more integrated networks. C_{CCA} showed a growing trend as K increases. With higher connected nodes, more segregated networks will be obtained, resulting in higher values of C. As the proposed multiplex parameters followed a similar behavior compared with the classical network parameters, they can be interpreted in similar network terms: multiplex global average connectivity for s_{CCA}, multiplex network integration for L_{CCA}, and multiplex network segregation for C_{CCA}.

Figure 5.7 shows the distribution plots for s_{CCA}, L_{CCA}, and C_{CCA} obtained using the real EEG recordings from HC and the different AD severity groups. Firstly, s_{CCA} results showed higher values as the disease progresses, excluding the case of AD_{mil} that had the lowest connectivity values. In the particular case of the AD_{sev} group, these differences were statistically significant for all comparisons, making AD_{sev} differentiable from the rest of the groups. Significant differences were also found between AD_{mil} and AD_{mod} using s_{CCA}. Secondly, L_{CCA} showed a clear increasing trend as dementia severity increases. However, only the HC vs AD_{sev} comparison showed statistically significant differences. Finally, C_{CCA} revealed more segregated multiplex networks as the disease progresses. C_{CCA}

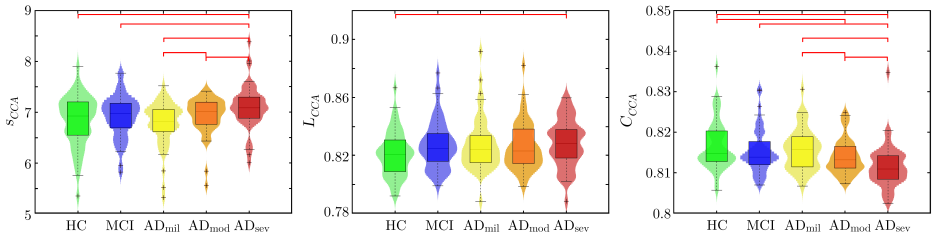

Figure 5.7: s_{CCA}, L_{CCA}, and C_{CCA} value distributions obtained using real EEG recordings from subjects at different stages of AD continuum: HC subjects, MCI patients, AD_{mil} patients, AD_{mod} patients, and AD_{sev} patients. Statistically significant pairwise differences are marked with red brackets (p-values < 0.05, Mann-Whitney U-test). Figure from Ruiz-Gómez et al. (2021).

results showed a decreasing trend from HC subjects to AD_{sev} patients. Similarly to s_{CCA}, the AD_{sev} patients could be discriminable from other groups. Additionally, the comparisons between HC subjects and AD_{mod}, and between AD_{mil} and AD_{mod} also showed statistically significant differences.

Chapter 6

Discussion

In the current Doctoral Thesis, the characterization of the neural changes in AD and MCI using local activation measures, neural coupling methods and network parameters derived from Complex Network Theory has been addressed. Firstly, further evidences for the progressive slowing and complexity loss of spontaneous EEG activity during AD continuum were found. These alterations lead us to propose a screening strategy of AD based on the results of a three-way classification MLP model. Secondly, abnormal coupling patterns in the early stages of dementia were found using novel nonlinear coupling metrics. Particularly, a widespread global decrease of similarity in all frequency bands was reported, with β as the frequency band where the early changes in prodromal stages of AD are highlighted. Thirdly, the possible bias in the connectivity estimation introduced by EEG volume conduction effects was evaluated using a surface-based computational model of the human head and a set of several coupled oscillators. Despite the fact that none of the functional connectivity metrics was immune to volume conduction, PLI was the metric less affected by its spurious effects. Our results using PLI revealed connectivity increases in low frequency bands and decreases in high frequency bands. Finally, a novel methodology to integrate all frequency-specific information in a multiplex framework based on CCA was proposed. Based on the results using synthetic signals, the CCA-based multiplex parameters can be analogous to their frequency-specific counterparts. Furthermore, our findings revealed decreases in integration and segregation as the disease progresses, increasing the multiplex networks vulnerability.

During this chapter, the aforementioned findings are further discussed following the same structure previously described in the hypotheses and results. At the end

of this chapter, the main limitations of this Doctoral Thesis are presented.

6.1 Local activation: towards a screening protocol of AD

The changes that AD neurodegenerative processes provokes in the EEG activity have been traditionally analyzed using simple signal processing methods, such as spectral techniques, and more complex ones, such as nonlinear analysis techniques. These metrics could provide complementary information useful to characterize the brain alterations during early stages of AD. They also could be effective features to fed an EEG-based methodology aimed at diagnosing MCI and AD (Ruiz-Gómez et al., 2018a).

One of the mayor effects that MCI and AD causes is the progressive slowing of the EEG spontaneous activity. Particularly, they are associated with an increase of power in low frequencies and a decrease in high frequency bands (Dauwels et al., 2010; Jeong, 2004). Our results using RP followed the same trend with higher values for AD patients in θ and lower values in β and γ bands, with MCI patients showing intermediate values. These progressive slow-down of the EEG was also observed by means of MF and IAF. The physiological explanations underlying the slowing of the EEG activity remain not clear after decades of research. However, the most extended hypothesis are based on the cerebral cholinergic deficit and the loss of neurotransmitter acetylcholine (Osipova et al., 2003). The loss of cholinergic innervation of the neocortex underlies different cognitive symptoms, such as memory loss, and might play a critical role in the slow-down of the EEG activity (Dauwels et al., 2010). Analogously, the cholinergic system modulates spontaneous cortical activity at low frequencies, hence the loss of neurotransmitter acetylcholine could produce the slowing of neural oscillations (Dauwels et al., 2010).

Concerning the nonlinear methods our findings suggest that the EEG activity seems to be less complex and more regular as the disease progresses. These findings are in line with previous studies that reported a loss of complexity and irregularity associated with early AD and MCI by means of nonlinear measures (Abásolo et al., 2006; Cao et al., 2015; Hornero et al., 2009; Jeong et al., 2001). The decrease of EEG complexity can be related with alterations in information processing at the cerebral cortex (Baraniuk et al., 2001). The loss of neurons or synapses between them could also explain the decrease of EEG complexity, since they are associated

with the complex dynamical processing within the brain neural networks (Baraniuk et al., 2001). Moreover, the hypothesis that states that is possible that the reduced complexity may be related with slowing EEG and its causes (Dauwels et al., 2011), as signals with higher low-frequency content are intrinsically more regular, may be discarded as it has been demonstrated that both metrics provide complementary information and reflect different aspects of the neural network.

Multiple studies have previously explored the use of several of these features to feed different classifiers with the aim of discriminating AD and MCI from HC subjects (Bertè et al., 2014; Buscema et al., 2015; Iqbal et al., 2005; Poza et al., 2017). However, they always were focused on binary discrimination problems. Only one study performed a three-way classification via binary classifiers (McBride et al., 2014). Although their discrimination results are slightly higher than ours (78.43% when comparing HC vs. all and 76.47% for AD vs. all in our study, and 85.42% and 83.33% in McBride's study, respectively), our proposal presented several advantages to consider it as a screening protocol. Beside the database limitations (we have 111 subjects in contrast to the 47 recruited in their study), we obtained a unique model consequence of the hold-out approach, easy to feed with new data, while they obtained a different model for each iteration in the LOO-CV procedure.

In addition to the three-class classification task, the proposed model based on MLP could also be used in binary assessments of healthy vs. cognitively impaired subjects. The model has shown the ability to detect whether a subject suffers from AD or MCI (correctly detecting 28 out of the 34 non-healthy subjects) only predicting 2 out of 17 AD patients as HC subjects. Additionally, it was also able to discard AD in 27 out of the 34 subjects not suffering from it (79.41% Sp), including 15 out of the 17 HC (88.24%). These results highlight the clinical usefulness of our proposal as an automatic tool to help in the early AD diagnosis, which might be expressed as a screening strategy depending on its predictions similar to:

1. If the model predicts AD, recommend beginning a treatment since most probably (89.47%, 17 out of 19 subjects) the patient suffers from AD or MCI.

2. If the model predicts HC, do not treat the patient, since most probably (88.89%, 16 out of 18 subjects) he/she does not suffer from AD; consider a regular evaluation of the subject in the persistence of symptoms in order to minimize the number of AD and MCI missed subjects.

3. If the model predicts MCI, conduct a regular evaluation of the patient since

doubts arise about the cognitive status of the subject.

6.2 Interaction between sensors: abnormal coupling patterns in AD

A full characterization of the brain dynamics is not possible using only spectral and non-lineal techniques. For this reason, connectivity approaches have become essential to gain further understanding of how the brain is organized as a functional network. Previous studies have found contradictory results depending on the database and the connectivity metric, although decreases in high frequency bands and increases in low frequency bands have been reported by many authors (Engels et al., 2015; Koenig et al., 2005; Tóth et al., 2014). In this Doctoral Thesis, two studies were carried out in this regard.

In the first one, two cross-entropy metrics, Cross-ApEn and Cross-SampEn, and their parameter configurations were compared to determine which of them yields a better characterization of the abnormal coupling patterns in AD and MCI (Ruiz-Gómez et al., 2018b). Lower values of run length m showed better performances for both metrics, suggesting that the fast nature of EEG fluctuations could be easier to capture with small length windows. On the other hand, too large values of m are inappropriate for detecting the dynamical changes in EEG recordings. Additionally, taking into account that Cross-SampEn revealed a high number of significant connections among the three groups for all parameters combinations and its technical advantages over Cross-ApEn, we could say that Cross-SampEn is more adequate to characterize the neural coupling patters in MCI and AD. This characterization suggests that EEG signals from different brain regions become gradually less similar as dementia progresses, with β band playing a key role in the early changes in prodromal stages of AD. Furthermore, these changes allowed us to discriminate when a subject does not suffer from AD and when a subject does not suffer from MCI with high classification values: specificities of 94.12% and 88.24%, and negative predictive values of 76.19% and 68.18%, respectively. These findings are in line with the well-known hypothesis of AD as a disconnection syndrome and could be associated with both alterations in information processing at the cerebral cortex and to the decreased levels of acetylcholine that disturb the synaptic transmission (Baraniuk et al., 2001; Jeong et al., 2001). Although several previous connectivity results support this hypothesis, they may be biased due to EEG volume conduction effects.

In the second study (Ruiz-Gómez et al., 2019b), a new model to build synthetic signals based on Kuramoto oscillators was proposed to study how different functional connectivity metrics are effected by volume conduction and to evaluate if they are able to detect real changes in synchronization. Furthermore, the brain alterations in the different stages of AD continuum were characterized using the metric less affected by the spurious influences of volume conduction, thus reducing the possible bias.

Our simulations using synthetic signals proved that the proposed modifications to existing functional metrics (i.e. iCOH, lagCOH, and ciPLV) and new proposed measures (i.e. AEC and PLI) were less affected by volume conduction compared to the original ones, as expected from theory (i.e. MSCOH, SL, and PLV). None of the analyzed metric was immune to volume conduction but these effects were smaller for PLI, making this metric the more suitable for increasing the insight into the underlying neural alterations in AD. Our results using PLI revealed coupling increases in low frequency bands, becoming more pronounced as dementia progresses. On the other hand, connectivity decreases were progressively found on high frequency bands, being statistically significant at the last stage of dementia in the α band. The loss of acetylcholine could support the decrease in high-frequency and the increase in low-frequency coupling, which led to the well-established 'cholinergic hypothesis of AD' (Bartus et al., 1982; Francis et al., 1999). Nevertheless, other hypothesis should be taken into account, such as structural brain changes (i.e., decreased hippocampal volume, atrophy of the medial, and neuronal loss) and a possible atrophic brain process that derives in global and regional gray matter density loss in AD patients (Cho et al., 2008; Karas et al., 2004). Therefore, this analysis using PLI to estimate the coupling between distant brain regions has allowed us to reduce the EEG volume conduction bias when building the brain network. As volume conduction effects are minimized, we can be sure that our findings represent true neuronal alterations.

6.3 Network organization: a novel methodology to build multiplex networks

Previous network organization studies reported contradictory results depending on the frequency band under analysis, and inconsistent results between them when studying the same frequency band. On one hand, significant clustering coefficient decreases were obtained in alpha band, while increases in theta were also reported

in the same study (Afshari and Jalili, 2017; Stam et al., 2009). On the other hand, some works found significant decreases for clustering in AD (Stam et al., 2009; Tijms et al., 2013) while other studies found increases as the disease progresses (He et al., 2008; Yao et al., 2010; Zhao et al., 2012). All these inconsistent results tangle the possible clinical interpretations and makes it difficult to extract conclusions about the changes in the global brain network provoked by the AD neurodegeneration process. Then, a multiplex approach that considers the information of all layers together could capture the relevant information of the whole brain network.

Despite the advantages over singles-layer methodologies, two common problems in multiplex network theory arises. Most of the proposed techniques require having the link values between homologous nodes of different layers to build the multiplex network, but these interlayer links are not usually available. Additionally, some of these methodologies tend to blur the differences between groups when opposite trends were reported depending on the frequency band under analysis. For example, clustering coefficient decreases in alpha but increases in theta bands are commonly reported in different AD characterization studies (Afshari and Jalili, 2017; Stam et al., 2009).

These concerns motivate us to propose and evaluate a novel methodology to build multiplex networks (Ruiz-Gómez et al., 2021). In particular, we used CCA to determine the coefficients that maximize the correlation between electrode-level and source-level results used to build the multiplex network. Furthermore, we studied how three different CCA multiplex parameters are affected by variations of connectivity using synthetic signals and evaluated if they are able to characterize the brain alterations during the different stages of AD continuum. The selected parameters (strength, characteristic path length, and clustering coefficient) were sufficiently representative and intuitive of the properties of the network and provide complementary information about how the brain network could work.

The distribution results for the proposed CCA-based multiplex parameters applied to the synthetic signals followed an analogous behavior compared with their classical network parameters, so they can be interpreted in similar network terms. Our findings applying the proposed methodology to the real EEG recordings indicated that dementia due to AD is characterized by a loss of 'small-world' properties as the disease progresses (revealed by decreases in integration and segregation), a trend that would would increase the network vulnerability. Clinically, this could reflect a progressive disruption in local information exchange between frequency bands (Cai et al., 2020). The increases in clustering coefficient could be a com-

pensatory mechanism that is triggered by the dysfunctional integration in the AD brain networks (Kabbara et al., 2018; Palesi et al., 2016).

Furthermore, this CCA-based methodology can be applied using different recording configurations for different groups or subjects, when the results at source-level are analyzed. Source reconstructed networks are comparable regardless of the EEG recording system configuration when the same atlas is used to reduce the signal dimensionality into ROIs. Then, the only possible bias that could be introduced into the observations is the one added during the source reconstruction process due to sLORETA limitations. Further studies in this line should be carried out, which could provide valuable insights into the brain network organization changes consequence of the neurodegenerative process.

6.4 Limitations of the study

Despite the fact that we have shown the utility of our proposals for characterizing the alterations in the neural dynamics during the different stages of the AD continuum, some limitations need to be addressed.

The first limitation is related to the sample size of the used databases. Although EEG studies aimed at characterizing AD alterations usually employ smaller databases, the sample size should be increased to enhance the generalization ability of our proposals as possible diagnostic tools.Despite that during the development of this Doctoral Thesis a new database that allowed us to study the AD continuum has been recorded, as it is stratified into five severity groups (controls, MCI subjects, mild AD patients, moderate AD patients, and severe AD patients), it would be very useful to also perform a longitudinal study, mainly focused on MCI subjects. This group is the most clinically interesting group, since two distinct subgroups of patients with MCI can be distinguished: those that remain stable at MCI condition and those that progress to AD. This research could provide deeper understanding on the complex neural changes during MCI and may allow to predict AD progression at an early stage.

Also associated with the characteristics of the databases, the second limitation is related to the number of electrodes. Particularly, graph analyses are more accurate using as many nodes as possible. To address this problem, we estimated the brain sources before the computation of the multiplex network parameters. In our case, we lose the spatial information as these parameters were averaged for all the ROIs. Studying the specific value for these parameters in each ROI could lead us to accurately identify brain areas with abnormal neural patters and gain

further insights on AD continuum neurodegeneration processes. However, source estimation is highly sensitive to small changes in the noisy data. In most cases, an ill-conditioned equation has to be solved and some methods add spatial weighting of the current estimations at the source positions. Hence, results obtained at the source-level must be carefully interpreted.

Even though our model that combines a realistic surface-based head model and a model of Kuramoto oscillators have demonstrated its utility to build synthetic signals, it simulated an isotropic electric propagation for all cerebral tissues. This approach has allowed us to evaluate the effect of EEG volume conduction in different measures of functional connectivity. However, some of the cerebral tissues, such as the white matter and the skull, present anisotropic conduction features that could influence connectivity results. This is an important issue to take into account for the construction of a more realistic brain model.

A final limitation concerns to the methods employed in the papers of this compendium of publications. Despite we have used a high variety of complementary parameters to characterize the spontaneous EEG activity in each of the described levels of analysis, there are other methods that could provide additional information about the alterations during the AD neurodegeneration, such as High Frequential Resolution Networks. These methods could lead us to identify the most plausible *in-silico* models that simulate the neurodegeneration mechanisms associated with AD progression.

Chapter 7

Conclusions

The studies included in this Doctoral Thesis are focused on applying different signal processing techniques with the aim of characterizing the brain alterations during the different stages of the AD continuum. These studies are intended to be a starting point to understand the underlying neural dynamics in AD and MCI, a crucial point for an early diagnosis and for adopting effective treatments.

The signal processing approaches were selected following three different levels of analysis: local activation patterns in individual sensors, analysis of interactions between sensors, and organization of brain networks. Based on local activation, we found that spectral and nonlinear features provide complementary information that allow us to characterize the previously reported brain abnormalities associated with AD and MCI: slowing of EEG rhythms, complexity loss, regularity increase, and variability decrease. These alterations have allowed us to build a model with high diagnostic ability, particularly for predicting AD and healthy status. Regarding the interaction between sensors, connectivity studies have proven to be useful to gain a deeper understanding on how different functional connectivity metrics are affected by the EEG volume conduction effects and how the complex neural substrates are altered as a consequence of the cognitive impairment preceding AD. Our results suggest connectivity increases in low frequency bands as the disease progresses, meanwhile connectivity decreases in high frequency bands when the severity increases. Starting from these connectivity results obtained using PLI, a new methodology to build multiplex networks was proposed. The interpretation of the obtained parameters can be analogous to their frequency-specific counterparts and they revealed that dementia due to AD altered progressively the small-world network properties, increasing multiplex networks vulnerability as a consequence

of the neurodegenerative processes.

In this chapter, the original contributions of the present Doctoral Thesis are described in section 7.1. Then, the main conclusions of these studies are indicated in section 7.2. Finally, the future research lines derived from this investigation are listed in section 7.3.

7.1 Contributions

The main contributions provided in the present Doctoral Thesis are listed below:

1) Development and evaluation of a three-way classification model (AD, MCI, and HC subjects) based on the complementary information provided by spectral measures and nonlinear methods, which can be used in a simplified clinical screening strategy for AD (Ruiz-Gómez et al., 2018a). Although a previous study performed a three-way classification methodology based on binary classifiers, this is the first time that a three-way classification model is developed.

2) Comparison of coupling metrics derived from nonlinear methods (Cross-ApEn and Cross-SampEn) for the analysis of spontaneous EEG activity in AD and MCI (Ruiz-Gómez et al., 2018b). To the best of our knowledge, only a few studies have applied Cross-ApEn and Cross-SampEn to biological systems, but they have never been used for the EEG characterization.

3) Development of a model to build synthetic EEG signals. This model is based on the combination of a surface-based computational model of the human head obtained from anatomical cryosection images, and a model of coupled oscillators that simulate the electrical activity of brain sources (Ruiz-Gómez et al., 2019b). Although a previous study simulated the brain source activity, they conclude that their model exaggerated the effects of volume conduction, as it was simulated in a quite simple way because modeling realistic sources was beyond the scope of their study.

4) Evaluation of the behavior of different functional connectivity metrics under the effect of simulated volume conduction (Ruiz-Gómez et al., 2019b). Applying a metric slightly affected by EEG volume conduction effects will lead us to findings that are mainly due to neuronal alterations and not because the spurious effects introduced by volume conduction.

5) Design, development and evaluation of a new methodology to build multiplex network parameters based on CCA (Ruiz-Gómez et al., 2021). Results obtained using the proposed method can summarize the available information across all frequency-dependent layers in one single value, making the global brain network easier to interpret from a clinical point of view.

7.2 Main conclusions

The analysis and discussion of the results of the studies included in this compendium of publications allow to draw the main conclusions of this Doctoral Thesis:

1) Resting state EEG provides valuable information about the abnormalities provoked by the AD neurodegenerative processes, which can be extracted using different signal processing techniques. The use of these methods leads an appropriate characterization and comprehension of the alterations that occur inside the brain during the different stages of the disease continuum.

2) The local changes in the EEG background activity are associated with the progression of AD, with MCI subjects showing intermediate values between HC subjects and AD patients. The typical alterations are a slowing of EEG rhythms (power spectrum shift from high-frequency components towards low-frequency components), a complexity loss, and a regularity increase.

3) Spectral and nonlinear features provide complementary information. This information is useful in the proposed three-way classification model, which can be used as a screening protocol for AD diagnosis.

4) The estimation of coupling between different brain regions is affected by the spurious effects of EEG volume conduction. Therefore, in order to achieve a correct interpretation of the results, it is important to employ coupling metrics that are able to detect real brain interactions minimizing the effect of volume conduction distortion.

5) The information exchange between distant brain areas produces a coordinated activation of neural assemblies, which is disrupted due to the neurodegenerative processes. Particularly, AD is characterized by a progressive reduction of functional connectivity in high frequency bands, and a increase in low frequency bands. These findings support the hypothesis of AD as a

disconnection syndrome. However, the coupling increases are thought to be caused by compensatory mechanisms in the brain.

6) The use of an objective procedure that can assign negative weights to build multiplex networks avoid to compensate the typical AD opposite trends in the different frequency bands. Particularly, the proposed methodology based on CCA leads us to obtain multiplex parameters that can be interpreted in an analogous way compared to their frequency-specific counterparts, facilitating their clinical interpretation.

7) AD multiplex network topologies tend to be less integrated and less segregated as the disease severity increases. Hence, AD is characterized by a loss of small-world network properties, increasing the global brain network vulnerability as a consequence of the neurodegenerative processes.

7.3 Future research lines

Several questions derived from this research may be studied in the future to complement the findings reported in this Doctoral Thesis. In this regard, the most interesting future research lines are discussed next.

Even if we had two large databases, larger databases are always desirable to improve the statistical power of the studies. In this regard, the study of longitudinal recordings following up the evolution of the MCI subjects for an specific period of time would be a crucial point to characterize different MCI subtypes, those with stable MCI and those who progress to AD. Moreover, including subjects affected by other forms of dementia could be also interesting, as it allow us to perform differential predictive diagnoses.

Concerning the employed signal processing techniques, different methods in each of the three levels of analysis were applied. Most of them can be applied to other electrophysiological signals, such as MEG or fMRI, and other pathologies. However, some improvements could be made by using other approaches:

1) In order to develop an automatic AD diagnostic tool, improving the classification ability of the discrimination models is needed. In this regard, the combination of data extracted from all of the three levels of analysis could provide additional and complementary information that could improve the diagnostic performances for the early AD detection. On the other hand, deep learning architectures could be able to deliver high-quality results, as

they extract new features that are the best for the specific classification task by themselves. However, bigger databases are needed to train and validate a deep learning methodology.

2) All the studies have been performed analyzing the signals in the electrode level. Increasing the number of electrodes of the EEG could lead to more accurate source level signals after the reconstruction procedure. Source analyses would be helpful for localizing the spatial source of electrical abnormalities, overcoming the volume conduction issue. Furthermore, graph analyses from high density EEG could lead us to accurately identify brain areas with abnormal neural patters, as they are more accurate using as many nodes as possible.

3) The assessment of effective connectivity metrics, which estimate the directionality of the relationships and the information flux, was out of the scope of this Thesis. However, they might also have a similar performances under volume conduction conditions compared to functional metrics and they could provide additional information about the brain alterations in AD and MCI.

4) All the network analyses have been made considering the well-known classical frequency bands. Although these bands have been useful to gain further insights into the underlying brain organization, other approaches could be an interesting future line of investigation. They overcome the limitations of predefined bands by increasing the frequency resolution of the analyses, the so-called High Frequential Resolution Networks.

Despite the findings described in the present Doctoral Thesis, further efforts must be addressed to gain further insights into the underlying brain dynamics in the different stages of AD continuum, focusing on the development of cognitive models that explain the brain alterations and the differences found during the different stages of AD continuum.

Appendix A

Papers included in this Doctoral Thesis

Automated Multiclass Classification of Spontaneous EEG Activity in Alzheimer's Disease and Mild Cognitive Impairment

Saúl J. Ruiz-Gómez[1], Carlos Gómez[1], Jesús Poza[1,2,3], Gonzalo C. Gutiérrez-Tobal[1], Miguel A. Tola-Arribas[4], Mónica Cano[5], Roberto Hornero[1,2,3]

[1] *Biomedical Engineering Group, E.T.S.I. Telecomunicación, University of Valladolid, Paseo de Belén 15, 47011, Valladolid, Spain*

[2] *Instituto de Investigación en Matemáticas (IMUVA), University of Valladolid, Paseo de Belén S/N, 47011, Valladolid, Spain*

[3] *Instituto de Neurociencias de Castilla y León (INCYL), University of Salamanca, Calle Pintor Fernando Gallego 1, 37007 Salamanca, Spain*

[4] *Servicio de Neurología, Hospital Universitario Río Hortega, Calle Dulzaina 2, 47012 Valladolid, Spain*

[5] *Servicio de Neurofisiología Clínica, Hospital Universitario Río Hortega, Calle Dulzaina 2, 47012 Valladolid, Spain*

Entropy
Volume 20, No. 35, January 2018, Pages 1–15

Abstract

The discrimination of early Alzheimer's disease (AD) and its prodromal form (i.e., mild cognitive impairment, MCI) from cognitively healthy control (HC) subjects is crucial since the treatment is more effective in the first stages of the dementia. The aim of our study is to evaluate the usefulness of a methodology based on electroencephalography (EEG) to detect AD and MCI. EEG rhythms were recorded from 37 AD patients, 37 MCI subjects and 37 HC subjects. Artifact-free trials were analyzed by means of several spectral and nonlinear features: relative power in the conventional frequency bands, median frequency, individual alpha frequency, spectral entropy, Lempel–Ziv complexity, central tendency measure, sample entropy, entropy, and auto-mutual information. Relevance and redundancy analyses were also conducted through the fast correlation-based filter (FCBF) to derive an optimal set of them. The selected features were used to train three different models aimed at classifying the trials: linear discriminant analysis (LDA), quadratic discriminant analysis (QDA) and multi-layer perceptron artificial neural network (MLP). Afterwards, each subject was automatically allocated in a particular group by applying a trial-based majority vote procedure. After feature extraction, the FCBF method selected the optimal set of features: individual alpha frequency, relative power at delta frequency band, and sample entropy. Using the aforementioned set of features, MLP showed the highest diagnostic performance in determining whether a subject is not healthy (sensitivity of 82.35% and positive predictive value of 84.85% for HC vs. all classification task) and whether a subject does not suffer from AD (specificity of 79.41% and negative predictive value of 84.38% for AD vs. all comparison). Our findings suggest that our methodology can help physicians to discriminate AD, MCI and HC.

Keywords: Alzheimer's disease, mild cognitive impairment, electroencephalography (EEG), spectral analysis, nonlinear analysis, multiclass classification approach

1. Introduction

Dementia due to Alzheimer's disease (AD) is a progressive neurodegenerative disorder associated with cognitive, behavioral and functional alterations. AD prevalence increases exponentially with age, from 1% in people between 60 and 64 years up to 38% in people over 85 years (Alzheimer's Association, 2017). Since AD is increasingly being recognized as a modern epidemic, growing efforts have been devoted to exploring its underlying brain dynamics. Despite the considerable progress made to understand AD pathophysiology, a better characterization of its early stages is still required (Alzheimer's Association, 2017). Mild cognitive impairment (MCI) subjects exhibit a memory impairment beyond what would be expected for their age, but do not fully accomplish the criteria for dementia diagnosis (Petersen, 2010). In this regard, further research is essential to identify incipient AD, since subjects with MCI have high risk of developing it (Mufson et al., 2012). Recent studies estimated

Email addresses: saul.ruiz@gib.tel.uva.es (Saúl J. Ruiz-Gómez[1]), carlos.gomez@tel.uva.es (Carlos Gómez[1]), jesus.poza@tel.uva.es (Jesús Poza[1,2,3]), gonzalo.gutierrez@gib.tel.uva.es (Gonzalo C. Gutiérrez-Tobal[1]), mtola.nrl@gmail.com (Miguel A. Tola-Arribas[4]), monica.cano.delpozo@gmail.com (Mónica Cano[5]), robhor@tel.uva.es (Roberto Hornero[1,2,3])

DOI: https://doi.org/10.3390/e20010035

that the conversion rate from MCI to AD is approximately 15% per year (Davatzikos et al., 2011), whereas this rate is only 1–2% from global population (Alzheimer's Association, 2017). Despite the fact that current pharmacological treatments and non-pharmacological therapies are not able to heal AD or MCI, an early diagnosis is still crucial since these are more effective in the first stages of the dementia (Lin and Neumann, 2013).

Several neuroimaging techniques have been used during the last decades with the aim of distinguishing AD and MCI patients from cognitively healthy control (HC) subjects: functional magnetic resonance imaging (fMRI), positron emission tomography (PET), magnetic resonance spectroscopy, electroencephalography (EEG), and magnetoencephalography (MEG), among others (Ewers et al., 2011). PET and fMRI show a good structural accuracy, but both offer a limited temporal resolution. By contrast, EEG and MEG are non-invasive techniques with high temporal resolution, allowing for studying the dynamical processes involved in the regulation of complex functional brain systems (Poza et al., 2014). Particularly, EEG is widely used due to its portability, low cost, and availability. Moreover, EEG has already shown its usefulness to characterize brain dynamics in AD and MCI (Poza et al., 2014; Fernández et al., 2010; Hornero et al., 2009; Stam, 2005; Woon et al., 2007; Abásolo et al., 2006; Schreiter Gasser et al., 2008; Baker et al., 2008).

The abnormalities that AD and MCI elicit in EEG activity have been traditionally analyzed using simple signal processing methods, such as spectral techniques (Schreiter Gasser et al., 2008; Baker et al., 2008). Spectral analyses seem to discriminate AD and MCI patients from HC subjects through a power increase in low frequency bands, as well as a decrease in higher frequencies (Schreiter Gasser et al., 2008; Baker et al., 2008). Since the mid 1990s, nonlinear analysis techniques have also been widely used in order to provide complementary information to spectral measures (Stam, 2005). Previous studies suggested a more regular EEG activity for AD and MCI patients when compared to HC subjects (Woon et al., 2007; Baker et al., 2008). Other authors reported a decrease of variability and complexity as the disease worsens (Poza et al., 2014; Fernández et al., 2010; Hornero et al., 2009; Abásolo et al., 2006). However, almost all these studies only applied one or a few methods to partially characterize the brain dynamics in AD and MCI.

The main objective of this study is to evaluate the diagnostic usefulness of an EEG-based methodology by means of different multiclass classifiers: logistic discriminant analysis (LDA), quadratic discriminant analysis (QDA) and multi-layer perceptron neural network (MLP). We hypothesize that the combination of spectral measures and nonlinear methods can be useful to help in AD and MCI diagnosis. For this reason, our proposed methodology is based on both frequency (spectral features) and time domain (nonlinear features) analyses applied to EEG recordings. However, this exhaustive characterization of EEG may lead to obtaining redundant features sharing similar information. In order to avoid this issue, an automatic feature selection stage based on the fast correlation-based filter (FCBF) is followed (Yu and Liu, 2004). Finally, a classification approach is also conducted. Previous studies performed a binary classification approach facing AD vs. HC, MCI vs. HC and AD vs. MCI (Bertè et al., 2014; Buscema et al., 2015; Huang et al., 2000; Iqbal et al., 2005; Poza et al., 2017). Only McBride et al. reported a three-way classification, but via binary classifiers (McBride et al., 2014). Additionally, their approach was validated through a leave-one-out cross-validation procedure, leading to multiple models. By contrast, our proposal focuses on building a single multiclass model to determine the group for each subject. This is an essential feature for a simplified screening protocol in the future. Afterwards, the group for each subject was settled with a trial-based majority vote procedure, as proposed in previous studies involving early AD recognition (Petrosian et al., 2001).

2. Materials and Methods

2.1. Subjects

EEG data were recorded from 111 subjects: (Ben-Mizrachi et al., 1984) AD patients, (Ben-Mizrachi et al., 1984) MCI patients, and (Ben-Mizrachi et al., 1984) elderly HC subjects. Patients with dementia or MCI due to AD were diagnosed according to the clinical National Institute on Aging and Alzheimer's Association (NIA-AA) criteria, whereas HC were elderly subjects without a cognitive impairment and with no history of neurological or psychiatric disorder (Albert et al., 2011). Inclusion and exclusion criteria for each group can be found in our previous study (Poza et al., 2017).

All participants and patients' caregivers were informed about the research background and the study protocol. Moreover, all of them gave their written informed consent to be included in the study. The Ethics Committee at the Río Hortega University Hospital (Valladolid, Spain) endorsed the study protocol, according to The Code of Ethics of the World Medical Association (Declaration of Helsinki).

2.2. EEG Recording

Five minutes of spontaneous EEG activity were recorded using a 19-channel EEG system (XLTEK®, Natus Medical, Pleasanton, CA, USA). Specifically, EEG activity was acquired from Fp1, Fp2, Fz, F3, F4, F7, F8, Cz, C3, C4, T3, T4, T5, T6, Pz, P3, P4, O1, and O2, at a sampling frequency of 200 Hz. Subjects were asked to stay in a relaxed state, awake, and with closed eyes during EEG acquisition. During the recording procedure, EEG traces were visually monitored in real time, and muscle activity was identified to avoid high-frequency noise. Additionally, independent component analysis (ICA) was

performed to minimize the presence of oculographic, cardiographic, and myographic artifacts (Poza et al., 2014). Afterwards, EEG signals were digitally filtered using a finite impulse response filter designed with a Hamming window between 1 and 70 Hz and a notch filter to remove the power line frequency interference (50 Hz, Butterworth filter). Finally, an experienced technician selected artifact-free epochs of 5-s by visual inspection.

We randomly divided our EEG database into training and test sets. The training set was formed by: 20 AD patients (45.85 $\pm$ 8.36 trials per subject, mean $\pm$ standard deviation, SD), 20 MCI subjects (46.85 $\pm$ 10.68 trials per subject) and 20 HC subjects (45.60 $\pm$ 7.93 trials per subject). The recordings not selected for the training set were assigned to the test set: 17 AD patients (44.53 $\pm$ 10.10 trials per subject), 17 MCI subjects (49.82 $\pm$ 8.29 trials per subject) and 17 HC subjects (44.24 $\pm$ 7.81 trials per subject). No statistically significant differences were found in age (p-value $>$ 0.05, Kruskal–Wallis test) and gender (p-value > 0.05, chi-squared test) among AD, MCI, and HC groups. Table 1 shows relevant socio-demographic and clinical data for each group.

2.3. Methods

The methodology followed in this study is represented in Figure 1. After EEG-signal recording and data preprocessing, both spectral and nonlinear features were computed. Then, FCBF was applied to the training set to automatically select an optimum set of features. Finally, three different multiclass classification approaches (LDA, QDA, and MLP) were adopted to settle the group for each trial and subject.

2.3.1. Feature Extraction

Spectral Analysis

A typical approach to characterize electromagnetic brain recordings is based on the analysis of their spectral content (Jeong, 2004; Dauwels et al., 2010; Osipova et al., 2003). Spectral parameters are based on the normalized power spectral density in the frequency band of interest (PSD_n). In this request, the following spectral parameters have been calculated from the PSD_n: relative power (RP), median frequency (MF), individual alpha frequency (IAF), and spectral entropy (SE).

- RP represents the relative contribution of different frequency components to the global power spectrum. RP is more appropriate than absolute power to analyze EEG data, as RP provides independent thresholds from the measurement equipment and lower inter-subject variability (Rodriguez et al., 1999). RP is obtained by summing the contribution of the desired spectral components:

$$\mathrm{RP}(f_1, f_2) = \sum_{f_1}^{f_2} \mathrm{PSD_n}(f), \tag{1}$$

where f_1 and f_2 are the low and the high cut-off frequencies of each band, respectively.

In this study, RP was calculated in the conventional EEG frequency bands: delta (δ, 1–4 Hz), theta (θ, 4–8 Hz), alpha (α, 8–13 Hz), beta-1 (β_1, 13–19 Hz), beta-2 (β_2, 19–30 Hz) and gamma (γ, 30–70 Hz).

- MF offers an alternative way to quantify the spectral changes of the EEG, and it is a simple index that summarizes the whole spectral content of the PSD_n. MF is defined as the frequency that comprises 50% of the PSD_n power:

$$\sum_{1\ \mathrm{Hz}}^{\mathrm{MF}} \mathrm{PSD_n}(f) = 0.5 \sum_{1\ \mathrm{Hz}}^{70\ \mathrm{Hz}} \mathrm{PSD_n}(f). \tag{2}$$

Previous studies suggested that MF provides a better performance for the characterization of brain activity than mean frequency, whose original definition is based on the computation of the spectral centroid (Poza et al., 2007).

- IAF evaluates the frequency at which the maximum alpha power is reached. Alpha oscillations are dominant in the EEG of resting normal subjects, with the exception of irregular activity in the delta band and lower frequencies. This issue involves that the PSD displays a peak around the alpha band. The IAF estimation in the present work is based on the calculation of the MF in the extended alpha band (4–15 Hz), as previous EEG studies on AD recommended (Moretti et al., 2004). This is shown in the following equation:

$$\sum_{4\ \mathrm{Hz}}^{\mathrm{IAF}} \mathrm{PSD_n}(f) = 0.5 \sum_{4\ \mathrm{Hz}}^{15\ \mathrm{Hz}} \mathrm{PSD_n}(f). \tag{3}$$

- SE estimates the signal irregularity in terms of the flatness of the power spectrum (Powell and Percival, 1979). On the one hand, a uniform power spectrum with a broad spectral content (e.g., a highly irregular signal like white noise) provides a high entropy value. On the other hand, a narrow power spectrum with only a few spectral components (e.g., a highly predictable signal like a sum of sinusoids) yields a low SE value. The equation for calculating SE would be:

$$\mathrm{SE} = -\sum_{1\ \mathrm{Hz}}^{70\mathrm{Hz}} \mathrm{PSD_n}(f) \cdot \log|\mathrm{PSD_n}(f)|. \tag{4}$$

Nonlinear Analysis

Alterations caused by AD and MCI also modify complexity, variability and the irregularity of the EEG activity (Hornero et al., 2009; Abásolo et al., 2006, 2008; Gómez et al., 2007; Jeong et al., 2001; Cao et al., 2015). Hence, to complement the spectral analysis, five global nonlinear

Table 1: Socio-demographic and clinical data for each group in the training set

	Training Set			Test Set		
	HC	**MCI**	**AD**	**HC**	**MCI**	**AD**
Number of subjects	20	20	20	17	17	17
Number of trials	912	937	917	752	847	757
Age (years) (median [IQR])	75.6 [74.1, 77.6]	77.9 [67.9, 79.8]	80.7 [74.7, 78.9]	76.4 [73.6, 78.9]	75.3 [69.8, 82.0]	82.4 [77.7, 83.9]
Gender (Male : Female)	8 : 12	8 : 12	5 : 15	4 : 13	8 : 9	7 : 10
MMSE[1] (median [IQR])	29 [28, 30]	27.5 [26.5, 29]	21 [18.5, 22.5]	29 [28, 30]	27. [27, 28]	22 [20, 24]
B-ADL[2] (median [IQR])	1.1 [1.0, 1.2]	2.9 [2.4, 3.3]	5.8 [5.1, 7.2]	1.2 [1.0, 1.3]	2.5 [2.3, 2.8]	5.0 [4.3, 6.4]
Education level (A : B)[3]	5 : 15	11 : 9	8 : 12	5 : 12	12 : 5	10 : 7

[1]MMSE: Mini Mental State Examination; [2]B-ADL: Bayer-Activities of Daily Living; [3]A: Primary education or below, B: Secondary education or above.

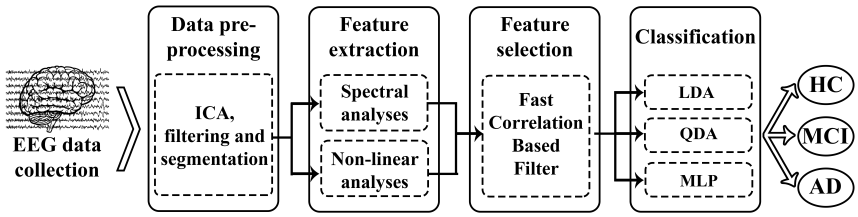

Figure 1: Block diagram of the steps followed in the EEG analysis: data collection, pre-processing, feature extraction, feature selection and classification.

methods were also calculated: Lempel–Ziv complexity (LZC), central tendency measure (CTM), sample entropy (SampEn), fuzzy entropy (FuzzyEn), and auto-mutual information (AMI).

- LZC estimates the complexity of a finite sequence of symbols. LZC analysis is based on a coarse-graining of measurements. Therefore, the EEG signal must be previously transformed into a finite symbol string. In this study, we used the simplest possible way: a binary sequence conversion (zeros and ones). By comparison with a threshold T_d, the original signal samples are converted into a 0−1 sequence $P = s(1), s(2), \ldots, s(N)$ with $s(i)$ defined by:

$$s(i) = \begin{cases} 1 & \text{if } x(i) < T_d \\ 0 & \text{if } x(i) \geq T_d \end{cases} \tag{5}$$

  The threshold T_d is estimated as the median value of the signals amplitude in each channel because it is more robust to outliers. The string P is then scanned from left to right and a complexity counter $c(N)$ is increased by one every time a new subsequence of consecutive characters is encountered in the scanning process. In order to obtain a complexity measure that is independent of the sequence length, $c(N)$ should be normalized. For a binary conversion, the upper bound of $c(N)$ is given by $b(N) = N/log2(N)$ and $c(N)$ can be normalized via $b(N)$:

$$C(n) = \frac{c(N)}{b(N)}, \tag{6}$$

  LZC values are normalized between 0 and 1, with higher LZC values for more complex time series. The detailed algorithm for LZC measure can be found in (Lempel and Ziv, 1976).

- CTM quantifies the variability of a given time series on the basis of its first-order differences. For CTM calculation, scatter plots of first differences of the data are drawn. The value of CTM is computed as the proportion of points in the plot that fall within a radius ρ, which must be specified (Cohen et al., 1996). For a time series with N samples, $N-2$ would be the total number of points in the scatter plot that can be plotted by representing $x(n+2) - x(n+1)$ versus $x(n+1) - x(n)$. Subsequently, the CTM of the time series can be computed as:

$$\text{CTM} = \frac{1}{N-2} \sum_{i=1}^{n-2} \delta(d_i), \tag{7}$$

  where

$$\delta(d_i) = \begin{cases} 1 & \text{if } \{(x[i+2] - x[i+1])^2 + \\ & (x[i+1] - x[i])^2\}^{\frac{1}{2}} \leq \rho \\ 0 & \text{otherwise.} \end{cases} \tag{8}$$

  Thus, CTM ranges between 0 and 1, with higher values corresponding to points more concentrated around the center of the plot (i.e., corresponding to less degree of variability).

- SampEn is an embedding entropy used to quantify the irregularity. It can be applied to short and relatively noisy time series (Ben-Mizrachi et al., 1984). To compute SampEn, two input parameters should be specified: a run length m and a tolerance window r. SampEn is the negative natural logarithm of the conditional probability that two sequences similar for m points remain similar at the next point, within a tolerance r, excluding self-matches (Ben-Mizrachi et al., 1984). Thus, SampEn assigns a non-negative number to a time series, with larger values corresponding to greater signal irregularity. For a time series of N points, $X(n) = x(1), x(2), \ldots, x(N)$, the $k = 1, \ldots, N - m + 1$ vectors of length m are formed as $X_m(k) = x(k + i), i = 0, \ldots, m - 1$. The distances among vectors are calculated as the maximum absolute distance between their corresponding scalar elements. B_i is the number of vectors that satisfy the condition that their distance is less than r. The counting number of different vectors is calculated and normalized as (Ben-Mizrachi et al., 1984):

$$B^m(r) = \frac{1}{N-m} \sum_{i=1}^{N-m} \frac{B_i}{N-m-1}. \quad (9)$$

Repeating the process for vectors of length m + 1, Bm+1(r) can be obtained and SampEn can be defined as:

$$\text{SampEn}(m, r) = -\ln \left[\frac{B^{m+1}(r)}{B^m(r)} \right], \quad (10)$$

- FuzzyEn provides information about how a signal fluctuates with time by comparing the time series with a delayed version of itself (Monge et al., 2015). As SampEn, higher FuzzyEn values are associated with more irregular time series. To compute FuzzyEn, three parameters must be fixed. The first parameter, m, is the length of the vectors to be compared, like in SampEn. The other ones, r and n, are the width and the gradient of the boundary of the exponential function, respectively (Monge et al., 2015). Given a time series $X(n) = x(1), x(2), \ldots, x(N)$, the FuzzyEn algorithm reads as follows:

  1. Compose $N - m + 1$ vectors of length m such that:

$$X_i^m = x(1), x(2), \ldots, x(N) - x_0(i), \quad (11)$$

where $x_0(i)$ is given by:

$$x_0(i) = \frac{1}{m} \sum_{j=0}^{m-1} x(i + j). \quad (12)$$

  2. Compute the distance, d_{ij}^m, between each two vectors, X_i^m and X_j^m, as the maximum absolute difference of their corresponding scalar components. Given n and r, calculate the similarity degree, d_{ij}^m, between X_i^m and X_j^m through a fuzzy function (d_{ij}^m, n, r):

$$D_{ij}^m(n, r) = \mu(d_{ij}^m, n, r) = \exp \left[-\frac{(d_{ij}^m)^n}{r} \right]. \quad (13)$$

  3. Define the function ϕ^m as:

$$\phi^m(n, r) = \frac{1}{N-m} \sum_{i=1}^{N-m} \left(\frac{1}{N-m+1} \sum_{j=1, j\neq i}^{N-m} D_{ij}^m \right). \quad (14)$$

  4. Increase the dimension to $m + 1$, form the vector X_i^{m+1} and the function $m + 1$. Finally, FuzzyEn(m, n, r) is defined as the negative natural logarithm of the deviation of m from $m+1$:

$$\text{FuzzyEn}(m, n, r) = \ln |\phi^m(n, r)| - \ln |\phi^{m+1}(n, r)|. \quad (15)$$

- AMI is the particularization of mutual information applied to time-delayed versions of the same sequence. Mutual information is a metric derived from Shannon's information theory to estimate the information gain from observations of one random event on another (Abásolo et al., 2008). AMI estimates, on average, the degree to which a time-delayed version of a signal can be predicted from the original one. Thus, more predictable time series, and accordingly more regular, lead to higher AMI values. The AMI between $X(n)$ and $X(n + k)$ is (Abásolo et al., 2008):

$$\text{AMI} = \sum_{X(n), X(n+k)} P_{XX_k}[X(n), X(n + k)] \cdot \log_2 \frac{P_{XX_k}[X(n), X(n + k)]}{P_X[X(n)] \cdot P_{X_k}[X(n + k)]} \quad (16)$$

where $P_{X_k}[X(n)]$ is the probability density for the measurement $X(n)$, while $P_{XX_k}[X(n), X(n + k)]$ is the joint probability density for the measurements of $X(n)$ and $X(n + k)$. In this study, the AMI was estimated over a time delay from 0 to 0.5 s and was then normalized, so that AMI($k = 0$)=1.

2.3.2. Feature Selection

The aforementioned characterization of the EEG may lead to the extraction of several features that provide similar information about the brain dynamics in AD, MCI, and HC. Consequently, a feature selection stage was also included. In our study, FCBF was used to discard those redundant features that share more information with the other ones than with the variable that defines the group

membership. FCBF is based on symmetrical uncertainty (SU), which is a normalized quantification of the information gain between each feature and the group membership variables (Yu and Liu, 2004). It consists of two steps: relevance and redundancy analyses of the features.

1. In the first step, a relevance analysis of the features is done. Thus, SU between each feature X_i and the group membership Y is computed as follows:

$$SU(X_i, Y) = 2\left[\frac{H(X_i) - H(X_i|Y)}{H(X_i) + H(Y)}\right], \quad i = 1, 2, ..., I \quad (17)$$

   where $H(\cdot)$ is the well-known Shannon's entropy, $H(X_i|Y)$ is the Shannon's entropy of X_i conditioned on Y, and I is the number of features extracted (in our study, I = 14 features). SU is normalized to the range [0, 1], with a value of SU = 1, indicating that, when knowing one feature, it is possible to completely predict the other, and a value of SU = 0 indicates that the two variables are independent. Then, a ranking of features is done based on their relevance since the higher the value of SU is, the more relevant the feature is.

2. The second step is a redundancy analysis used to discard redundant features. SU between each pair of features $SU(X_i, X_j)$ is sequentially estimated beginning from the first-ranked ones. If X_i shares more information with X_j than with the corresponding group Y, $SU(X_i, X_j) \geq SU(X_i, Y)$ (with X_i being more highly ranked than X_j), the feature j is discarded due to redundancy and it is not considered in subsequent comparisons. The optimal features are those not discarded when the algorithm ends.

2.3.3. Classification Approach

The described AD-MCI-HC diagnosis problem corresponds to a pattern classification task. Specifically, it can be modeled as a three-class classification problem. Bayesian decision theory establishes the rule to make such a decision to minimize the probability of misclassification (Bishop, 1995). We have implemented LDA, QDA, and MLP models to ensure that our conclusions take into account a variety of classification methodologies. In this study, we classify trials using each trained model, and, then, every subject is classified by means of a majority vote of all its trials (Petrosian et al., 2001).

- Linear and Quadratic Discriminant Analysis (LDA and QDA)

  LDA takes an input vector and assigns it to one out of the K classes using linear hyperplanes as decision surfaces (Bishop, 2007). This classifier assumes that different classes generate data based on different Gaussian distributions, whose parameters are estimated with the fitting function during the training. In order to predict the classes of new data, the trained model finds the class with the smallest misclassification cost assuming that the covariance matrices of each class are identical (homoscedasticity) (Bishop, 2007).

  QDA is a classification approach closely related to LDA. However, there is no assumption that the covariance of all classes are identical among them and it establishes a quadratic decision boundary between classes in the feature space (Bishop, 2007).

- Multi-Layer Perceptron Artificial Neural Network (MLP)

  MLP is an artificial neural network that maps an input vector onto a set of output variables using a nonlinear function controlled by a vector of adjustable parameters. The use of neural networks for classification issues has some advantages. First, no prior assumptions about the distribution of the data are required, since neural network algorithms adjust themselves to the environment by means of the training or learning process. Thus, complex relationships can be modeled by these algorithms (Zhang, 2000).

  An MLP consists of three or more layers (an input and an output layer with one or more hidden layers) of neurons, with each layer fully connected to the next one. In our study, we have evaluated MLP networks with a single hidden layer of neurons, since networks with this architecture are capable of universal approximation (Hornik, 1991). MLP utilizes backpropagation in conjunction with an optimization method, such as gradient descent, with the aim of finding appropriate weights to connect neurons each other. Backpropagation is based on the definition of a suitable error function, which is minimized by updating the weights in the network (Bishop, 1995).

  In order to predict the classes for new data, the trained MLP model provides the posterior probability of belonging to each class. A three-class classification problem involves the use of three output neurons, one neuron per group. In our study, the number of neurons in the hidden layer (n_h) and a regularization parameter (u) were optimized by cross-validation leaving all trials of a subject out in every iteration in the training set. This procedure was carried out 30 times to minimize the effect of network random initialization and then the results were averaged (Gutiérrez-Tobal et al., 2013). NETLAB toolbox was used to implement the neural network classifier (Nabney, 2002).

2.3.4. Statistical Analysis

The three-class diagnostic ability of the models was assessed in terms of accuracy (Acc, overall percentage of subjects rightly classified) and Cohen's kappa (κ). κ

measures the agreement between predicted and observed classes, avoiding the part of agreement by chance (Witten et al., 2011). On the other hand, the performance of the models for HC vs. all and AD vs. all comparison was described by sensitivity (Se, percentage of positive subjects appropriately classified), specificity (Sp, percentage of negative subjects correctly classified), Acc, positive predictive value (PPV, proportion of positive estimations of the models that are true positive results) and negative predictive value (NPV, proportion of negative estimations of the models that are true negative results).

3. Results

According to the proposed methods, we calculated 14 features from each EEG channel. Nine spectral features: RP(δ) (where RP(δ) represents de RP value for the δ band), RP(θ), RP(α), RP(β_1), RP(β_2), RP(γ), MF, IAF, and SE, and five derived from the nonlinear methods: LZC, CTM, SampEn, FuzzyEn, and AMI. The results were obtained based on all the artifact-free trials within the five-minute period of recording. Results from all EEG channels were averaged in order to achieve one value per trial for each method.

3.1. Training Set

In order to select the optimal value of the different input parameters of each feature, only a training set was used. The optimal value for r (CTM) was obtained by evaluating the range $r \in [0.01, 0.5]$ (step = 0.005). Values of $r < 0.01$ were not considered, since they led to a CTM value close to 0 for every subject, whereas values of $r > 0.5$ were also discarded since they led to CTM values equal to 1 regardless the group. For both SampEn and FuzzyEn, m and r optimal values were obtained by evaluating all the combinations for $m = 1, 2$ and $r \in (0.1 \cdot \text{SD}, 0.25 \cdot \text{SD})$ (step = 0.05), where SD is the standard deviation of the time series (Monge et al., 2015; Richman and Moorman, 2000). In the case of FuzzyEn, values of n = 1, 2, 3 were also evaluated to obtain its optimal value (Monge et al., 2015). We chose those configurations (r = 0.075 for CTM; m = 1 and $r = 0.1 \cdot$ SD for SampEn; and m = 1, $r = 0.1 \cdot$ SD, and n = 3 for FuzzyEn) for which the corresponding CTM, SampEn, and FuzzyEn values showed the lowest *p*-value (Kruskal–Wallis test) among the three groups. Table 2 summarizes the averaged results for each group, taking into account only the training set. After feature extraction, FCBF was applied to the training set. The final FCBF optimal set was composed of three features: two spectral measures (IAF and RP(δ)) and a nonlinear one (SampEn).

The MLP model was obtained according to the optimal values for n_h and u. Both were optimized by cross-validation, leaving all trials for each subject out in every iteration. For each value of u between 0 and 100 (step = 5), we varied the number of neurons in the hidden layer from 1 to 20 (step = 1) in order to compute the κ value. This procedure was carried out 30 times to minimize the effect of network random initialization. Then, the k values were averaged (Gutiérrez-Tobal et al., 2013). The optimal values (highest κ for trials) were u = 45 and 11 neurons in the hidden layer, as Figure 2 shows. On the other hand, since LDA and QDA models have no tuning parameters to be optimized, these were trained using all trials in the training set.

3.2. Test Set

Once the models were trained, their diagnostic ability was only evaluated using the test set. The overall accuracy of the models in the three-class classification task was 58.82% with LDA, 60.78% with QDA, and 62.75% with MLP. Additionally, we obtained k values of 0.3824 with LDA, 0.4118 with QDA and 0.4412 with MLP. These results show that MLP outperformed the discriminant analyses classifiers.

Table 3 displays the confusion matrices of each model, i.e., the model class estimation for each subject versus their actual group. As expected, the three models had higher difficulties when classifying MCI trials and subjects, as this is an intermediate state between HC and AD.

Table 4 shows Se, Sp, Acc, PPV and NPV for each method for HC vs. all and AD vs. all, derived from confusion matrices. MLP showed the highest diagnostic performance when determining whether a subject is not healthy (HC vs. all classification tasks: Se = 82.35% and PPV = 84.85%). Furthermore, the network showed the highest diagnostic capability when determining whether a subject does not suffer from AD (AD vs. all comparison: Sp = 79.41% and NPV = 84.38%). LDA and QDA showed similar tendencies although reaching lower diagnostic performance than MLP, as Table 4 shows.

4. Discussion

4.1. Spectral and Nonlinear Characterization of AD and MCI

Our spectral results suggested that AD and MCI elicit a slowing of spontaneous EEG activity. Further inspection of RP values revealed that AD patients reached higher RP values in low frequency bands (δ) and lower RP values in high frequency bands (β_1, β_2 and γ) than HC subjects. For the MCI group, a slight slowing of neural oscillations was found in comparison with HC. This increase of slow rhythms in spontaneous EEG activity was also observed by means of MF and IAF. Both spectral parameters were lower for AD patients than for MCI and HC subjects. These findings confirm the trend reported in previous studies: AD and MCI are accompanied by a progressive slow-down of EEG (Jeong, 2004; Dauwels et al., 2010). Finally, our SE results showed changes in the frequency distribution of the power spectrum. However, the physiological explanations for all of these alterations are not clear. The most

Table 2: Averaged results (median (interquartile range)) for each group and for each feature taking into account only the training set. The selected features that formed the FCBF optimal set are highlighted in bold.

	Feature	Healthy controls	MCI patients	AD patients
Spectral	**RP(δ)**	**0.227 [0.179, 0.277]**	**0.164 [0.102, 0.221]**	**0.158 [0.103, 0.229]**
	RP(θ)	0.111 [0.083, 0.131]	0.122 [0.087, 0.155]	0.143 [0.103, 0.188]
	RP(α)	0.243 [0.174, 0.291]	0.317 [0.224, 0.544]	0.279 [0.192, 0.447]
	RP(β_1)	0.128 [0.101, 0.155]	0.101 [0.081, 0.160]	0.101 [0.073, 0.141]
	RP(β_2)	0.111 [0.084, 0.138]	0.105 [0.048, 0.135]	0.091 [0.060, 0.119]
	RP(γ)	0.097 [0.074, 0.168]	0.087 [0.037, 0.145]	0.089 [0.047, 0.141]
	MF	10.584 [9.690, 11.900]	10.467 [8.639, 12.285]	9.971 [9.030, 10.997]
	IAF	**9.502 [8.751, 9.996]**	**9.404 [8.519, 9.972]**	**8.811 [8.510, 9.474]**
	SE	0.813 [0.760, 0.822]	0.796 [0.695, 0.816]	0.782 [0.733, 0.809]
Nonlinear	LZC	0.684 [0.6331, 0.7360]	0.667 [0.551, 0.731]	0.663 [0.589, 0.713]
	CTM[1]	0.101 [0.076, 0.129]	0.111 [0.086, 0.165]	0.116 [0.077, 0.183]
	SampEn[1]	**1.366 [1.288, 1.540]**	**1.312 [1.103, 1.489]**	**1.274 [1.034, 1.489]**
	FuzzyEn[1]	0.532 [0.466, 0.624]	0.514 [0.395, 0.618]	0.508 [0.427, 0.584]
	AMI	-0.149 [-0.184,-0.130]	-0.149 [-0.175,-0.124]	-0.145 [-0.164,-0.128]

[1]These results were obtained using the optimal parameters for each feature: $r = 0.075$ for CTM; $m = 1$ and $r = 0.1 \cdot SD$ for SampEn; and $m = 1$, $r = 0.1 \cdot SD$, and $n = 3$ for FuzzyEn (SD: standard deviation).

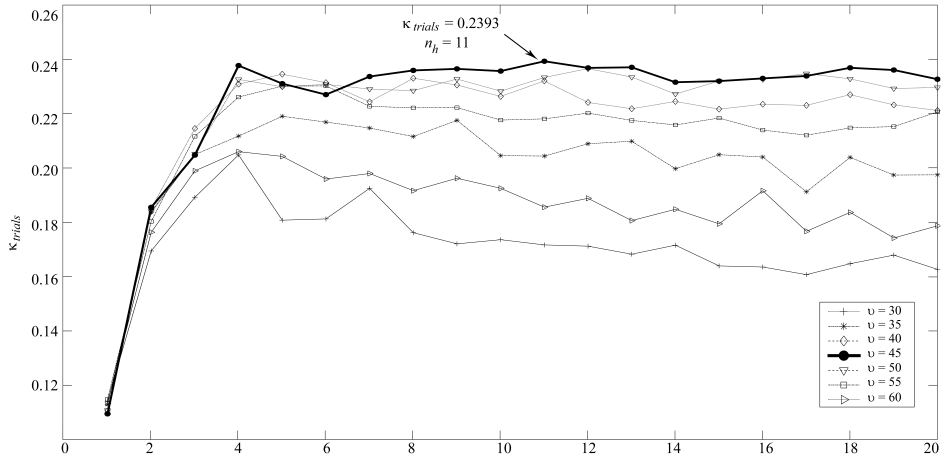

Figure 2: Optimal regularization parameter (u) and number of neurons in the hidden layer (n_h) for MLP.

Table 3: Confusion matrices of each model using the test set: subjects' classification applying a trial-based majority vote procedure.

	LDA			QDA			MLP		
Actual / Estimated	**HC**	**MCI**	**AD**	**HC**	**MCI**	**AD**	**HC**	**MCI**	**AD**
HC	11	4	2	13	3	1	12	3	2
MCI	4	7	6	4	7	6	4	8	5
AD	2	3	12	3	3	11	2	3	12

extended hypothesis is that a significant cerebral cholinergic deficit underlies cognitive symptoms, as memory loss. A loss of cholinergic innervation of the neocortex might play a critical role in the EEG slowing associated with AD (Jeong, 2004). Analogously, the slowing of neural oscillations in AD could also be due to the loss of neurotransmitter acetylcholine, since the cholinergic system modulates spontaneous cortical activity at low frequencies (Osipova et al., 2003).

Regarding the nonlinear parameters that quantify the complexity and irregularity of EEG recordings, our findings showed lower LZC, SampEn, FuzzyEn and higher AMI

Table 4: Diagnostic performance for HC vs. all and AD vs. all, derived from confusion matrices.

	HC vs. All			AD vs. All		
	LDA	**QDA**	**MLP**	**LDA**	**QDA**	**MLP**
Se (%)	82.35	79.41	82.35	70.59	64.71	70.59
Sp (%)	64.71	76.47	70.59	76.47	79.41	79.41
Acc (%)	76.47	78.43	78.43	74.51	74.51	76.47
PPV (%)	82.35	87.10	84.85	60.00	61.11	63.16
NPV (%)	64.71	65.00	66.67	83.87	81.82	84.38

values for AD patients than for HC subjects. For these measures, MCI subjects showed intermediate values between AD and HC. Previous EEG studies also reported a loss of complexity and irregularity associated with early AD and MCI by means of nonlinear measures (Hornero et al., 2009; Abásolo et al., 2006, 2008; Gómez et al., 2007; Jeong et al., 2001; Cao et al., 2015). Additionally, CTM values were higher in AD patients and lower in HC subjects. This result suggests a decrease on variability in AD, as Abásolo et al. previously reported (Abásolo et al., 2006). Taking into account the different nature of the nonlinear parameters, our results showed that the brain activity from AD patients is less complex, more regular and less variable than in MCI and HC subjects. These changes can be associated with both loss of information content and alterations in information processing at the cerebral cortex (Baraniuk et al., 2001). The decrease of EEG complexity can also be due to the loss of neurons or synapses, since they are associated with the complex dynamical processing within the brain neural networks (Jeong et al., 2001).

4.2. Towards a Screening Protocol of AD

Previous studies explored several EEG features for AD and MCI discrimination from HC, focusing on binary discrimination problems (AD vs. HC, MCI vs. HC and AD vs. MCI) (Bertè et al., 2014; Buscema et al., 2015; Huang et al., 2000; Iqbal et al., 2005; Poza et al., 2017). To the best of our knowledge, only one study performed a three-way classification, although via binary classifiers (McBride et al., 2014). McBride et al. reached an accuracy value of 85.42% when comparing HC vs. all and 83.33% for AD vs. all (eyes closed resting condition) (McBride et al., 2014). Although their results are slightly higher than ours (78.43% and 76.47% for both comparisons, respectively), several advantages of our methodology should be noticed. Firstly, their database was composed by only 47 subjects, in contrast to the 111 subjects recruited for our study. This data limitation also led the authors to validate its proposal through a leave-one-out cross-validation procedure instead of using a hold-out approach (training and test sets). As they obtained a different model for each iteration, the inclusion of new subjects would imply changes in every iteration of cross-validation. However, once our model is trained, the subsequent runtime to apply new data is trivial. It allows us to classify new data just feeding the trained model with the standardized version of them, simplifying the screening protocol. In contrast to the above-mentioned studies, our MLP single model can be used not only for the three-class classification task but also in binary assessments of healthy vs. cognitively impaired subjects. As derived from Table 3 and Table 4, it has shown the ability to detect whether a subject suffers from AD or MCI in 28 out of the 34 non-healthy subjects (82.53% Se)—with a positive post-test probability of 84.85% (28 subjects rightly classified out of 33 subjects predicted as AD or MCI)—and only predicting two out of 17 AD patients as HC. In addition, the same model also showed the ability to discard AD in 27 out of the 34 subjects not suffering from it (79.41% Sp), including 15 out of the 17 HC (88.24%). These results highlight the clinical usefulness of our proposal, which might be expressed as a screening strategy similar to:

1. If the MLP model predicts AD, recommend beginning a treatment since most probably (89.47%, 17 out of 19 subjects) the patient suffers from AD or MCI.
2. If the MLP model predicts HC, do not treat the patient, since most probably (88.89%, 16 out of 18 subjects) he/she does not suffer from AD; consider a regular evaluation of the subject in the persistence of symptoms in order to minimize the number of AD and MCI missed subjects.
3. If the MLP predicts MCI, conduct a regular evaluation of the patient since doubts arise about the cognitive status of the subject.

4.3. Limitations and Future Research Lines

Despite the fact that we showed the usefulness of our proposal, some limitations need to be addressed. Although we used a large data sample to train and validate the models (5122 trials), they were obtained from 111 subjects. Hence, analyzing more recordings from different subjects would enhance the generalization ability of our results. Moreover, taking into account the MCI heterogeneity, it would be useful to characterize different subtypes and conduct a longitudinal analysis to characterize subjects with stable MCI and those who progress to AD. Finally, only three classification approaches (LDA, QDA, and MLP) have been used in this study. In future research works, the usefulness of other advanced classification methods, such as spiking neural networks and support vector machines, should be evaluated.

5. Conclusions

To sum up, our results show that both AD and MCI elicit changes in the EEG background activity: a slowing of EEG rhythms, alterations in the frequency distribution of the power spectrum, a complexity loss, a regularity increase and a variability decrease. Our proposal has shown that

spectral and nonlinear features allows us to characterize the brain abnormalities associated with AD and MCI. In addition, we have shown the high diagnostic ability of different three-class models trained with this EEG information, particularly when predicting AD and HC status. These results highlight the usefulness of our proposal in order to help physicians classify AD, MCI and HC from EEG data.

Acknowledgments

This research was supported by the 'Ministerio de Economía y Competitividad' and 'European Regional Development Fund' (FEDER) under project TEC2014-53196-R, by 'European Commission' and FEDER under project 'Análisis y correlación entre el genoma completo y la actividad cerebral para la ayuda en el diagnóstico de la enfermedad de Alzheimer' ('Cooperation Programme Interreg V-A Spain-Portugal, POCTEP 2014–2020'), and by 'Consejería de Educación de la Junta de Castilla y León' and FEDER under project VA037U16. Saúl J. Ruiz-Gómez has a predoctoral scholarship from the 'Junta de Castilla y León' and European Social Fund.

References

Abásolo, D., Escudero, J., Hornero, R., Gómez, C., Espino, P., 2008. Approximate entropy and auto mutual information analysis of the electroencephalogram in Alzheimer's disease patients. Medical and Biological Engineering and Computing 46 (10), 1019–1028.

Abásolo, D., Hornero, R., Carlos, G., Miguel, L., 2006. Analysis of EEG background activity in Alzheimer ' s disease patients with Lempel – Ziv complexity and central tendency measure. Medical Engineering and Physics Physics 28, 315–322.

Albert, M. S., DeKosky, S. T., Dickson, D., Dubois, B., Feldman, H. H., Fox, N. C., Gamst, A., Holtzman, D. M., Jagust, W. J., Petersen, R., Snyder, P. J., Carrillo, M. C., Thies, B., Phelps, C. H., 2011. The diagnosis of mild cognitive impairment due to Alzheimer's disease: Recommendations from the National Institute on Aging-Alzheimer's Association workgroups on diagnostic guidelines for Alzheimer's disease. Alzheimer's and Dementia 7, 270–279.

Alzheimer's Association, 2017. 2017 Alzheimer's Disease Facts and Figures. Alzheimers Dement 13, 325–373.

Baker, M., Akrofi, K., Schiffer, R., Boyle, M. W. O., 2008. EEG Patterns in mild cognitive impairment (MCI) patients. The open neuroimaging journal 2, 52–55.

Baraniuk, R. G., Flandrin, P., Janssen, A. J., Michel, O. J., 2001. Measuring time-frequency information content using the Reényi entropies. IEEE Transactions on Information Theory 47 (4), 1391–1409.

Ben-Mizrachi, A., Procaccia, I., Grassberger, P., feb 1984. Characterization of experimental (noisy) strange attractors. Physical Review A 29 (2), 975–977.

Bertè, F., Lamponi, G., Calabrò, R. S., Bramanti, P., 2014. Elman neural network for the early identification of cognitive impairment in Alzheimer's disease. Functional neurology 29 (1), 57–65.

Bishop, C. M., 1995. Neural Networks for Pattern Recognition. Vol. 1995.

Bishop, C. M., jan 2007. Pattern Recognition and Machine Learning. Journal of Electronic Imaging 16 (4), 049901.

Buscema, M., Vernieri, F., Massini, G., Scrascia, F., Breda, M., Rossini, P. M., Grossi, E., 2015. An improved I-FAST system for the diagnosis of Alzheimer's disease from unprocessed electroencephalograms by using robust invariant features. Artificial Intelligence in Medicine 64 (1), 59–74.

Cao, Y., Cai, L., Wang, J., Wang, R., Yu, H., Cao, Y., Liu, J., 2015. Characterization of complexity in the electroencephalograph activity of Alzheimer's disease based on fuzzy entropy. Chaos 25, 083116.

Cohen, M., Hudson, D., Deedwania, P., 1996. Applying continuous chaotic modeling to cardiac signal analysis. IEEE Engineering in Medicine and Biology Magazine 15 (5), 97–102.

Dauwels, J., Vialatte, F., Cichocki, A., 2010. Diagnosis of Alzheimer's disease from EEG signals: where are we standing? Current Alzheimer Research 7 (6), 487–505.

Davatzikos, C., Bhatt, P., Shaw, L. M., Batmanghelich, K. N., Trojanowski, J. Q., 2011. Prediction of MCI to AD conversion, via MRI, CSF biomarkers, and pattern classification. Neurobiology of Aging 32 (12), 2322.e19–2322.e27.

Ewers, M., Sperling, R. A., Klunk, W. E., Weiner, M. W., Hampel, H., 2011. Neuroimaging markers for the prediction and early diagnosis of Alzheimer's disease dementia. Trends in Neurosciences 34 (8), 430–442.

Fernández, A., Hornero, R., Gómez, C., Turrero, A., Gil-Gregorio, P., Matías-Santos, J., Ortiz, T., 2010. Complexity analysis of spontaneous brain activity in Alzheimer disease and mild cognitive impairment: an MEG study. Alzheimer disease and associated disorders 24 (2), 182–189.

Gómez, C., Hornero, R., Abásolo, D., Fernández, A., Escudero, J., sep 2007. Analysis of the magnetoencephalogram background activity in Alzheimer's disease patients with auto-mutual information. Computer Methods and Programs in Biomedicine 87 (3), 239–247.

Gutiérrez-Tobal, G., Álvarez, D., Marcos, J., Del Campo, F., Hornero, R., 2013. Pattern recognition in airflow recordings to assist in the sleep apnoea–hypopnoea syndrome diagnosis. Medical and Biological Engineering and Computing 51 (12), 1367–1380.

Hornero, R., Abasolo, D., Escudero, J., Gomez, C., 2009. Nonlinear analysis of electroencephalogram and magnetoencephalogram recordings in patients with Alzheimer's disease. Philosophical Transactions of the Royal Society A: Mathematical, Physical and Engineering Sciences 367 (1887), 317–336.

Hornik, K., 1991. Approximation capabilities of multilayer feedforward networks. Neural Networks 4 (2), 251–257.

Huang, C., Wahlund, L.-O., Dierks, T., Julin, P., Winblad, B., Jelic, V., nov 2000. Discrimination of Alzheimer's disease and mild cognitive impairment by equivalent EEG sources: a cross-sectional and longitudinal study. Clinical Neurophysiology 111 (11), 1961–1967.

Iqbal, K., del C. Alonso, A., Chen, S., Chohan, M. O., El-Akkad, E., Gong, C.-X., Khatoon, S., Li, B., Liu, F., Rahman, A., Tanimukai, H., Grundke-Iqbal, I., jan 2005. Tau pathology in Alzheimer disease and other tauopathies. Biochimica et Biophysica Acta (BBA) - Molecular Basis of Disease 1739 (2-3), 198–210.

Jeong, J., jul 2004. EEG dynamics in patients with Alzheimer's disease. Clinical Neurophysiology 115 (7), 1490–1505.

Jeong, J., Gore, J. C., Peterson, B. S., 2001. Mutual information analysis of the EEG in patients with Alzheimer's disease. Clinical Neurophysiology 112 (5), 827–835.

Lempel, A., Ziv, J., 1976. On the complexity of finite sequences. IEEE Transactions on Information Theory 22 (1), 75–81.

Lin, P. J., Neumann, P. J., 2013. The economics of mild cognitive impairment. Alzheimer's and Dementia 9 (1), 58–62.

McBride, J. C., Zhao, X., Munro, N. B., Smith, C. D., Jicha, G. A., Hively, L., Broster, L. S., Schmitt, F. A., Kryscio, R. J., Jiang, Y., 2014. Spectral and complexity analysis of scalp EEG characteristics for mild cognitive impairment and early Alzheimer's disease. Computer Methods and Programs in Biomedicine 114 (2), 153–163.

Monge, J., Gómez, C., Poza, J., Fernández, A., Quintero, J., Hornero, R., 2015. MEG analysis of neural dynamics in attention-deficit/hyperactivity disorder with fuzzy entropy. Medical Engineering and Physics 37 (4), 416–423.

Moretti, D. V., Babiloni, C., Binetti, G., Cassetta, E., Dal Forno, G., Ferreric, F., Ferri, R., Lanuzza, B., Miniussi, C., Nobili, F., Rodriguez, G., Salinari, S., Rossini, P. M., 2004. Individual analysis of EEG frequency and band power in mild Alzheimer's disease. Clinical Neurophysiology 115 (2), 299–308.

Mufson, E. J., Binder, L., Counts, S. E., DeKosky, S. T., DeToledo-Morrell, L., Ginsberg, S. D., Ikonomovic, M. D., Perez, S. E., Scheff, S. W., jan

2012. Mild cognitive impairment: pathology and mechanisms. Acta Neuropathologica 123 (1), 13–30.

Nabney, I. T., 2002. NETLAB: Algorithms for pattern recognition. Springer Science and Business Media, New York.

Osipova, D., Ahveninen, J., Kaakkola, S., Jääskeläinen, I. P., Huttunen, J., Pekkonen, E., 2003. Effects of scopolamine on MEG spectral power and coherence in elderly subjects. Clinical Neurophysiology 114 (10), 1902–1907.

Petersen, R. C., 2010. Alzheimer's disease: progress in prediction. The Lancet Neurology 9 (1), 4–5.

Petrosian, A., Prokhorov, D., Lajara-Nanson, W., Schiffer, R., 2001. Recurrent neural network-based approach for early recognition of Alzheimer's disease in EEG. Clinical Neurophysiology 112, 1378–1387.

Powell, G. E., Percival, I. C., 1979. A spectral entropy method for distinguishing regular and irregular motion of Hamiltonian systems. Journal of Physics A: Mathematical and General 12 (11), 2053–2071.

Poza, J., Gómez, C., García, M., Corralejo, R., Fernández, A., Hornero, R., 2014. Analysis of neural dynamics in mild cognitive impairment and Alzheimer's disease using wavelet turbulence. Journal of Neural Engineering 11 (2), 26010.

Poza, J., Gómez, C., García, M., Tola-Arribas, M. A., Carreres, A., Cano, M., Hornero, R., 2017. Spatio-Temporal Fluctuations of Neural Dynamics in Mild Cognitive Impairment and Alzheimer's Disease. Current Alzheimer research 14 (9), 924–936.

Poza, J., Hornero, R., Abásolo, D., Fernández, A., García, M., 2007. Extraction of spectral based measures from MEG background oscillations in Alzheimer's disease. Medical Engineering and Physics 29 (10), 1073–1083.

Richman, J. S., Moorman, J. R., 2000. Physiological time-series analysis using approximate entropy and sample entropy. American journal of physiology. Heart and circulatory physiology 278 (6), 2039–49.

Rodriguez, G., Copello, F., Vitali, P., Perego, G., Nobili, F., 1999. EEG spectral profile to stage Alzheimer's disease. Clinical Neurophysiology 110 (10), 1831–1837.

Schreiter Gasser, U., Rousson, V., Hentschel, F., Sattel, H., Gasser, T., oct 2008. Alzheimer disease versus mixed dementias: An EEG perspective. Clinical Neurophysiology 119 (10), 2255–2259.

Stam, C., oct 2005. Nonlinear dynamical analysis of EEG and MEG: Review of an emerging field. Clinical Neurophysiology 116 (10), 2266–2301.

Witten, I. H., Frank, E., Hall, M. A., 2011. Data Mining: Practical Machine Learning Tools and Techniques. Morgan Kaufmann Publishers, Burlington.

Woon, W. L., Cichocki, A., Vialatte, F., Musha, T., 2007. Techniques for early detection of Alzheimer's disease using spontaneous EEG recordings. Physiological Measurement 28 (4), 335–347.

Yu, L., Liu, H., 2004. Efficient feature selection via analysis of relevance and redundancy. Journal of Machine Learning Research 5, 1205–1224.

Zhang, G., 2000. Neural networks for classification: a survey. IEEE Transactions on Systems, Man and Cybernetics, Part C (Applications and Reviews) 30 (4), 451–462.

Measuring Alterations of Spontaneous EEG Neural Coupling in Alzheimer's Disease and Mild Cognitive Impairment by Means of Cross-Entropy Metrics

Saúl J. Ruiz-Gómez[1], Carlos Gómez[1], Jesús Poza[1,2,3], Mario Martínez-Zarzuela[4], Miguel A. Tola-Arribas[5], Mónica Cano[6], Roberto Hornero[1,2,3]

[1]*Biomedical Engineering Group, E.T.S.I. Telecomunicación, University of Valladolid, Paseo de Belén 15, 47011, Valladolid, Spain*

[2]*Instituto de Investigación en Matemáticas (IMUVA), University of Valladolid, Paseo de Belén S/N, 47011, Valladolid, Spain*

[3]*Instituto de Neurociencias de Castilla y León (INCYL), University of Salamanca, Calle Pintor Fernando Gallego 1, 37007 Salamanca, Spain*

[4]*Imaging and Telematics Group, University of Valladolid, Paseo de Belén 15, 47011, Valladolid, Spain*

[5]*Servicio de Neurología, Hospital Universitario Río Hortega, Calle Dulzaina 2, 47012 Valladolid, Spain*

[6]*Servicio de Neurofisiología Clínica, Hospital Universitario Río Hortega, Calle Dulzaina 2, 47012 Valladolid, Spain*

Frontiers in Neuroinformatics
Volume 12, No. 76, October 2018, Pages 1–11

Abstract

Alzheimer's Disease (AD) represents the most prevalent form of dementia and is considered a major health problem due to its high prevalence and its economic costs. An accurate characterization of the underlying neural dynamics in AD is crucial in order to adopt effective treatments. In this regard, mild cognitive impairment (MCI) is an important clinical entity, since it is a risk-state for developing dementia. In the present study, coupling patterns of 111 resting-state electroencephalography (EEG) recordings were analyzed. Specifically, we computed Cross-Approximate Entropy (Cross-ApEn) and Cross-Sample Entropy (Cross-SampEn) of 37 patients with dementia due to AD, 37 subjects with MCI and 37 healthy control (HC) subjects. Our results showed that Cross-SampEn outperformed Cross-ApEn, revealing higher number of significant connections among the three groups (Kruskal-Wallis test, FDR-corrected p-values < 0.05). AD patients exhibited statistically significant lower similarity values at θ and β_1 frequency bands compared to HC. MCI is also characterized by a global decrease of similarity in all bands, being only significant at β_1. These differences shows that β band might play a significant role in the identification of early stages of AD. Our results suggest that Cross-SampEn could increase the insight into brain dynamics at different AD stages. Consequently, it may contribute to develop early AD biomarkers, potentially useful as diagnostic information.

Keywords: Alzheimer's disease, mild cognitive impairment, electroencephalography (EEG), neural coupling, cross-entropy metrics

1. Introduction

The human brain is an extremely complex network comprised of billions of interconnected neurons (Babiloni et al., 2016). Abnormal neural patterns at cellular coupling can provoke cognitive, behavioral, and functional alterations. Dementia due to Alzheimer's disease (AD) is the most common cause of neurodegenerative pathology, affecting up to 38% of people over 85 years (Alzheimer's Association, 2017). Neural activity in AD is progressively modified as a consequence of the neurodegenerative process and disturbances in information transmission and processing in the brain arise (Babiloni et al., 2016). Current interest in the field is focused on the detection of AD at its earliest possible stages. In this regard, mild cognitive impairment (MCI) appears as an important clinical entity, since it is considered as a prodromal stage of AD. Previous research have shown that MCI subjects progress to AD at a rate of approximately 15% per year (Davatzikos et al., 2011), whereas healthy controls develop dementia at a rate of 1–2% per year (Alzheimer's Association, 2017). Thus, MCI can be considered a prodromal form of AD. MCI subjects exhibit objective evidence of memory impairment greater than expected for their age and edu-

Email addresses: saul.ruiz@gib.tel.uva.es (Saúl J. Ruiz-Gómez[1]), carlos.gomez@tel.uva.es (Carlos Gómez[1]), jesus.poza@tel.uva.es (Jesús Poza[1,2,3]), marmar@tel.uva.es (Mario Martínez-Zarzuela[4]), mtola.nrl@gmail.com (Miguel A. Tola-Arribas[5]), monica.cano.delpozo@gmail.com (Mónica Cano[6]), robhor@tel.uva.es (Roberto Hornero[1,2,3])

DOI: https://doi.org/10.3389/fninf.2018.00076

cation level. Nonetheless, MCI does not necessarily interfere in their daily activities (Petersen, 2010).

Several techniques have been used to study neural dynamics in AD and MCI, such as positron emission tomography (PET), functional magnetic resonance imaging (fMRI), electroencephalography (EEG), and magnetoencephalography (MEG) (Ewers et al., 2011). In this study, the electrical brain activity was measured via EEG due to its high temporal resolution in contrast to PET and fMRI, which offer lower temporal resolution (Poza et al., 2014). Moreover, EEG is a non-invasive technique widely used in clinical settings to take advantage of its low cost compared to MEG. EEG measures the electrical activity of the brain generated by synchronized neurons (Poza et al., 2017). This information can help to further understand the relationship between neuronal dynamics and the alterations in brain function (Babiloni et al., 2016; Vecchio and Babiloni, 2011). Moreover, EEG has already shown its usefulness to characterize brain dynamics in AD and MCI (Babiloni et al., 2009; Dauwels et al., 2010b; Koenig et al., 2005).

In past decades, the abnormalities in AD and MCI neural activity were typically characterized using local activation analyses in individual sensors, by means of spectral and nonlinear measures. Spectral analyses reflect a power increase in low frequency bands as the disease worsens, and a decrease in higher frequencies (Baker et al., 2008; Gasser et al., 2008; Ruiz-Gómez et al., 2018). Parameters derived from nonlinear techniques have revealed that AD and MCI are characterized by a decrease in complexity and variability (Ruiz-Gómez et al., 2018; Jeong, 2004; McBride et al., 2014; Dauwels et al., 2010a). Particularly, different notions of entropy, such as Approximate Entropy (*ApEn*) and Sample Entropy (*SampEn*), have paid great attention in discriminating AD patients, MCI subjects, and cognitively healthy control (HC) subjects, mostly using binary approaches. In these studies, AD patients showed significant lower *ApEn* and *SampEn* values than MCI patients and HC subjects (Abásolo et al., 2005, 2006; Hornero et al., 2008; Gómez et al., 2009). These results support the well-known hypothesis that the EEG activity becomes more regular as the disease progresses.

However, spectral and nonlinear parameters are no longer sufficient for a full characterization of brain dynamics (Stam and van Straaten, 2012). For this reason, increasing efforts have been made to gain further understanding of how the brain is organized as a functional network. Similarities between time series are traditionally quantified with linear methods, such as coherency and spectral estimations (Koenig et al., 2005; Babiloni et al., 2006; Moretti et al., 2008; Tóth et al., 2014; Frantzidis et al., 2014b). Nevertheless, these methods are not suitable for characterizing nonstationary signals. For this reason, most of them only found subtle alterations that depend on the particular coupling parameter. Since different entropy-based measures, such as *ApEn* and *SampEn*, are very well suited to analyze short and noisy one-dimensional time series (Pincus, 1991), the multidimensional versions of these methods are a good option for the analysis of multiple signals recorded from many electrodes, like EEG. Cross-Approximate Entropy (Cross-ApEn) and Cross-Sample Entropy (Cross-SampEn) algorithms can be applied to two signals, to quantify the statistical similarity between them (Pincus, 2001). It is neccessary to address that Cross-ApEn has some limitations: it is not consistent for every condition and is not always defined. Cross-SampEn was proposed to overcome these drawbacks, remaining relatively consistent for all conditions and being always defined (Richman and Moorman, 2000). Finally, there is other important difference between these two measures: whereas Cross-ApEn analysis exhibits direction dependence (i.e. it is an asymmetric method), Cross-SampEn is a direction independent measure. Usually, higher values of cross-entropy metrics indicate less similarity between signals, and they are associated with weaker coupling (Hudetz et al., 2003). Only a few studies have applied Cross-ApEn and Cross-SampEn to biological systems (Pincus and Singer, 1996; Licinio et al., 1998; Martínez-Zarzuela et al., 2013). To the best of our knowledge, only our preliminary study has analyzed spontaneous EEG activity in AD by means of Cross-SampEn and graph theory parameters (Gómez et al., 2016).

In this study, we hypothesized that the coupling patterns between different functional brain regions are disrupted in dementia, even at prodromal stages. These alterations involved in cognitive decline affect the EEG activity and could be characterized by means of cross-entropy metrics. Accordingly, in the current research we attempt to address the following questions: (i) can Cross-SampEn overcome the Cross-ApEn technical drawbacks and provide additional information about spontaneous EEG activity?; (ii) which of these measures yield a better characterization of the abnormal coupling patterns in AD and MCI?; and (iii) can these metrics be useful to discriminate AD and MCI patients from HC subjects?

2. Materials

2.1. Participants

In this study, we recruited a total of 111 subjects: 37 AD patients (12 males and 25 females), 37 MCI patients (16 males and 21 females), and 37 age-matched HC subjects (12 males and 25 females). Patients with dementia due to AD and MCI were diagnosed following the criteria of the National Institute on Aging and Alzheimer's Association (NIA-AA). HC volunteers had no pathological background and underwent a medical examination and cognitive assessment in order to discard any symptoms of neurological disorder (Albert et al., 2011). Exclusion criteria were the same used in our previous studies (Poza et al., 2017; Ruiz-Gómez et al., 2018): (1) presence or history of another neurological or psychiatric disease, different from

Table 1: Socio-demographic and clinical data for each group in the training set.

	HC	MCI	AD
Number of subjects	20	20	20
Number of trials	912	937	917
Age (years) (median [IQR])	75.6 [74.1, 77.6]	77.9 [67.9, 79.8]	80.7 [74.7, 78.9]
Gender (Male : Female)	8 : 12	8 : 12	5 : 15
MMSE[1] (median [IQR])	29 [28, 30]	27.5 [26.5, 29]	21 [18.5, 22.5]
B-ADL[2] (median [IQR])	1.1 [1.0, 1.2]	2.9 [2.4, 3.3]	5.8 [5.1, 7.2]
Education level (A:B)[3]	5 : 15	11 : 9	8 : 12

[1]MMSE: Mini Mental State Examination; [2]B-ADL: Bayer-Activities of Daily Living; [3]A: Primary education or below, B: Secondary education or above.

Table 2: Socio-demographic and clinical data for each group in the test set.

	HC	MCI	AD
Number of subjects	17	17	17
Number of trials	752	847	757
Age (years) (median [IQR])	76.4 [73.6, 78.9]	75.3 [69.8, 82.0]	82.4 [77.7, 83.9]
Gender (Male : Female)	4 : 13	8 : 9	7 : 10
MMSE[1] (median [IQR])	29 [28, 30]	27 [27, 28]	22 [20, 24]
B-ADL[2] (median [IQR])	1.2 [1.0, 1.3]	2.5 [2.3, 2.8]	6.4 [5.0, 7.3]
Education level (A:B)[3]	5 : 12	12 : 5	10 : 7

[1]MMSE: Mini Mental State Examination; [2]B-ADL: Bayer-Activities of Daily Living; [3]A: Primary education or below, B: Secondary education or above.

MCI or dementia due to AD; (2) atypical course or uncommon clinical presentations according to the NIA-AA criteria; (3) advanced dementia (Clinical Dementia Rating = 3); (4) institutionalized patients; (5) medication that could affect EEG activity; and (6) lack of cooperation during EEG acquisition. This study was carried out in accordance with the recommendations of the Code of Ethics of the World Medical Association with written informed consent from all subjects. All subjects and caregivers gave written informed consent in accordance with the Declaration of Helsinki. The protocol was approved by The Ethics Committee at the Río Hortega University Hospital (Valladolid, Spain). Relevant socio-demographic and clinical characteristics are specified in Tables 1 and 2 for training and test sets, respectively.

2.2. EEG recording

Resting-state EEG activity was acquired using a 19-channel EEG system (XLTEK®, Natus Medical) at a sampling frequency of 200 Hz. The electrodes were located at the positions Fp1, Fp2, Fz, F3, F4, F7, F8, Cz, C3, C4, T3, T4, T5, T6, Pz, P3, P4, O1, and O2 according to the international 10–20 system. Common average referencing (CAR) was chosen as the reference technique for EEG recoding because previous studies found that CAR outperforms standard types of electrical referencing (Ludwig et al., 2009). Subjects were asked to remain awake with closed eyes during EEG acquisition. For each five-minute EEG recording, the following pre-processing procedure was applied: (i) digital filtering using a Hamming window bandpass finite impulse response (FIR) filter between 0.4 and 98 Hz and a notch filter to remove the power line frequency interference (50 Hz); (ii) independent component analysis (ICA) to minimize the presence of oculographic, cardiographic, and myographic artifacts; (iii) digital filtering using a Hamming window bandpass FIR filter in the band of interest (1–70 Hz); and (iv) selection of 5-s artifact-free epochs by visual inspection.

In our previous study (Ruiz-Gómez et al., 2018), we randomly divided the EEG database into training and test sets. The training set was composed of 60 subjects (20 of each group), while the remaining 51 subjects were assigned to the test set (17 of each group). In addition, for every comparison between groups no statistically significant differences were found in age and gender (p-value > 0.05, Kruskal-Wallis test and chi-squared test, respectively). In order to compare our results with the previous ones, training and test sets remain unchanged (Ruiz-Gómez et al., 2018).

3. Methods

The followed methodology is explained below:

1. Training set:

   (a) First, after data collection and pre-processing, Cross-ApEn and Cross-SampEn were computed in the following frequency bands: delta (δ, 1–4 Hz), theta (θ, 4–8 Hz), alpha (α, 8–13 Hz), beta-1 (β_1, 13–19 Hz), beta-2 (β_2, 19–30 Hz), and gamma (γ, 30–70 Hz). Also, both measures were computed for different combinations of their configuration parameters, the run length m and the tolerance window r. The optimal values for m and r were obtained by evaluating the ranges suggested by Pincus (Pincus, 2001): $m \in [1, 2]$ and $r \in [0.10, 0.15, 0.20, 0.25]$. The result of computing each measure for all pair-wise combinations of channels was an $M \times M$ matrix ($M = 19$), where each entry $M_{i,j}$ contains the Cross-ApEn or Cross-SampEn between the channels i and j.

   (b) Then, we selected the parameters combination for which the corresponding Cross-ApEn or Cross-SampEn values showed the highest number of significant connections among the three groups using false discovery rate (FDR) (Benjamini and Hochberg, 1995) (FDR-corrected p-values < 0.05, Kruskal-Wallis test).

   (c) After determining the measure and m and r values that provides a better discrimination among

the three groups, fast correlation-based filter (FCBF) (Yu and Liu, 2004) was applied to select two optimal sets of connections for discriminating HC vs. MCI and HC vs. AD, respectively.

(d) Afterwards, quadratic discriminant analysis (QDA), support vector machines (SVM), and decision trees (DT) models were trained with these optimal sets of features using training data.

2. Test set:

(e) For the chosen metric in step (b), coupling patterns were obtained for the subjects comprised in the test set. Statistical differences were evaluated between groups for HC vs. MCI and HC vs. AD comparisons.

(f) Finally, the binary discrimination ability of the optimal sets of features obtained were evaluated by means of QDA, SVM, and DT approaches trained in step (d) using test data.

3.1. Cross-Approximate Entropy

Cross-ApEn quantifies the statistical dissimilarity between two paired signals (Pincus, 2000). The Cross-ApEn algorithm is quite similar to *ApEn*, but it is applied to two time series rather than an individual signal. Thus, Cross-ApEn affords a coupling metric from which you can directly determine the changes in interconnected networks (Pincus, 2000). The procedure for Cross-ApEn estimation requires two time series, u and v, of N samples. It is also necessary to determine the value of the run length m and the tolerance window r. Conceptually, Cross-ApEn quantifies the asynchrony between two time series by determining the frequency in which m-length patterns in v are similar to reference m-length patterns in u within a tolerance r.

Given the aforementioned time series $u = [u(1), u(2), ..., u(N)]$ and $v = [v(1), v(2), ..., v(N)]$, the algorithm to calculate Cross-ApEn is described as follows (Pincus, 2000):

1. Normalize u and v into u^* and v^*, by subtracting the mean of each time series and dividing by its standard deviation.

2. Form the sequences of m consecutive u^* and v^* values starting with the ith and jth point, respectively.

$$x(i) = [u^*(i), u^*(i+1), ..., u^*(i+m-1)] \quad (1)$$

$$y(j) = [v^*(j), v^*(j+1), ..., v^*(j+m-1)] \quad (2)$$

3. Compute the distance between $x(i)$ and $y(j)$, $d[x(i), y(j)]$, defined as the maximum absolute difference of their scalar components:

$$d[x(i), y(j)] = \max_{k=0,1,...,m-1} |u^*(i+k) - v^*(j+k)| \quad (3)$$

4. For each $x_m(i)$, find the number of j so that $d[x_m(i), x_m(j)]$ is smaller or equal to r, denoted as $N_i^m(r)$. Then, for $i = 1, 2, ..., N-m+1$, set:

$$C_i^m(r)(v||u) = \frac{N_i^m(r)}{N-m+1} \quad (4)$$

5. Obtain $\phi^m(r)$, averaging the natural logarithm of $C_i^m(r)$ over i:

$$\phi^m(r)(v||u) = \frac{1}{N-m+1} \sum_{i=1}^{N-m+1} \ln C_i^m(r)(v||u) \quad (5)$$

6. Similarly, obtain $C^{m+1}(r)$ and then compute $\phi^{m+1}(r)$ following similar steps:

$$C_i^{m+1}(r)(v||u) = \frac{N_i^{m+1}(r)}{N-m+1} \quad (6)$$

$$\phi^{m+1}(r)(v||u) = \frac{1}{N-m+1} \sum_{i=1}^{N-m+1} \ln C_i^{m+1}(r)(v||u) \quad (7)$$

7. Finally, Cross-ApEn is defined as:

$$\text{Cross-ApEn}(r, m, N)(v||u) = \phi^m(r)(v||u) - \phi^{m+1}(r)(v||u) \quad (8)$$

The absence of similar patterns between u and v may lead to non-defined values of Cross-ApEn. Thus, two correction strategies have been proposed to assign non zero values in the absence of matches: *bias* 0 and *bias max* (Richman and Moorman, 2000). In this study, the *bias max* correction strategy has been applied (Martínez-Zarzuela et al., 2013). This strategy assigns the values $C_i^m(r) = C_i^{m+1}(r)$ and $C_i^{m+1}(r) = (N-m+1)^{-1}$ if originally $C_i^m(r) = 0$ and $C_i^{m+1}(r) = 0$, respectively.

3.2. Cross-Sample Entropy

Cross-SampEn was proposed by Richman and Moorman to overcome the drawbacks of Cross-ApEn (Richman and Moorman, 2000). Cross-SampEn is always defined and remains relatively consistent for conditions where Cross-ApEn does not. As Cross-ApEn, Cross-SampEn allows assessing the degree of dissimilarity between two time series. To compute Cross-SampEn is also necessary to specify the values of the run length m and the tolerance window r. Thus, the algorithm to compute Cross-SampEn between the previously described time series, u and v, is the following (Richman and Moorman, 2000):

1. Normalize u and v into u^* and v^*, by subtracting the mean of each time series and dividing by its standard deviation.

2. Form the sequences of m consecutive u^* and v^* values starting with the ith and jth point, respectively.

$$x(i) = [u^*(i), u^*(i+1), ..., u^*(i+m-1)] \quad (9)$$

$$y(j) = [v^*(j), v^*(j+1), ..., v^*(j+m-1)] \quad (10)$$

3. Compute the distance between $x(i)$ and $y(j)$, $d[x(i), y(j)]$, defined as the maximum absolute difference of their scalar components:

$$d[x(i), y(j)] = \max_{k=0,1,...,m-1} |u^*(i+k) - v^*(j+k)| \quad (11)$$

4. For each $x_m(i)$, find the number of j so that $d[x_m(i), x_m(j)]$ is smaller or equal to r with $i \neq j$, denoted as $b_i^m(r)$. Then, for $i = 1, 2, ..., N-m$, set:

$$B_i^m(r)(v||u) = \frac{b_i^m(r)}{N-m} \quad (12)$$

5. Define $B^m(r)(v||u)$ as:

$$B^m(r)(v||u) = \frac{1}{N-m} \sum_{i=1}^{N-m} \ln B_i^m(r)(v||u) \quad (13)$$

6. Similarly, define $A^m(r)(v||u)$ as $1/(N-m)$ times the number of j ($j = 1, 2, ..., N-m+1$), such the distance between $x_{m+1}(i)$ and $y_{m+1}(i)$ is less or equal to r. Then, calculate:

$$A^m(r)(v||u) = \frac{1}{N-m} \sum_{i=1}^{N-m} \ln A_i^m(r)(v||u) \quad (14)$$

7. Finally, Cross-SampEn is defined as:

$$\text{Cross-SampEn}(r, m, N)(v||u) = -\ln \left[\frac{A^m(r)(v||u)}{B^m(r)(v||u)} \right] \quad (15)$$

3.3. Statistical analysis

Firstly, a descriptive analysis was carried out to study the distribution of the coupling results. Kolmogorov–Smirnov and Shapiro–Wilks tests were used to evaluate the normality of the data, whereas Levene test was employed to assess the homogeneity of variances. As Cross-ApEn and Cross-SampEn results did not meet the parametric test assumptions, a nonparametric test was used. Statistical differences among three groups were evaluated by Kruskal–Wallis test, whereas statistical differences between HC and MCI subjects and between HC and AD subjects were evaluated with Mann-Whitney U-test. In order to correct for multiple comparisons, FDR controlling procedure was used (Benjamini and Hochberg, 1995).

Signal processing was carried out using Matlab (version R2017a, Mathworks, Natick, MA), whereas statistical analyses were computed using SPSS Statistics (version 20, IBM Corp, Armonk, NY).

3.4. Classification analysis

The binary classification performance of the optimum sets of features for each comparison (HC vs. MCI and HC vs. AD) was assessed by means of QDA, SVM, and DT. These techniques are widely employed for data classification from EEG recordings (Spyrou et al., 2016; Ruiz-Gómez et al., 2018; Chriskos et al., 2018). In order to compare our results with those of our previous study (Ruiz-Gómez et al., 2018), the performances of the models were described by the same statistical measures: accuracy (*Acc*), sensitivity (*Se*), specificity (*Sp*), positive predictive value (*PPV*), and negative predictive value (*NPV*).

3.4.1. Quadratic Discriminant Analysis (QDA)

QDA is commonly used due to its advantages over linear discriminant analysis (LDA). While LDA assumes both data normality (Gaussian or normal distribution) and homoscedasticity (equal variances) to model each class-conditional density function for an input feature, QDA does not presume homoscedasticity (Bishop, 2007). Then, in order to predict the classes of new data, the QDA models find the class with the smallest misclassification by establishing a quadratic decision boundary between classes in the feature space, instead the linear decision threshold of LDA (Bishop, 2007).

3.4.2. Support Vector Machines (SVM)

SVM is a binary classifier that searches for the optimal hyperplane boundary, built in a transformed high-dimensional space to maximize separation. The weight vector w is obtained by solving an optimization problem based on Lagrange multipliers η^n, expressed as follows (Vapnik, 1999):

$$w = \sum_{n \in S} \eta^n t^n \varphi(x^n), \quad (16)$$

where t^n is the target or desired output and $\varphi(\cdot)$ maps training vectors into the higher dimensional space. The output of the SVM classifier is expressed in terms of these support vectors as follows (Vapnik, 1999):

$$y = \sum_{n \in S} \eta^n t^n K(x^n, x) + w_0, \quad (17)$$

Table 3: Total number of significant connections among the three groups (FDR-corrected p-values < 0.05, Kruskal-Wallis test) for each parameter combination in the training set.

	Cross-ApEn		Cross-SampEn	
	m=1	**m=2**	**m=1**	**m=2**
r=0.10	182	0	468	0
r=0.15	486	213	508	12
r=0.20	403	228	**514**	48
r=0.25	349	255	502	196

where S is a subset of the indices $\{1, ..., N\}$ corresponding to the support vector and $K(\cdot, \cdot)$ represents the inner product kernel function in the transformed space. In the present study, a polynomial kernel is used. This kernel represents the similarity of vectors in a feature space over polynomials of the original variables, allowing learning of non-linear models (Goldberg and Elhadad, 2008).

3.4.3. Decision Trees (DT)

DT models predict responses to data and can be viewed as a combination of models in which only one model is responsible for making predictions at any given point in input space. The input space is partitioned into cuboid regions, whose edges are aligned with the axes. For any new input x, the region it falls into is determined by starting at the top of the tree (root node) and following a path down to a specific leaf node according to the decision criteria at each node (Breiman et al., 1984).

4. Results

According to the proposed methodology, we obtained a Cross-ApEn and a Cross-SampEn coupling matrix value per subject and frequency band. These matrices were obtained by averaging results from all artifact-free trials from five-minute recordings of each subject.

4.1. Training set

In order to chose the values for m and r to compute Cross-ApEn and Cross-SampEn, only the training set was used. They were obtained by evaluating all the combinations for $m \in [1, 2]$ and $r \in [0.10, 0.15, 0.20, 0.25]$. Table 3 shows the total number of significant connections among the three groups (FDR-corrected p-values < 0.05, Kruskal-Wallis test) as the sum for all frequency bands for each parameters combination. The results of Table 3 show that Cross-SampEn with $m = 1$ and $r = 0.2$ exhibits the higher number of significant connections. Therefore, we chose that configuration for further analyses.

After determining the optimal metric, FCBF was applied to derive the two optimal sets for binary classifications tasks (HC vs. MCI and HC vs. AD). For this purpose, each connection between two electrodes in every frequency band was interpreted as a feature. Table 4 shows the FCBF-selected features that formed optimal sets for HC vs. MCI and HC vs. AD classification tasks. These sets of features were used to train the QDA, SVM and DT models. For each classifier, two models were trained: one with the aim of classifying MCI and HC subjects, and the other one for AD patients vs. HC subjects comparison.

Table 4: Optimal FCBF sets of features for HC vs. MCI and HC vs. AD comparisons.

	Selected Features			
HC vs. MCI	Fz-T4 (δ)	Cz-C3 (θ)	C4-Fp2 (α)	P3-Fz (β_1)
HC vs. AD	F7-Fp2 (δ)	Fp1-C3 (θ)	T3-T5 (θ)	C3-Pz (γ)

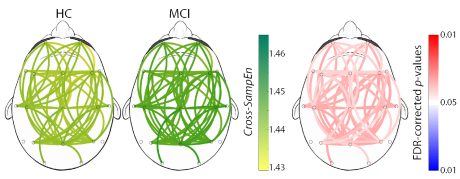

Figure 1: Cross-SampEn results for HC vs. MCI comparison at β_1 band. Left and central columns depict Cross-SampEn values for controls and MCI patients, respectively. Right column displays statistical results, where connections were only displayed when statistically significant differences were obtained (FDR-corrected p-values<0.05, Mann-Whitney U-test). Red color tones indicate significant Cross-SampEn increases in MCI compared with controls, whereas blue color tones denote significant decreases.

4.2. Test set

For the previously chosen measure, Cross-SampEn ($m = 1$, $r = 0.2$), coupling patterns were obtained for the subjects comprised in the test set. Only those frequency bands that showed statistically significant connections are presented in Fig 1 (HC vs. MCI) and Fig 2 (HC vs. AD). In these figures, the left column shows Cross-SampEn values for the healthy group, while the outcomes for patients groups are presented in the center column. Finally, statistically significant connections (FDR-corrected p-values<0.05, Mann-Whitney U-test) between groups are displayed in the right column using the following color-code: red color tones indicate significant Cross-SampEn increases in AD or MCI patients compared to controls, whereas blue color tones denote significant decreases. Note that for all columns, only statistically significant differences are displayed.

Our Cross-SampEn results showed that EEG activity in MCI patients is characterized by an overall similarity decrease in β_1 band, as shown in Fig 1. Additionally, AD patients present significant higher Cross-SampEn values in θ and β_1 frequency bands, as displayed in Fig 2 (a) and (b), respectively.

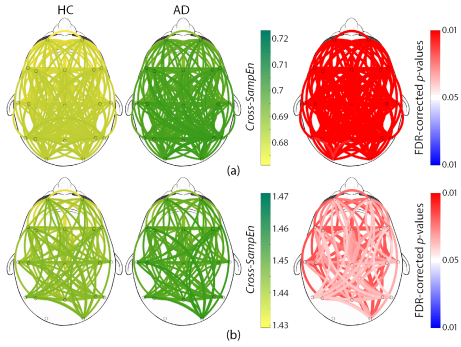

Figure 2: Cross-SampEn results for HC vs. AD comparison (a) at θ band, and (b) at β_1 band. Left and central columns depict Cross-SampEn values for controls and AD patients, respectively. Right column displays statistical results, where connections were only displayed when statistically significant differences were obtained (FDR-corrected p-values$<$0.05, Mann-Whitney U-test). Red color tones indicate significant Cross-SampEn increases in AD compared with controls, whereas blue color tones denote significant decreases.

In order to evaluate the diagnostic ability of the previously trained models (QDA, SVM, and DT), only the test set was used. In the case of the HC vs. MCI classification task, higher diagnostic results were found with SVM and DT ($Acc = 73.53\%$, $Se = 58.82\%$, and $Sp = 88.24\%$), compared with QDA ($Acc = 67.65\%$, $Se = 52.95$, and $Sp = 82.35$). Also SVM and DT reached higher diagnostic performance for the HC vs. AD comparison ($Acc = 82.35\%$, $Se = 70.59\%$, and $Sp = 94.12\%$) compared with QDA ($Acc = 76.47\%$, $Se = 76.47\%$, and $Sp = 76.47\%$). Furthermore, both SVM and DT models present a good diagnostic capability for discriminating when a subject does not suffer AD ($Sp = 94.12\%$ and $NPV = 76.19\%$) and MCI ($Sp = 88.24\%$ and $NPV = 68.18\%$).

5. Discussion

The aim of this study was to assess the performance of Cross-ApEn and Cross-SampEn in order to find abnormal coupling patterns in the early stages of dementia. For that purpose, three main objectives based on the research questions were set.

5.1. Cross-ApEn vs. Cross-SampEn

The first research question was focused on determining whether Cross-SampEn can provide additional information about spontaneous EEG activity in AD and MCI compared to Cross-ApEn.

Only a few studies have applied these metrics to biological systems. For instance, Cross-ApEn has been applied to analyze secretory patterns of luteinizing hormone and testosterone in young and aged healthy men (Pincus and Singer, 1996), concentrations of circulating leptin, luteinizing hormone, and estradiol in healthy women (Licinio et al., 1998), blood oxygen saturation and heart rate signals from nocturnal oximetry (Álvarez et al., 2009) and bihemispheric EEGs from rats (Hudetz et al., 2003). On the other hand, Pritchard *et al.* (Pritchard et al., 2014) applied Cross-SampEn to resting-state fMRI data with the aim of establish functional connectivity between different brain areas. To the best of our knowledge, only Xie *et al.* (Xie et al., 2010) have compared the performance of Cross-ApEn and Cross-SampEn in order to prove the theoretical advantages of the last one. Firstly, they compared both measures quantitatively using five different coupled systems. Then, they applied both measures to a real-life problem in which they analyzed the synchronization patterns of left inter-hemisphere rats' EEG signals. Both analyses showed that Cross-SampEn could be more conveniently applied to different dynamical neural systems contaminated by noise.

Our results using the training set revealed a high number of significant connections among the three groups for all Cross-SampEn combinations with $m = 1$, as shown in Table 3. In our particular case, Cross-SampEn showed statistical differences among the three groups that Cross-ApEn could not detect. Therefore, taking into account that Cross-SampEn shows technical advantages over Cross-ApEn and our results, we could say that Cross-SampEn is more adequate to characterize the neural coupling patters in MCI and AD. Additionally, both metrics show better performances for $m = 1$ compared to $m = 2$. This could be due to the fast nature of EEG fluctuations which could be easier to detect with low values of m. Too large m values are inappropriate for detecting the dynamical changes in EEG recordings (Li et al., 2013). Finally, in order to avoid possible biases, it is important to optimize these configuration parameters for each particular database using a hold-out approach. That is, splitting the original dataset into a training set used to optimize these parameters and a test set used to measure the generalization performance of the metrics, as we have done in the current study.

5.2. Abnormal coupling patterns in MCI and AD

After comparing the usefulness of both measures and determining the optimal configuration, characterization of MCI and AD was assessed. Our Cross-SampEn ($m = 1$, $r = 0.2$) results revealed that MCI and AD groups are characterized by a global decrease of similarity in all frequency bands. However, significant differences were only found in β_1 band for MCI and in θ and β_1 bands for AD.

Previous EEG studies have shown evidences of coupling loss in AD through different connectivity measures. In line with our results, Besthorn *et al.* (Besthorn et al.,

1994) found a coherence decrease in AD, specifically in θ, α and β bands. Synchronization likelihood (*SL*) also showed lower values for AD patients in all frequency bands, but they were statically significant only in the 14–18 and 18–22 Hz bands (corresponding with our β_1 band, approximately) (Stam et al., 2003). Koenig *et al.* (Koenig et al., 2005) analyzed different databases using global field synchrony (*GFS*), finding significant differences in α and β bands. Furthermore, Jeong *et al.* (Jeong et al., 2001) reported lower values of cross-mutual information in AD subjects than in controls, confirming the disconnection syndrome in AD. To the best of our knowledge, only our previous study addressed the characterization AD by means of Cross-SampEn (Gómez et al., 2009), but the whole frequency range (1-40 Hz) was analyzed, instead of dividing it into the classical EEG bands. Our results in this preliminary study suggested that dementia due to AD is characterized by a lower degree of similarity among channels. The current research do not follow the same trend, since AD patients present widespread significant higher Cross-SampEn values in θ and β_1 bands, with long-range connections being more common, since it is one of the main characteristics of pathological aging (Frantzidis et al., 2014a). Several authors have suggested that the observed abnormal coupling patterns may be due to the loss of acetylcholine, long-distance association fibers or gray matter volume (Kikuchi et al., 2000; Francis et al., 1999; Cook and Leuchter, 1996; Cho et al., 2008; Karas et al., 2004). Acetylcholine is a major excitatory modulator of cortical synaptic function and the effect of blocking the cholinergic system is the reduction of resting EEG coupling (Kikuchi et al., 2000; Francis et al., 1999). Additionally, the loss of long distance association fibers produce interhemispheric corticocortical disconnection that could contribute to cognitive impairment (Cook and Leuchter, 1996; Cho et al., 2008). Finally, global and regional gray matter density loss in AD patients indicate an ongoing atrophic process in their brains, that could produce the disconnection between different brain areas (Karas et al., 2004). Other authors suggested that the neuron loss may cause the coupling decrease (Moretti et al., 2011). Nevertheless, if the loss of EEG coupling in AD would simply be caused by a loss of neurons, it would be difficult to understand why all frequencies are not equally affected (Stam et al., 2003).

Despite the fact that MCI studies are less common, a few ones have reported that this pathology is also associated with less connected brain networks. Connectivity decrease in MCI was revealed also by lower *SL* values in δ and α bands (Babiloni et al., 2006). This trend of lower *SL* values for MCI is also present in β band from MEG data (Gómez et al., 2009). Koenig *et al.* (Koenig et al., 2005) showed intermediate *GFS* values between AD and HC for MCI subjects in α and β frequency bands. The aforementioned studies provide evidences for considering MCI as a disconnection syndrome, at least in α and β frequency bands. This inconsistency on the results may be due to the heterogeneity of MCI, different neuroimaging techniques, different coupling measures, or a combination of these factors. Nonetheless, it has been demonstrated that the β band may have a special significance in AD, especially in the early stages. Our results showed that EEG activity in MCI patients is characterized by an overall similarity decrease in β_1 band. Clinically, this reduced coupling may be due to the structural brain changes suffered by patients with MCI: decreased hippocampal volume, atrophy of the medial temporal lobe, or loss of gray matter volume (Karas et al., 2004).

Our findings suggest that EEG signals from different channels are more dissimilar among them in healthy people and they become gradually more similar as dementia progresses. It should be noticed the importance of β as the frequency band where the early changes in prodromal stages of AD are highlighted. Then, as the disease progresses, the abnormal coupling patterns also appear in low frequency bands, mainly at θ band in the current study, but also at α in previous ones (Koenig et al., 2005; Babiloni et al., 2006). These changes reflected the well-known disconnection syndrome and could be associated with both alterations in information processing at the cerebral cortex and to the disturbed synaptic transmission (e.g. decreased levels of acetylcholine), since they are associated with the complex dynamical processing within the brain neural networks (Jeong et al., 2001; Baraniuk et al., 2001).

5.3. Discrimination of MCI and AD patients from HC subjects

In order to evaluate the discrimination ability of Cross-SampEn, three different models (QDA, SVM, and DT) with two optimal set of features were used depending on the classification task (HC vs. MCI or HC vs. AD). Our results showed that the highest classification accuracy for HC vs. AD comparison was obtained using SVM and DT ($Acc = 82.35\%$, $Se = 70.59\%$, and $Sp = 94.12\%$). Also SVM and DT obtained the highest accuracy for the HC vs. MCI classification problem ($Acc = 73.53\%$, $Se = 52.95\%$, and $Sp = 82.35\%$). In our previous study (Ruiz-Gómez et al., 2018), where same training and test sets were used, we obtained precision values of 78.43% and 76.47% for HC vs. All and AD vs. All comparisons using a multi-layer perceptron artificial neural network, respectively. Our accuracy results using cross-entropy metrics are slightly better, but it should be noted that we are using different models for each binary classification instead of one multiclass model as in our previous work. Other previous studies achieved similar precision values, between 76.2% and 87.5% for AD vs. HC, and between 66.7% and 79.2% for MCI vs. HC (Poza et al., 2017, 2014; McBride et al., 2015; Huang et al., 2000). These results should be cautiously interpreted due to the use of different databases, usually with small sample sizes.

5.4. Limitations and future research lines

Despite the promising usefulness of Cross-SampEn as a measure to characterize brain dynamics in AD and its prodromal form, several limitations need to be addressed. Although we had a quite large database composed of 111 subjects, we divided our database to determine the optimal cross-entropy based metric and its configuration parameters that fit better to the characterization of coupling patterns in MCI and AD and to train and validate the models. It would also be possible to determine the optimal metric and its configuration with synthetic EEG signals generated from surrogate data with known dependencies or other models, as Kuramoto models (Acebrón et al., 2005). Moreover, it would be useful to conduct a longitudinal study of MCI subjects to gain a deeper understanding on the complex neural changes provoked by cognitive impairment; this would allow us to classify those with stable MCI and those who progress to AD. Finally, features derived from only one metric (Cross-SampEn) have been applied in this study to discriminate MCI and AD patients from HC subjects. It is noteworthy that in the case we would like to improve the classification ability of the models, features extracted from several other coupling metrics, like *SL*, *GFS*, phase-lag index (*PLI*) or directed transfer function (*DTF*), might also provide complementary information about neuronal alterations in this disorder that would improve the models.

6. Conclusions

This study provides original insights into the characterization of spontaneous neural activity in AD and MCI. Cross-SampEn has proven to be useful to gain a deeper understanding on the complex neural substrates underlying cognitive impairment preceding AD. Our results suggest that MCI and AD are associated with an overall similarity decrease between different brain regions, mainly at β_1 frequency band. Furthermore, optimal FCBF-derived sets of these abnormalities have proved their usefulness to discriminate MCI and AD patients from controls, reaching relatively high accuracy values. These results highlight the usefulness of cross-entropy metrics in order to further understand the underlying brain dynamics in MCI and AD.

Conflict of Interest Statement

The authors declare that the research was conducted in the absence of any commercial or financial relationships that could be construed as a potential conflict of interest.

Author Contributions

Saúl J. Ruiz-Gómez processed the signals, analyzed the data, and wrote the manuscript. Carlos Gómez, Mario Martínez-Zarzuela and Roberto Hornero designed the study and interpreted the results. Jesús Poza interpreted the results. Miguel A. Tola-Arribas and Mónica Cano took part in the diagnosis of subjects and the collection of data. All authors have read and approved the final manuscript.

Funding

This research was supported by 'European Commission' and 'European Regional Development Fund' (FEDER) under project 'Análisis y correlación entre el genoma completo y la actividad cerebral para la ayuda en el diagnóstico de la enfermedad de Alzheimer' ('Cooperation Programme Interreg V-A Spain-Portugal, POCTEP 2014-2020'), and by 'Ministerio de Ciencia, Innovación y Universidades' and FEDER under project DPI2017-84280-R. Saúl J. Ruiz-Gómez has a predoctoral scholarship from the 'Junta de Castilla y León' and European Social Fund.

References

Abásolo, D., Hornero, R., Espino, P., Álvarez, D., Poza, J., 2006. Entropy analysis of the EEG background activity in Alzheimer's disease patients. Physiological Measurement 27 (3), 241–53.

Abásolo, D., Hornero, R., Espino, P., Poza, J., Sánchez, C. I., De La Rosa, R., 2005. Analysis of regularity in the EEG background activity of Alzheimer's disease patients with Approximate Entropy. Clinical Neurophysiology 116 (8), 1826–1834.

Acebrón, J. A., Bonilla, L. L., Vicente, C. J., Ritort, F., Spigler, R., 2005. The Kuramoto model: A simple paradigm for synchronization phenomena. Reviews of Modern Physics.

Albert, M. S., DeKosky, S. T., Dickson, D., Dubois, B., Feldman, H. H., Fox, N. C., Gamst, A., Holtzman, D. M., Jagust, W. J., Petersen, R. C., Snyder, P. J., Carrillo, M. C., Thies, B., Phelps, C. H., 2011. The diagnosis of mild cognitive impairment due to Alzheimer's disease: Recommendations from the National Institute on Aging-Alzheimer's Association workgroups on diagnostic guidelines for Alzheimer's disease. Alzheimer's & Dementia 7, 270–279.

Álvarez, D., Hornero, R., Abásolo, D., Del Campo, F., Zamarrón, C., López, M., 2009. Nonlinear measure of synchrony between blood oxygen saturation and heart rate from nocturnal pulse oximetry in obstructive sleep apnoea syndrome. Physiological Measurement 30 (9), 967–982.

Alzheimer's Association, 2017. 2017 Alzheimer's Disease Facts and Figures. Alzheimers Dement 13, 325–373.

Babiloni, C., Ferri, R., Binetti, G., Cassarino, A., Forno, G. D., Ercolani, M., Ferreri, F., Frisoni, G. B., Lanuzza, B., Miniussi, C., Nobili, F., Rodriguez, G., Rundo, F., Stam, C. J., Musha, T., Vecchio, F., Rossini, P. M., 2006. Fronto-parietal coupling of brain rhythms in mild cognitive impairment: A multicentric EEG study. Brain Research Bulletin 69 (1), 63–73.

Babiloni, C., Ferri, R., Binetti, G., Vecchio, F., Frisoni, G. B., Lanuzza, B., Miniussi, C., Nobili, F., Rodriguez, G., Rundo, F., Cassarino, A., Infarinato, F., Cassetta, E., Salinari, S., Eusebi, F., Rossini, P. M., 2009. Directionality of EEG synchronization in Alzheimer's disease subjects. Neurobiology of Aging 30 (1), 93–102.

Babiloni, C., Lizio, R., Marzano, N., Capotosto, P., Soricelli, A., Triggiani, A. I., Cordone, S., Gesualdo, L., Del Percio, C., 2016. Brain neural synchronization and functional coupling in Alzheimer's disease as revealed by resting state EEG rhythms. International Journal of Psychophysiology 103, 88–102.

Baker, M., Akrofi, K., Schiffer, R., O'Boyle, M. W., 2008. EEG Patterns in Mild Cognitive Impairment (MCI) Patients. The Open Neuroimaging Journal 2 (Mci), 52–55.

Baraniuk, R. G., Flandrin, P., Janssen, A. J., Michel, O. J. J., 2001. Measuring time-frequency information content using the Reényi entropies. IEEE Transactions on Information Theory 47 (4), 1391–1409.

Benjamini, Y., Hochberg, Y., 1995. Controlling the false discovery rate: a practical and powerful approach to multiple testing. Journal of the Royal Statistical Society B 57 (1), 289–300.

Besthorn, C., Förstl, H., Geiger-Kabisch, C., Sattel, H., Gasser, T., Schreiter-Gasser, U., 1994. EEG coherence in Alzheimer disease. Electroencephalography and Clinical Neurophysiology 90 (3), 242–245.

Bishop, C. M., 2007. Pattern Recognition and Machine Learning. Journal of Electronic Imaging 16 (4), 049901.

Breiman, L., Friedman, J. H., Olshen, R. A., Stone, C. J., 1984. Classification and Regression Trees. In: The Wadsworth statisticsprobability series. Wadsworth International Group, Belmont, California.

Cho, H., Dong, W. Y., Young, M. S., Beum, S. K., Yeong, I. K., Young, B. C., Kwang, S. L., Yong, S. S., Yoon, B., Kim, W., Kook, J. A., 2008. Abnormal integrity of corticocortical tracts in mild cognitive impairment: A diffusion tensor imaging study. Journal of Korean Medical Science 23 (3), 477–483.

Chriskos, P., Frantzidis, C. A., Gkivogkli, P. T., Bamidis, P. D., Kourtidou-Papadeli, C., 2018. Achieving Accurate Automatic Sleep Staging on Manually Pre-processed EEG Data Through Synchronization Feature Extraction and Graph Metrics. Frontiers in Human Neuroscience.

Cook, I., Leuchter, F., 1996. Synaptic dysfunction in Alzheimer's disease: clinical assessment using quantitative EEG. Behavioural Brain Research 78 (1), 15–23.

Dauwels, J., Vialatte, F., Cichocki, A., 2010a. Diagnosis of Alzheimer's disease from EEG signals: where are we standing? Curr Alzheimer Res 7 (6), 487–505.

Dauwels, J., Vialatte, F., Musha, T., Cichocki, A., 2010b. A comparative study of synchrony measures for the early diagnosis of Alzheimer's disease based on EEG. NeuroImage 49 (1), 668–693.

Davatzikos, C., Bhatt, P., Shaw, L. M., Batmanghelich, K. N., Trojanowski, J. Q., 2011. Prediction of MCI to AD conversion, via MRI, CSF biomarkers, and pattern classification. Neurobiology of Aging 32 (12).

Ewers, M., Sperling, R. A., Klunk, W. E., Weiner, M. W., Hampel, H., 2011. Neuroimaging markers for the prediction and early diagnosis of Alzheimer's disease dementia. Trends in Neurosciences 34 (8), 430–442.

Francis, P. T., Palmer, A. M., Snape, M., Wilcock, G. K., 1999. The cholinergic hypothesis of Alzheimer's disease: a review of progress. Journal of Neurology, Neurosurgery & Psychiatry 66 (2), 137–147.

Frantzidis, C. A., Ladas, A. K. I., Vivas, A. B., Tsolaki, M., Bamidis, P. D., 2014a. Cognitive and physical training for the elderly: Evaluating outcome efficacy by means of neurophysiological synchronization. International Journal of Psychophysiology.

Frantzidis, C. A., Vivas, A. B., Tsolaki, A., Klados, M. A., Tsolaki, M., Bamidis, P. D., 2014b. Functional disorganization of small-world brain networks in mild Alzheimer's disease and amnestic Mild cognitive impairment: An EEG study using Relative Wavelet Entropy (RWE). Frontiers in Aging Neuroscience 6 (AUG).

Gasser, U. S., Rousson, V., Hentschel, F., Sattel, H., Gasser, T., 2008. Alzheimer disease versus mixed dementias: An EEG perspective. Clinical Neurophysiology 119 (10), 2255–2259.

Goldberg, Y., Elhadad, M., 2008. splitSVM: fast, space-efficient, non-heuristic, polynomial kernel computation for NLP applications. HLT '08: Proceedings of the 46th Annual Meeting of the Association for Computational Linguistics on Human Language Technologies.

Gómez, C., Hornero, R., Abásolo, D., Fernández, A., Escudero, J., 2009. Analysis of MEG background activity in Alzheimer's disease using nonlinear Methods and ANFIS. Annals of Biomedical Engineering 37 (3), 586–594.

Gómez, C., Poza, J., Gomez-Pilar, J., Bachiller, A., Juan-Cruz, C., Tola-Arribas, M. A., Carreres, A., Cano, M., Hornero, R., 2016. Analysis of spontaneous EEG activity in Alzheimer's disease using cross-sample entropy and graph theory. In: Proceedings of the Annual International Conference of the IEEE Engineering in Medicine and Biology Society, EMBS. pp. 2830–2833.

Hornero, R., Escudero, J., Fernández, A., Poza, J., Gómez, C., 2008. Spectral and nonlinear analyses of MEG background activity in patients with Alzheimer's disease. IEEE Transactions on Biomedical Engineering 55 (6), 1658–1665.

Huang, C., Wahlund, L. O., Dierks, T., Julin, P., Winblad, B., Jelic, V., 2000. Discrimination of Alzheimer's disease and mild cognitive impairment by equivalent EEG sources: a cross-sectional and longitudinal study. Clinical Neurophysiology 111 (11), 1961–1967.

Hudetz, A. G., Wood, J. D., Kampine, J. P., 2003. Cholinergic Reversal of Isoflurane Anesthesia in Rats as Measured by Cross-approximate Entropy of the Electroencephalogram. Anesthesiology 99 (5), 1125–1131.

Jeong, J., 2004. EEG dynamics in patients with Alzheimer's disease. Clinical Neurophysiology 115 (7), 1490–1505.

Jeong, J., Gore, J. C., Peterson, B. S., 2001. Mutual information analysis of the EEG in patients with Alzheimer's disease. Clin.Neurophysiol. 112, 827–835.

Karas, G. B., Scheltens, P., Rombouts, S. A. R. B., Visser, P. J., Van Schijndel, R. A., Fox, N. C., Barkhof, F., 2004. Global and local gray matter loss in mild cognitive impairment and Alzheimer's disease. NeuroImage 23 (2), 708–716.

Kikuchi, M., Wada, Y., Koshino, Y., Nanbu, Y., Hashimoto, T., 2000. Effects of Scopolamine on Interhemispheric EEG Coherence in Healthy Subjects: Analysis during Rest and Photic Stimulation. Clinical EEG and Neuroscience 31 (2), 109–115.

Koenig, T., Prichep, L., Dierks, T., Hubl, D., Wahlund, L. O., John, E. R., Jelic, V., 2005. Decreased EEG synchronization in Alzheimer's disease and mild cognitive impairment. Neurobiology of Aging 26 (2), 165–171.

Li, D., Liang, Z., Wang, Y., Hagihira, S., Sleigh, J. W., Li, X., 2013. Parameter selection in permutation entropy for an electroencephalographic measure of isoflurane anesthetic drug effect. Journal of Clinical Monitoring and Computing 27 (2), 113–123.

Licinio, J., Negrão, B., Mantzoros, C., Kaklamani, V., Wong, M. L., Bongiorno, P. B., Mulla, A., Cearnal, L., Veldhuis, J. D., Flier, J. S., McCann, S. M., Gold, P. W., 1998. Synchronicity of frequently sampled, 24-h concentrations of circulating leptin, luteinizing hormone, and estradiol in healthy women. Proceedings of the National Academy of Sciences of the United States of America 95 (5), 2541–2546.

Ludwig, K. A., Miriani, R. M., Langhals, N. B., Joseph, M. D., Anderson, D. J., Kipke, D. R., 2009. Using a Common Average Reference to Improve Cortical Neuron Recordings From Microelectrode Arrays. Journal of Neurophysiology.

Martínez-Zarzuela, M., Gómez, C., Díaz-Pernas, F. J., Fernández, A., Hornero, R., 2013. Cross-Approximate Entropy parallel computation on GPUs for biomedical signal analysis. Application to MEG recordings. Computer Methods and Programs in Biomedicine 112 (1), 189–199.

McBride, J., Zhao, X., Munro, N. B., Jicha, G., Smith, C., Jiang, Y., 2015. Discrimination of mild cognitive impairment and Alzheimer's disease using transfer entropy measures of scalp EEG. Journal of Healthcare Engineering 6 (1), 55–70.

McBride, J. C., Zhao, X., Munro, N. B., Smith, C. D., Jicha, G. A., Hively, L., Broster, L. S., Schmitt, F. A., Kryscio, R. J., Jiang, Y., 2014. Spectral and complexity analysis of scalp EEG characteristics for mild cognitive impairment and early Alzheimer's disease. Computer Methods and Programs in Biomedicine 114 (2), 153–163.

Moretti, D. V., Frisoni, G. B., Binetti, G., Zanetti, O., 2011. Anatomical substrate and scalp EEG markers are correlated in subjects with cognitive impairment and Alzheimer's disease. Frontiers in Psychiatry 1.

Moretti, D. V., Frisoni, G. B., Pievani, M., Rosini, S., Geroldi, C., Binetti, G., Rossini, P. M., 2008. Cerebrovascular disease and hippocampal atrophy are differently linked to functional coupling of brain areas: An EEG coherence study in MCI subjects. Journal of Alzheimer's Disease 14 (3), 285–299.

Petersen, R. C., 2010. Alzheimer's disease: progress in prediction. The Lancet Neurology 9 (1), 4–5.

Pincus, S. M., 1991. Approximate entropy as a measure of system complexity. Proceedings of the National Academy of Sciences of the United States of America 88 (6), 2297–2301.

Pincus, S. M., 2000. Irregularity and asynchrony in biologic network signals. Methods in Enzymology 321, 149–182.

Pincus, S. M., 2001. Assessing Serial Irregularity and Its Implications for Health. Annals of the New York Academy of Sciences 954 (1), 245–

267.
Pincus, S. M., Singer, B. H., 1996. Randomness and degrees of irregularity. Proceedings of the National Academy of Sciences of the United States of America 93 (5), 2083–2088.
Poza, J., Gómez, C., García, M., Corralejo, R., Fernández, A., Hornero, R., 2014. Analysis of neural dynamics in mild cognitive impairment and Alzheimer's disease using wavelet turbulence. Journal of Neural Engineering 11 (2), 026010.
Poza, J., Gómez, C., García, M., Tola-Arribas, M. A., Carreres, A., Cano, M., Hornero, R., 2017. Spatio-Temporal Fluctuations of Neural Dynamics in Mild Cognitive Impairment and Alzheimer's Disease. Current Alzheimer research 14 (9), 924–936.
Pritchard, W. S., Laurienti, P. J., Burdette, J. H., Hayasaka, S., 2014. Functional Brain Networks Formed Using Cross-Sample Entropy Are Scale Free. Brain Connectivity 4 (6), 454–464.
Richman, J. S., Moorman, J. R., 2000. Physiological time-series analysis using approximate entropy and sample entropy. American Journal of Physiology 278 (6), 2039–49.
Ruiz-Gómez, S. J., Gómez, C., Poza, J., Gutiérrez-Tobal, G. C., Tola-Arribas, M. A., Cano, M., Hornero, R., 2018. Automated Multiclass Classification of Spontaneous EEG Activity in Alzheimer's Disease and Mild Cognitive Impairment. Entropy 20 (1), 35.
Spyrou, I. M., Frantzidis, C., Bratsas, C., Antoniou, I., Bamidis, P. D., 2016. Geriatric depression symptoms coexisting with cognitive decline: A comparison of classification methodologies. Biomedical Signal Processing and Control.
Stam, C. J., Van Der Made, Y., Pijnenburg, Y. A. L., Scheltens, P., 2003. EEG synchronization in mild cognitive impairment and Alzheimer's disease. Acta Neurologica Scandinavica 108 (2), 90–96.
Stam, C. J., van Straaten, E. C. W., 2012. The organization of physiological brain networks. Clinical Neurophysiology 123 (6), 1067–1087.
Tóth, B., File, B., Boha, R., Kardos, Z., Hidasi, Z., Gaál, Z. A., Csibri, É., Salacz, P., Stam, C. J., Molnár, M., 2014. EEG network connectivity changes in mild cognitive impairment - Preliminary results. International Journal of Psychophysiology 92 (1), 1–7.
Vapnik, V. N., 1999. An overview of statistical learning theory. IEEE transactions on neural networks / a publication of the IEEE Neural Networks Council.
Vecchio, F., Babiloni, C., 2011. Direction of Information Flow in Alzheimer's Disease and MCI Patients. International Journal of Alzheimer's Disease 2011, 1–7.
Xie, H. B., Guo, J. Y., Zheng, Y. P., 2010. A comparative study of pattern synchronization detection between neural signals using different cross-entropy measures. Biological Cybernetics 102 (2), 123–135.
Yu, L., Liu, H., 2004. Efficient Feature Selection via Analysis of Relevance and Redundancy. Journal of Machine Learning Research 5, 1205–1224.

Computational modeling of the effects of EEG volume conduction on functional connectivity metrics. Application to Alzheimer's disease continuum

Saúl J. Ruiz-Gómez[1], Roberto Hornero[1,2], Jesús Poza[1,2], Aarón Maturana-Candelas[1], Nádia Pinto[3,4,5], Carlos Gómez[1]

[1] *Biomedical Engineering Group, E.T.S.I. Telecomunicación, University of Valladolid, Paseo de Belén 15, 47011, Valladolid, Spain*

[2] *Instituto de Investigación en Matemáticas (IMUVA), University of Valladolid, Paseo de Belén S/N, 47011, Valladolid, Spain*

[3] *IPATIMUP, Instituto de Patologia e Imunologia Molecular da Universidade do Porto, Rua Júlio Amaral de Carvalho 45, 4200-135 Porto, Portugal*

[4] *Instituto de Investigação e Inovação em Saúde, Rua Alfredo Allen 208, 4200-135 Porto, Portugal*

[5] *Center of Mathematics of the University of Porto (CMUP), Rua do Campo Alegre 687, 4169-007 Porto, Portugal*

Journal of Neural Engineering
Volume 16, No. 6, October 2019, Pages 066019

Abstract

Objective. The aim of this study was to evaluate the effect of electroencephalographic (EEG) volume conduction in different measures of functional connectivity and to characterize the EEG coupling alterations at the different stages of dementia due to Alzheimer's disease (AD). *Approach*. Magnitude Squared Coherence (MSCOH), imaginary part of Coherence (iCOH), lagged Coherence (lagCOH), Amplitude Envelope Correlation (AEC), Synchronization Likelihood (SL), Phase Lag Index (PLI), Phase Locking Value (PLV), and corrected imaginary PLV (ciPLV) were applied to: (i) synthetic signals generated with a Kuramoto-based model of several coupled oscillators; and (ii) a resting-state EEG database of real recordings from 51 cognitively healthy controls, 51 mild cognitive impairment (MCI) subjects, 51 mild AD (AD_{mil}) patients, 50 moderate AD (AD_{mod}) patients, and 50 severe AD (AD_{sev}) patients. *Main results*. Our results using synthetic signals showed that PLI was the least affected parameter by spurious influences in a simulated volume conduction environment. Results using real EEG recordings showed that spontaneous activity of MCI patients is characterized by a significant coupling increase in the θ band. As dementia progresses, this increase in the θ band became more pronounced, and a significant widespread decrease in α band appeared at the last stage of dementia. *Significance*. Our results revealed that the estimation of functional EEG connectivity using PLI could reduce the bias introduced by the spurious influence of volume conduction, and it could increase the insight into the underlying brain dynamics at different stages of the AD continuum.

Keywords: Alzheimer's disease, mild cognitive impairment, electroencephalography (EEG), synthetic signals, volume conduction, neural coupling

1. Introduction

The human brain contains billions of interconnected neurons forming a complex network of innumerable connections (Babiloni et al., 2016). These networks are continuously changing and adapting themselves due to external and internal stimuli throughout the entire life span (D'Amelio and Rossini, 2012). Specifically, the combination of different factors, such as synaptic pruning, the neuronal apoptosis, and the loss of cortico-cortical connections, is responsible for physiological brain aging (D'Amelio and Rossini, 2012). However, some physiopathological processes can alter normal brain aging and cause dementia.

Dementia due to Alzheimer's disease (AD) is the most common cause of dementia, with an estimated 60–80% of cases (Alzheimer's Association, 2017). Depending on the affected brain regions and the symptoms, different stages can be distinguished during the course of AD continuum. The initial symptoms of AD are usually preceded by a stage known as mild cognitive impairment due to AD (MCI). MCI subjects exhibit a memory impairment beyond what would be expected for their age, but do not fully accomplish the criteria for dementia diagnosis (Petersen, 2016). Therefore, MCI can be considered a prodromal stage of AD, since previous research has

Email addresses: saul.ruiz@gib.tel.uva.es (Saúl J. Ruiz-Gómez[1]), robhor@tel.uva.es (Roberto Hornero[1,2]), jesus.poza@tel.uva.es (Jesús Poza[1,2]), aaron.maturana@gib.tel.uva.es (Aarón Maturana-Candelas[1]), npinto@ipatimup.pt (Nádia Pinto[3,4,5]), carlos.gomez@tel.uva.es (Carlos Gómez[1])

DOI: https://doi.org/10.1088/1741-2552/ab4024

shown that the conversion rate to AD is approximately 15% per year (Davatzikos et al., 2011), whereas healthy controls develop dementia at a rate of only 1–2% per year (Alzheimer's Association, 2017). Then, in the earliest AD stage, known as mild AD (AD_{mil}), patients may function independently but they show symptoms as reading problems and clear deficits on clinical examination. In the next stage, moderate AD (AD_{mod}), patients require a greater level of care because they show increasingly poor judgment and deepening confusion. Finally, severe AD (AD_{sev}) is the last stage of this disease, in which patients loose the ability to respond to their environment and, eventually, to control movement.

During the last decades, several neuroimaging techniques have been used to detect brain changes associated with neurodegeneration and cognitive decline (Ewers et al., 2011). Methods like functional magnetic resonance imaging (fMRI) and positron emission tomography (PET) have been used to investigate functional and metabolic brain changes in AD and MCI (Martínez et al., 2017; Li et al., 2015). However, fMRI and PET do not offer enough temporal resolution to study real-time brain dynamics. In order to study the dynamical processes involved in complex brain systems, techniques with high temporal resolution, such as electroencephalography (EEG) and magnetoencephalography (MEG), are required (Poza et al., 2014). Specifically, EEG is widely used in clinical settings to take advantage of its low cost and portability compared to MEG. Moreover, EEG has already shown its usefulness to characterize brain dynamics in AD and MCI (Stam et al., 2007; Moretti et al., 2008; Tóth et al., 2014; Ruiz-Gómez et al., 2018).

EEG measures the electrical activity generated by synchronized cortical neuronal pools with electrodes placed at the scalp (Poza et al., 2017). However, these signals suffer from attenuation, expansion and noise contamination when traveling across different surfaces in the head. These effects cause that there is no unique solution when estimating the active neuronal sources in the brain from the time series recorded on the scalp (Stam et al., 2007). This is known as 'volume conduction' problem and can provoke spurious correlations between time series recorded by nearby electrodes, because they are very likely to pick up electrical activity from the same brain sources, even if their are independent (Stam et al., 2007; Schoffelen and Gross, 2009). In order to achieve a correct interpretation of the results, it is important to employ coupling metrics that do not yield significant connectivity estimations between independent sources (Khadem and Hossein-Zadeh, 2014). Consequently, these connectivity estimations are indicators of real brain interactions, minimizing the effect of volume conduction distortion (Ewald et al., 2012).

In order to simulate the neuronal current propagation from the source regions within the brain to the EEG electrodes, several electrical models have been proposed: from simple n-sphere models (in which each concentric spherical region represents different brain layers) to more accurate models based on information from other neuroimaging techniques (Nunez and Srinivasan, 2009). To simulate the source activity, also different procedures have been used, such as dipole generators, potential meshes, and oscillators (Stam et al., 2007; Ahmadi et al., 2019; Nunez and Srinivasan, 2009). The most extended electrical model in EEG source analysis is the boundary element method (BEM) (Mosher et al., 1999). The BEM quasi-analytic solution can be obtained within n-shell geometry using spherical harmonics expansions (SHE) of the electric lead fields (Nolte and Dassios, 2005). On the other hand, finite element based (FEM) approaches use real-head models assuming realistic information of where the different tissues (e.g. skin, skull, cerebrospinal fluid (CSF), gray and white matter) are inside the head (Vorwerk et al., 2014; Cho et al., 2015). However, these methods do not allow the characterization of the influence of volume conduction in coupling estimators, since the simulation of ideal scenarios without volume conduction is not feasible (Stam et al., 2007; Ahmadi et al., 2019). A first approach to evaluate the influence of EEG volume conduction in different connectivity metrics was performed by *Stam et al.* (Stam et al., 2007), and another recent study replicated this one with the same limitations (Ahmadi et al., 2019). In both studies, brain source activity was simulated using the well-known Kuramoto model (Kuramoto, 1975), a set of globally coupled limit-cycle oscillators centered at a single frequency of 10 Hz. This value was selected as it is the predominant frequency in resting-state eyes-closed EEG activity (Stam et al., 2007). To model volume conduction, they proposed three different scenarios of increasing common sources by allowing more than a single oscillator to contribute to each simulated EEG channel (Stam et al., 2007). They conclude that this approach allowed them to test the behavior of various measures under exaggerated effects of volume conduction, but in a quite simple way because modeling realistic sources in a volume conductor is beyond the scope of their study (Stam et al., 2007). Starting from this point, we wanted to go a step further and simulate the brain activity with multiple oscillators centered at different frequencies within all the available EEG spectrum, as well as a more realistic model of the electrical propagation of the electric signals from sources to electrodes.

In the present study, we used the combination of a surface-based computational model of the human head obtained from anatomical cryosection images, and a model of coupled oscillators that simulate the electrical activity of brain sources. Then, two different scenarios were considered: the first one is a volume-conduction free case, while the other one is the real case with volume conduction. This model allows us to quantify how different functional connectivity metrics are affected by volume conduction. In this regard, eight measures, which have been developed to analyze neural connections, were evaluated: Magnitude Squared Coherence

(MSCOH), imaginary part of Coherence (iCOH), lagged Coherence (lagCOH), Amplitude Envelope Correlation (AEC), Synchronization Likelihood (SL), Phase Lag Index (PLI), Phase Locking Value (PLV), and corrected imaginary PLV (ciPLV). Many previous EEG studies have focused on the application of different connectivity metrics, since local activation studies are no longer sufficient for a full characterization of AD brain dynamics (Stam and van Straaten, 2012). Their results support the well-established hypothesis of AD as a 'disconnection syndrome' (D'Amelio and Rossini, 2012), but all these results may be biased due to volume conduction effects. Therefore, the aim of this study was to analyze which functional connectivity measures are able to detect real changes in synchronization without being affected by volume conduction and if they are able to characterize the brain alterations during AD continuum.

2. Materials

2.1. Subjects

In this study, resting-state EEG activity was recorded from a total of 253 subjects: 51 cognitively healthy control (HC) subjects, 51 MCI subjects, 51 AD_{mil} patients, 50 AD_{mod} patients, and 50 AD_{sev} patients. Firstly, information from the recordings of HC subjects, combined with the Kuramoto model and the real-head model, was used to create the synthetic data. Then, all recordings were used to study the neural interactions of the aforementioned stages during AD continuum.

Healthy controls had no pathological background, and underwent a cognitive assessment in order to discard any symptoms of neurological disorder. Patients with MCI and dementia due to AD were diagnosed following the criteria of the National Institute on Aging and Alzheimer's Association (NIA-AA) (McKhann et al., 2011). No significant differences between groups were found in age ($p > 0.05$, Kruskal-Wallis test). Socio-demographic and clinical data are provided in table 1.

This study was carried out in accordance with the recommendations of the Code of Ethics of the World Medical Association with written informed consent from all subjects. All subjects and caregivers gave written informed consent in accordance with the Declaration of Helsinki. The protocol was approved by the Ethics Committee of Porto University (Portugal).

2.2. EEG recordings

For each subject, five minutes of resting-state EEG activity were recorded using a 19-channel system at the electrodes Fp1, Fp2, Fz, F3, F4, F7, F8, Cz, C3, C4, T3, T4, T5, T6, Pz, P3, P4, O1, and O2 following the International System 10-20. Signals were recorded at a sampling frequency of 500 Hz using the Nihon Kohden Neurofax JE-921A system with common average reference (CAR).

Subjects were asked to remain awake with closed eyes during EEG acquisition. For each recording, the same pre-processing procedure was applied (Ruiz-Gómez et al., 2018). It consists of the following steps: (i) digital filtering using a Hamming window bandpass FIR filter in the band of interest (1–70 Hz) and a notch filter to remove the power line frequency interference (50 Hz); (ii) independent component analysis (ICA) to minimize the presence of oculographic, cardiographic, and myographic artifacts; and (iii) selection of 5-s artifact-free epochs by visual inspection.

3. Methods

Our methodology is divided into the following steps:

1. Firstly, the modeling of synthetic signals from the 19 simulated EEG channels is performed. We used a surface-based model built from information of the Visible Human Project® (VHP) dataset (U.S. National Library of Medicine, 2018) (see Section 3.1). The electrical activity of brain sources was simulated using 200 oscillators forming a the Kuramoto model, where each oscillator represents the electrical activity generated by synchronized neuronal pools (see Section 3.2). The amplitude of the oscillators was determined based on the spectral content of HC subjects' EEG activity (see Section 3.3). Then, two different scenarios were simulated: the first one is a volume-conduction free case, while the second one is a simulated case with volume conduction (see Section 3.3).

2. Secondly, the selected eight connectivity metrics (MSCOH, iCOH, lagCOH, AEC, SL, PLI, PLV, and ciPLV) were computed for these two scenarios in order to quantitatively determine which of the analyzed connectivity metrics are able to detect real changes in synchronization without being affected by volume conduction. We used the Two-sample Kolmogorov-Smirnov test for this purpose (see Section 3.5).

3. Finally, for the chosen metrics in the previous step, coupling patterns were obtained for the five groups of our database. Then, statistical differences were evaluated between groups comparing healthy controls with each stage of dementia (MCI, AD_{mil}, AD_{mod}, and AD_{sev}).

3.1. Real-head model

In order to analyze the effect of volume conduction on the different functional connectivity metrics, we simulated synthetic signals using artificial sources inside the brain surface of a real-head model. Surface-based models describe each individual tissue as a triangular surface mesh. In this study, the surface-based computational

Table 1: Socio-demographic and clinical data.

	HC	MCI	AD_{mil}	AD_{mod}	AD_{sev}
Number of subjects	51	51	51	50	50
Age (years) (mean ± SD[a])	80.14 ± 7.09	85.53 ± 7.25	80.69 ± 7.05	81.30 ± 8.04	79.98 ± 7.82
Gender (Male:Female)	26:25	15:36	21:30	7:43	7:43
MMSE[b] (mean ± SD[a])	28.82 ± 1.13	23.33 ± 2.84	22.49 ± 2.27	13.60 ± 2.76	2.42 ± 3.70

[a]SD: standard deviation; [b]MMSE, Mini Mental State Examination score; HC: cognitively healthy control subjects; MCI: Mild Cognitive Impairment patients; AD_{mil}: mild Alzheimer's disease patients; AD_{mod}: moderate Alzheimer's disease patients; AD_{sev}: severe Alzheimer's disease patients.

model of the human head was constructed from the open-source Visible Human Project® (VHP) dataset (U.S. National Library of Medicine, 2018). The VHP dataset contains a large amount of magnetic resonance images, computed tomographies, and anatomical cryosection images from both males and females.

In our particular case, we used a previously created model described at (Makarov et al., 2016). This model is also available online at https://www.wiley.com/legacy/wileychi/makarov/matlab.html and has already been used in different studies to provide insight into the propagation of electromagnetic fields through the human head and transcranial direct current stimulation (Elloian et al., 2014; Noetscher et al., 2014).

This model used anatomical cryosection images from a patient in the construction of the model. These images have a resolution of 2048 x 1216 pixels, which corresponds with a spatial resolution of 0.33 mm. Then, the main structures of the head were identified and hand-segmented using ITK-Snap (Yushkevich et al., 2006). Specifically, the brain, the CSF, the skull, and the skin were identified. The results of this segmentation were very fine meshes with a large number of nodes for each tissue. Then, in order to reduce the computational cost of the simulations, the number of nodes was reduced, eliminating defects and discrepancies.

In this study, 19 simulated EEG electrodes were placed according to the International System 10-20. Thus, the final result of the real-head model is shown in figure 1. The electrical activity produced by synchronized neuronal pools generates electromagnetic waves (in our simulations, the electrical activity of each brain source is simulated with a coupled oscillator of the Kuramoto model). As the electromagnetic waves propagate from sources to electrodes, their amplitudes experience some attenuation. This attenuation defines the rate of amplitude loss of an electromagnetic wave defined by the parameter α (electrical attenuation). For each of the aforementioned modeled tissues, α was assigned according to: $\alpha_{brain} = 0.002726$, $\alpha_{CSF} = 0.016624$, $\alpha_{skull} = 0.001665$, and $\alpha_{skin} = 0.000165$. The procedure to compute α from relative permittivity and electrical conductivity values for each tissue (taken from Hasgal database, available at http://www.itis.ethz.ch/database) is detailed in the Table A of the Supplementary Material.

Once the model was created, the electrical activity of brain sources was simulated using a set of coupled oscillators forming a Kuramoto model.

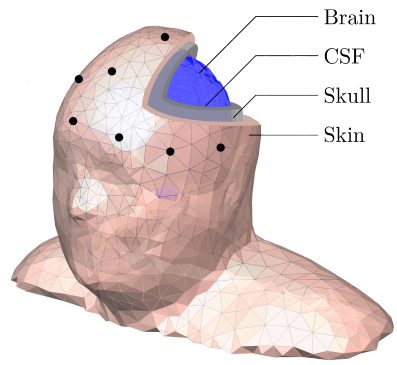

Figure 1: Real-head model from the VHP dataset (U.S. National Library of Medicine, 2018).

3.2. Kuramoto model

The original model proposed by Kuramoto described the phase dynamics of N equally weighted and purely sinusoidal coupled oscillators. The phase dynamics of each oscillator is described by the following differential equation (Kuramoto, 1975):

$$\frac{d\theta_i}{dt} = \omega_i + \frac{K}{N}\sum_{j=1}^{N}\sin(\omega_j - \omega_i), \tag{1}$$

where θ_i represents the phase of the ith oscillator, whose natural frequency is ω_i, and K is the global coupling strength between all oscillators. This equation reflects that the phase evolution of each oscillator is determined by its natural frequency, ω_i, and the average influence of all other oscillators.

The natural frequencies ω_i are distributed according to some unimodal and symmetric probability distribution $g(\omega)$. Thus, the distribution should fulfill that $g(\omega) =$

$g(-\omega)$ for all ω. Typically, Lorentzian distributions centered around ω_0 and with width γ are used to determine these natural frequencies (Strogatz, 2000):

$$g(\omega) = \frac{\gamma}{\pi[\gamma^2 + (\omega - \omega_0)^2]}. \quad (2)$$

The global level of synchronization between the N oscillators that compose the system over time, $r(t)$, is defined as:

$$r(t) = \frac{1}{N}\sum_{j=1}^{N} e^{j\theta_i(t)}. \quad (3)$$

If the model is integrated numerically varying the global coupling K, two different scenarios appear. On one hand, for simulations with K less than a certain threshold K_{crit}, $r(t)$ evolves towards zero. This means that the oscillators act as if they were unsynchronized. On the other hand, when K exceeds K_{crit}, $r(t)$ grows exponentially, reflecting the emergence of a single cluster of synchronized oscillators (Strogatz, 2000). As the natural frequencies are taken from a Lorentzian distribution, this critical value K_{crit} is only determined by the distribution width and is given by $K_{crit} = 2\gamma$ (Stam et al., 2007).

For each oscillator, equation (1) was numerically integrated using the Runge-Kutta method of order 4 (Stam et al., 2007). Then, the state of the i-th oscillator, which was obtained from ω_0, at time t is given by:

$$O_{i,\omega_0}(t) = A_{\omega_0} \sin\theta_i(t), \quad (4)$$

where A_{ω_0} was a constant amplitude for all the oscillators obtained with the same ω_0, but frequency-dependent. The resulting time series represent the electrical activity of the brain sources.

3.3. Model simulations

Many parameters of the previously described Kuramoto model should be set for the simulation of the synthetic EEG signals that represent the electrical activity of the brain sources. Firstly, we divided the available spectrum of the real EEG signals from HC subjects (between 1 and 70 Hz) into spectral bands of 1 Hz wide. Then, we took the central frequencies ω_0 of each oscillator by evaluating the range $f_0 \in [1.5, 69.5]$ Hz (step=1 Hz), as $\omega_0 = 2\pi f$, as described in our previous work (Ruiz-Gómez et al., 2019). For each frequency band, a total number of $N = 200$ oscillators randomly placed inside the brain mesh were simulated, each one representing an active cerebral source. In order to extract analytical results, an infinite number of oscillators is needed, but it has been demonstrated that a limited number of them can be used to explain empirical results (Kiss et al., 2002). Also, this number of brain sources was determined as a trade-off that reduced computational costs and allowed every synthetic electrode to have a closest brain source. Specific oscillation frequencies were determined by a Lorentzian distribution of central frequency ω_0 and width $\gamma = 1$ (Stam et al., 2007; Ahmadi et al., 2019; Ruiz-Gómez et al., 2019).

The state of each oscillator was obtained by numerical integration with a time step of 2 ms (corresponding to a sample frequency of 500 Hz, according to the sample frequency of the real EEG recordings). With the aim of simulating the state of the oscillator $O_{i,\omega_0}(t)$, values of A_{ω_0} were determined as the squared root of the relative power in each 1-Hz frequency band centered at ω_0, only taking into account real EEG recordings.

Then, we simulated two different scenarios:

1. Firstly, an ideal volume-conduction free case in which each source is only registered by the closest EEG electrode. Thus, the voltage $V_j(t)$ of the jth simulated EEG channel at a time t was related to the state $O_{i,\omega_0}(t)$ of the ith oscillator (centered at ω_0) at a time t as:

$$V_j(t) = \sum_{\omega_0}\sum_{i}\sum_{\alpha} O_{i,\omega_0}(t) \cdot e^{-\alpha \cdot d_{i,J}(\alpha)}, \quad (5)$$

with $d_{i,J} = \min(d_{i,j})$ for all j. α represents the electrical attenuation of each modeled tissues of the head, $d_{i,j}$ represents the total distance (in meters) between the simulated brain source i and the simulated EEG electrode j, and $d_{i,J}(\alpha)$ represents the distance (in meters) between the simulated brain source i and the simulated EEG electrode j in the modeled tissue with electrical attenuation α.

2. The second scenario represents the real-case with volume conduction, where each source activity is registered by all simulated EEG electrodes. Therefore, the voltage $V_j(t)$ can be defined as:

$$V_j(t) = \sum_{\omega_0}\sum_{i}\sum_{\alpha} O_{i,\omega_0}(t) \cdot e^{-\alpha \cdot d_{i,j}(\alpha)}, \quad (6)$$

For each value of global coupling K, 300 trials were simulated, resulting 300 time series of 19 simulated channels and 2500 samples. It is noteworthy that in all trials, the initial 5000 samples were discarded to eliminate transitory states of the oscillators.

3.4. Functional connectivity metrics

Functional connectivity between each pair of electrodes was estimated using eight different functional coupling metrics, complementary from the point of view of the inference process: MSCOH, iCOH, lagCOH, AEC, SL, PLI, PLV, and ciPLV.

MSCOH is a well-known method that combines sensitivity to both amplitude and phase synchrony based on the normalized cross-spectral density. Given two time series X and Y two time series (from two different EEG channels), it is defined as (Roach and Mathalon, 2008):

$$\text{MSCOH}_{X,Y} = |\text{COH}_{X,Y}|^2 = \frac{|S_{XY}|^2}{P_X P_Y}, \quad (7)$$

where S_{XY} is the cross-spectrum of X and Y, and P_X and P_Y are the power spectral density of X and Y respectively.

iCOH is the result of the projection of $\text{COH}_{X,Y}$ into the imaginary axis. Its main advantage is that it rules out instantaneous interactions, which may be due to volume conduction (Nolte et al., 2004). Its mathematical formulation reads:

$$\text{iCOH}_{X,Y} = \Im\{\text{COH}_{X,Y}\}, \tag{8}$$

where $\Im\{\cdot\}$ represents the imaginary part.

lagCOH was proposed by Pascual-Marqui *et al.* (Pascual-Marqui et al., 2011) to estimate connectivity between different brain regions removing the instantaneous contribution, which could be mainly due to volume conduction. It is defined as (Pascual-Marqui et al., 2011):

$$\text{lagCOH}_{X,Y} = \frac{[\Im\{S_{X,Y}\}]^2}{S_X S_Y - \Re\{S_{XY}\}^2}, \tag{9}$$

where $\Re\{\cdot\}$ represents the real part.

AEC estimates the correlation of two signals based on their amplitudes. Firstly, time series are orthogonalized for each trial separately (O'Neill et al., 2018). Then, their power envelopes are obtained using the Hilbert transform. Finally, coupling is calculated as the Pearson correlation between the log-transformed power envelopes (Brookes et al., 2014).

SL represents the likelihood that if a system is in the same state at two different times, another system will also be in the same state at these two times. The detailed mathematical procedure to compute SL proposed by Stam *et al.* can be found in (Stam and Van Dijk, 2002).

PLI was also proposed by Stam *et al.* (Stam et al., 2007) to overcome SL limitations and quantifies the asymmetry of the phase difference distributions of two signals. It is non sensitive to shared signals at zero phase lag, and the stronger this nonzero phase locking is, the larger the PLI will be. Mathematically, it is defined as (Stam et al., 2007):

$$\text{PLI}_{X,Y} = |\langle sign \sin(\Delta\phi_{X,Y})\rangle|, \tag{10}$$

where $\langle\cdot\rangle$ indicates the expectation operator and $\Delta\phi_{X,Y}$ is the phase difference or relative phase between signals X and Y.

PLV is a time-dependent connectivity measure that looks for latencies at which the phase difference between the signals varies little across trials (Lachaux et al., 1999). For resting-state data, it is defined as (Mormann et al., 2000):

$$\text{PLV}_{X,Y}(t) = \frac{1}{T}|\sum_{t=1}^{T} e^{-i(\phi_X(t)-\phi_Y(t))}|, \tag{11}$$

where T is the data length and ϕ is the instantaneous phase of the signals X and Y at time t.

ciPLV was proposed by Bruña *et al.* (Bruña et al., 2018) to remove the contribution of the zero phase differences of PLV. Thus, this measure is insensitive to zero-lag effects and it is corrected in a similar way to lagCOH. Mathematically, it is defined as (Bruña et al., 2018):

$$\text{ciPLV}_{X,Y}(t) = \frac{\frac{1}{T}\Im\{e^{-i(\phi_X(t)-\phi_Y(t))}\}}{\sqrt{1-(\frac{1}{T}\Re\{e^{-i(\phi_X(t)-\phi_Y(t))}\})^2}} \tag{12}$$

3.5. Statistical and classification analyses

Firstly, in order to evaluate the influence of volume conduction with synthetic data, Two-sample Kolmogorov-Smirnov test (ks statistic) was used. The lower the values of ks, the lesser the differences between both curves. Specifically, the red curve corresponds to volume-conduction free case and the blue one to the real-case with volume conduction. Therefore, the more similar the curves of volume-conduction free scenario and the real case scenario with volume conduction are, the metric has a better behavior detecting real changes in synchronization without being affected by volume conduction.

Then, an exploratory analysis was carried out to assess the distribution of the coupling values with the real EEG recordings. As our results did not meet the parametric test assumptions of normality (Shapiro-Wilk test) and homoscedasticity (Levene's test), statistical differences between healthy control subjects and the rest of the groups were evaluated with the Mann-Whitney U-test. In order to deal with multiple simultaneous comparisons, a false discovery rate (FDR) controlling procedure was applied (Benjamini and Hochberg, 1995).

Finally, a classification approach using a leave-one-out cross validation procedure was performed to evaluate the clinical value of our metrics. As the characterization of the EEG may lead to the extraction of several redundant features, a feature selection stage based on stepwise multilinear regression with a conditional forward selection approach was included to select an optimal set of features. Afterwards, a linear discriminant analysis (LDA) was used to classify the subjects (Bishop, 2006).

4. Results

4.1. Model simulations

Before any further analyses, we performed a qualitative analysis of the generated synthetic signals comparing them with the real EEG signals in the frequency domain by means of the normalized power spectral density (PSD_n), and in the time domain by visual inspection. Figure 2 displays the grand-averaged PSD_n across trials and all channels for a real HC subject (figure 2.a), and a the grand-averaged PSD_n across trials and all simulated channels for a synthetic signal generated with the Kuramoto model (figure 2.b). Grand averaged PSD_n from real EEG signals and from synthetic signals are very similar.

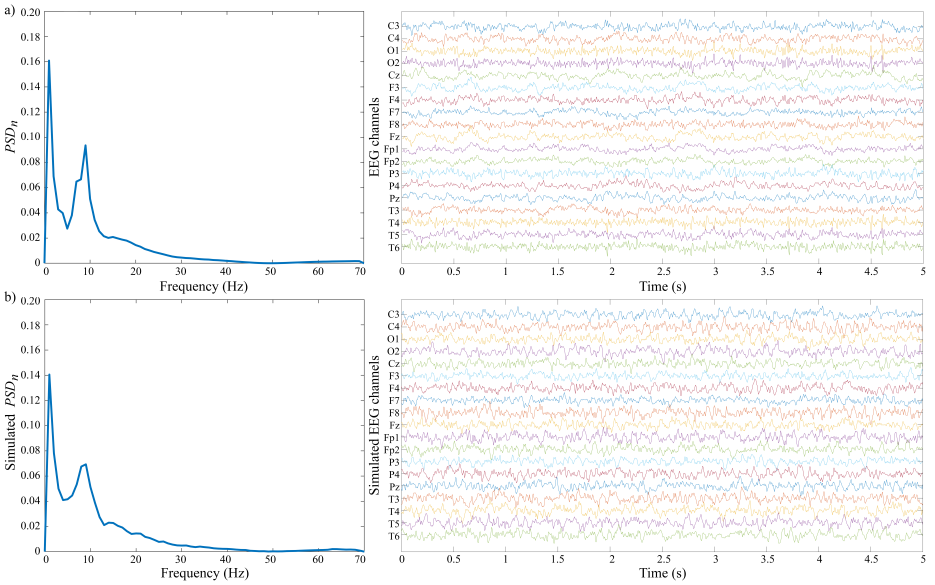

Figure 2: Normalized power spectral density (PSD_n) function grand-averaged over all trials and channels (left panels), and two random 5-s EEG epochs from all EEG channels (right panels): (a) HC subject, and (b) synthetic signal obtained with the Kuramoto model (simulated scenario with volume conduction).

Similarity between real and synthetic signals is also supported by two randomly selected 5-s EEG epochs from all channels, as figure 2 also shows.

Then, in order to determine the coupling metric that is less affected by volume conduction, all metrics were calculated from the time series generated with the Kuramoto model as a function of coupling strength K for the different scenarios. Connectivity results are summarized in figure 3, where the solid lines indicate the average coupling values over all pairs of the 19 simulated channels, and the shaded areas represent the standard deviation of the 300 simulated epochs.

Firstly, the results for MSCOH, iCOH, and lagCOH are shown in figures 3.a, 3.b, and 3.c, respectively. In the scenario without volume conduction, MSCOH stayed constant but higher than 0.2 for K lower than $K_{crit} = 2$ (when the expected value should be 0), and then increased for higher values of K, as expected from theory. When volume conduction was introduced in the second scenario, the resulting curve was shifted toward higher MSCOH values showing that MSCOH was very affected by spurious influences of common sources ($ks = 0.56$). Both iCOH and lagCOH stayed relatively constant around 0.04 and lagCOH stayed constant for K lower than K_{crit}, and then increased for higher values of K in both scenarios. Furthermore, they also were slightly affected by volume conduction ($ks = 0.15$ and $ks = 0.16$, for iCOH and lagCOH respectively).

Secondly, figure 3.d shows that AEC stayed stable around 0.1 for $K < K_{crit}$ in both simulated scenarios. For $K > K_{crit}$, AEC started to increase slowly, never reaching values much higher than 0.2. When volume conduction was introduced, AEC became slightly lower for all values of K. Thus, AEC is slightly underestimating the true level of coupling. Quantitatively, the test statistic ks showed that AEC is not highly affected by volume conduction ($ks = 0.3$).

Thirdly, figures 3.e and 3.f show the SL and PLI results, respectively. In both scenarios, SL values remained very low for $K < K_{crit}$, and slightly increased from K_{crit} onwards. However, SL was the metric most affected by the spurious influences of common sources as the resulting curve was shifted toward higher SL values when volume conduction was introduced, as it showed the highest value of ks, 0.61). Figure 3.f shows the PLI results. In both scenarios, PLI values remained very low for $K < K_{crit}$, and increased from K_{crit} onwards. However, it can be noticed that PLI started to increase at $K = 1.5$, rather than

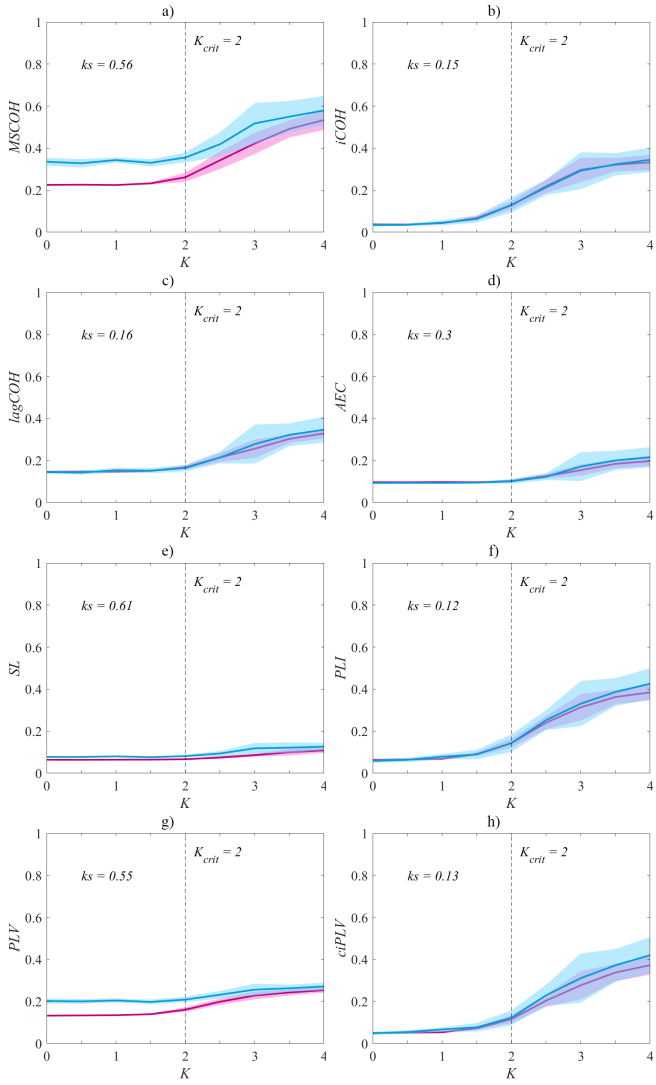

Figure 3: MSCOH, iCOH, lagCOH, AEC, SL, PLI, PLV, and ciPLV values as a function of global coupling intensity (K) for the ideal volume-conduction free scenario (red) and the real-case with volume conduction scenario (blue). The solid lines indicate the average values and the shaded areas represent the standard deviation of the 300 simulated epochs. Two-sample Kolmogorov-Smirnov test values (ks statistic) are specified for each metric.

at the theoretic value of $K_{crit} = 2$. When the influence of volume conduction is added, average PLI values were very similar for $K > K_{crit}$ compared with the volume conduction free scenario. Furthermore, PLI is slightly affected by the spurious influence of volume conduction as revealed by the test statistic ks ($ks = 0.12$).

Finally, the results for PLV and ciPLV are shown in figures 3.g and 3.h, respectively. PLV stayed constant but around 0.15 for K lower than K_{crit} in the scenario without volume conduction, and then slightly increased for higher values of K. For the second scenario, higher PLV values were obtained when oscillators were not coupled. Thus, PLV was very affected by the spurious influences of common sources ($ks = 0.55$). However, ciPLV was able to overcome this limitation minimizing the volume conduction distortion as very similar values for both scenarios were obtained ($ks = 0.13$), starting with values around 0.06 for $K < K_{crit}$, and increasing ciPLV values as K increased.

To summarize, our model simulations showed that the eight analyzed metrics are sensitive to increases in the coupling strength for $K > K_{crit}$. For K values lower than K_{crit}, iCOH, lagCOH, AEC, PLI and ciPLV showed low values of connectivity in both simulated scenarios. However, MSCOH showed higher values compared with PLI (over 0.2 against 0.06) in the volume-conduction free scenario and higher values compared with PLI (around 0.35 against 0.06) under volume conduction conditions. For K higher than K_{crit}, all metrics responded to increases in the coupling strength. MSCOH, SL, and PLV overestimated connectivity and were very affected by spurious influences of volume conduction, while PLI, AEC, and ciPLV were weakly influenced by the simulated volume conduction and underestimated the real coupling level. Quantitatively, the two-sample Kolmogorov-Smirnov test revealed that PLI was the metric least affected by the spurious influence of volume conduction ($ks = 0.12$), although none of the analyzed metrics are immune to it. For these reasons, the subsequent analysis with the real EEG recordings was performed using only PLI.

4.2. Real EEG recordings

For the metric chosen using synthetic data (PLI), coupling patterns were obtained for the five groups of our database. The characterization of the different AD stages was assessed comparing healthy elderly controls with each stage of dementia.

Since results are frequency-dependent, PLI was computed for the six classical EEG-frequency bands: delta (δ, 1-4 Hz), theta (θ, 4-8 Hz), alpha (α, 8-13 Hz), beta-1 (β_1, 13-19 Hz), beta-2 (β_2, 19-30 Hz), and gamma (γ, 30-70 Hz). Connectivity patterns obtained for each frequency band are presented in figure 4. Only statistically significant connections between groups (FDR-corrected p-values$<$0.05, Mann-Whitney U-test) were displayed using the following color-code: red color tones indicated significant PLI increases in patients compared to controls, whereas blue color tones denoted significant decreases.

PLI results showed that EEG activity in MCI subjects is characterized by statistically significant connectivity increases in the θ band when compared to HC subjects, especially for long-distance interhemispheric connections. PLI increases in θ band were also found for the HC vs. AD_{mil} comparison after the FDR correction. Furthermore, some connections in the β_2 band showed significant connectivity decreases for AD_{mil} patients compared with HC subjects. The aforementioned trend of coupling increases in the θ frequency band as the disease progresses continued, reaching its maximum number of significant differences for the comparison between HC subjects and AD_{mod} patients. Additionally, our results revealed that AD_{sev} spontaneous EEG activity is characterized not only by widespread significant increases of PLI values in θ band, but also by an overall decrease of connectivity in α band. Finally, only a few connections showed statistically significant decreases in connectivity in β_2 band for AD_{sev} patients compared with HC subjects.

The combination of stepwise multilinear regression and LDA with a leave-one-out cross-validation procedure was used to assess the diagnostic value of our PLI results. The overall accuracy of the model in the five-class classification task was 41.50% (Cohen's kappa = 0.2688). Our model was also able to determine whether a subject is not healthy with an accuracy of 79.84% (Sensitivity = 86.63%; Positive Predictive Value = 84.85%). Furthermore, the model showed an accuracy of 77.47% when determining whether a subject suffer from AD (Sensitivity = 82.12%; Positive Predictive Value = 81.58%).

5. Discussion

In the present study, we evaluated the behavior of eight different functional connectivity metrics (MSCOH, iCOH, lagCOH, AEC, SL, PLI, PLV, and ciPLV) under the effect of volume conduction and their ability to characterize the brain alterations of the different stages during the AD progression.

5.1. Model simulations

In order to asses the effect of volume conduction and the changes in true synchronization, we used a surface-based computational model of the human head and a set of many coupled oscillators in a Kuramoto model. This combination allowed us to simulate the oscillatory nature of the EEG activity generated by brain sources and recorded at the scalp. The Kuramoto model behavior has been well-studied and it has been previously employed to simulate EEG activity (Stam et al., 2007; Ahmadi et al., 2019). However, in these previous works they modeled volume conduction by allowing various oscillators contribute to each simulated EEG channel, because modeling realistic sources in a volume conductor was beyond the scope of the studies. As they concluded, this

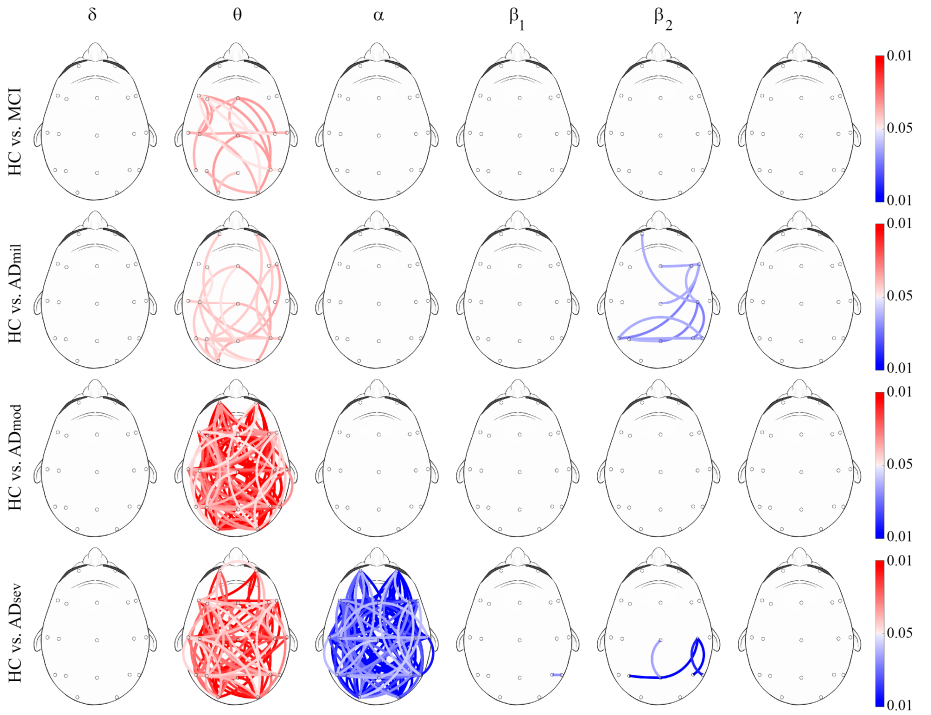

Figure 4: PLI results for each classical EEG-frequency band. Connections between electrodes were only displayed when statistically significant within group differences were obtained (Mann-Whitney U-test, FDR-corrected p-values < 0.05). Red color tones indicate statistically significant connectivity increases in patients compared to controls, whereas blue color tones denote significant decreases.

approximation was quite 'simplistically', but it allowed them for testing the behavior of different coupling metrics under extreme conditions (Stam et al., 2007; Ahmadi et al., 2019). Starting from this point, we wanted to go a step further and simulate the brain activity with multiple oscillators centered at different frequencies within all the available EEG spectrum, as well as a more realistic model of the electrical propagation of the EEG signals from sources to electrodes.

Our connectivity results obtained with the synthetic signals showed that all analyzed metrics responded as expected from theory, reflecting the increases in coupling strength as continuously growing connectivity values for $K > K_{crit}$. Particularly, iCOH, PLI and ciPLV were also able to quantify the synchronization between oscillators with lower K values and the bifurcation point at K_{crit} is less pronounced. Taking into account the lowest and highest coupling values obtained with the models for all these metrics, MSCOH, iCOH, PLI and ciPLV had a relatively high dynamic range. Compared with them, the dynamic ranges of AEC and SL were much smaller, probably because our models were able to simulate a greater phase-based coupling instead of amplitude-based coupling. Qualitatively, when volume conduction was introduced in the simulations, our results showed that these effects were clearly smaller for iCOH, lagCOH, PLI and ciPLV. On the other hand, MSCOH, SL and PLV were strongly influenced by volume conduction, specially for low coupling strength values. After performing the quantitative analysis, it revealed that all eight metrics were not immune to volume conduction but these effects were clearly smaller for PLI. This result is closely related with

the dynamic range of the metrics, since slight variations of lagCOH and AEC due to volume conduction induced higher differences between both scenarios. However, similar variations of PLI produced less differences between scenarios, and it can be interpreted as PLI was less affected by volume conduction.

Comparing metrics from the point of view of the inference process, iCOH and lagCOH were proposed to remove instantaneous contributions, which could be mainly due to volume conduction (Nolte et al., 2004; Pascual-Marqui et al., 2011). Our simulations showed that, as expected, both metrics were less affected by volume conduction compared to MSCOH. PLI was a new metric proposed by *Stam et al*. (Stam et al., 2007) to overcome limitations of SL, a previously described metric proposed also by them (Stam and Van Dijk, 2002). Our results also showed that PLI was able to minimize the effect of volume conduction distortion compared to SL. Following a similar way to remove the contribution of zero phase differences compared to lagCOH, ciPLV was proposed as a PLV modification to overcome its limitations (Bruña et al., 2018). Our results showed that ciPLV stayed less affected by volume conduction distortion compared to PLV. Thus, our simulations proved that the proposed modifications to existing metrics and new proposed measures were less affected by volume conduction compared to the original ones, as expected from theory.

Only a few previous studies tried to analyze the effects of volume conduction in various connectivity metrics simulating the volume conduction problem by means of different methods (Stam et al., 2007; Ahmadi et al., 2019; Khadem and Hossein-Zadeh, 2014; Peraza et al., 2012). Firstly, Stam *et al*. (Stam et al., 2007) used a 'simple' approximation based on linear mixing of Kuramoto oscillators. Then, they evaluated the ability of phase coherence (PC), PLI, and iCOH to remain invariant against the presence of common sources. Their simulations showed that PLI responded to increases in the coupling strength of the oscillator and was less affected by volume conduction than PC and iCOH (Stam et al., 2007). Secondly, Ahmadi *et al*. (Ahmadi et al., 2019) replicated this previous study employing the same model and calculating the same metrics as well others based on the visibility graph algorithms (Lacasa and Toral, 2010). Their simulation results showed that PLI and visibility graph measures could predict the coupling degree correctly even in strongly overlapping environments (Ahmadi et al., 2019). Thirdly, Peraza *et al.* (Peraza et al., 2012) used a simple head model based on four concentric-spheres to simulate the EEG activity at the scalp generated by surrogate sources located at the brain level. Then, they estimated PLI, MSCOH and PC networks and calculated diverse parameters derived from graph theory. Agreeing with our results, they showed that MSCOH and PC were highly affected by volume conduction, while PLI was partially invariant to this effect (Peraza et al., 2012). Finally, Khadem *et al.* (Khadem and Hossein-Zadeh, 2014) tried to discriminate brain interactions and instantaneous linear mixing effects using two surrogate datasets. They ranked the estimated connectivity measures using a proposed sensitivity index, which quantifies the sensitivity of the metric to detect dependencies caused by brain interactions in the presence of instantaneous linear mixing effects (Khadem and Hossein-Zadeh, 2014). Based on this rank and in line with our results, iCOH and PLI (also weighted PLI) showed higher sensitivity levels compared to mutual information and MSCOH.

Therefore, taking into account previous findings and our results, which showed that PLI was the metric least affected by volume conduction effects, we could say that PLI could increase the insight into the underlying neural alterations at the different stages of AD.

5.2. Abnormal coupling patterns in AD progression

After reducing the possible bias that volume conduction could introduce by using PLI as a coupling metric, the characterization of neural changes in the AD progression was assessed. Our PLI results revealed that dementia due to AD is characterized by connectivity increases in low frequency bands and decreases in high frequency bands. Specifically, our results showed that EEG activity in MCI patients is characterized by a coupling increase in the θ band (see figure 4), and a decrease in the α and β_1 bands (see Supplementary Material, figures C and D), with only the connectivity increases being statistically significant. As dementia progresses, this increase in the θ band becomes more pronounced as more connections showed statistical differences. Furthermore, the aforementioned decrease in α band gets statistically significant at the last stage of dementia (AD_{sev}).

Only few previous studies analyzed the EEG connectivity changes in MCI (Tóth et al., 2014; Babiloni et al., 2019). Tóth *et al.* (Tóth et al., 2014) reported PLI decreases in patients diagnosed with an amnestic subtype of MCI at δ (0.5-4 Hz) and α_1 (8-10 Hz) frequency bands. Following the same trend, Babiloni *et al.* (Babiloni et al., 2019) estimated the source distribution of the electrical activity from the surface EEG data, and then they measured the functional connectivity between all regions of interest (ROIs). They reported that patients suffering from MCI due to AD showed statistically significant lower lagged linear connectivity values in the α frequency band, for both interhemispheric and intrahemispheric analyses (Babiloni et al., 2019). Other previous EEG studies have shown evidences of functional connectivity loss for AD patients at the lower α band (8-10 Hz) in the posterior region, taking into account HC and three AD groups (AD_{mil}, AD_{mil}, and AD_{sev}) (Engels et al., 2015). In line with our results, Stam *et al.* (Stam et al., 2009) found similar trends in spontaneous MEG activity of AD patients compared to HC subjects. Their mean PLI values were significantly lower for the AD group in the 8–10 Hz and 13–30 Hz bands. Additionally, their results also showed a non-significant coupling increase in the 4-8 Hz band, which agrees with

our results in the θ band. Caunet *et al.* (Canuet et al., 2012) found that source connectivity patterns between ROIs of AD patients (including AD_{mil}, AD_{mod}, and AD_{sev}, as the AD group) were characterized by a reduction of connectivity (by means of lagged phase synchronization) in the 10-13 Hz band and an increase in the θ band, involving mainly temporal and frontal connections. However, to the best of our knowledge, there is no previous study that analyzed the EEG activity stratifying the AD continuum in four groups from its prodromal form (MCI) to its last stage (AD_{sev}).

The proposed LDA model has shown the ability to detect whether a subject suffers from AD or MCI in 175 out of the 202 non-healthy subjects (Sensitivity = 86.63%), with a positive post-test probability of 87.94%. In addition, the model also showed the ability to confirm AD in 124 out of the 151 subjects suffering from this pathology (Sensitivity = 82.12%), with a positive post-test probability of 81.58%. A previous study carried out a classification approach using the same database and a leave-one-out cross-validation procedure (Maturana-Candelas et al., 2019). They proposed a quadratic discriminant analysis model based on Multiscale Sample Entropy and Refined Multiscale Spectral Entropy results. They obtained a Cohen's kappa value of 0.2541, while our model obtained a slightly higher Cohen's kappa value (0.2688). Thus, our classification results highlight the diagnostic usefulness of our proposal, which might be used as an AD screening strategy.

Clinically, the variation of connectivity metrics reflects the underlying changes in amplitude and phase coupling of different oscillating neuronal populations. A well-known feature during AD continuum is the decrease in connectivity at high frequency bands between both close and distant channels, suggesting functional disconnections among cortical regions (Jeong, 2004). Some studies suggested that these connectivity decreases could be produced by structural brain changes, such as decreased hippocampal volume, atrophy of the medial temporal lobe or neuronal loss (Karas et al., 2004; Cho et al., 2008). Also, the disconnection between different brain areas could be due to global and regional gray matter density loss in AD patients, indicating an ongoing atrophic process in the brain (Karas et al., 2004). Nevertheless, if the loss of neural coupling during neurodegeneration would simply be caused by a loss of neurons, it would be difficult to explain why all frequencies are not equally affected (Stam et al., 2003). Finally, another previous explanation for the observed decreases in α and β frequency bands is the loss of acetylcholine (a major excitatory modulator of cortical synaptic function), which led to the well-known 'cholinergic hypothesis of AD' (Bartus et al., 1982; Francis et al., 1999). In addition, an animal study showed that the loss of acetylcholine results in a decrease in high-frequency coupling and an increase in low-frequency coupling (Villa et al., 2000). Thus, the loss of acetylcholine could support our PLI results, explaining both the connectivity decrease in high frequency bands and the increase in low frequency bands during AD continuum.

5.3. Limitations and future research lines

In spite of the promising performance of PLI as a connectivity metric to detect changes in synchronization under simulated volume conduction conditions and its usefulness to characterize the brain alterations during the different stages of AD continuum, the present study has some limitations.

Firstly, although we analyzed the effect of volume conduction with the combination of a realistic surface-based head model and a model of Kuramoto oscillators, another way to mitigate this effect is to first solve the EEG inverse problem and then estimate functional connectivity between the estimated source activity. Solving the inverse problem could reduce the bias introduced by volume conduction, thus making source-connectivity results a more reliable estimation of the underlying coupling. However, the EEG inverse problem is ill-posed because for admissible output voltages, the solution is non-unique and unstable (the solution is highly sensitive to small changes in the noisy data) (Grech et al., 2008). In most cases, an ill-conditioned equation has to be solved and some methods add spatial weighting of the current estimations at the source positions. These issues influence the estimation of source activity, so their results must be carefully interpreted (Grech et al., 2008).

Secondly, we simulated an isotropic electric propagation from cerebral sources to electrodes for all tissues. Some of the cerebral tissues, such as the white matter and the skull, present anisotropic conduction features that could influence connectivity results. This is an important issue to take into account in future studies, as it could lead to the construction of a more realistic brain model.

Thirdly, eight functional connectivity metrics were applied in this study to characterize their ability to detect real changes in synchronization without being affected by volume conduction. Our results revealed that none of them is immune to the volume conduction, despite these effects were smaller for PLI. Effective coupling metrics (e.g., Granger Causality, Cross-Sample Entropy, Partial Directed Coherence) might also have a similar performances under volume conduction conditions and could provide valuable information about neuronal organization.

Fourthly, even if we had a large database to characterize the brain abnormalities during the AD continuum, it would be useful to conduct a longitudinal study of subjects at early AD stages, such as MCI, to gain a deeper understanding on the complex neural changes of those that progress to AD and those remain stable in the MCI stage. Moreover, it could be also interesting to perform differential predictive diagnoses comparing AD and other neurodegenerative disorders in order to draw further clinical conclusions in future works.

Finally, starting from the weighted networks obtained by means of PLI, a complex analysis based on graph theory metrics could be addressed to characterize functional networks at the different stages of dementia due to AD. Other approaches using sub-networks, such as minimum spanning trees (Tewarie et al., 2015), may also provide valuable insights on the structural and functional organization of neural networks during the AD progression.

6. Conclusions

Our research provides an original approach to the characterization of EEG volume conduction using a real-head model and its effects on eight connectivity measures. We have proven that none of these metrics are immune to volume conduction, but PLI is the least affected. PLI has also proven its usefulness to reflect the neural changes caused by the AD progression in its different stages, from MCI to AD_{sev}. Our results suggest that functional connectivity increases in θ frequency band with increasing disease severity, meanwhile connectivity decreases in α band with the disease progression. Furthermore, we can conclude that all these findings are mainly due to neuronal alterations in dementia because we have used PLI, a metric that is slightly affected by volume conduction effects.

Acknowledgments

This research was supported by 'European Commission' and 'European Regional Development Fund' (FEDER) under project 'Análisis y correlación entre el genoma completo y la actividad cerebral para la ayuda en el diagnóstico de la enfermedad de Alzheimer' ('Cooperation Programme Interreg V-A Spain-Portugal, POCTEP 2014-2020'), by 'Ministerio de Ciencia, Innovación y Universidades' and FEDER under projects PGC2018-098214-A-I00 and DPI2017-84280-R, and by 'Fundação para a Ciência e a Tecnologia/Ministério da Ciência, Tecnologia e Inovação' and FEDER under projects POCI-01-0145-FEDER-007274 and UID/MAT/00144/2013. Saúl J. Ruiz-Gómez was in receipt of a predoctoral scholarship from the 'Junta de Castilla y León' and the 'European Social Fund'.

References

Ahmadi, N., Pei, Y., Pechenizkiy, M., 2019. Effect of linear mixing in EEG on synchronization and complex network measures studied using the Kuramoto model. Physica A: Statistical Mechanics and its Applications 520, 289–308.

Alzheimer's Association, 2017. 2017 Alzheimer's Disease Facts and Figures. Alzheimers Dementia 13, 325–373.

Babiloni, C., Del Percio, C., Pascarelli, M. T., Lizio, R., Noce, G., Lopez, S., Rizzo, M., Ferri, R., Soricelli, A., Nobili, F., Arnaldi, D., Famà, F., Orzi, F., Buttinelli, C., Giubilei, F., Salvetti, M., Cipollini, V., Franciotti, R., Onofrj, M., Stirpe, P., Fuhr, P., Gschwandtner, U., Ransmayr, G., Aarsland, D., Parnetti, L., Farotti, L., Marizzoni, M., D'Antonio, F., De Lena, C., Güntekin, B., Hanoğlu, L., Yener, G., Emek-Savaş, D. D., Triggiani, A. I., Taylor, J. P., McKeith, I., Stocchi, F., Vacca, L., Hampel, H., Frisoni, G. B., De Pandis, M. F., Bonanni, L., 2019. Abnormalities of functional cortical source connectivity of resting-state electroencephalographic alpha rhythms are similar in patients with mild cognitive impairment due to Alzheimer's and Lewy body diseases. Neurobiology of Aging 77, 112–127.

Babiloni, C., Lizio, R., Marzano, N., Capotosto, P., Soricelli, A., Triggiani, A. I., Cordone, S., Gesualdo, L., Del Percio, C., 2016. Brain neural synchronization and functional coupling in Alzheimer's disease as revealed by resting state EEG rhythms. International Journal of Psychophysiology 103, 88–102.

Bartus, R., Dean, R., Beer, B., Lippa, A., 1982. The cholinergic hypothesis of geriatric memory dysfunction. Science 217, 408–414.

Benjamini, Y., Hochberg, Y., 1995. Controlling the false discovery rate: a practical and powerful approach to multiple testing. Journal of the Royal Statistical Society B 57 (1), 289–300.

Bishop, C. M., 2006. Pattern Recognition and Machine Learning. Springer Science & Business Media, New York.

Brookes, M. J., O'Neill, G. C., Hall, E. L., Woolrich, M. W., Baker, A., Palazzo Corner, S., Robson, S. E., Morris, P. G., Barnes, G. R., 2014. Measuring temporal, spectral and spatial changes in electrophysiological brain network connectivity. NeuroImage 91, 282–299.

Bruña, R., Maestú, F., Pereda, E., 2018. Phase locking value revisited: Teaching new tricks to an old dog. Journal of Neural Engineering 15, 056011.

Canuet, L., Tellado, I., Couceiro, V., Fraile, C., Fernandez-Novoa, L., R., I., Takeda, M., 2012. Resting-State Network Disruption and APOE Genotype in Alzheimer's Disease: A lagged Functional Connectivity Study. PLoS ONE 7 (9), 1–12.

Cho, H., Dong, W. Y., Young, M. S., Beum, S. K., Yeong, I. K., Young, B. C., Kwang, S. L., Yong, S. S., Yoon, B., Kim, W., Kook, J. A., 2008. Abnormal integrity of corticocortical tracts in mild cognitive impairment: A diffusion tensor imaging study. Journal of Korean Medical Science 23 (3), 477–483.

Cho, J. H., Vorwerk, J., Wolters, C. H., Knösche, T. R., 2015. Influence of the head model on EEG and MEG source connectivity analyses. NeuroImage 110, 60–77.

D'Amelio, M., Rossini, P. M., 2012. Brain excitability and connectivity of neuronal assemblies in Alzheimer's disease: From animal models to human findings. Progress in Neurobiology 99, 42–60.

Davatzikos, C., Bhatt, P., Shaw, L. M., Batmanghelich, K. N., Trojanowski, J. Q., 2011. Prediction of MCI to AD conversion, via MRI, CSF biomarkers, and pattern classification. Neurobiology of Aging 32 (12), 2322.e19–2322.e27.

Elloian, J. M., Noetscher, G. M., Makarov, S. N., Pascual-Leone, A., 2014. Continuous wave simulations on the propagation of electromagnetic fields through the human head. IEEE Transactions on Biomedical Engineering 61, 1676–1683.

Engels, M. M., Stam, C. J., van der Flier, W. M., Scheltens, P., de Waal, H., van Straaten, E. C., 2015. Declining functional connectivity and changing hub locations in Alzheimer's disease: An EEG study. BMC Neurology 15, 1–8.

Ewald, A., Marzetti, L., Zappasodi, F., Meinecke, F. C., Nolte, G., 2012. Estimating true brain connectivity from EEG/MEG data invariant to linear and static transformations in sensor space. NeuroImage 60, 476–488.

Ewers, M., Sperling, R. A., Klunk, W. E., Weiner, M. W., Hampel, H., 2011. Neuroimaging markers for the prediction and early diagnosis of Alzheimer's disease dementia. Trends in Neurosciences 34 (8), 430–442.

Francis, P. T., Palmer, A. M., Snape, M., Wilcock, G. K., 1999. The cholinergic hypothesis of Alzheimer's disease: A review of progress. Journal of Neurology Neurosurgery and Psychiatry 66, 137–147.

Grech, R., Cassar, T., Muscat, J., Camilleri, K. P., Fabri, S. G., Zervakis, M., Xanthopoulos, P., Sakkalis, V., Vanrumste, B., 2008. Review on solving the inverse problem in EEG source analysis. Journal of NeuroEngineering and Rehabilitation 5 (25), 1–33.

Jeong, J., jul 2004. EEG dynamics in patients with Alzheimer's disease. Clinical Neurophysiology 115 (7), 1490–1505.

Karas, G. B., Scheltens, P., Rombouts, S. A. R. B., Visser, P. J., Van Schijndel, R. A., Fox, N. C., Barkhof, F., 2004. Global and local gray matter

loss in mild cognitive impairment and Alzheimer's disease. NeuroImage 23 (2), 708–716.

Khadem, A., Hossein-Zadeh, G. A., 2014. Quantification of the effects of volume conduction on the EEG/MEG connectivity estimates: An index of sensitivity to brain interactions. Physiological Measurement 35, 2149–2164.

Kiss, I. Z., Zhai, Y., Hudson, J. L., 2002. Emerging coherence in a population of chemical oscillators. Science 296, 1676–1678.

Kuramoto, Y., 1975. Self-entrainment of a population of coupled nonlinear oscillators. In: International Symposium on Mathematical Problems in Theoretical Physics. Vol. 39. Berlin, Heidelberg, pp. 420–422.

Lacasa, L., Toral, R., 2010. Description of stochastic and chaotic series using visibility graphs. Physical Review E - Statistical, Nonlinear, and Soft Matter Physics 82, 036120.

Lachaux, J. P., Rodriguez, E., Martinerie, J., Varela, F. J., 1999. Measuring phase synchrony in brain signals. Human Brain Mapping 8, 194–208.

Li, H. J., Hou, X. H., Liu, H. H., Yue, C. L., He, Y., Zuo, X. N., 2015. Toward systems neuroscience in mild cognitive impairment and Alzheimer's disease: A meta-analysis of 75 fMRI studies. Human Brain Mapping 36, 1217–1232.

Makarov, S. N., Noetscher, G. M., Nazarian, A., 2016. Low-Frequency Electromagnetic Modeling for Electrical and Biological Systems Using MATLAB. John Wiley & Sons, Hoboken, New Jersey.

Martínez, G., Vernooij, R. W., Fuentes Padilla, P., Zamora, J., Flicker, L., Bonfill Cosp, X., 2017. 18F PET with flutemetamol for the early diagnosis of Alzheimer's disease dementia and other dementias in people with mild cognitive impairment (MCI). The Cochrane Database of Systematic Reviews 11, 1–50.

Maturana-Candelas, A., Gómez, C., Poza, J., Pinto, N., Hornero, R., 2019. EEG characterization of the Alzheimer's disease continuum by means of multiscale entropies. Entropy 21 (6), 1–15.

McKhann, G. M., Knopman, D. S., Chertkow, H., Hyman, B. T., Jack, C. R., Kawas, C. H., Klunk, W. E., Koroshetz, W. J., Manly, J. J., Mayeux, R., Mohs, R. C., Morris, J. C., Rossor, M. N., Scheltens, P., Carrillo, M. C., Thies, B., Weintraub, S., Phelps, C. H., 2011. The diagnosis of dementia due to Alzheimer's disease: Recommendations from the National Institute on Aging-Alzheimer's Association workgroups on diagnostic guidelines for Alzheimer's disease. Alzheimer's and Dementia 7, 263–269.

Moretti, D. V., Frisoni, G. B., Pievani, M., Rosini, S., Geroldi, C., Binetti, G., Rossini, P. M., 2008. Cerebrovascular disease and hippocampal atrophy are differently linked to functional coupling of brain areas: An EEG coherence study in MCI subjects. Journal of Alzheimer's Disease 14, 285–299.

Mormann, F., Lehnertz, K., David, P., E. Elger, C., 2000. Mean phase coherence as a measure for phase synchronization and its application to the EEG of epilepsy patients. Physica D: Nonlinear Phenomena 144, 358–369.

Mosher, J. C., Leahy, R. M., Lewis, P. S., 1999. EEG and MEG: Forward solutions for inverse methods. IEEE Transactions on Biomedical Engineering 46, 245–259.

Noetscher, G. M., Yanamadala, J., Makarov, S. N., Pascual-Leone, A., 2014. Comparison of cephalic and extracephalic montages for transcranial direct current stimulation-a numerical study. IEEE Transactions on Biomedical Engineering 61, 2488–2498.

Nolte, G., Bai, O., Wheaton, L., Mari, Z., Vorbach, S., Hallett, M., 2004. Identifying true brain interaction from EEG data using the imaginary part of coherency. Clinical Neurophysiology 115, 2292–2307.

Nolte, G., Dassios, G., 2005. Analytic expansion of the EEG lead field for realistic volume conductors. Physics in Medicine and Biology 50, 3807–3823.

Nunez, P. L., Srinivasan, R., 2009. Electric Fields of the Brain: The neurophysics of EEG, 3rd Edition. Oxford University Press Inc., New York.

O'Neill, G. C., Tewarie, P., Vidaurre, D., Liuzzi, L., Woolrich, M. W., Brookes, M. J., 2018. Dynamics of large-scale electrophysiological networks: A technical review. NeuroImage 180, 559–576.

Pascual-Marqui, R. D., Lehmann, D., Koukkou, M., Kochi, K., Anderer, P., Saletu, B., Tanaka, H., Hirata, K., John, E. R., Prichep, L., Biscay-Lirio, R., Kinoshita, T., 2011. Assessing interactions in the brain with exact low-resolution electromagnetic tomography. Philosophical Transactions of the Royal Society A: Mathematical, Physical and Engineering Sciences 2, 3768–3784.

Peraza, L. R., Asghar, A. U., Green, G., Halliday, D. M., 2012. Volume conduction effects in brain network inference from electroencephalographic recordings using phase lag index. Journal of Neuroscience Methods 207, 189–199.

Petersen, R. C., 2016. Mild cognitive impairment. Continuum (Minneap Minn) 22, 404–418.

Poza, J., Gómez, C., García, M., Corralejo, R., Fernández, A., Hornero, R., 2014. Analysis of neural dynamics in mild cognitive impairment and Alzheimer's disease using wavelet turbulence. Journal of Neural Engineering 11, 26010.

Poza, J., Gómez, C., García, M., Tola-Arribas, M. A., Carreres, A., Cano, M., Hornero, R., aug 2017. Spatio-Temporal Fluctuations of Neural Dynamics in Mild Cognitive Impairment and Alzheimer's Disease. Current Alzheimer Research 14 (9), 924–936.

Roach, B. J., Mathalon, D. H., 2008. Event-related EEG time-frequency analysis: An overview of measures and an analysis of early gamma band phase locking in schizophrenia. Schizophrenia Bulletin 34 (5), 907–926.

Ruiz-Gómez, S. J., Gómez, C., Poza, J., Martínez-Zarzuela, M., Tola-Arribas, M. A., Cano, M., Hornero, R., 2018. Measuring Alterations of Spontaneous EEG Neural Coupling in Alzheimer's Disease and Mild Cognitive Impairment by Means of Cross-Entropy Metrics. Frontiers in Neuroinformatics 12 (76), 1–11.

Ruiz-Gómez, S. J., Gómez, C., Poza, J., Maturana-Candelas, A., Tola-Arribas, M. A., Cano, M., Hornero, R., 2019. Analysis of Volume Conduction Effects on Different Functional Connectivity Metrics: Application to Alzheimer's Disease EEG Signals. Proceedings of the Annual International Conference of the IEEE Engineering in Medicine and Biology Society, EMBS Accepted for publication.

Schoffelen, J. M., Gross, J., 2009. Source connectivity analysis with MEG and EEG. Human Brain Mapping 30, 1857–1865.

Stam, C. J., De Haan, W., Daffertshofer, A., Jones, B. F., Manshanden, I., Van Cappellen Van Walsum, A. M., Montez, T., Verbunt, J. P., De Munck, J. C., Van Dijk, B. W., Berendse, H. W., Scheltens, P., 2009. Graph theoretical analysis of magnetoencephalographic functional connectivity in Alzheimer's disease. Brain 132 (1), 213–224.

Stam, C. J., Nolte, G., Daffertshofer, A., 2007. Phase lag index: Assessment of functional connectivity from multi channel EEG and MEG with diminished bias from common sources. Human Brain Mapping 28, 1178–1193.

Stam, C. J., Van Der Made, Y., Pijnenburg, Y. A. L., Scheltens, P., 2003. EEG synchronization in mild cognitive impairment and Alzheimer's disease. Acta Neurologica Scandinavica 108, 90–96.

Stam, C. J., Van Dijk, B. W., 2002. Synchronization likelihood: An unbiased measure of generalized synchronization in multivariate data sets. Physica D: Nonlinear Phenomena 163, 236–251.

Stam, C. J., van Straaten, E. C., 2012. The organization of physiological brain networks. Clinical Neurophysiology 123 (6), 1067–1087.

Strogatz, S. H., 2000. From Kuramoto to Crawford: Exploring the onset of synchronization in populations of coupled oscillators. Physica D: Nonlinear Phenomena 143, 1–20.

Tewarie, P., van Dellen, E., Hillebrand, A., Stam, C. J., 2015. The minimum spanning tree: An unbiased method for brain network analysis. NeuroImage 104, 177–188.

Tóth, B., File, B., Boha, R., Kardos, Z., Hidasi, Z., Gaál, Z. A., Csibri, É., Salacz, P., Stam, C. J., Molnár, M., 2014. EEG network connectivity changes in mild cognitive impairment - Preliminary results. International Journal of Psychophysiology 92 (1), 1–7.

U.S. National Library of Medicine, 2018. The Visible Human Project.

Villa, A. E., Tetko, I. V., Dutoit, P., Vantini, G., 2000. Non-linear cortico-cortical interactions modulated by cholinergic afferences from the rat basal forebrain. BioSystems 58, 219–228.

Vorwerk, J., Cho, J. H., Rampp, S., Hamer, H., Knösche, T. R., Wolters, C. H., 2014. A guideline for head volume conductor modeling in EEG and MEG. NeuroImage 100, 590–607.

Yushkevich, P. A., Piven, J., Hazlett, H. C., Smith, R. G., Ho, S., Gee, J. C., Gerig, G., 2006. User-guided 3D active contour segmentation of anatomical structures: Significantly improved efficiency and reliability. NeuroImage 31, 1116–1128.

Supplementary material

For the sake of replicability and completeness, additional methodological details and further analyses are included in this supplementary material.

Electrical attenuation

Electrical attenuation is calculated as:

$$\alpha = \omega \left(\frac{\mu \mathcal{E}'}{2} \left[\left(\sqrt{1 + \left(\frac{\mathcal{E}''}{\mathcal{E}'} \right)^2} - 1 \right) \right] \right)^{1/2} \quad (1)$$

with $\mathcal{E}' = \mathcal{E}_r \mathcal{E}_0$, $\mathcal{E}'' = \sigma/\omega$, and $\omega = 2\pi f$. Constant values: $\mathcal{E}_0 = 8.8541 \cdot 10^{-12}$ F/m, $\mu_0 = 4 \cdot \pi \cdot 10 - 7$ H/m, and $\mu_r = 1$.

Relative permittivity ($\mathcal{E}_r$) and electrical conductivity (σ) for all the simulated tissues (brain, CSF, skull annd skin) at 35 Hz are shown in Table A.

Results

Mean PLI results for each group (top panel) and statistically significant connectivity patterns between groups (bottom panel) in the conventional frequency bands are shown in figures A - F.

In the bottom panel, connections between electrodes were only displayed when statistically significant within group differences were obtained (Mann-Whitney U-test, FDR-corrected p-values<0.05). Red color tones indicate statistically significant connectivity increases in patients compared to controls, whereas blue color tones denote significant decreases.

Table A: Dielectric properties for all the simulated tissues (brain, CSF, skull and skin) at 35 Hz.

	Relative Permittivity[a], $\mathcal{E}_r$	**Electrical Conductivity**[a], σ **(S/m)**	**Electrical attenuation,** α **(Np/m)**
Brain	$1.93 \cdot 10^7$	$8.33 \cdot 10^2$	0.002726
CSF	$1.09 \cdot 10^2$	2.00	0.016624
Skull	$1.26 \cdot 10^4$	$2.01 \cdot 10^{-2}$	0.001665
Skin	$1.14 \cdot 10^3$	$2.00 \cdot 10^{-4}$	0.000165

[a] Relative permittivity ($\mathcal{E}_r$) and electrical conductivity (σ) are taken from the Hasgal database (available at http://www.itis.ethz.ch/database).

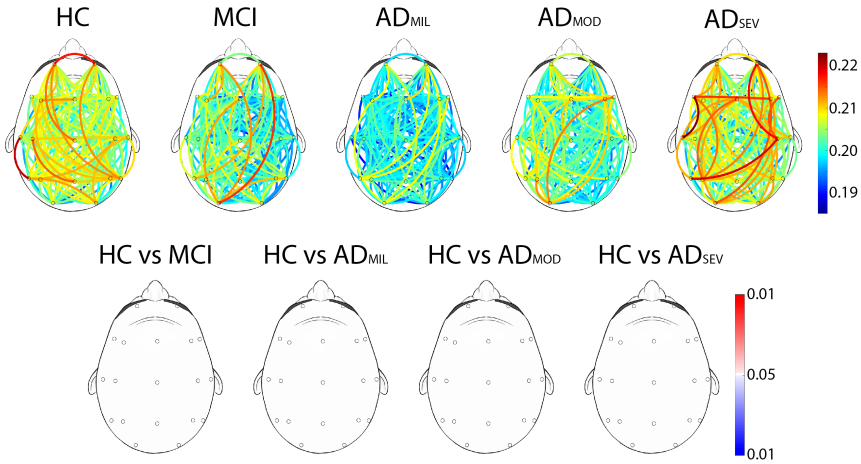

Figure A: Mean PLI results for each group in the δ band (top panel) and statistically significant connectivity patterns between groups (bottom panel). In the bottom panel, connections between electrodes were only displayed when statistically significant within group differences were obtained (Mann-Whitney U-test, FDR-corrected p-values$<$0.05). HC: healthy controls; MCI: mild cognitive impairment subjects; AD_{mil}: mild Alzheimer's disease patients; AD_{mod}: moderate Alzheimer's disease patients; AD_{sev}: severe Alzheimer's disease patients.

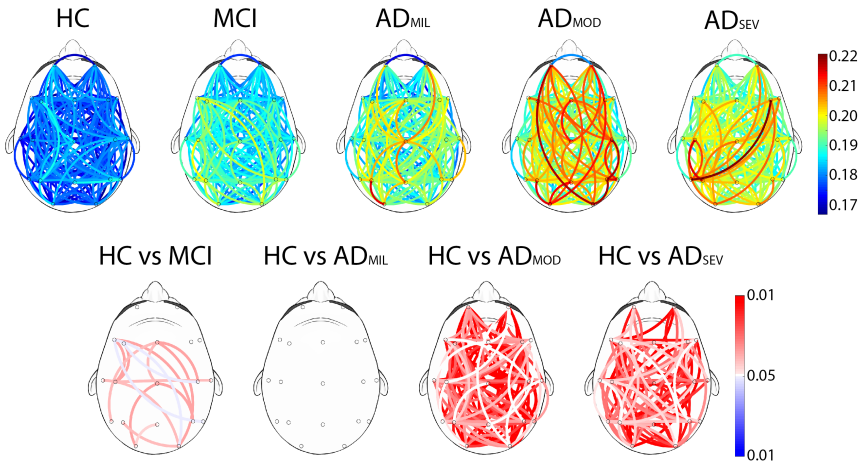

Figure B: Mean PLI results for each group in the θ band (top panel) and statistically significant connectivity patterns between groups (bottom panel). In the bottom panel, connections between electrodes were only displayed when statistically significant within group differences were obtained (Mann-Whitney U-test, FDR-corrected p-values$<$0.05). HC: healthy controls; MCI: mild cognitive impairment subjects; AD_{mil}: mild Alzheimer's disease patients; AD_{mod}: moderate Alzheimer's disease patients; AD_{sev}: severe Alzheimer's disease patients.

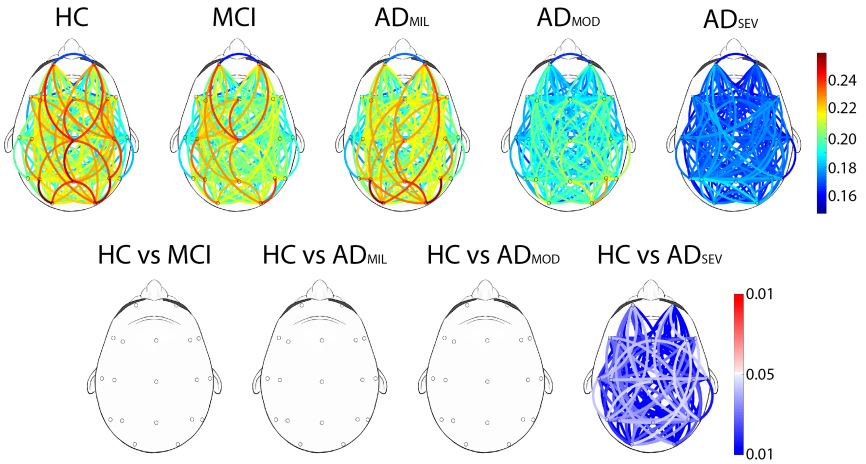

Figure C: Mean PLI results for each group in the α band (top panel) and statistically significant connectivity patterns between groups (bottom panel). In the bottom panel, connections between electrodes were only displayed when statistically significant within group differences were obtained (Mann-Whitney U-test, FDR-corrected p-values$<$0.05). HC: healthy controls; MCI: mild cognitive impairment subjects; AD_{mil}: mild Alzheimer's disease patients; AD_{mod}: moderate Alzheimer's disease patients; AD_{sev}: severe Alzheimer's disease patients.

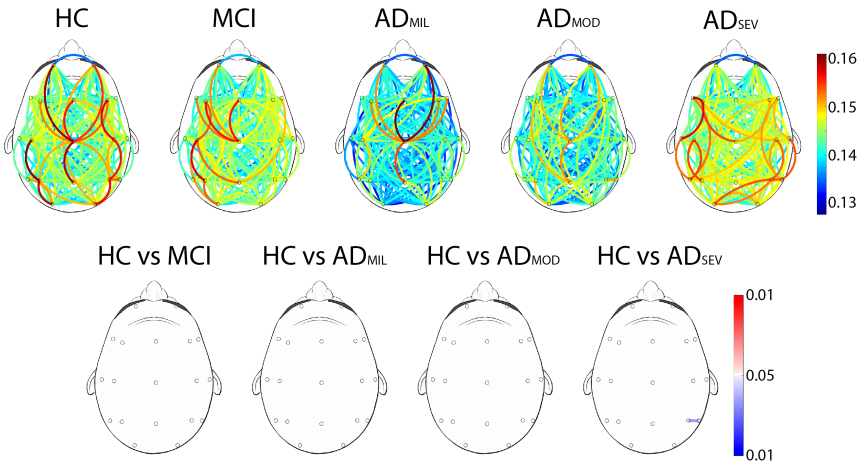

Figure D: Mean PLI results for each group in the β_1 band (top panel) and statistically significant connectivity patterns between groups (bottom panel). In the bottom panel, connections between electrodes were only displayed when statistically significant within group differences were obtained (Mann-Whitney U-test, FDR-corrected p-values$<$0.05). HC: healthy controls; MCI: mild cognitive impairment subjects; AD_{mil}: mild Alzheimer's disease patients; AD_{mod}: moderate Alzheimer's disease patients; AD_{sev}: severe Alzheimer's disease patients.

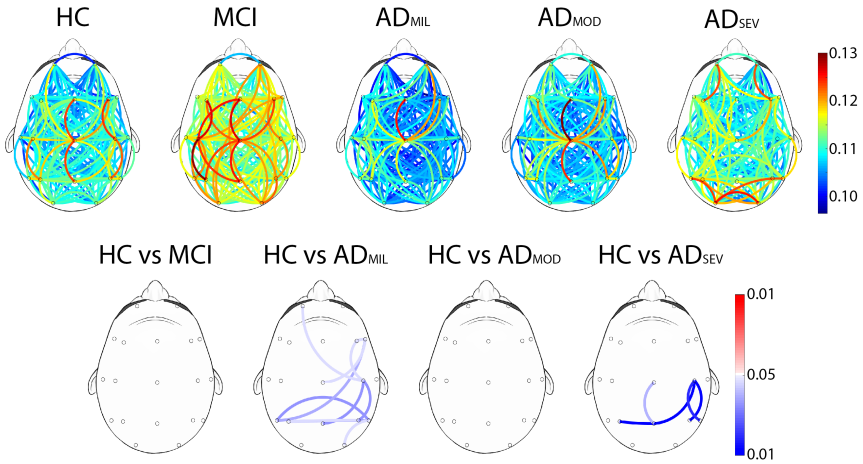

Figure E: Mean PLI results for each group in the β_2 band (top panel) and statistically significant connectivity patterns between groups (bottom panel). In the bottom panel, connections between electrodes were only displayed when statistically significant within group differences were obtained (Mann-Whitney U-test, FDR-corrected p-values$<$0.05). HC: healthy controls; MCI: mild cognitive impairment subjects; AD$_{mil}$: mild Alzheimer's disease patients; AD$_{mod}$: moderate Alzheimer's disease patients; AD$_{sev}$: severe Alzheimer's disease patients.

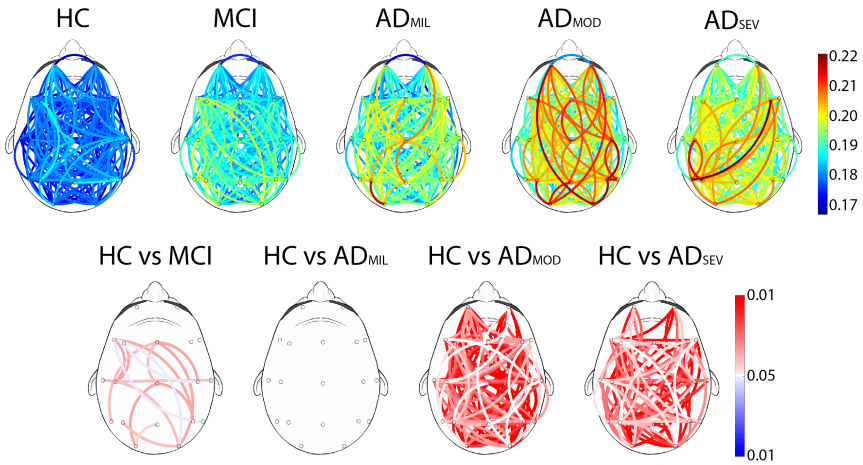

Figure F: Mean PLI results for each group in the γ band (top panel) and statistically significant connectivity patterns between groups (bottom panel). In the bottom panel, connections between electrodes were only displayed when statistically significant within group differences were obtained (Mann-Whitney U-test, FDR-corrected p-values$<$0.05). HC: healthy controls; MCI: mild cognitive impairment subjects; AD$_{mil}$: mild Alzheimer's disease patients; AD$_{mod}$: moderate Alzheimer's disease patients; AD$_{sev}$: severe Alzheimer's disease patients.

A new method to build multiplex networks using Canonical Correlation Analysis for the characterization of the Alzheimer's disease continuum

Saúl J. Ruiz-Gómez[1,2], Roberto Hornero[1,2,3], Jesús Poza[1,2,3], Eduardo Santamaría-Vazquez[1,2], Víctor Rodríguez-González[1,2], Aarón Maturana-Candelas[1,2], Carlos Gómez[1,2]

[1] *Biomedical Engineering Group, E.T.S.I. Telecomunicación, University of Valladolid, Paseo de Belén 15, 47011, Valladolid, Spain*

[2] *Centro de Investigacion Biomedica en Red en Bioingeniería, Biomateriales y Nanomedicina (CIBER-BBN), Instituto de Salud Carlos III, Avenida Monforte de Lemos 3-5, 28029, Madrid, Spain*

[3] *Instituto de Investigación en Matemáticas (IMUVA), University of Valladolid, Paseo de Belén S/N, 47011, Valladolid, Spain*

Journal of Neural Engineering
Volume 18, No. 2, January 2021, Pages 026002

Abstract

Objective. The aim of this study was to solve one of the current limitations for the characterization of the brain network in the Alzheimer's disease (AD) continuum. Nowadays, frequency-dependent approaches have reached contradictory results depending on the frequency band under study, tangling the possible clinical interpretations. *Approach*. To overcome this issue, we proposed a new method to build multiplex networks based on canonical correlation analysis (CCA). Our method determines two basis vectors using the source and electrode-level frequency-specific network parameters for a reference group, and then project the results for the rest of the groups into these hyperplanes to make them comparable. It was applied to: (i) synthetic signals generated with a Kuramoto-based model; and (ii) a resting-state EEG database formed by recordings from 51 cognitively healthy controls, 51 mild cognitive impairment subjects, 51 mild AD patients, 50 moderate AD patients, and 50 severe AD patients. *Main Results*. Our results using synthetic signals showed that the interpretation of the proposed CCA-based multiplex parameters (multiplex strength, multiplex characteristic path length and multiplex clustering coefficient) can be analogous to their frequency-specific counterparts, as they displayed similar behaviors in terms of average connectivity, integration, and segregation. Findings using real EEG recordings revealed that dementia due to AD is characterized by a significant increase in average connectivity, and by a loss of integration and segregation. *Significance*. We can conclude that CCA can be used to build multiplex networks based from frequency-specific results, summarizing all the available information and avoiding the limitations of possible frequency-specific conflicts. Additionally, our method supposes a novel approach for the construction and analysis of multiplex networks during AD continuum.

Keywords: canonical correlation analysis, connectivity, multiplex networks, synthetic signals, electroencephalography (EEG), Alzheimer's disease, mild cognitive impairment

1. Introduction

In terms of graph theory, a network can be defined as a set of elements (nodes) linked by connections or interactions (edges) (Mijalkov et al., 2017). In this regard the human brain can be seen as a dynamic, complex network, where brain regions are the nodes and the connections between them are the edges. Cerebral networks are continuously adapting themselves following external and internal stimuli, as well as physiological sculpture changes during brain maturation and throughout the life span (D'Amelio and Rossini, 2012). However, normal brain aging can be altered by some physiopathological processes, like those associated to neurodegeneration.

Dementia due to Alzheimer's disease (AD) is the most common cause of dementia, accounting for an estimated 60 to 80 % cases (Alzheimer's Association, 2019). Based on current research advances, AD is best conceptualized as a biological and clinical continuum, covering from the preclinical to symptomatic phases of AD. Cognition (including episodic memory, executive function, and verbal fluency) and function (basic and complex activities of daily living) appear to decline in a very subtle way at AD early stages. While the concept of a continuum appears to be more appropriate for the characterization of

Email addresses: saul.ruiz@gib.tel.uva.es (Saúl J. Ruiz-Gómez[1,2]), robhor@tel.uva.es (Roberto Hornero[1,2,3]), jesus.poza@tel.uva.es (Jesús Poza[1,2,3]), eduardo.santamaria@gib.tel.uva.es (Eduardo Santamaría-Vazquez[1,2]), victor.rodriguez@gib.tel.uva.es (Víctor Rodríguez-González[1,2]), aaron.maturana@gib.tel.uva.es (Aarón Maturana-Candelas[1,2]), carlos.gomez@tel.uva.es (Carlos Gómez[1,2])

DOI: https://doi.org/10.1088/1741-2552/abd82c

AD course, some degree of staging has been helpful for clinical purposes. Traditionally, two key stages have been considered: mild cognitive impairment (MCI) due to AD, and dementia due to AD (McKhann et al., 2011; Aisen et al., 2017). MCI is usually considered a prodromal stage of AD in which patients exhibit cognitive deficits, but do not fully accomplish the criteria for dementia diagnosis (Petersen, 2016). Then, depending on the symptoms, AD dementia can be further divided into mild (AD_{mil}), moderate (AD_{mod}), and severe AD (AD_{sev}) (Aisen et al., 2017). Firstly, AD_{mil} patients show clear deficits on clinical examination but they may function independently. In the next stage, AD_{mod} patients suffer increasingly poor judgment and deepening confusion, and require a greater level of care. Finally, AD_{sev} patients are completely dependent as they loose the ability to respond to their environment and to control movement.

Nowadays, AD diagnosis is complex and with a high degree of subjectivity (Alzheimer's Association, 2019). Notwithstanding, whole-brain neuroimaging techniques have shown their potential to study MCI and AD brain alterations, claiming their role as interesting methodologies to find relevant biomarkers and develop new objective diagnostic tools (McBride et al., 2014; Buscema et al., 2015; Poza et al., 2017; Ruiz-Gómez et al., 2018a). Among them, neurophysiological techniques provide the ability to study fast changing neural networks. This is the case of electroencephalography (EEG), which is a brain imaging method that measures the electrical activity generated by synchronized cortical neurons pools (Poza et al., 2017).

EEG has already proven it usefulness to characterize MCI and AD pathophysiological brain dynamics during resting state (Dauwels et al., 2010). Traditionally, three major effects of MCI and AD have been observed from EEG recordings: slowing of the EEG, reduced complexity of EEG signals, and perturbations in EEG connectivity (Dauwels et al., 2010). Based on connectivity results, graphs can be constructed as an abstract representation of the cerebral activity, providing insights into the specific organization of the brain. The organization of these graphs has been quantified using parameters derived from complex network theory in the conventional EEG frequency bands: delta, theta, alpha, beta-1, beta-2, and gamma. Recent functional network studies have reported that AD is mainly associated with a decrease of integration (local information processing) and a increase of segregation (global information processing) (Stam et al., 2009; Afshari and Jalili, 2017). However, previous studies that compared graph properties between AD and healthy control networks in specific frequency bands, using EEG, MEG, and fMRI data, did not report consistent result between them. On one hand, contradictory results depending on the frequency band under analysis were showed. For example, Stam *et al.* reported significant clustering coefficient decreases in alpha, but increases in theta (Stam et al., 2009). The opposite trend was reported for the characteristic path length, with significant increases in alpha and decreases in theta (Stam et al., 2009). This makes difficult to extract conclusions about the alterations that AD neurodegeneration elicits in the global brain network. On the other hand, previous studies also reported inconsistent results between them when studying the same frequency band. Some works that investigated the average clustering coefficient did not find differences between AD and control subjects (Stam et al., 2007a; Lo et al., 2010; Sanz-Arigita et al., 2010), others found significant decreases in AD (Stam et al., 2009; Tijms et al., 2013) and other studies also found an increased clustering in AD (He et al., 2008; Yao et al., 2010; Zhao et al., 2012). This issue also happens with the characteristic path length, as higher values as the disease progresses were reported (Stam et al., 2007a; Lo et al., 2010; He et al., 2008; Yao et al., 2010; Zhao et al., 2012), but also lower values (Sanz-Arigita et al., 2010; Tijms et al., 2013). All these results tangle the possible clinical interpretations about the brain changes provoked by the AD neurodegeneration process. Furthermore, analyzing single layers separately could not capture relevant information of the whole brain network that could be provided by a multiplex approach. Then, analyzing the multiplex network considering the information of all layers together has focused a great attention.

Multiplex network theory has been applied in different real-world multiplex networks, such as social systems (Battiston et al., 2014) and interconnected hyperlink networks (De Domenico et al., 2016). In the case of EEG-based networks, each frequency-specific network (typically: delta, theta, alpha, beta-1, beta-2, and gamma) corresponds to a layer. These layers are interconnected by the links between the same set of electrodes across layers. Different methods have been used to build these multiplex networks: from a simple parameter sum across all frequency-specific layers to more complex approaches (Battiston et al., 2014; Boccaletti et al., 2014; Yu et al., 2017), such as using a quality function to determine the value of the links across the different layers (Kabbara et al., 2018). However, these methods present some limitations. The estimation of multiplex parameters and the comparison between multiplex networks could be biased if the link weights are different across studies (Stam, 2014). Furthermore, these approaches could compensate opposite trends between groups for the analyzed frequency bands and blur the differences between groups.

In this study, we proposed a new approach to build multiplex networks based on Cononical Correlation Analysis (CCA). The proposed method shows several benefits over single-layer methodologies, and over other previously proposed multiplex approaches. Regarding the advantages over single-layer methodologies, results obtained using the proposed method can summarize the available information across all layers in one single value, making the global brain network easier to interpret from the clinical point of view. Having only one value that represents a particular network feature instead of one value

per frequency-band also avoids the problem of contradictory results depending on the frequency band under study, which are commonly obtained in AD studies (Stam et al., 2009; Ruiz-Gómez et al., 2020). With regard to the advantages over previously proposed multiplex approaches, most of them require having the link values between homologous nodes of different layers to build the multiplex network, including those described in the studies of De Domenico, Boccaletti, and Buldú (De Domenico et al., 2016; Boccaletti et al., 2014; Buldú and Porter, 2018). However, these interlayer links are not usually available, as in our study. Other authors have proposed multiplex approaches for scenarios where the interlayer links are not available, such as the sum of the different parameters for each layer (Battiston et al., 2014; Boccaletti et al., 2014). However, considering the results of some previous studies (Stam et al., 2009; Ruiz-Gómez et al., 2020), where opposite trends were reported depending on the frequency band under analysis (e.g., significant clustering coefficient decreases in alpha, but increases in theta), it could be expected that this approach could compensate the opposite trends for the analyzed frequency bands and blur the differences between groups. In our method, the different weights assigned to each layer during the procedure of computing the multiplex parameters are given by an objective procedure (CCA). These weights define the hyperplane where the correlation between source and electrode-level results is maximized and they could be negative, thus avoiding to compensate the aforementioned AD opposite trends in the different frequency bands. CCA has been previously applied as a feature extraction method in Brain Computer Interface applications (Zhang et al., 2018; Santamaría-Vázquez et al., 2019), to investigate the relationship between synchronous neural interactions and cognitive neuropsychological domains in AD patients (Karageorgiou et al., 2012), and to improve the accuracy in coherence estimation by means of weighting (Cui et al., 2018). We propose a new methodology to build multiplex networks based on CCA, which determines the coefficients that maximize the correlation between electrode-level and source-level results. Firstly, in order to evaluate the behavior of the multiplex parameters under controlled coupling conditions, we used our previously published synthetic signals (Ruiz-Gómez et al., 2019), generated by the combination of a surface based computational model of the human head and a model of coupled oscillators. Then, we applied the proposed methodology to real EEG recordings to obtain new multiplex parameters that summarize all the frequency-band information for each subject under study. Therefore, the aim of this study was to analyze how three different CCA multiplex parameters (CCA global strength s_{CCA}, CCA characteristic path length L_{CCA}, and CCA clustering coefficient C_{CCA}) are affected by variations of connectivity using synthetic signals, and if they are able to characterize the brain alterations during AD continuum.

2. Materials

2.1. Synthetic signals

Firstly, in order to analyze the behavior of the new proposed metrics, we used a set of simulated signals using artificial brain sources and a realistic head model previously published by our research group (Ruiz-Gómez et al., 2019). The surface-based model was constructed from the open-source Visible Human Project® (VHP) dataset (U.S. National Library of Medicine, 2018). The brain, the cerebrospinal fluid, the skull, and the skin were identified and hand-segmented using ITK-Snap (Yushkevich et al., 2006). Then, neuronal activity was propagated from synthetic brain sources to 19 simulated EEG electrodes placed following the international 10-20 system.

Once the model was created, the electrical source activity was simulated using a set of coupled oscillators to generate a Kuramoto model by varying the global coupling parameter K. For each value of global coupling K, 300 trials were simulated using 200 oscillators randomly placed inside the brain mesh. This procedure results in 300 time series of 19 simulated channels and 2500 samples. It is noteworthy that in all trials, the initial 5000 samples were discarded to eliminate transitory states of the oscillators. Further details about the generation of these synthetic signals can be found in our previous study (Ruiz-Gómez et al., 2019).

2.2. Real EEG signals

The real dataset formed by 253 resting-state EEG recordings. They were recorded from 51 cognitively healthy control (HC) subjects, 51 MCI subjects, 51 AD_{mil} patients, 50 AD_{mod} patients, and 50 AD_{sev} patients. HC group was composed by elderly subjects with no neurological disorders. On the other hand, patients with MCI and dementia due to AD were diagnosed following the criteria of the National Institute on Aging and Alzheimer's Association (NIA-AA) (McKhann et al., 2011; Albert et al., 2011). The socio-demographic and clinical characteristics of each group are provided in table 1.

For each subject, five minutes of resting state EEG activity were recorded by means of a 19-channel EEG system Nihon Kohden Neurofax JE-921A at a sampling frequency of 500 Hz. The electrodes were placed following the specifications of the international 10–20 system at Fp1, Fp2, Fz, F3, F4, F7, F8, Cz, C3, C4, T3, T4, T5, T6, Pz, P3, P4, O1, and O2. Signals were re-referenced by means of common average referencing. Then, they were preprocessed in three steps (Ruiz-Gómez et al., 2019, 2018b): (i) band-pass digital filtering to limit the spectral content to the wide frequency band between 1 and 70 Hz (Hamming window, filter order 2000, forward and backward filtering) and band-stop digital filtering to remove the 50-Hz noise power (Hamming window, filter order 2000, forward and backward filtering); (ii) independent component analysis

(ICA) to minimize the presence of oculographic, cardiographic, and myographic artifacts; and (iii) selection of 5 s artifact-free epochs by visual inspection.

During the ICA analysis, an average of 2.01 $\pm$ 1.88 (mean $\pm$ standard deviation) components were discarded per subject from a total number of 19 components. After the visual inspection, an average of 38.81 $\pm$ 13.03 5-s artifact-free epochs per subject were considered for further analysis.

3. Methods

Firstly, synthetic signals were used to study the behavior of the CCA multiplex parameters under different connectivity conditions. For this purpose, we performed the following steps:

1. Estimation of connectivity between pair-wise nodes using Phase Lag Index (PLI) (see Section 3.2) at the electrode-level and source-level synthetic signals.
2. Calculation of frequency-specific network parameters: global strength (s), characteristic path length (L), and clustering coefficient (C) were obtained from PLI matrices both at electrode-level and at source-level (see Section 3.3).
3. These electrode and source frequency-specific parameters formed the multidimensional variables to compute CCA. Then, two basis vectors were obtained (electrode-level and source-level) using the less connected synthetic signals, which were computed with $K = 2$ in the Kuramoto model (see Sections 3.4 and 3.5).
4. Finally, in order to make results comparable, network parameters from all groups ($K = 2$, 2.5, 3, and 3.5) were projected onto these hyperplanes computing the linear combination of the frequency-dependent results multiplied by the reference basis vectors.

Then, real EEG signals were used to analyze the trends of the CCA multiplex parameters during AD continuum. This procedure is represented in figure 1, and it is divided into the following steps:

1. Source level signals were reconstructed from real EEG recordings using standardized low resolution brain electromagnetic tomography (sLORETA) (see Section 3.1).
2. Connectivity between pair-wise electrodes was computed using PLI for the real EEG recordings, and between pair-wise Regions of Interest (ROIs) for reconstructed source-level signals (see Section 3.2).
3. The aforementioned frequency-specific network parameters were also obtained from PLI matrices (see Section 3.3).
4. Two basis vectors were obtained (electrode-level and source-level) using only the HC results (see Sections 3.4 and 3.5).
5. Then, results from all groups (HC, MCI, AD_{mil}, AD_{mod}, and AD_{sev}) were projected into these hyperplanes computing the linear combination of the frequency-dependent results multiplied by the reference basis vectors (see Section 3.5).”

It is noteworthy that, in both cases, we only analyzed the source-level results, since source-reconstructed networks are comparable regardless of the EEG recording system configuration. That is, if the Desikan-Killiany atlas is used to reduce signal dimensionality into ROIs, the derived networks will have always 68 nodes. Otherwise, electrode-level networks size depends on the number of acquisition channels, that can vary depending on the configuration. Furthermore, source-level results will allow us to analyze and compare new groups that could have been recorded with different EEG configurations, or even using MEG, with the healthy control group used in this study. This would not be possible if we use the electrode-level results.

3.1. Source reconstruction: sLORETA

Time series at source level from real EEG recordings were obtained using sLORETA, available in Brainstorm (http://neuroimage.usc.edu/brainstorm) (Tadel et al., 2011). sLORETA is based on a model of lineal distributed sources and provides a solution maximizing the correlation between neighboring sources, assuming that nearby neurons are synchronized (Pascual-Marqui, 2002). In addition, sLORETA reduces the errors on the estimated source activity applying some physiological restrictions. sLORETA provides high-dimensionality source-level signals, which were projected in 68 ROIs using the Desikan-Killiany atlas. Technical details of the method are described in (Pascual-Marqui, 2002).

3.2. Connectivity

In order to construct the brain networks, adjacency matrices were computed using PLI. PLI is a connectivity metric proposed by Stam *et al.* (Stam et al., 2007b) that quantifies the phase difference distribution between two time series. The stronger the phase locking is, the larger the PLI will be, except the case of shared signals at zero phase lag (where it is non sensitive). Moreover, our previous work using synthetic signals (Ruiz-Gómez et al., 2019) demonstrated that PLI can detect real changes in synchronization. Additionally, this work also showed that PLI is less affected by the volume conduction problem than other measures, such as magnitude squared coherence, imaginary part of coherence, amplitude envelope correlation, synchronization likelihood, or phase locking value (Ruiz-Gómez et al., 2019).

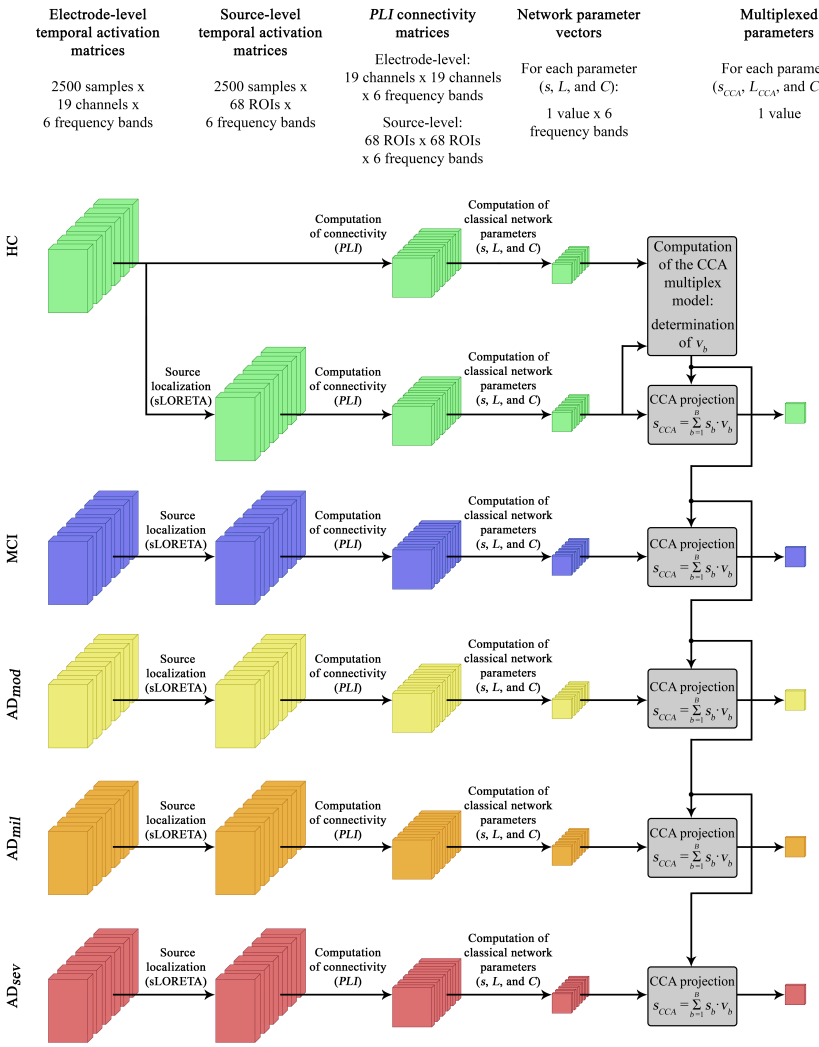

Figure 1: Block diagram of the used methodology with the real EEG signals. It is divided into the following steps: (i) reconstruction of the source-level signals from real EEG recordings (see Section 3.1); (ii) estimation of connectivity between pair-wise nodes (see Section 3.2); (iii) computation of frequency-specific network parameters (see Section 3.3); (iv) Computation of the multiplex model based on CCA: determination of the basis vector (v_b) that defines the reference hyperplane using the healthy control results (see Sections 3.4 and 3.5); (v) CCA projection: projection of the results onto these hyperplanes computing the linear combination of the frequency-dependent results multiplied by the reference basis vectors: $s_{CCA} = \sum_{b=1}^{B} s_b \cdot v_b$ (see Section 3.5).

Table 1: Socio-demographic and clinical data.

	HC	MCI	AD_{mil}	AD_{mod}	AD_{sev}
Number of subjects	51	51	51	50	50
Age (years) (mean ± SD[a])	80.14 ± 7.09	85.53 ± 7.25	80.6 9± 7.05	81.30 ± 8.04	79.98 ± 7.82
Gender (Male:Female)	26:25	15:36	21:30	7:43	7:43
MMSE[b] (mean ± SD[a])	28.82 ± 1.13	23.33 ± 2.84	22.49 ± 2.27	13.60 ± 2.76	2.42 ± 3.70

[a]SD: standard deviation; [b]MMSE, Mini Mental State Examination score; HC: cognitively healthy control subjects; MCI: Mild Cognitive Impairment patients; AD_{mil}: mild Alzheimer's disease patients; AD_{mod}: moderate Alzheimer's disease patients; AD_{sev}: severe Alzheimer's disease patients.

Mathematically, PLI is defined as (Stam et al., 2007b):

$$PLI_{X,Y} = |\langle sign \sin(\Delta\phi_{X,Y})\rangle|, \quad (1)$$

where $\langle\cdot\rangle$ indicates the expectation operator and $\Delta\phi_{X,Y}$ is the phase difference or relative phase between signals X and Y.

PLI was computed for the six conventional EEG-frequency bands: delta (δ, 1-4 Hz), theta (θ, 4-8 Hz), alpha (α, 8-13 Hz), beta-1 (β_1, 13-19 Hz), beta-2 (β_2, 19-30 Hz), and gamma (γ, 30-70 Hz).

3.3. Network parameters

Three network parameters derived from graph theory were computed from PLI matrices to summarize diverse aspects of global and local brain connectivity: global strength (s), characteristic path length (L), and clustering coefficient (C).

s is a basic network metric that is commonly used as a measure of density, representing the total 'wiring cost' of the network (Rubinov and Sporns, 2010). It is computed as the mean number of links connected to the nodes:

$$s = \frac{1}{N}\sum_{i\in N} s_i = \frac{1}{N}\sum_{i\in N}\sum_{j\in N} a_{ij}, \quad (2)$$

where a_{ij} is the PLI value between nodes i and j and N is the total number of nodes.

L is the most commonly used measure of functional integration. Brain integration resumes the ability to combine specialized information from distributed brain regions. Anatomically, paths are sequences of nodes and links that represent potential routes of information flow between different brain regions. Specifically, L is defined as the average shortest path length between all pairs of nodes in the network (Rubinov and Sporns, 2010):

$$L = \frac{1}{N}\sum_{i\in N}\frac{\sum_{j\in N, j\neq i} l_{ij}}{N-1}, \quad (3)$$

where l_{ij} is the shortest path length (distance) between nodes i and j.

C is a simple segregation metric based on the number of triangles in the network. Segregation quantifies the ability of the brain to process information in densely interconnected groups of brain regions. Mathematically, C reflects the prevalence of clustered connectivity around individual nodes and represents the fraction of the node neighbors that are also neighbors of each other (Rubinov and Sporns, 2010):

$$C = \frac{1}{N}\sum_{i\in N}\frac{2t_i}{s_i(s_i-1)}, \quad (4)$$

where t_i is the geometric mean of triangles around node i and s_i is the strength of a node i.

Since PLI results are frequency dependent, one value for every network parameter was obtained for each of the previously defined frequency bands. These frequency-specific values were then used to compute the multiplex parameters by means of CCA.

3.4. Canonical Correlation Analysis (CCA)

CCA is a statistical method for measuring the linear relationship between two datasets of multidimensional variables $X \in \Re^{m\times N}$ and $Y \in \Re^{n\times N}$, where N is the number of observations which must be the same for both datasets, and m and n are the number of variables in each dataset, respectively (Jobson, 2012). CCA can be defined as the problem of finding two sets of basis vectors $w \in \Re^{m\times 1}$ and $v \in \Re^{n\times 1}$, such that the correlations between the projections of the variables onto these basis vectors are mutually maximized (Jobson, 2012):

$$\rho = \arg\max_{w,v} \frac{w^T X Y^T v}{\sqrt{w^T X X^T w}\sqrt{v^T Y Y^T v}} \quad (5)$$

3.5. CCA: A new way to build multiplex networks

In this study, we propose to use the basis vectors obtained with CCA to reduce the frequency band dimensionality of every network parameter and to obtain multiplex metrics. Specifically, electrode and source-level network parameters in every frequency band formed the two datasets of multidimensional variables: $X, Y \in \Re^{B\times N}$ and $w, v \in \Re^{B\times 1}$ where N is the number of observations, and $B = 6$ corresponds to the six conventional EEG frequency bands. Then, we computed new CCA multiplex parameters as the projection of the results onto these hyperplanes, which is equivalent to compute the linear combination of the frequency-dependent results multiplied by the basis vectors. In terms of notation, our new CCA multiplex parameters are defined as s_{CCA}, L_{CCA}, and C_{CCA} corresponding to those obtained from the classical measures in each frequency band s, L, and C, respectively.

Mathematically, s_{CCA} is defined as:

$$s_{CCA} = \sum_{b=1}^{B} s_b \cdot v_b, \quad (6)$$

where s_b is the value of s in the bth frequency band and v_b is the bth value of the basis vectors obtained with CCA. L_{CCA} and C_{CCA} can be defined analogously.

3.6. Statistical analysis

For both analyses, an exploratory analysis was carried out to assess the distribution of the CCA multiplex values with the synthetic and real EEG recordings. As our results did not meet the parametric test assumptions of normality (Shapiro-Wilk test) and homoscedasticity (Levene's test), statistical differences between groups were evaluated with the Mann-Whitney U-test.

4. Results

4.1. Synthetic signals

In order to analyze the behavior of the new CCA multiplex parameters depending on the level of connectivity, they were calculated from the time series generated with the Kuramoto model. Firstly, we calculated the source-level basis vector for each network parameter obtained with the less connected signals and then projected the results from the rest of the groups onto these hyperplanes.

Distribution results for s_{CCA}, L_{CCA}, and C_{CCA} using synthetic signals are shown in figures 2(a)-(c), respectively. Firstly, our s_{CCA} results revealed an increasing trend as connectivity increases. It is also possible to observe that differences between consecutive groups are getting larger as the Kuramoto global coupling parameter (K) increases. This trend is similar to the one expected for the classical network parameter s: as connectivity increases, networks are more connected and the values of s become higher. Secondly, L_{CCA} followed the opposite trend, as L_{CCA} results were smaller for higher values of global coupling. These results are in line with the one expected for L, as connectivity increases will lead to more integrated networks, associated with lower values of L. Finally, our results using C_{CCA} showed a growing trend as connectivity increases. This increasing segregation trend was also supported by the expected values of C for each frequency band. With higher connected nodes, more segregated networks will be obtained, since more node neighbors could be also neighbors of each other.

To sum up, our proposed method provides results that are able to summarize the available information across all layers in one single value, overcoming the existing problems derived from the traditional frequency-dependent network analysis. Additionally, the proposed multiplex parameters followed a similar behavior compared with the classical network parameters. Then, they can be interpreted in similar network terms: multiplex global average connectivity for s_{CCA}, multiplex network integration for L_{CCA}, and multiplex network segregation for C_{CCA}.

4.2. Real EEG recordings

The distribution plots for s_{CCA}, L_{CCA}, and C_{CCA} obtained using the real EEG recordings from HC and the different AD severity groups are displayed in figure 3. Statistically significant differences between groups (p-values $<$ 0.05, Mann–Whitney U-test) are also displayed.

Firstly, in the case of s_{CCA}, our results showed that HC subjects displayed low average connectivity levels and they rise as the disease progresses, excluding the case of AD_{mil} that had the lowest connectivity values. Mann-Whitney U-tests revealed that the AD_{sev} group could be differentiated from the rest of the groups, as statistically significant differences were found for all these comparisons. Significant differences between AD_{mil} and AD_{mod} s_{CCA} values were also found. Secondly, L_{CCA} results showed slightly higher values as dementia severity increases, being only statistically significant for HC vs AD_{sev} comparison. Finally, C_{CCA} results revealed more segregated multiplex networks as the disease progresses, as it showed a decreasing trend from HC subject to AD_{sev} patients. Only AD_{mil} were slightly shifted up from this trend. The Mann-Whitney U-tests revealed statistically significant differences between AD_{sev} patients and all the rest of the groups, HC subjects vs. AD_{mod}, and AD_{mil} vs. AD_{mod} comparisons.

5. Discussion

In the present study, we proposed a new methodology to build multiplex networks based on CCA. Additionally, we evaluated the behavior of these new metrics using synthetic signals varying their connectivity, and we analyzed their ability to characterize the brain network alterations during the different stages of AD continuum.

5.1. CCA multiplex network parameter interpretations

In order to asses the interpretation of the new CCA-based multiplex network parameters, a set of synthetic signals was used. This approach allowed us to study the behavior of the proposed multiplex parameters (s_{CCA}, L_{CCA}, and C_{CCA}) in different connectivity scenarios and relate them with their frequency-specific counterparts. Previous studies have evaluated the performance of various connectivity metrics by simulating different scenarios with the well-studied Kuramoto model (Ruiz-Gómez et al., 2019; Stam et al., 2007b; Moretti et al., 2008). To the best of our knowledge, no previous work has analyzed the performance of frequency-specific network parameters nor multiplex ones.

In the frequency-specific case, the strength represents the sum of the weighted links connected to that node (Rubinov and Sporns, 2010). Then, the global strength s is most commonly used as a measure of density, with higher values for more connected networks (Rubinov and Sporns, 2010). Our results using s_{CCA} followed the

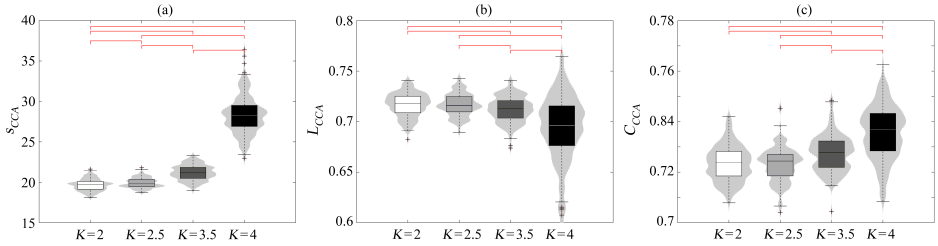

Figure 2: s_{CCA}, L_{CCA}, and C_{CCA} value distributions obtained using synthetic signals as a function of the Kuramoto model global coupling intensity (K). Statistically significant pairwise differences are marked with red brackets ($p < 0.05$, Mann-Whitney U-test).

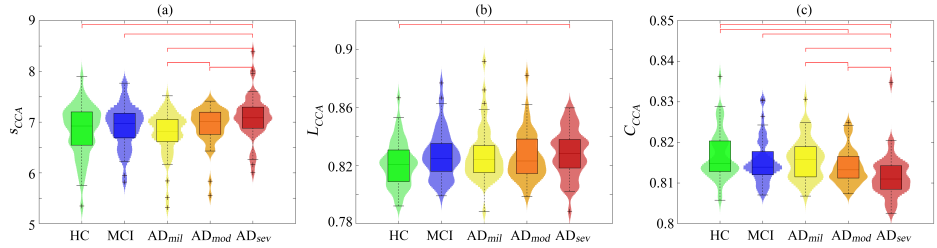

Figure 3: s_{CCA}, L_{CCA}, and C_{CCA} value distributions obtained using real EEG recordings from subjects at different stages of AD continuum: HC subjects, MCI patients, AD_{mil} patients, AD_{mod} patients, and AD_{sev} patients. Statistically significant pairwise differences are marked with red brackets ($p < 0.05$, Mann-Whitney U-test).

same trend, showing bigger increases between consecutive groups as connectivity grows. Thus, the interpretation of the CCA-based multiplex parameter obtained from s can be analogous to the frequency-specific metric.

The characteristic path length L is most commonly used integration metric and measures the average shortest path length between all pair-wise nodes (Rubinov and Sporns, 2010; Watts and Strogatz, 1998). Theoretically, more disconnected networks lead to higher values of L. In the extreme case, paths between disconnected nodes are defined to have infinite length (Rubinov and Sporns, 2010). This trend is also observed for our multiplex L_{CCA} results, as lower values are obtained as connectivity grows. Consequently, connectivity increases elicits decreases in the values of L_{CCA}, which can be interpreted as more integrated multiplex networks.

The mean clustering coefficient C is a simple measure of segregation, computed as the average fraction of triangles around an individual node (Rubinov and Sporns, 2010; Watts and Strogatz, 1998). Therefore, lower connected networks result in higher segregated network, as nodes with a low strength may not have clustered connectivity around them (Rubinov and Sporns, 2010). When our proposed CCA-based multiplex approach is applied, C_{CCA} results followed the same trend, showing higher segregation for more connected multiplex networks.

Therefore, considering these results, we can conclude that the interpretation of the CCA-based multiplex parameters can be analogous to their frequency-specific counterparts, as they revealed the same behavior using synthetic signals. Additionally, our proposed method is able to capture and summarize all the relevant information of the whole brain network, while a single-layer approach only provides a limited perspective of the neural network properties.

5.2. Abnormal multiplex network patterns in AD progression

Network organization has conventionally been analyzed in diverse frequency bands, as they are considered to be associated with different cognitive processes. Previous EEG studies have shown that functional connectivity patters in AD networks are frequency-dependent (Yu et al., 2017; Hillebrand et al., 2016). Specifically, in our database, network topologies in low-frequency bands tend to be less integrated and more segregated as the disease severity increases, reducing their global performance and enhancing their local performance (Ruiz-Gómez et al., 2020). Here, we integrate all frequency-specific networks in a multiplex framework using CCA to

study the brain changes during AD continuum. Our results indicated that multiplex networks are characterized by higher average connectivity as AD severity increases, revealed by an increasing trend in s_{CCA}. Furthermore, these networks tended to be less integrated (revealed by a increase in L_{CCA}) and less segregated (decrease in C_{CCA}) as the disease progresses.

Firstly, a consensus with decreased functional connectivity in alpha band has been reached by previous studies (Dauwels et al., 2010; Ruiz-Gómez et al., 2019; Wang et al., 2014; Babiloni et al., 2018). However, inconsistent results have been found for other frequency bands (Ruiz-Gómez et al., 2019; Hata et al., 2016). These frequency-dependent connectivity variations lead to contradictory results in terms of global strength, which depends on the frequency under analysis. Our previous work using the same database supports these frequency-dependent results, as significant increases of s in the theta band and significant decreases of s in the alpha band were reported as the disease severity increases (Ruiz-Gómez et al., 2020). To the best of our knowledge, no previous study has analyzed the mean average connectivity in multiplex networks during AD continuum. This could be due to this parameter alone does not give further information about network organization, but it can be useful combined with the integration and segregation information given by L_{CCA} and C_{CCA} results, respectively.

Secondly, our L_{CCA} results are in line with previous studies that reported lower integration in AD networks compared to HC subjects, revealed by an increase in the characteristic path length values (Stam, 2014), a decrease in the network global efficiency (Afshari and Jalili, 2017), and a decrease in the participation coefficient (De Haan et al., 2012). From the clinical point of view, the global propensity to facilitate information exchange is progressively reduced as a consequence of neurodegeneration as dementia severity increases (Guillon et al., 2017).

Finally, many previous studies showed decreases in global segregation for the AD group using both multiplex and frequency-specific networks (Stam et al., 2009; Supekar et al., 2008; Cai et al., 2020), in line with our C_{CCA} results. Clinically, this could reflect that local information exchange between frequency bands is progressively disrupted as a consequence of AD (Cai et al., 2020). However, increases in clustering coefficient are also reported as a possible compensatory mechanism that is triggered by the dysfunctional integration in the AD brain networks (Kabbara et al., 2018; Palesi et al., 2016). This compensatory effect could explain the C_{CCA} values obtained for the AD_{mil} group, as it did not follow the declining trend of C_{CCA} as AD severity increases.

Putting these results together, our findings indicated that dementia due to AD is characterized by a loss of 'small-world' networks as the disease progresses (revealed by decreases in integration and segregation) (Sanz-Arigita et al., 2010; Bullmore and Sporns, 2009). This progressive loss of small-world network properties would increase multiplex networks vulnerability (Vecchio et al., 2017).

5.3. Limitations and future research lines

Despite the fact that we have reduced the volume-conduction bias (by using PLI to build the connectivity network), reduced the frequency-specific results bias (by adopting a multiplex approach), and facilitated the comparison with other EEG-channel configurations and neuroimaging methods (by using source-level results obtained with a standard atlas), the present study has some limitations that should be considered.

Firstly, multiplex network parameters were averaged for all ROIs. Future studies should be carried out taking into account the specific value for each ROI. These spatial analyses could lead us to accurately identify brain areas with abnormal neural patters to gain further insights on AD continuum neurodegeneration processes.

Secondly, even if we had a large database composed of 253 recordings to characterize the brain abnormalities during the AD progression, subjects were divided into five groups depending on their stage. Thus, each group was formed by only 50 or 51 subjects; this sample size is not big enough to perform a classification analysis and prove the usefulness of our proposed methodology as a generalizable diagnostic tool.

Finally, despite we had the AD continuum stratified into five severity groups, it would be useful to perform a longitudinal study focused only on MCI subjects. This group is the most clinically interesting group, since two distinct subgroups of patients with MCI can be distinguished: those that remain stable at MCI condition, and those that progress to AD. This research could provide deeper understanding on the complex neural changes during MCI and may allow to predict AD progression at an early stage.

6. Conclusions

In the present study, an original methodology to build multiplex networks is proposed, evaluated with synthetic signals, and applied to real EEG recordings from patients in different stages of AD continuum. We proved that the proposed CCA-based multiplex parameters can be interpreted in an analogous way compared to their frequency-specific counterparts, as they revealed the same behavior against coupling variations using synthetic signals. Furthermore, our results using real EEG recordings revealed that dementia due to AD altered progressively the small-world network properties, increasing multiplex networks vulnerability as a consequence of the neurodegenerative processes.

Acknowledgments

This research was supported by 'Ministerio de Ciencia e Innovación - Agencia Estatal de Investigación'

and 'European Regional Development Fund' (FEDER) under project PGC2018-098214-A-I00, by 'European Commission' and 'FEDER' under projects 'Análisis y correlación entre el genoma completo y la actividad cerebral para la ayuda en el diagnóstico de la enfermedad de Alzheimer' and 'Análisis y correlación entre la epigenética y la actividad cerebral para evaluar el riesgo de migraña crónica y episódica en mujeres' ('Cooperation Programme Interreg V-A Spain-Portugal POCTEP 2014–2020'), and by 'CIBER de Bioingeniería, Biomateriales y Nanomedicina (CIBER-BBN)' through 'Instituto de Salud Carlos III' co-funded with FEDER funds. Saúl J. Ruiz-Gómez, Eduardo Santamaría-Vázquez, and Aarón Maturana-Candelas were in receipt of a predoctoral scholarship from the 'Junta de Castilla y León' and the 'European Social Fund'. Víctor Rodríguez-González was in receipt of a PIF-UVa grant from the 'University of Valladolid'.

References

Afshari, S., Jalili, M., 2017. Directed Functional Networks in Alzheimer's Disease: Disruption of Global and Local Connectivity Measures. IEEE Journal of Biomedical and Health Informatics 21, 949–955.

Aisen, P. S., Cummings, J., Jack, C. R., Morris, J. C., Sperling, R., Frölich, L., Jones, R. W., Dowsett, S. A., Matthews, B. R., Raskin, J., Scheltens, P., Dubois, B., 2017. On the path to 2025: Understanding the Alzheimer's disease continuum. Alzheimer's Research and Therapy 9 (60), 1–10.

Albert, M. S., DeKosky, S. T., Dickson, D., Dubois, B., Feldman, H. H., Fox, N. C., Gamst, A., Holtzman, D. M., Jagust, W. J., Petersen, R. C., Snyder, P. J., Carrillo, M. C., Thies, B., Phelps, C. H., 2011. The diagnosis of mild cognitive impairment due to Alzheimer's disease: Recommendations from the National Institute on Aging-Alzheimer's Association workgroups on diagnostic guidelines for Alzheimer's disease. Alzheimer's and Dementia 7, 270–279.

Alzheimer's Association, 2019. 2019 Alzheimer's disease facts and figures. Alzheimer's & Dementia.

Babiloni, C., Del Percio, C., Lizio, R., Noce, G., Lopez, S., Soricelli, A., Ferri, R., Nobili, F., Arnaldi, D., Famà, F., Aarsland, D., Orzi, F., Buttinelli, C., Giubilei, F., Onofrj, M., Stocchi, F., Stirpe, P., Fuhr, P., Gschwandtner, U., Ransmayr, G., Garn, H., Fraioli, L., Pievani, M., Frisoni, G. B., D'Antonio, F., De Lena, C., Güntekin, B., Hanoğlu, L., Başar, E., Yener, G., Emek-Savaş, D. D., Triggiani, A. I., Franciotti, R., Taylor, J. P., Vacca, L., De Pandis, M. F., Bonanni, L., 2018. Abnormalities of resting-state functional cortical connectivity in patients with dementia due to Alzheimer's and Lewy body diseases: an EEG study. Neurobiology of Aging 65, 18–40.

Battiston, F., Nicosia, V., Latora, V., 2014. Structural measures for multiplex networks. Physical Review E - Statistical, Nonlinear, and Soft Matter Physics 89, 032804.

Boccaletti, S., Bianconi, G., Criado, R., del Genio, C. I., Gómez-Gardeñes, J., Romance, M., Sendiña-Nadal, I., Wang, Z., Zanin, M., 2014. The structure and dynamics of multilayer networks. Physics Reports 544, 1–122.

Buldú, J. M., Porter, M. A., 2018. Frequency-based brain networks: From a multiplex framework to a full multilayer description. Network Neuroscience 2 (4), 418–441.

Bullmore, E., Sporns, O., 2009. Complex brain networks: graph theoretical analysis of structural and functional systems. Nature Reviews Neuroscience 10 (10), 186–198.

Buscema, M., Vernieri, F., Massini, G., Scrascia, F., Breda, M., Rossini, P. M., Grossi, E., 2015. An improved I-FAST system for the diagnosis of Alzheimer's disease from unprocessed electroencephalograms by using robust invariant features. Artificial Intelligence in Medicine 64, 59–74.

Cai, L., Wei, X., Liu, J., Zhu, L., Wang, J., Deng, B., Yu, H., Wang, R., 2020. Functional Integration and Segregation in Multiplex Brain Networks for Alzheimer's Disease. Frontiers in Neuroscience 14, 1–14.

Cui, D., Qi, S., Gu, G., Li, X., Li, Z., Wang, L., Yin, S., 2018. Magnitude Squared Coherence Method based on Weighted Canonical Correlation Analysis for EEG Synchronization Analysis in Amnesic Mild Cognitive Impairment of Diabetes Mellitus. IEEE Transactions on Neural Systems and Rehabilitation Engineering 26 (10), 1908–1917.

D'Amelio, M., Rossini, P. M., 2012. Brain excitability and connectivity of neuronal assemblies in Alzheimer's disease: From animal models to human findings. Progress in Neurobiology 99, 42–60.

Dauwels, J., Vialatte, F., Cichocki, A., 2010. Diagnosis of Alzheimer's disease from EEG signals: where are we standing? Current Alzheimer Research 7 (6), 487–505.

De Domenico, M., Sasai, S., Arenas, A., 2016. Mapping multiplex hubs in human functional brain networks. Frontiers in Neuroscience 10, 1–14.

De Haan, W., Van der Flier, W. M., Koene, T., Smits, L. L., Scheltens, P., Stam, C. J., 2012. Disrupted modular brain dynamics reflect cognitive dysfunction in Alzheimer's disease. NeuroImage 59, 3085–3093.

Guillon, J., Attal, Y., Colliot, O., La Corte, V., Dubois, B., Schwartz, D., Chavez, M., De Vico Fallani, F., 2017. Loss of brain inter-frequency hubs in Alzheimer's disease. Scientific Reports 7, 1–13.

Hata, M., Kazui, H., Tanaka, T., Ishii, R., Canuet, L., Pascual-Marqui, R. D., Aoki, Y., Ikeda, S., Kanemoto, H., Yoshiyama, K., Iwase, M., Takeda, M., 2016. Functional connectivity assessed by resting state EEG correlates with cognitive decline of Alzheimer's disease - An eLORETA study. Clinical Neurophysiology 127, 1269–1278.

He, Y., Chen, Z., Evans, A., 2008. Structural insights into aberrant topological patterns of large-scale cortical networks in Alzheimer's disease. Journal of Neuroscience 28 (18), 4756–4766.

Hillebrand, A., Tewarie, P., Van Dellen, E., Yu, M., Carbo, E. W., Douw, L., Gouw, A. A., Van Straaten, E. C., Stam, C. J., 2016. Direction of information flow in large-scale resting-state networks is frequency-dependent. Proceedings of the National Academy of Sciences of the United States of America 113, 3867–3872.

Jobson, J. D., 2012. Applied Multivariate Data Analysis: Volume II: Categorical and Multivariate Methods: Categorical and Multivariate Methods. Springer, New York, NY, USA.

Kabbara, A., Eid, H., El Falou, W., Khalil, M., Wendling, F., Hassan, M., 2018. Reduced integration and improved segregation of functional brain networks in Alzheimer's disease. Journal of Neural Engineering 15, 026023.

Karageorgiou, E., Lewis, S. M., McCarten, J. R., Leuthold, A. C., Hemmy, L. S., McPherson, S. E., Rottunda, S. J., Rubins, D. M., Georgopoulos, A. P., 2012. Canonical correlation analysis of synchronous neural interactions and cognitive deficits in Alzheimer's dementia. Journal of Neural Engineering 9, 056003.

Lo, C. Y., Wang, P. N., Chou, K. H., Wang, J., He, Y., Lin, C. P., 2010. Diffusion tensor tractography reveals abnormal topological organization in structural cortical networks in Alzheimer's disease. Journal of Neuroscience 30 (50), 16876–16885.

McBride, J. C., Zhao, X., Munro, N. B., Smith, C. D., Jicha, G. A., Hively, L., Broster, L. S., Schmitt, F. A., Kryscio, R. J., Jiang, Y., 2014. Spectral and complexity analysis of scalp EEG characteristics for mild cognitive impairment and early Alzheimer's disease. Computer Methods and Programs in Biomedicine 114 (2), 153–163.

McKhann, G. M., Knopman, D. S., Chertkow, H., Hyman, B. T., Jack, C. R., Kawas, C. H., Klunk, W. E., Koroshetz, W. J., Manly, J. J., Mayeux, R., Mohs, R. C., Morris, J. C., Rossor, M. N., Scheltens, P., Carrillo, M. C., Thies, B., Weintraub, S., Phelps, C. H., 2011. The diagnosis of dementia due to Alzheimer's disease: Recommendations from the National Institute on Aging-Alzheimer's Association workgroups on diagnostic guidelines for Alzheimer's disease. Alzheimer's and Dementia 7 (3), 263–269.

Mijalkov, M., Kakaei, E., Pereira, J. B., Westman, E., Volpe, G., 2017. BRAPH: A graph theory software for the analysis of brain connectivity. PLoS ONE 12 (8), 1–23.

Moretti, D. V., Frisoni, G. B., Pievani, M., Rosini, S., Geroldi, C., Binetti, G., Rossini, P. M., 2008. Cerebrovascular disease and hippocampal atrophy are differently linked to functional coupling of brain areas: An

EEG coherence study in MCI subjects. Journal of Alzheimer's Disease 14 (3), 285–299.

Palesi, F., Castellazzi, G., Casiraghi, L., Sinforiani, E., Vitali, P., Gandini Wheeler-Kingshott, C. A., D'Angelo, E., 2016. Exploring patterns of Alteration in Alzheimer's disease brain networks: A combined structural and functional connectomics analysis. Frontiers in Neuroscience 10, 1–16.

Pascual-Marqui, R. D., 2002. Standardized low-resolution brain electromagnetic tomography (sLORETA): Technical details. Methods and Findings in Experimental and Clinical Pharmacology 24 Suppl D, 5–12.

Petersen, R. C., 2016. Mild cognitive impairment. Continuum 22, 404–418.

Poza, J., Gómez, C., García, M., Tola-Arribas, M. A., Carreres, A., Cano, M., Hornero, R., aug 2017. Spatio-Temporal Fluctuations of Neural Dynamics in Mild Cognitive Impairment and Alzheimer's Disease. Current Alzheimer research 14 (9), 924–936.

Rubinov, M., Sporns, O., 2010. Complex network measures of brain connectivity: Uses and interpretations. NeuroImage 52, 1059–1069.

Ruiz-Gómez, S. J., Gómez, C., Poza, J., Gutiérrez-Tobal, G. C., Tola-Arribas, M. A., Cano, M., Hornero, R., 2018a. Automated multiclass classification of spontaneous EEG activity in Alzheimer's disease and mild cognitive impairment. Entropy 20, 1–15.

Ruiz-Gómez, S. J., Gómez, C., Poza, J., Marcos, R.-V., Gutiérrez-de Pablo, V., Rodríguez-González, V., Maturana-Candelas, A., 2020. Volume Conduction Effects on Connectivity Metrics: Application of Network Parameters to Characterize Alzheimer's Disease Continuum. Proceedings of the 42nd Annual International Conference of the IEEE Engineering in Medicine and Biology Society (EMBC), Montreal (Canada), 30–33.

Ruiz-Gómez, S. J., Gómez, C., Poza, J., Martínez-Zarzuela, M., Tola-Arribas, M. A., Cano, M., Hornero, R., 2018b. Measuring alterations of spontaneous EEG neural coupling in alzheimer's disease and mild cognitive impairment by means of cross-entropy metrics. Frontiers in Neuroinformatics 12 (76), 1–11.

Ruiz-Gómez, S. J., Hornero, R., Poza, J., Maturana-Candelas, A., Pinto, N., Gómez, C., 2019. Computational modeling of the effects of EEG volume conduction on functional connectivity metrics. Application to Alzheimer's disease continuum. Journal of Neural Engineering 16, 066019.

Santamaría-Vázquez, E., Martínez-Cagigal, V., Gomez-Pilar, J., Hornero, R., 2019. Asynchronous Control of ERP-Based BCI Spellers Using Steady-State Visual Evoked Potentials Elicited by Peripheral Stimuli. IEEE Transactions on Neural Systems and Rehabilitation Engineering 27 (9), 1883–1892.

Sanz-Arigita, E. J., Schoonheim, M. M., Damoiseaux, J. S., Rombouts, S. A., Maris, E., Barkhof, F., Scheltens, P., Stam, C. J., 2010. Loss of 'Small-World' Networks in Alzheimer's Disease: Graph Analysis of fMRI Resting-State Functional Connectivity. PLoS ONE 5, 1–14.

Stam, C. J., 2014. Modern network science of neurological disorders. Nature Reviews Neuroscience 15, 683–695.

Stam, C. J., De Haan, W., Daffertshofer, A., Jones, B. F., Manshanden, I., Van Cappellen Van Walsum, A. M., Montez, T., Verbunt, J. P., De Munck, J. C., Van Dijk, B. W., Berendse, H. W., Scheltens, P., 2009. Graph theoretical analysis of magnetoencephalographic functional connectivity in Alzheimer's disease. Brain 132, 213–224.

Stam, C. J., Jones, B. F., Nolte, G., Breakspear, M., Scheltens, P., 2007a. Small-world networks and functional connectivity in Alzheimer's disease. Cerebral Cortex 17 (1), 92–99.

Stam, C. J., Nolte, G., Daffertshofer, A., 2007b. Phase lag index: Assessment of functional connectivity from multi channel EEG and MEG with diminished bias from common sources. Human Brain Mapping 28, 1178–1193.

Supekar, K., Menon, V., Rubin, D., Musen, M., Greicius, M. D., 2008. Network analysis of intrinsic functional brain connectivity in Alzheimer's disease. PLoS Computational Biology 4, 1–11.

Tadel, F., Baillet, S., Mosher, J. C., Pantazis, D., Leahy, R. M., 2011. Brainstorm: A user-friendly application for MEG/EEG analysis. Computational Intelligence and Neuroscience 879716, 1–13.

Tijms, B. M., Möller, C., Vrenken, H., Wink, A. M., de Haan, W., van der Flier, W. M., Stam, C. J., Scheltens, P., Barkhof, F., 2013. Single-Subject Grey Matter Graphs in Alzheimer's Disease. PLoS ONE 8 (3), 1–9.

U.S. National Library of Medicine, 2018. The Visible Human Project. URL https://www.nlm.nih.gov/research/visible/visible_human.html

Vecchio, F., Miraglia, F., Piludu, F., Granata, G., Romanello, R., Caulo, M., Onofrj, V., Bramanti, P., Colosimo, C., Rossini, P. M., 2017. 'Small World' architecture in brain connectivity and hippocampal volume in Alzheimer's disease: a study via graph theory from EEG data. Brain Imaging and Behavior 11, 473–485.

Wang, R., Wang, J., Yu, H., Wei, X., Yang, C., Deng, B., 2014. Decreased coherence and functional connectivity of electroencephalograph in Alzheimer's disease. Chaos 24, 033136.

Watts, D., Strogatz, S., 1998. Collective dynamics of 'small world' networks. Nature 393, 440–442.

Yao, Z., Zhang, Y., Lin, L., Zhou, Y., Xu, C., Jiang, T., 2010. Abnormal cortical networks in mild cognitive impairment and alzheimer's disease. PLoS Computational Biology 6 (11), e1001006.

Yu, M., Engels, M. M., Hillebrand, A., Van Straaten, E. C., Gouw, A. A., Teunissen, C., Van Der Flier, W. M., Scheltens, P., Stam, C. J., 2017. Selective impairment of hippocampus and posterior hub areas in Alzheimer's disease: An MEG-based multiplex network study. Brain 140, 1466–1485.

Yushkevich, P. A., Piven, J., Hazlett, H. C., Smith, R. G., Ho, S., Gee, J. C., Gerig, G., 2006. User-guided 3D active contour segmentation of anatomical structures: Significantly improved efficiency and reliability. NeuroImage 31, 1116–1128.

Zhang, Y., Yin, E., Li, F., Zhang, Y., Tanaka, T., Zhao, Q., Cui, Y., Xu, P., Yao, D., Guo, D., 2018. Two-Stage Frequency Recognition Method Based on Correlated Component Analysis for SSVEP-Based BCI. IEEE Transactions on Neural Systems and Rehabilitation Engineering 26, 1314–1323.

Zhao, X., Liu, Y., Wang, X., Liu, B., Xi, Q., Guo, Q., Jiang, H., Jiang, T., Wang, P., 2012. Disrupted small-world brain networks in moderate Alzheimer's disease: A resting-state fMRI study. PLoS ONE 7 (3), e33540.

Appendix B

Scientific achievements

B.1 Publications

B.1.1 Papers indexed in the JCR

1. **Saúl J. Ruiz-Gómez**, Carlos Gómez, Jesús Poza, Gonzalo C. Gutiérrez-Tobal, Miguel A. Tola-Arribas, Mónica Cano, Roberto Hornero, "Automated Multiclass Classification of Spontaneous EEG Activity in Alzheimer's Disease and Mild Cognitive Impairment", *Entropy*, vol. 20 (1), pp. 35, January, 2018, DOI: 10.3390/e20010035

2. Carlos Gómez, Celia Juan-Cruz, Jesús Poza, **Saúl J. Ruiz-Gómez**, Javier Gomez-Pilar, Pablo Núñez, María García, Alberto Fernández, Roberto Hornero, "Alterations of Effective Connectivity Patterns in Mild Cognitive Impairment: An MEG Study", *Journal of Alzheimers Disease*, vol. 65 (3), pp. 843–854, September, 2018, DOI: 10.3233/JAD-170475

3. **Saúl J. Ruiz-Gómez**, Carlos Gómez, Jesús Poza, Mario Martínez-Zarzuela, Miguel A. Tola-Arribas, Mónica Cano, Roberto Hornero, "Measuring Alterations of Spontaneous EEG Neural Coupling in Alzheimer's Disease and Mild Cognitive Impairment by Means of Cross-Entropy Metrics", *Frontiers in Neuroinformatics*, vol. 12 (76), pp. 1–11, October, 2018, DOI: 10.3389/fninf.2018.00076

4. **Saúl J. Ruiz-Gómez**, Roberto Hornero, Jesús Poza, Aarón Maturana-Candelas, Nádia Pinto, Carlos Gómez, "Computational modeling of the effects of EEG volume conduction on functional connectivity metrics. Appli-

cation to Alzheimer's disease continuum", *Journal of Neural Engineering*, vol. 16 (6), pp. 066019, October, 2019, DOI: 10.1088/1741-2552/ab4024

5. Aarón Maturana-Candelas, Carlos Gómez, Jesús Poza, **Saúl J. Ruiz-Gómez**, Roberto Hornero, "Inter-band Bispectral Analysis of EEG Background Activity to Characterize Alzheimer's Disease Continuum", *Frontiers in Computational Neuroscience*, vol. 14 (70), pp. 1–11, September, 2020, DOI: 10.3389/fncom.2020.00070

6. Miguel Rebelo, Carlos Gómez, Iva Gomes, Jesús Poza, Sandra Martins, Aarón Maturana-Candelas, **Saúl J. Ruiz-Gómez**, Luís Durães, Patricia Sousa, Manuel Figueruelo, María Rodríguez, Carmen Pita, Miguel Arenas, Luis Álvarez, Roberto Hornero, Nádia Pinto, "Genome-wide scan for five brain oscillatory phenotypes identifies a new QTL associated with theta EEG band", *Brain Sciences*, vol. 10 (11), pp. 870, November, 2020, DOI: 10.3390/brainsci10110870

7. **Saúl J. Ruiz-Gómez**, Roberto Hornero, Jesús Poza, Eduardo Santamaría-Vázquez, Víctor Rodríguez-González, Aarón Maturana-Candelas, Carlos Gómez, "A new method to build multiplex networks using Canonical Correlation Analysis for the characterization of the Alzheimer's disease continuum", *Journal of Neural Engineering*, vol. 18 (2), pp. 0260002, January, 2021, DOI: 10.1088/1741-2552/abd82c

B.1.2 International conferences

1. Carlos Gómez, Fernando Vaquerizo-Villar, Jesús Poza, **Saúl J. Ruiz-Gómez**, Miguel A. Tola-Arribas, Mónica Cano, Roberto Hornero, "Bispectral Analysis of Spontaneous EEG Activity from Patients with Moderate Dementia Due to Alzheimer's Disease", *39th Annual International Conference of the IEEE Engineering in Medicine and Biology Society*, ISBN: 978-1-5090-2809-2, pp. 422–425, Jeju (South Korea), July 11 - July 15, 2017. DOI: 10.1109/EMBC.2017.8036852

2. Pablo Núñez, Jesús Poza, Carlos Gómez, **Saúl J. Ruiz-Gómez**, Víctor Rodríguez-González, Miguel A. Tola-Arribas, Mónica Cano, Roberto Hornero, "Analysis of Electroencephalographic Dynamic Functional Connectivity in Alzheimer's Disease", *World Congress on Medical Physics & Biomedical Engineering (IUPESM 2018)*, pp. 165–168, Praga (Czech Republic), June 3 - June 8, 2018. DOI: 10.1007/978-981-10-9038-7_30

3. Carlos Gómez, **Saúl J. Ruiz-Gómez**, Jesús Poza, Aarón Maturana-Candelas, Nádia Pinto, Miguel A. Tola-Arribas, Mónica Cano, Roberto Hornero, "Assessment of EEG Connectivity Patterns in Mild Cognitive Impairment Using Phase Slope Index", *40th Annual International Conference of the IEEE Engineering in Medicine and Biology Society*, ISBN: 978-1-5386-3646-6, pp. 263–266, Honolulu (United States), July 17 - July 21, 2018. DOI: 10.1109/EMBC.2018.8512270

4. **Saúl J. Ruiz-Gómez**, Carlos Gómez, Jesús Poza, Pablo Núñez, Víctor Rodríguez-González, Aarón Maturana-Candelas, Roberto Hornero, "Analysis of Information Flux in Alzheimer's Disease and Mild Cognitive Impairment by Means of Graph-Theory Parameters", *International Conference on NeuroRehabilitation (ICNR 2018)*, ISBN: 978-3-030-01844-3, pp. 569–573, Pisa (Italy), October 16 - October 20, 2018.

5. Pablo Núñez, Jesús Poza, Carlos Gómez, Víctor Rodríguez-González, **Saúl J. Ruiz-Gómez**, Aarón Maturana-Candelas, Roberto Hornero, "Characterizing Non-stationarity in Alzheimer's Disease and Mild Cognitive Impairment by Means of Kullback-Leibler Divergence", *International Conference on NeuroRehabilitation (ICNR 2018)*, ISBN: 978-3-030-01844-3, pp. 574–578, Pisa (Italy), October 16 - October 20, 2018.

6. Aarón Maturana-Candelas, Carlos Gómez, Jesús Poza, **Saúl J. Ruiz-Gómez**, María Rodríguez, Miguel Figueruelo, Nádia Pinto, Sandra Martins, Alexandra M. Lopes, Iva Gomes, Roberto Hornero, "Analysis of Spontaneous EEG Activity in Alzheimer's Disease Patients by Means of Multiscale Spectral Entropy", *International Conference on NeuroRehabilitation (ICNR 2018)*, ISBN: 978-3-030-01844-3, pp. 579–583, Pisa (Italy), October 16 - October 20, 2018.

7. Pablo Núñez, Jesús Poza, Carlos Gómez, Verónica Barroso-García, **Saúl J. Ruiz-Gómez**, Aarón Maturana-Candelas, Miguel A. Tola-Arribas, Mónica Cano, Roberto Hornero, "Characterization of EEG Resting-state Activity in Alzheimer's Disease by Means of Recurrence Plot Analyses", *41st Annual International Conference of the IEEE Engineering in Medicine and Biology Society*, pp. 5786–5789, Berlin (Germany), July 23 - July 27, 2019. DOI: 10.1109/EMBC.2019.8856600

8. **Saúl J. Ruiz-Gómez**, Carlos Gómez, Jesús Poza, Aarón Maturana-Candelas, Víctor Rodríguez-González, María García, Miguel A. Tola-

Arribas, Mónica Cano, Roberto Hornero, "Analysis of Volume Conduction Effects on Different Functional Connectivity Metrics: Application to Alzheimer's Disease EEG Signals", *41st Annual International Conference of the IEEE Engineering in Medicine and Biology Society*, pp. 6434–6437, Berlin (Germany), July 23 - July 27, 2019. DOI: 10.1109/EMBC.2019.8856548

9. **Saúl J. Ruiz-Gómez**, Carlos Gómez, Jesús Poza, Marcos Revilla-Vallejo, Víctor Gutiérrez-de-Pablo, Víctor Rodríguez-González, Aarón Maturana-Candelas, Roberto Hornero, "Volume Conduction Effects on Connectivity Metrics: Application of Network Parameters to Characterize Alzheimer's Disease Continuum", *42nd Annual International Conference of the IEEE Engineering in Medicine and Biology Society*, pp. 30–33, Virtual conference Montreal (Canada), July 20 - July 24, 2020. DOI: 10.1109/EMBC44109.2020.9176398

B.1.3 National conferences

1. Pablo Núñez, Jesús Poza, Carlos Gómez, **Saúl J. Ruiz-Gómez**, Miguel A. Tola-Arribas, Mónica Cano, Roberto Hornero, "Análisis de los patrones de conectividad neuronal mediante EEG en la enfermedad de Alzheimer", *XXXIV Congreso Anual de la Sociedad Española de Ingeniería Biomédica (CASEIB 2016)*, ISBN: 978-84-9048-531-6, pp. 240–243, Valencia (Spain), October 23 - October 25, 2016.

2. **Saúl J. Ruiz-Gómez**, Carlos Gómez, Jesús Poza, Alberto Fernández, Pablo Núñez, Roberto Hornero, "Análisis de la actividad MEG en pacientes con deterioro cognitivo leve mediante la probabilidad de sincronización y parámetros derivados de la teoría de redes complejas", *XXXIV Congreso Anual de la Sociedad Española de Ingeniería Biomédica (CASEIB 2016)*, ISBN: 978-84-9048-531-6, pp. 404–407, Valencia (Spain), October 23 - October 25, 2016.

3. Carlos Gómez, Jesús Poza, Javier Gomez-Pilar, Lucía Martín, Pablo Núñez, María Rodríguez, Manuel Figueruelo, **Saúl J. Ruiz-Gómez**, Roberto Hornero, "Caracterización de la actividad neuronal en pacientes con la enfermedad de Alzheimer tras una sesión de estimulación multisensorial", *XXXIV Congreso Anual de la Sociedad Española de Ingeniería Biomédica (CASEIB*

2016), ISBN: 978-84-9048-531-6, pp. 400–403, Valencia (Spain), October 23 - October 25, 2016.

4. Carlos Gómez, Jesús Poza, Javier Gomez-Pilar, Lucía Martín, Pablo Núñez, María Rodríguez, Manuel Figueruelo, **Saúl J. Ruiz-Gómez**, Roberto Hornero, "Caracterización de la actividad neuronal en pacientes con enfermedad de Alzheimer tras una sesión de estimulación multisensorial", *VII Congreso Nacional de Alzheimer 2017*, pp. 1, Málaga (Spain), November 9 - November 11, 2017.

5. **Saúl J. Ruiz-Gómez**, Carlos Gómez, Jesús Poza, Pablo Núñez, Víctor Rodríguez-González, Miguel A. Tola-Arribas, Mónica Cano, Roberto Hornero, "Caracterización de los Patrones de Flujo de Información en el EEG de Pacientes con Deterioro Cognitivo Leve", *XXXV Congreso Anual de la Sociedad Española de Ingeniería Biomédica (CASEIB 2017)*, ISBN: 978-84-9082-797-0, pp. 217–220, Bilbao (Spain), November 29 - December 1, 2017.

6. Pablo Núñez, Jesús Poza, Carlos Gómez, **Saúl J. Ruiz-Gómez**, Adrián Martín-Montero, Miguel A. Tola-Arribas, Mónica Cano, Roberto Hornero, "Estudio de la conectividad neuronal dinámica en la enfermedad de Alzheimer", *XXXV Congreso Anual de la Sociedad Española de Ingeniería Biomédica (CASEIB 2017)*, ISBN: 978-84-9082-797-0, pp. 341–344, Bilbao (Spain), November 29 - December 1, 2017.

7. Adrián Martín-Montero, Gonzalo C. Gutiérrez-Tobal, Jesús Poza, Daniel Álvarez, Fernando Vaquerizo-Villar, Verónica Barroso-García, **Saúl J. Ruiz-Gómez**, Leila Kheirandish-Gozal, Félix del Campo, David Gozal, Roberto Hornero, "Caracterización de la apnea del sueño infantil mediante nuevas bandas espectrales del EEG", *XXXVI Congreso Anual de la Sociedad Española de Ingeniería Biomédica (CASEIB 2018)*, ISBN: 978-84-09-06253-9, pp. 249–252, Ciudad Real (Spain), November 21 - November 23, 2018.

8. **Saúl J. Ruiz-Gómez**, Carlos Gómez, Jesús Poza, Pablo Núñez, Víctor Rodríguez-González, Adrián Martín-Montero, Aarón Maturana-Candelas, Roberto Hornero, "Estudio del efecto de la conducción de volumen en medidas de conectividad funcional derivadas de la coherencia", *XXXVI Congreso Anual de la Sociedad Española de Ingeniería Biomédica (CASEIB 2018)*, ISBN: 978-84-09-06253-9, pp. 241–244, Ciudad Real (Spain), November 21 - November 23, 2018.

9. Víctor Rodríguez-González, Jesús Poza, Carlos Gómez, Pablo Núñez, **Saúl J. Ruiz-Gómez**, Aarón Maturana-Candelas, Roberto Hornero, "Localización de fuentes cerebrales para la caracterización de la demencia debida a enfermedad de Alzheimer", *XXXVI Congreso Anual de la Sociedad Española de Ingeniería Biomédica (CASEIB 2018)*, ISBN: 978-84-09-06253-9, pp. 195–198, Ciudad Real (Spain), November 21 - November 23, 2018.

10. Carmen Pita, Manuel Figueruelo, María Rodríguez, Lucía Martín, Elena Ramos, Aarón Maturana-Candelas, Roberto Hornero, Jesús Poza, **Saúl J. Ruiz-Gómez**, María García, Luís Durães, Ricardo González, Ana M. Macedo, Rita Rocha, Luis Álvarez, Sandra Martins, Alexandra M. Lopes, Iva Gomes, Miguel Arenas, Carlos Gómez, Patricia Sousa, Nádia Pinto, "Avances en el diagnóstico temprano de la enfermedad de Alzheimer mediante la correlación entre el genoma y la actividad cerebral", *VIII Congreso Nacional de Alzheimer*, Huesca (Spain), November 14 - November 16, 2019.

11. **Saúl J. Ruiz-Gómez**, Carlos Gómez, Jesús Poza, Aarón Maturana-Candelas, Miguel A. Tola-Arribas, Mónica Cano, Roberto Hornero, "Modelado computacional de la conducción de volumen en el EEG. Caracterización del deterioro cognitivo leve y su progresión a la enfermedad de Alzheimer", *XXXVII Congreso Anual de la Sociedad Española de Ingeniería Biomédica (CASEIB 2019)*, ISBN: 978-84-09-16707-4, pp. 199–202, Santander (Spain), November 27 - November 29, 2019.

12. Aarón Maturana-Candelas, Jesús Poza, Roberto Hornero, Pablo Núñez, **Saúl J. Ruiz-Gómez**, Víctor Gutiérrez-de-Pablo, Marcos Revilla-Vallejo, Carlos Gómez, "Estudio de la relación entre el gen MAPT y la conectividad cerebral en la demencia por enfermedad de Alzheimer", *XXXVIII Congreso Anual de la Sociedad Española de Ingeniería Biomédica (CASEIB 2020)*, ISBN: 978-84-09-25491-0, pp. 331–334, Valladolid (Spain), November 25 - November 27, 2020.

B.2 International internship

Three-month research internship at the Computational Neuroscience LAB Institute of Computer Science, University of Tartu, Tartu (Estonia).

i. Purpose of the internship

The main purpose of the research stay was the application of unsupervised classification techniques and deep learning techniques to the electroencephalographic (EEG) signals in the context of AD and MCI diagnosis. Apart from this activity, the relationship between cortical thickness and generic information was also investigated. It should be noted that genetics play an important role on the AD development risk. The cerebral cortex is also thought to play a key role in many of our cognitive functions, and its structural changes during aging are of interest to understand its normal and pathological development. The analysis was performed in two directions. In the direct problem, we aimed to build regressions models predicting cortical thickness from genotype (categorical regression). In the inverse problem, we aimed at inferring the genotype from the pattern of cortical thickness of the patient. For this purpose, the following activities were carried out: (i) extraction of the relevant genetic information (APoE, BIN1, CLU, ABCA7, CR1 and PICALM genes) and the cortical thickness information from all brain regions using the table of FreeSurfer cortical parcellation anatomical statistics per subject; (ii) study of the relation between the aforementioned genes and the cortical thickness of different brain areas in healthy aging patients; in particular, we explored different statistical and machine learning techniques to assess the potential relation between cortical thickness across the brain and the genes involved in pathological aging; and (iii) statistical testing to explore significant relationship between certain alleles and cortical thickness of several brain areas.

ii. Methodological summary

The main research activity has been the application of new techniques in the context of early AD diagnosis. Particularly, the application of new unsupervised and deep learning techniques to EEG signals in the context of AD diagnosis was evaluated. Furthermore, in the context of cortical thickness and genetics, different signal processing techniques were studied: (i) hierarchical clustering was used to determine and characterize different sub-groups

in the database; (ii) principal component analysis (PCA) was used to reduce the dimensionality of the data and describe them with new correlated variables; and (iii) non-negative Matrix Factorization (NMF) was used to group the genetic expression and find the representative genes from the groups. These analyses were performed with the specific values of cortical thickness and with the ranking of the cortical areas.

iii. Quality indicators of the institution

Founded in 1632, the University of Tartu is one of the oldest universities in Europe. Currently, it has more than 13,000 students (including 1,200 international students from 90 countries) and 3,600 employees. According to information in the ISI Web of Science, the University of Tartu belongs to the 1% of the most cited universities and research institutions in the world. The University of Tartu accounts for more than half of the Estonian national research output with almost 3,000 research articles published annually and 120 Doctoral Theses defended per year.

Specifically, the receiving research group (Computational Neuroscience LAB) has a total of 9 researchers, both pre-doctoral and post-doctoral. Their research is focused on the knowledge of different brain mechanisms in different pathologies through computational neuroscience. In addition, they have developed various deep learning and deep reinforcement learning algorithms. Regarding their research capacity, they have published a total of 45 articles in journals indexed in the JCR in the last 5 years, as well as a multitude of communications in prestigious international congresses. In addition, the group has numerous international collaborations, including the Brain Imaging Center (Goethe University, Frankfurt, Germany), the Max-Planck Institute for Brain Research (Frankfurt, Germany), the University of the Balearic Islands (Spain), Vancouver General Hospital (Vancouver, Canada) or University College London (London, UK).

Particularly, Dr. Raúl Vicente is the director of the Computational Neuroscience LAB and professor in 'Data Science'. He obtained a Doctorate in Physics from the University of the Balearic Islands in Spain, and was a post-doctoral fellow at the Max-Planck Institute for Brain Research in Germany for 7 years. His resume accredits a total of 29 publications in journals indexed in the JCR and numerous preprints in arXiv in the last 5 years. In addition, he currently has 3 active research projects funded by SA Archimedes, Archimedes Foundation, and AS Milrem (1 as principal in-

vestigator). Finally, he has participated in 3 research projects funded by the Estonian Research Council and the Estonian Ministry of Education and Research.

B.3 Awards and honors

12/2017: **Winner of the José María Ferrero Corral award at CASEIB 2017**, for the study entitled "Estudio de la conectividad neuronal dinámica en la enfermedad de Alzheimer", conducted by Pablo Núñez, Jesús Poza, Carlos Gómez, Saúl J. Ruiz-Gómez, Adrián Martín-Montero, Miguel Á. Tola-Arribas, Mónica Cano, and Roberto Hornero.

12/2018: **Finalist of the José María Ferrero Corral award at CASEIB 2018**, for the study entitled "Estudio del efecto de la conducción de volumen en medidas de conectividad funcional derivadas de la coherencia', conducted by Saúl J. Ruiz-Gómez, Carlos Gómez, Jesús Poza, Pablo Núñez, Víctor Rodríguez-González, Adrián Martín-Montero, Aarón Maturana-Candelas, and Roberto Hornero.

12/2018: **Winner of the José María Ferrero Corral award at CASEIB 2018**, for the study entitled "Caracterización de la apnea del sueño infantil mediante nuevas bandas espectrales del EEG", conducted by Adrián Martín-Montero, Gonzalo C. Gutiérrez-Tobal, Jesús Poza, Daniel Álvarez, Fernando Vaquerizo-Villar, Verónica Barroso-García, Saúl J. Ruiz-Gómez, Leila Kheirandish-Gozal, Félix del Campo, David Gozal, and Roberto Hornero.

Apéndice C

Resumen en castellano

C.1 Introducción

Uno de los desarrollos más importantes en la historia de la neurología clínica fue la invención del electroencefalograma (EEG). Desde este momento, en 1929, se han realizado numerosos esfuerzos para comprender las relaciones entre las distintantas regiones cerebrales que explicarían el funcionamiento del cebrero. Sin embargo, a día hoy se necesitan más investigaciones con el fin de comprender cómo los grupos neuronales corticales intercambian información para formar una red neuronal compleja. En los últimos años, con los avances técnicos y computacionales, se han desarrollado herramientas más sofisticadas para registrar, analizar y modelar redes cerebrales funcionales.

Por lo general, la organización estructural y funcional de las redes neuronales en los trastornos cerebrales se ha evaluado siguiendo tres niveles de análisis según cómo se han estudiado las interacciones: (i) análisis de patrones de activación local en sensores individuales, (ii) análisis de interacciones entre sensores utilizando métricas de conectividad y sincronización, y (iii) análisis de la organización funcional de las redes cerebrales, aplicando parámetros derivados de la teoría de redes complejas. En este contexto, la presente Tesis Doctoral tiene como objetivo analizar los cambios neuronales subyacentes siguiendo los niveles de análisis antes mencionados en las diferentes etapas de la demencia debida a enfermedad de Alzhiemer (EA) y su etapa prodrómica: el deterioro cognitivo leve (DCL).

La demencia debida a EA es una enfermedad neurodegenerativa progresiva que provoca alteraciones cognitivas, conductuales y funcionales en los pacientes. Durante el progreso de la enfermedad se pueden distinguir tres fases dependiendo de

cómo los síntomas interfieran con la capacidad de los pacientes para realizar las actividades: EA leve, EA moderada y EA grave (Jack et al., 2011). En la etapa más temprana de la EA, los pacientes pueden conducir y trabajar, y pueden funcionar de forma independiente, pero muestran algunos síntomas, como problemas de lectura (Alzheimer's Association, 2020). En la etapa de EA moderada, que suele ser la más larga, los pacientes suelen mostrar cada vez más dificultades para comunicarse y realizar las actividades de la vida diaria (Alzheimer's Association, 2020). Finalmente, la EA grave es la última etapa de esta enfermedad, donde los pacientes requieren un mayor nivel de atención, ya que eventualmente pierden la capacidad de control del movimiento y quedan postrados en la cama (Alzheimer's Association, 2020).

Sin embargo, se pueden distinguir otras fases previas al desarrollo de la EA, como la EA preclínica y el DCL (Jack et al., 2011). En la EA preclínica los pacientes aún no han desarrollado ningún síntoma típico de la EA, pero presentan cambios cerebrales que indican los primeros signos de la EA. En esta etapa, los cerebros de los pacientes son capaces de compensar los niveles anormales de beta-amiloide y la disminución del metabolismo de la glucosa para seguir funcionando con normalidad (Bischof et al., 2016). Durante la etapa de DCL, las personas muestran evidencias de cambios cerebrales relacionados con la EA y un deterioro de la memoria más allá de lo que se esperaría para su edad, pero no cumplen completamente los criterios para el diagnóstico de demencia. El DCL es considerado una etapa prodrómica de la EA, ya que la tasa de conversión a la EA es mucho más elevada para personas con DCL que para sujetos sanos (Petersen, 2016). Pero no todos los sujetos con DCL progresan a la EA, sino que existe un subgrupo que permanece con DCL estable. Por lo tanto, identificar aquellos sujetos con DCL que tienen más probabilidades de desarrollar EA u otras demencias es un objetivo principal de la investigación actual.

El diagnóstico definitivo de la EA solo se puede hacer mediante el análisis microscópico del cerebro del paciente después de la muerte. En la práctica clínica diaria, el diagnóstico de EA probable está basado en la historia clínica del paciente y las distintas exploraciones clínicas, neurológicas y psiquiátricas (McKhann et al., 1984). Un diagnóstico temprano es crucial, ya que los tratamientos son más efectivos en las primeras etapas de la demencia y podrían detener o retrasar el proceso neurodegenerativo, a pesar de que las terapias actuales no pueden curar el DCL ni la EA (Alzheimer's Association, 2020). En este punto, algunos métodos de neuroimagen han mostrado resultados prometedores como herramientas de diagnóstico para la EA, como las mediciones de resonancia magnética de la atrofia

del lóbulo temporal medial, la obtención de imágenes de tomografía por emisión de positrones del metabolismo de la glucosa y los depósitos de Aβ y biomarcadores basados en el EEG (Khoury and Ghossoub, 2019). En la actualidad, algunas de estas técnicas de imagen están recomendadas en las guías para el diagnóstico de la EA.

En este contexto, la presente Tesis Doctoral se presenta como un compendio de cuatro publicaciones indexadas en el *Journal Citation Reports* (JCR) entre los años 2018 y 2021. El objetivo de estas publicaciones es la caracterización de los cambios neuronales subyacentes en las diferentes etapas de la EA y su etapa prodrómica, DCL, siguiendo los tres niveles de análisis antes mencionados. Siguiendo el orden cronológico, la primera publicación se centró en estudiar los cambios que provocan la demencia por EA y el DCL a nivel de activación local (Ruiz-Gómez et al., 2018a). La información proporcionada por varios parámetros espectrales y no lineales sirvió para entrenar diferentes clasificadores, que nos llevaron a proponer un protocolo de cribado de la EA. Los dos siguientes trabajos se centraron en los análisis de interacciones entre sensores. En particular, la segunda publicación tenía como objetivo evaluar la capacidad de dos métricas de conectividad no lineales derivadas de la entropía cruzada para caracterizar los patrones de acoplamiento durante el DCL y la EA (Ruiz-Gómez et al., 2018b). En el tercer artículo (Ruiz-Gómez et al., 2019b), se analizó cómo diferentes métricas de conectividad funcional se ven afectadas por los efectos espurios de la conducción de volumen utilizando un modelo que simulaba la actividad EEG, y si éstas son capaces de caracterizar las alteraciones cerebrales durante el continuo de la EA. Por último, la cuarta publicación se centró en el análisis de los cambios en la organización funcional de las redes cerebrales durante el continuo de la EA. Específicamente, el objetivo de este estudio fue proponer y evaluar un nuevo método para construir redes *multiplex* que integrasen la información de las redes obtenidas en las bandas de frecuencia convencionales utilizando análisis de correlación canónica (CCA, *Canonical Correlation Analysis*) (Ruiz-Gómez et al., 2021).

C.2 Hipótesis y objetivos

Durante las últimas décadas, los mecanismos neuronales asociados con la neurodegeneración y el deterioro cognitivo del cerebro han centrado una gran atención. Sin embargo, aún es necesaria una mejor identificación de los sustratos neurofisiológicos subyacentes a las lesiones biológicas en el DCL y la EA. Por tanto, nuestra hipótesis es que *el análisis de la actividad EEG espontánea mediante puede servir*

para tratar de caracterizar las alteraciones cerebrales durante las diferentes etapas del continuo de la EA. Particularmente, para llevar a cabo esta caracterización, los datos se examinaron siguiendo tres niveles de análisis: (i) análisis de patrones de activación local en sensores individuales; (ii) análisis de interacciones entre sensores usando métricas conectividad y sincronización; y (iii) análisis de la organización funcional de las redes cerebrales, aplicando parámetros derivados de la teoría de redes complejas.

La aplicación de diferentes métodos en los dominios de la frecuencia (medidas espectrales) y del tiempo (medidas no lineales) a la actividad de EEG en sensores individuales ha llevado a observar dos efectos principales en la EA y el DCL: ralentización del EEG y reducción de la complejidad de las señales EEG. Por lo tanto, es razonable plantear la siguiente hipótesis: *una metodología basada en la combinación de características espectrales y no lineales puede ser una herramienta útil para ayudar en el diagnóstico de la EA y el DCL.*

Sin embargo, los estudios de activación local no son suficientes para obtener una caracterización completa de la dinámica cerebral de la EA (Stam and van Straaten, 2012). Es por ello que muchos estudios de EEG se han centrado en el análisis de interacciones entre sensores (Canuet et al., 2012; Engels et al., 2015; Koenig et al., 2005; Moretti et al., 2008; Tóth et al., 2014). La mayoría de estudios utilizan métricas de conectividad funcional y apoyan la hipótesis bien establecida de la EA como un 'síndrome de desconexión'. Solo unos pocos estudios han aplicado métodos no lineales, como métricas de entropía cruzada, a sistemas biológicos con el objetivo de estimar los patrones de sincronización (Licinio et al., 1998; Martínez-Zarzuela et al., 2013; Pincus and Singer, 1996). Por lo tanto, planteamos la hipótesis de que *métricas de entropía cruzada pueden caracterizar patrones de acoplamiento alterados entre diferentes canales EEG en la EA y el DCL.*

Estos estudios de conectividad funcional pueden estar sesgados debido a los efectos de la conducción de volumen, ya que estas métricas podrían reflejar valores de acoplamiento espurios entre fuentes cerebrales independientes. Por lo tanto, se hipotetiza que *diversas medidas de conectividad funcional se ven afectadas de manera diferente por los efectos de conducción de volumen y podrían sesgar los resultados.*

Basándonos en los resultados obtenidos con las medidas de acoplamiento, se pueden construir grafos como una representación abstracta de la actividad cerebral. Estas representaciones se han cuantificado utilizando parámetros derivados de la teoría de redes complejas, proporcionando información sobre la organización específica del cerebro. En particular, la EA se asocia principalmente con una

disminución progresiva del procesamiento de la información global y un aumento progresivo del procesamiento de la información local. Sin embargo, se han obtenido resultados contradictorios en diferentes bandas de frecuencia (He et al., 2008; Lo et al., 2010; Sanz-Arigita et al., 2010; Stam et al., 2009; Tijms et al., 2013; Yao et al., 2010; Zhao et al., 2012). Esto complica las posibles interpretaciones clínicas sobre las alteraciones que provoca la neurodegeneración de la EA. Por lo tanto, planteamos la hipótesis de que *un enfoque multiplex que analice conjuntamente diferentes bandas de frecuencia podría capturar información relevante de toda la red cerebral.*

El objetivo general de la presente Tesis Doctoral es estudiar, diseñar y aplicar nuevos métodos de procesado para caracterizar las alteraciones de los sustratos neuronales durante el continuo de la demencia debida a EA. Para lograr este objetivo principal, se han planteado los siguientes objetivos específicos:

I. Revisar la bibliografía y el estado del arte relacionado con metodologías de procesamiento de señales biomédicas útiles para caracterizar datos EEG. En concreto, la metodología estará basada en 3 niveles: medidas de activación local, métricas de acoplamiento, y parámetros derivados de la teoría de grafos, con el fin de caracterizar de manera integral la dinámica neuronal cerebral.

II. Construir una base de datos de registros de actividad EEG espontánea y expandir la existente. Ambas bases de datos están formadas por los registros de EEG, datos sociodemográficos y variables clínicas de pacientes en las diferentes etapas del continuo de la EA, incluidos los pacientes con DCL y controles.

III. Seleccionar e implementar los métodos más adecuados para obtener medidas locales, de acoplamiento y de red que caractericen la dinámica cerebral durante el proceso de neurodegeneración y modelar los efectos de conducción de volumen en las señales EEG.

IV. Evaluar el rendimiento diagnóstico de los métodos seleccionados y su capacidad para caracterizar los cambios cerebrales en las diferentes etapas del continuo de la EA.

V. Comparar y discutir los resultados obtenidos con el objetivo de extraer las conclusiones oportunas. Este objetivo incluye la comparación con los estudios más recientes sobre el análisis del EEG en el DCL y la EA.

Tabla C.1: Datos socio-demográficos y clínicos de la base de datos del Hospital Universitario Río Hortega.

	Controles	**DCL**	**EA**
Número de sujetos	37	37	37
Edad (media ± SD[1])	76.3 ± 3.5	76.0 ± 7.3	79.8 ± 6.0
Género (Hombre:Mujer)	12:25	16:21	12:25
MMSE[2] (media ± SD[1])	28.9 ± 1.3	27.3 ± 1.9	21.2 ± 3.3

[1]SD: desviación estándar. [2]MMSE: resultado del test *Mini Mental State Examination.*
DCL: pacientes con deterioro cognitivo leve; EA: pacientes con enfermedad de Alzheimer.

Tabla C.2: Datos socio-demográficos y clínicos de la base de datos del proyecto AD-EEGWA.

	Controles	**DCL**	**EA_{mil}**	**EA_{mod}**	**EA_{sev}**
Número de sujetos	51	51	51	50	50
Edad (media ± SD[1])	80.1 ± 7.1	85.5 ± 7.2	80.7 ± 7.0	81.3 ±8.0	80.0 ± 7.8
Género (Hombre:Mujer)	26:25	15:36	21:30	7:43	7:43
MMSE[2] (media ± SD[1])	28.8 ± 1.1	23.3 ± 2.8	22.5 ± 2.3	13.6 ± 2.8	2.42 ± 3.7

[1]SD: desviación estándar. [2]MMSE: resultado del test *Mini Mental State Examination.*
DCL: pacientes con deterioro cognitivo leve; EA_{mil}: pacientes con enfermedad de Alzheimer leve; EA_{mod}: pacientes con enfermedad de Alzheimer moderada; EA_{sev}: pacientes con enfermedad de Alzheimer severa.

VI. Difundir los principales resultados y conclusiones de la investigación en revistas indexadas del JCR, así como en congresos internacionales y nacionales.

C.3 Sujetos

Para llevar a cabo los estudios que forman parte de este compendio se han utilizado dos bases de datos. La primera está compuesta por un total de 111 registros EEG adquiridos en un entorno clínico, en el Hospital Universitario Río Hortega (Valladolid, España) antes del comienzo de la Tesis. Cabe destacar que durante el desarrollo de la misma pero con posterioridad a la publicación de los estudios, el número de registros aumentó hasta 196, contando con los primeros registros longitudinales. Por su parte, la segunda base de datos fue registrada durante el desarrollo de la Tesis y está compuesta por 253 registros EEG adquiridos en un entorno de investigación como resultado del Proyecto POCTEP 2014-2020 'Análisis y correlación entre el genoma completo y la actividad cerebral para la ayuda en el diagnóstico de la enfermedad de Alzheimer'(AD-EEGWA). En las tablas C.1 y C.2 se recogen los datos sociodemográficos y clínicos de los sujetos incluidos en cada base de datos.

La adquisición del EEG fue muy similar para ambas bases de datos. Para ca-

da sujeto, se registraron cinco minutos de actividad EEG espontánea utilizando un sistema de 19 canales distribuidos siguiendo el Sistema Internacional 10-20. Se pidió a los sujetos que permanecieran en un estado relajado, despiertos y con los ojos cerrados durante la adquisición del EEG. Sin embargo, el equipo de adquisición de EEG y la frecuencia de muestreo varían dependiendo de la base de datos. Los registros del Hospital Universitario Río Hortega se adquirieron con un XLTEK® (Natus Medical, Pleasanton, CA, EE. UU.) a una frecuencia de muestreo de 200 Hz. Por otra parte, la base de datos POCTEP se registró con un equipo Nihon Kohden Neurofax JE-921A (Nihon Koden, Tokio, Japón) a una frecuencia de muestreo de 500 Hz. En ambos casos, las señales fueron re-referenciadas mediante referencia promedio común (CAR) y se llevaron a cabo las mismas etapas de preprocesamiento para eliminar artefactos.

C.4 Métodos

La metodología utilizada en las distintas publicaciones que forman el compendio sigue una misma estructura general. Todos los estudios comienzan con una etapa de pre-procesado, seguida de una de extracción de características. Posteriormente, en los trabajos que tienen un enfoque hacia la caracterización las alteraciones cerebrales durante las distintas etapas de la EA (Ruiz-Gómez et al., 2018b, 2019b, 2021), se incluye una etapa de análisis estadístico. Por otra parte, si el enfoque del estudio es la discriminación entre las distintas etapas de la EA, se incluyen etapas de selección y clasificación de características (Ruiz-Gómez et al., 2018a,b, 2019b). Además de estos análisis enfocados a la caracterización de la EA, en esta Tesis Doctoral se ha propuesto un nuevo método para modelar señales sintéticas para estudiar el efecto de la conducción de volumen del EEG y un nuevo método para crear redes *multiplex* a partir del análisis de CCA.

C.4.1 Señales EEG sintéticas

El nuevo método propuesto para generar señales EEG sintéticas está basado en la combinación de un modelo anatómico de las distintas capas de la cabeza, construido a partir de información de la base de datos del Visible Human Project® (VHP) (U.S. National Library of Medicine, 2018), y un conjunto de osciladores acoplados que forman un modelo Kuramoto (Kuramoto, 1975), utilizados para simular las fuentes cerebrales dentro del cerebro. Para estudiar el efecto de la conducción de volumen del EEG, se simularon dos escenarios diferentes: (i) un caso ideal sin

conducción de volumen en el que cada fuente solo es registrada por el electrodo más cercano, y (ii) el caso real con conducción de volumen, donde la actividad de cada fuente es registrada por todos los electrodos simulados (Ruiz-Gómez et al., 2019b).

C.4.2 Activación local

Después de la etapa de preprocesamiento, las épocas libres de artefactos se analizaron en primer lugar mediante métricas que se centran en determinar el nivel de activación de los grupos neuronales individuales. Desde el punto de vista de cómo se extrae la información, se pueden distinguir dos tipos diferentes de parámetros: espectrales y no lineales.

Los métodos espectrales extraen información del EEG en base a su contenido espectral y se calculan a partir de la densidad espectral de potencia normalizada (PSD_n). En nuestro caso se han calculado la potencia relativa (RP), que representa la contribución relativa de diferentes componentes de frecuencia al espectro de potencia global (Rodriguez et al., 1999), la frecuencia mediana (MF), que se define como la frecuencia que comprende la mitad de la potencia del espectro, la frecuencia individual alpha (IAF), que es la MF teniendo en cuenta únicamente la banda alpha extendida (4–15 Hz) (Moretti et al., 2004), y la entropía espectral (SE), que estima la irregularidad de la señal en términos de cómo de plano es el espectro de potencia de la misma (Powell and Percival, 1979).

Para complementar este análisis espectral, también se calcularon cinco métodos globales no lineales: la complejidad de Lempel-Ziv (LZC) (Lempel and Ziv, 1976), la medida de tendencia central (CTM) (Cohen et al., 1996), la entropía muestral (SampEn) (Richman and Moorman, 2000), la entropía difusa (FuzzyEn) (Chen et al., 2007), y la auto-información mutua (AMI) (Fraser and Swinney, 1986). Estos métodos cuantifican la complejidad, la variabilidad y la irregularidad de las señales EEG utilizando diferentes procedimientos.

C.4.3 Similitud entre pares de sensores

De forma análoga, en el segundo nivel de análisis también se ha estudiado el comportamiento de dos tipos diferentes de medidas de acoplamiento: métricas de conectividad funcional y métricas de acoplamiento derivadas de métodos no lineales.

Se han estudiado diferentes métricas de conectividad funcional complementarias desde el punto de vista del proceso de inferencia y algunas métricas que fue-

ron propuestas para superar algunas limitaciones de las existentes. En concreto, se han empleado la magnitud al cuadrado de la coherencia (MSCOH) (Roach and Mathalon, 2008), la parte imaginaria de coherencia (iCOH) (Nolte et al., 2004), la coherencia con el retardo de fase eliminado (lagCOH) (Pascual-Marqui et al., 2011), la correlación de envolvente de amplitud (AEC) (Brookes et al., 2014), la probabilidad de sincronización (SL) (Stam and Van Dijk, 2002), el índice de retardo de fase (PLI) (Stam et al., 2007), el valor de acoplamiento de fase (PLV) (Mormann et al., 2000), y el PLV corrigiendo la parte imaginaria (ciPLV) (Bruña et al., 2018).

Además, la aplicación de métodos no lineales sobre dos series temporales en lugar de a una única señal permite obtener métricas de acoplamiento derivadas de métodos no lineales, como las utilizadas en este compendio: la entropía aproximada cruzada (Cross-ApEn) (Pincus, 2000) y entropía muestral cruzada (Cross-SampEn) (Richman and Moorman, 2000).

C.4.4 Organización de red

Después de la estimación de la similitud entre todos los pares de sensores, estas matrices de adyacencia pueden ser interpretadas como una red utilizando parámetros de grafos derivados de la teoría de redes complejas. Hay que tener en cuenta que en todos los estudios se ha utilizado la matriz de conectividad completa para el cálculo de los parámetros de red, ya que la aplicación de un umbral arbitrario para binarizar o umbralizar la matriz podría introducir un sesgo.

Concretamente, en esta Tesis Doctoral se han utilizado tres medidas de grafos que aportan información complementaria de las características de la red y que son suficientemente representativas e intuitivas de las propiedades de la misma. Además, el coste computacional de las medidas es muy bajo. Específicamente, hemos estudiado la fuerza de la conectividad mediante el parámetro *strength* global (s), la integración de la red mediante la longitud de camino característica (L) y la segregación de la red mediante el coeficiente de agrupamiento (C) (Rubinov and Sporns, 2010). Dado que los resultados de conectividad dependen de la frecuencia, se obtuvo un valor para cada parámetro de red para cada una de las bandas de frecuencia de EEG convencionales.

Sin embargo, la interpreteción clínica de estos parámetros dependientes de la frecuencia es complicada. Es por ello que recientes estudios proponen la construcción de redes *multiplex*, que contengan toda la información de la red cerebral (Battiston et al., 2014; De Domenico et al., 2016). Se han utilizado diferentes méto-

dos para construir estas redes *multiplex*, desde una simple suma de los parámetros específicos de cada banda de frecuencia hasta enfoques más complejos, como usar una función de calidad para determinar el valor de los enlaces entre las diferentes capas (Kabbara et al., 2018). Estos métodos presentan algunas limitaciones, como que podrían compensar tendencias opuestas entre grupos para las bandas de frecuencia analizadas, perdiéndose las diferencias estadísticamente significativas entre ellos. Es por esta razón que en esta Tesis Doctoral se ha propuesto un nuevo método para construir redes *multiplex* utilizando los vectores base obtenidos con CCA, que pueden asignar valores negativos a los pesos asignados a cada banda.

C.4.5 Análisis estadístico

Para tratar de caracterizar los cambios cerebrales provocados por los procesos neurodegenerativos en las diferentes etapas del continuo de la EA, se utilizaron diferentes tests de hipótesis estadísticas. Dado que nuestros datos no cumplieron con los supuestos de normalidad y homocedasticidad (tests de Shapiro-Wilk y Levene, respectivamente), las diferencias estadísticas entre ellas se evaluaron con pruebas no paramétricas. Dado que en algunos estudios (Ruiz-Gómez et al., 2018b, 2019b) estamos aplicando estos tests un número muy elevado de veces, por ejemplo al comparar los valores de conectividad para cada par de electrodos de diferentes grupos de gravedad, la probabilidad de obtener un falso positivo aumenta drásticamente. Es por ello que ha sido necesario aplicar procedimientos de control de la tasa de falsos descubrimientos (FDR). En concreto, se ha aplicado el procedimiento de Benjamini-Hochberg para corregir los p-valores obtenidos (Benjamini and Hochberg, 1995).

C.4.6 Análisis de clasificación

Por otra parte, para evaluar la capacidad diagnóstica de nuestras propuestas, se han utilizado distintos modelos de clasificación de características. Sin embargo, la extracción de numerosas características puede llevar a la obtención de información redundante, por lo que una etapa previa de selección de características es necesaria. Con esta etapa se obtiene un conjunto óptimo de características para el problema de clasificación. Particularmente, dos métodos de selección de características se han utilizado en esta Tesis: regresión multilineal por pasos con una selección directa condicional (Guyon and Elisseeff, 2003) y un filtro basado en correlación (FCBF) (Yu and Liu, 2004). Particularmente, la regresión multilineal fue utilizada en Ruiz-Gómez et al. (2019b), mientras que FCBF se utilizó en Ruiz-Gómez et al. (2018a)

y Ruiz-Gómez et al. (2018b).

Una vez obtenido el conjunto óptimo de características, diferentes técnicas de aprendizaje automático han sido utilizadas para abordar la clasificación de los distintos sujetos. Entre las diferentes técnicas de aprendizaje supervisado, se han utilizado el análisis discriminante lineal (LDA) (Ruiz-Gómez et al., 2018a,b, 2019b), el análisis discriminante cuadrático (QDA) (Ruiz-Gómez et al., 2018a,b), las máquinas de vectores de soporte (SVM) (Ruiz-Gómez et al., 2018b), los árboles de decisión (DT) (Ruiz-Gómez et al., 2018b), y las redes neuronales artificiales de perceptrón multicapa (MLP) (Ruiz-Gómez et al., 2018a).

C.5 Resultados y discusión

Mediante las distintas técnicas de procesado previamente descritas, ha sido posible identificar algunas de las alteraciones en la actividad cerebral en las distintas etapas de la EA para cada uno de los niveles de análisis estudiados. Además, estas medidas nos permitieron discriminar entre los distintos grupos de severidad.

C.5.1 Activación local

En cuanto a los métodos espectrales, se ha podido observar una lentificación progresiva de la actividad espontánea del EEG con el DCL y la EA. Concretamente, los valores obtenidos para las medidas espectrales mostraron un aumento de potencia en las bajas frecuencias y una disminución en las bandas de alta frecuencia a medida que la severidad de la enfermedad aumentaba (Ruiz-Gómez et al., 2018a). Estos resultados apoyan la tendecia de lentificación del espectro como consecuencia de la EA, anteriormente sugerida por estudios previos (Dauwels et al., 2010; Jeong, 2004). Esta lentificación pueden estar relacionada con la pérdida de la inervación colinérgica del neocórtex, que puede provocar diferentes síntomas cognitivos como la pérdida de memoria, y con déficits del neurotransmisor acetilcolina, encargado de modular la actividad sináptica del sistema nervioso (Dauwels et al., 2010; Osipova et al., 2003). Por otra parte, con respecto a los métodos no lineales, nuestros resultados sugieren que la actividad del EEG parece ser menos compleja y más regular a medida que avanza la enfermedad. Estas alteraciones en el procesamiento de la información podrían estar relacionadas con la pérdida de neuronas o la pérdida de sinapsis entre ellas, ya que estos hechos afectan directamente al procesamiento dinámico de las redes neuronales del cerebro (Baraniuk et al., 2001; Dauwels et al., 2010). Además, dado que ambos tipos de métricas aportan infor-

mación complementaria y reflejan diferentes aspectos de la red neuronal, se podría descartar la hipótesis de que es posible que la menor complejidad pueda estar relacionada con la ralentización del EEG y sus causas, ya que las señales con mayor contenido en bajas frecuencias son intrínsecamente más regulares (Dauwels et al., 2011).

Además de esta caracterización, también se ha evaluado la capacidad diagnóstica de estas medidas utilizando diferentes clasificadores. La mayoría de estudios previos siempre se han centrado en problemas de discriminación binaria (Bertè et al., 2014; Buscema et al., 2015; Iqbal et al., 2005; Poza et al., 2017), mientras que nuestro enfoque ha sido una clasificación en tres grupos. Únicamente un estudio previo realizó una clasificación en tres grupos, pero mediante clasificadores binarios (McBride et al., 2014). Aunque sus resultados fueron ligeramente superiores a los nuestros (78.43 % al comparar controles sanos frente a todos y 76.47 % para EA frente a todos en nuestro caso, y 85.42 % y 83.33 % en sus caso, respectivamente), nuestra propuesta presenta varias ventajas. Principalmente, al utilizar un enfoque de dividir la base de datos en entrenamiento y test, nosotros obtuvimos un único modelo, mientras que ellos obtuvieron un modelo para cada iteración del proceso de validación cruzada. Además, nuestro modelo ha demostrado la capacidad de detectar si un sujeto padece EA o DCL (detectando correctamente 28 de los 34 sujetos no sanos) prediciendo únicamente 2 de 17 pacientes con EA como controles sanos, y también fue capaz de descartar EA en 27 de los 34 sujetos que no la padecían (79,41 %), incluidos 15 de los 17 controles (88,24 %) (Ruiz-Gómez et al., 2018a). Estos hechos hacen que sea más fácil evaluar posibles nuevos registros y establecer un protocolo de cribado.

C.5.2 Similitud entre pares de sensores

Sin embargo, no es posible llevar a cabo un caracterización completa de la dinámica cerebral utilizando únicamente técnicas espectrales y no lineales. Por esta razón, los enfoques de conectividad se han vuelto esenciales para comprender mejor la organización del cerebro. Se realizaron dos estudios al respecto (Ruiz-Gómez et al., 2018b, 2019b).

En el primero, se comparó el comportamiento de dos medidas de acoplamiento no lineales derivadas del concepto de entropía aplicado a dos series temporales, la Cross-ApEn y la Cross-SampEn (Ruiz-Gómez et al., 2018b). En primer lugar, los resultados obtenidos con las distintas configuraciones de parámetros mostraron que las ventanas de longitud pequeña (parámetro m en ambas medidas) son más

adecuadas para captar la naturaleza rápida de las fluctuaciones del EEG. Adicionalmente, teniendo en cuenta que la Cross-SampEn mostró un mayor número de conexiones significativas entre los tres grupos para todas las combinaciones de parámetros y sus ventajas técnicas sobre la Cross-ApEn, podríamos decir que la Cross-SampEn es más adecuada para caracterizar los patrones de acoplamiento neuronal en el DCL y la EA. Los resultados obtenidos sugieren que las señales de EEG de diferentes regiones del cerebro se vuelven gradualmente menos similares a medida que avanza la demencia, y además la banda β juega un papel clave en las etapas prodrómicas de la EA. Estos hallazgos apoyan la hipótesis de desconexión y siguen la misma tendencia de estudios previos (Engels et al., 2015; Koenig et al., 2005; Tóth et al., 2014), en los que se mostró una disminución de la conectividad en las bandas de altas frecuencias. Además, estos cambios nos permitieron discriminar cuando un sujeto no padece EA y cuando un sujeto no padece DCL con valores de clasificación bastante elevados: especificidades de 94,12 % y 88,24 %, y valores predictivos negativos del 76,19 % 68,18 %, respectivamente. Estos resultados apoyan la hipótesis de 'síndrome de desconexión' de la EA y podrían estar asociados tanto a alteraciones en el procesamiento de la información en la corteza cerebral como a la disminución de los niveles de acetilcolina que perturban la transmisión sináptica (Baraniuk et al., 2001; Jeong et al., 2001). Sin embargo, tanto estos resultados como los obtenidos en estudios previos pueden estar sesgados debido a los efectos de conducción del volumen del EEG.

Es por este hecho que nuestro segundo estudio se centró en estudiar cómo diferentes métricas de conectividad funcional se ven afectadas por la conducción de volumen del EEG y evaluar si son capaces de detectar cambios reales en la sincronización neuronal (Ruiz-Gómez et al., 2019b). Para ello, se propuso un nuevo modelo para construir señales sintéticas basado en osciladores de Kuramoto. Además, se caracterizaron las alteraciones cerebrales en las diferentes etapas del continuo de la EA utilizando la métrica menos afectada por las influencias espurias de la conducción de volumen (PLI), reduciendo así el posible sesgo. Nuestros resultados utilizando las señales sintéticas demostraron que las modificaciones propuestas a las métricas funcionales existentes (iCOH, lagCOH y ciPLV) y las nuevas medidas propuestas (AEC y PLI) se vieron menos afectadas por la conducción de volumen en comparación con las originales (MSCOH, SL y PLV), como se esperaba de la teoría. Sin embargo, ninguna de las métricas analizadas fue inmune a la conducción de volumen, pero estos efectos fueron menores para PLI, lo que hace que esta métrica sea más adecuada para estudiar las alteraciones neuronales subyacentes a la EA. Nuestros resultados utilizando PLI revelaron aumentos de acoplamiento en

bandas de baja frecuencia, volviéndose más pronunciados a medida que avanza la demencia. Por otro lado, progresivamente se encontraron disminuciones de conectividad en las bandas de alta frecuencia, siendo estadísticamente significativas en la última etapa de la demencia en la banda α. Estos resultados siguen las mismas tendencias que estudios previos (Engels et al., 2015; Koenig et al., 2005; Tóth et al., 2014). La pérdida de acetilcolina podría apoyar la disminución de acoplamiento en altas frecuencias y el aumento en bajas frecuencias, lo que se conoce como 'hipótesis colinérgica de la EA' (Bartus et al., 1982; Francis et al., 1999). Sin embargo, se deben tener en cuenta otras hipótesis, como cambios estructurales del cerebro (disminución del volumen del hipocampo, atrofia medial y pérdida neuronal) y un posible proceso de atrofia cerebral (Cho et al., 2008; Karas et al., 2004).

C.5.3 Organización de red

La caracterización de la red cerebral mediante medidas de grafos se ha realizado típicamente en las bandas de frecuencia convencionales del EEG. Sin embargo, estas redes no son capaces de reflejar el comportamiento de la red global y a menudo muestran resultados contradictorios dependiendo de las frecuencias estudiadas. Es por ello que durante los últimos años se ha tratado de integrar toda esta información mediante metodologías *multiplex*. Sin embargo, estas metodologías también presentan una serie de limitaciones, como que la mayoría de las técnicas propuestas requieren tener los valores de enlace entre nodos homólogos de diferentes capas para construir la red *multiplex* (estos enlaces entre capas no suelen estar disponibles (Battiston et al., 2014; De Domenico et al., 2016; Yu et al., 2017) y además algunas de estas metodologías tienden a difuminar las diferencias entre los grupos cuando se las tendencias en las distintas bandas de frecuencia son opuestas (como por ejemplo en el caso de la EA, donde el coeficiente de agrupamiento típicamente disminuye en la banda α pero aumenta en la banda θ (Afshari and Jalili, 2017; Stam et al., 2009)). Estos hechos fueron los que nos motivaron a proponer una nueva metodología para construir redes *multiplex* basada en CCA.

En primer lugar, los resultados *multiplex* de tres parámetros de grafos típicos (*strength*, longitud de camino característico y coeficiente de agrupamiento) obtenidos utilizando las señales sintéticas siguieron un comportamiento análogo en comparación con sus homólogos clásicos, por lo que pueden interpretarse en términos de red similares. Además, cuando esta metodología fue aplicada a los registros EEG reales pertenecientes a pacientes con EA, nuestros resultados revelaron un

aumento progresivo en la longitud de camino característica y una disminución progresiva del coeficiente de agrupamiento a medida que avanza la enfermedad (Ruiz-Gómez et al., 2021). Estos resultados indican una disminución en la integración y en la segregación de la red, es decir, hay un mayor coste para que exista el intercambio de información entre las distintas áreas del cerebro (Cai et al., 2020; Kabbara et al., 2018). Además, teniendo en cuenta ambos fenómenos, podemos decir que la demencia debida a la EA se aumenta la vulnerabilidad de la red, dado que existe una pérdida de sus propiedades de '*small-world*' a medida que avanza la enfermedad.

C.6 Conclusiones

El análisis y discusión de los resultados de los estudios incluidos en este compendio de publicaciones permiten extraer las principales conclusiones de esta Tesis Doctoral:

1) El EEG en estado de reposo proporciona información valiosa acerca de las alteraciones cerebrales provocadas por los procesos neurodegenerativos de la EA, que se pueden extraer mediante diferentes técnicas de procesamiento de señal. El uso de estos métodos nos lleva a una mejor caracterización y comprensión de los cambios que ocurren en el interior del cerebro durante las diferentes etapas del continuo de la enfermedad.

2) Los cambios locales en la actividad EEG espontánea parecen estar relacionados con la progresión de la enfermedad, ya que los sujetos con DCL muestran valores intermedios entre los controles sanos y los pacientes con EA. Las alteraciones típicas son una ralentización de los ritmos EEG (cambio del espectro de potencia de componentes de alta frecuencia a componentes de baja frecuencia), una pérdida de complejidad, y un aumento de regularidad.

3) Los métodos espectrales y no lineales proporcionan información complementaria útil para llevar a cabo un modelo de clasificación en tres grupos, que se puede utilizar como un protocolo de detección para el cribado y diagnóstico de la EA.

4) La estimación del acoplamiento entre diferentes regiones del cerebro se ve afectada por los efectos espurios de la conducción de volumen asociada al EEG. Por lo tanto, para lograr una interpretación correcta de los resultados, es importante emplear métricas de acoplamiento que sean capaces de detectar

interacciones cerebrales reales minimizando el efecto de la distorsión por conducción de volumen.

5) El intercambio de información entre áreas distantes del cerebro produce una activación coordinada de grupos neuronales, que pueden alterarse debido a los procesos neurodegenerativos. Particularmente, la EA se caracteriza por una reducción progresiva de la conectividad funcional en las bandas altas de frecuencia y un aumento en las bandas bajas de frecuencia. Se cree que los aumentos de acoplamiento pueden ser causados por mecanismos compensatorios en el cerebro. Sin embargo, estos hallazgos apoyan la hipótesis del síndrome de desconexión.

6) El uso de un procedimiento objetivo que permite asignar pesos negativos para construir redes *multiplex* evita compensar las típicas tendencias opuestas que se han obtenido previamente en la EA según la banda de frecuencia analizada. En particular, la metodología propuesta basada en CCA nos lleva a obtener parámetros *multiplex* que pueden ser interpretados de forma análoga a sus homólogos utilizados típicamente en bandas específicas de frecuencia, facilitando así su interpretación clínica.

7) Las topologías de red *multiplex* en la EA tienden a estar menos integradas y menos segregadas a medida que aumenta la gravedad de la enfermedad. Por lo tanto, la EA se caracteriza por una pérdida de las propiedades '*small-world*' de la red, lo que aumenta la vulnerabilidad de la red cerebral global como consecuencia de los procesos neurodegenerativos.

Bibliography

Abásolo, D., Escudero, J., Hornero, R., Gómez, C., Espino, P., 2008. Approximate entropy and auto mutual information analysis of the electroencephalogram in Alzheimer's disease patients. Medical and Biological Engineering and Computing 46, 1019–1028.

Abásolo, D., Hornero, R., Carlos, G., Miguel, L., 2006. Analysis of EEG background activity in Alzheimer ' s disease patients with Lempel – Ziv complexity and central tendency measure. Medical Engineering and Physics Physics 28, 315–322.

Afshari, S., Jalili, M., 2017. Directed Functional Networks in Alzheimer's Disease: Disruption of Global and Local Connectivity Measures. IEEE Journal of Biomedical and Health Informatics 21 (4), 949–955.

Ahmadi, N., Pei, Y., Pechenizkiy, M., 2019. Effect of linear mixing in EEG on synchronization and complex network measures studied using the Kuramoto model. Physica A: Statistical Mechanics and its Applications 520, 289–308.

Aisen, P. S., may 2002. The potential of anti-inflammatory drugs for the treatment of Alzheimer's disease.

Albert, M. S., DeKosky, S. T., Dickson, D., Dubois, B., Feldman, H. H., Fox, N. C., Gamst, A., Holtzman, D. M., Jagust, W. J., Petersen, R. C., Snyder, P. J., Carrillo, M. C., Thies, B., Phelps, C. H., 2011. The diagnosis of mild cognitive impairment due to Alzheimer's disease: Recommendations from the National Institute on Aging-Alzheimer's Association workgroups on diagnostic guidelines for Alzheimer's disease. Alzheimer's and Dementia 7 (3), 270–279.

Alzheimer's Association, 2020. Alzheimer's Disease Facts and Figures 2020. Alzheimer's and Dementia 16 (3), 1–94.

Babiloni, C., Del Percio, C., Lizio, R., Noce, G., Cordone, S., Lopez, S., Soricelli, A., Ferri, R., Pascarelli, M. T., Nobili, F., Arnaldi, D., Aarsland, D., Orzi, F., Buttinelli, C., Giubilei, F., Onofrj, M., Stocchi, F., Stirpe, P., Fuhr, P., Gschwandtner, U., Ransmayr, G., Caravias, G., Garn, H., Sorpresi, F., Pievani, M., Frisoni, G. B., D'Antonio, F., De Lena, C., Güntekin, B., Hanoğlu, L., Başar, E., Yener, G., Emek-Savaş, D. D., Triggiani, A. I., Franciotti, R., De Pandis, M. F., Bonanni, L., jul 2017. Abnormalities of cortical neural synchronization mechanisms in patients with dementia due to Alzheimer's and Lewy body diseases: an EEG study. Neurobiology of Aging 55, 143–158.

Baraniuk, R. G., Flandrin, P., Janssen, A. J., Michel, O. J., 2001. Measuring time-frequency information content using the Reényi entropies. IEEE Transactions on Information Theory 47 (4), 1391–1409.

Bartus, R., Dean, R., Beer, B., Lippa, A., 1982. The cholinergic hypothesis of geriatric memory dysfunction. Science 217, 408–414.

Battiston, F., Nicosia, V., Latora, V., 2014. Structural measures for multiplex networks. Physical Review E - Statistical, Nonlinear, and Soft Matter Physics 89 (3), 032804.

Benjamini, Y., Hochberg, Y., 1995. Controlling the false discovery rate: a practical and powerful approach to multiple testing. Journal of the Royal Statistical Society B 57 (1), 289–300.

Bertè, F., Lamponi, G., Calabrò, R. S., Bramanti, P., 2014. Elman neural network for the early identification of cognitive impairment in Alzheimer's disease. Functional neurology 29 (1), 57–65.

Bischof, G. N., Jesse, F., Fliessbach, K., Dronse, J., Hammes, J., Neumaier, B., Onur, O., Fink, G. R., Kukolja, J., Drzezga, A., van Eimeren, T., 2016. Impact of tau and amyloid burden on glucose metabolismin Alzheimer's disease. Annals of Clinical and Translational Neurology 3 (12), 934–939.

Bishop, C. M., 2006. Pattern recognition and machine learning. Springer.

Blennow, K., de Leon, M. J., Zetterberg, H., 2006. Alzheimer's disease. Lancet 368 (9533), 387–403.

Boccaletti, S., Bianconi, G., Criado, R., del Genio, C. I., Gómez-Gardeñes, J., Romance, M., Sendiña-Nadal, I., Wang, Z., Zanin, M., 2014. The structure and dynamics of multilayer networks. Physics Reports 544 (1), 1–122.

Briels, C. T., Briels, C. T., Schoonhoven, D. N., Schoonhoven, D. N., Stam, C. J., De Waal, H., Scheltens, P., Gouw, A. A., jun 2020. Reproducibility of EEG functional connectivity in Alzheimer's disease. Alzheimer's Research and Therapy 12 (1), 1–14.

Briggs, R., Kennelly, S. P., O'Neill, D., 2016. Drug treatments in Alzheimer's disease. Clinical Medicine Journal 16 (3), 247–253.

Brodaty, H., Ames, D., Snowdon, J., Woodward, M., Kirwan, J., Clarnette, R., Lee, E., Lyons, B., Grossman, F., 2003. A randomized placebo-controlled trial of risperidone for the treatment of aggression, agitation, and psychosis of dementia. Journal of Clinical Psychiatry 64 (2), 134–143.

Bronzino, J. D., Peterson, D. R., 2014. Biomedical Engineering Fundamentals. CRC Press.

Brookes, M. J., O'Neill, G. C., Hall, E. L., Woolrich, M. W., Baker, A., Palazzo Corner, S., Robson, S. E., Morris, P. G., Barnes, G. R., 2014. Measuring temporal, spectral and spatial changes in electrophysiological brain network connectivity. NeuroImage 91, 282–299.

Bruña, R., Maestú, F., Pereda, E., 2018. Phase locking value revisited: Teaching new tricks to an old dog. Journal of Neural Engineering 15 (5), 056011.

Buscema, M., Vernieri, F., Massini, G., Scrascia, F., Breda, M., Rossini, P. M., Grossi, E., 2015. An improved I-FAST system for the diagnosis of Alzheimer's disease from unprocessed electroencephalograms by using robust invariant features. Artificial Intelligence in Medicine 64 (1), 59–74.

Cai, L., Wei, X., Liu, J., Zhu, L., Wang, J., Deng, B., Yu, H., Wang, R., 2020. Functional Integration and Segregation in Multiplex Brain Networks for Alzheimer's Disease. Frontiers in Neuroscience 14 (51), 1–14.

Cammisuli, D. M., Danti, S., Bosinelli, F., Cipriani, G., feb 2016. Non-pharmacological interventions for people with Alzheimer's Disease: A critical review of the scientific literature from the last ten years. European Geriatric Medicine 7 (1), 57–64.

Canuet, L., Tellado, I., Couceiro, V., Fraile, C., Fernandez-Novoa, L., R., I., Takeda, M., 2012. Resting-State Network Disruption and APOE Genotype in Alzheimer's Disease: A lagged Functional Connectivity Study. PLoS ONE 7 (9), 1–12.

Cao, Y., Cai, L., Wang, J., Wang, R., Yu, H., Cao, Y., Liu, J., 2015. Characterization of complexity in the electroencephalograph activity of Alzheimer's disease based on fuzzy entropy. Chaos 25, 083116.

Chen, W., Wang, Z., Xie, H., Yu, W., 2007. Characterization of surface EMG signal based on fuzzy entropy. IEEE Transactions on Neural Systems and Rehabilitation Engineering 15 (2), 266–272.

Cho, H., Dong, W. Y., Young, M. S., Beum, S. K., Yeong, I. K., Young, B. C., Kwang, S. L., Yong, S. S., Yoon, B., Kim, W., Kook, J. A., 2008. Abnormal integrity of corticocortical tracts in mild cognitive impairment: A diffusion tensor imaging study. Journal of Korean Medical Science 23 (3), 477–483.

Cohen, J., 1960. A Coefficient of Agreement for Nominal Scales. Educational and Psychological Measurement 20 (1), 37–46.

Cohen, M. E., Hudson, D. L., Deedwania, P. Ć., 1996. Applying continuous chaotic modeling to cardiac signal analysis. IEEE Engineering in Medicine and Biology Magazine 15 (5), 97–102.

Cohen, M. X., 2014. Analyzing Neural Time Series Data: Theory and Practice. MIT press.

Coronel, C., Garn, H., Waser, M., Deistler, M., Benke, T., Dal-Bianco, P., Ransmayr, G., Seiler, S., Grossegger, D., Schmidt, R., mar 2017. Quantitative EEG markers of entropy and auto mutual information in relation to MMSE scores of probable Alzheimer's disease patients. Entropy 19 (3), 1–14.

Cummings, J., Vinters, H., Felix, J., 2003. The Neuropsychiatry of Alzheimer's Disease and Related Dementias. CRC Press.

D'Amelio, M., Rossini, P. M., 2012. Brain excitability and connectivity of neuronal assemblies in Alzheimer's disease: From animal models to human findings. Progress in Neurobiology 99, 42–60.

Dauwels, J., Srinivasan, K., Ramasubba Reddy, M., Musha, T., Vialatte, F. B., Latchoumane, C., Jeong, J., Cichocki, A., 2011. Slowing and loss of complexity in Alzheimer's EEG: Two sides of the same coin? International Journal of Alzheimer's Disease 539621, 1–10.

Dauwels, J., Vialatte, F., Cichocki, A., 2010. Diagnosis of Alzheimer's Disease from EEG Signals: Where Are We Standing? Current Alzheimer Research 7 (6), 487–505.

De Domenico, M., Sasai, S., Arenas, A., 2016. Mapping multiplex hubs in human functional brain networks. Frontiers in Neuroscience 10 (326), 1–14.

de Haan, W., Pijnenburg, Y. A., Strijers, R. L., van der Made, Y., van der Flier, W. M., Scheltens, P., Stam, C. J., aug 2009. Functional neural network analysis in frontotemporal dementia and Alzheimer's disease using EEG and graph theory. BMC Neuroscience 10 (101), 1–12.

Delorme, A., Makeig, S., mar 2004. EEGLAB: An open source toolbox for analysis of single-trial EEG dynamics including independent component analysis. Journal of Neuroscience Methods 134 (1), 9–21.

Desikan, R. S., Ségonne, F., Fischl, B., Quinn, B. T., Dickerson, B. C., Blacker, D., Buckner, R. L., Dale, A. M., Maguire, R. P., Hyman, B. T., Albert, M. S., Killiany, R. J., 2006. An automated labeling system for subdividing the human cerebral cortex on MRI scans into gyral based regions of interest. NeuroImage 31, 968–980.

Deture, M. A., Dickson, D. W., 2019. The neuropathological diagnosis of Alzheimer's disease. Molecular Neurodegeneration 14 (32), 1–18.

Dickson, D. W., Crystal, H. A., Mattiace, L. A., Masur, D. M., Blau, A. D., Davies, P., Yen, S. H., Aronson, M. K., 1992. Identification of normal and pathological aging in prospectively studied nondemented elderly humans. Neurobiology of Aging 13 (1), 179–189.

Elloian, J. M., Noetscher, G. M., Makarov, S. N., Pascual-Leone, A., 2014. Continuous wave simulations on the propagation of electromagnetic fields through the human head. IEEE Transactions on Biomedical Engineering 61, 1676–1683.

Engels, M. M., Stam, C. J., van der Flier, W. M., Scheltens, P., de Waal, H., van Straaten, E. C., 2015. Declining functional connectivity and changing hub locations in Alzheimer's disease: An EEG study. BMC Neurology 15 (145), 1–8.

Escudero, J., Abásolo, D., Hornero, R., Espino, P., López, M., 2006. Analysis of electroencephalograms in Alzheimer's disease patients with multiscale entropy. Physiological Measurement 27 (11), 1091–1106.

Farcomeni, A., 2008. A review of modern multiple hypothesis testing, with particular attention to the false discovery proportion. Statistical Methods in Medical Research 17 (4), 347–388.

Farina, F. R., Emek-Savaş, D. D., Rueda-Delgado, L., Boyle, R., Kiiski, H., Yener, G., Whelan, R., jul 2020. A comparison of resting state EEG and structural MRI for classifying Alzheimer's disease and mild cognitive impairment. NeuroImage 215, 116795.

Flemons, W. W., Littner, M. R., 2003. Measuring Agreement Between Diagnostic Devices. Chest 124 (4), 1535–1542.

Folstein, M. F., Folstein, S. E., McHugh, P. R., 1975. "Mini-mental state". A practical method for grading the cognitive state of patients for the clinician. Journal of Psychiatric Research 12 (3), 189–198.

Francis, P. T., Palmer, A. M., Snape, M., Wilcock, G. K., 1999. The cholinergic hypothesis of Alzheimer's disease: A review of progress. Journal of Neurology Neurosurgery and Psychiatry 66, 137–147.

Fraser, A. M., Swinney, H. L., 1986. Independent coordinates for strange attractors from mutual information. Physical Review A 33 (2), 1134—-1140.

Friedman, J. H., 1989. Regularized discriminant analysis. Journal of the American Statistical Association 55 (11), 119–139.

Fuchs, E. C., Zivkovic, A. R., Cunningham, M. O., Middleton, S., LeBeau, F. E., Bannerman, D. M. M., Rozov, A., Whittington, M. A., Traub, R. D., Rawlins, J. N. P., Monyer, H., 2007. Recruitment of Parvalbumin-Positive Interneurons Determines Hippocampal Function and Associated Behavior. Neuron 53 (4), 591–604.

Gaubert, S., Raimondo, F., Houot, M., Corsi, M. C., Naccache, L., Sitt, J. D., Hermann, B., Oudiette, D., Gagliardi, G., Habert, M. O., Dubois, B., De Vico Fallani, F., Bakardjian, H., Epelbaum, S., jul 2019. EEG evidence of compensatory mechanisms in preclinical Alzheimer's disease. Brain 142 (7), 2096–2112.

Goldberg, Y., Elhadad, M., 2008. splitSVM: fast, space-efficient, non-heuristic, polynomial kernel computation for NLP applications. In: HLT '08: Proceedings of the 46th Annual Meeting of the Association for Computational Linguistics on Human Language Technologies. pp. 237–240.

Gómez, C., Poza, J., Gomez-Pilar, J., Bachiller, A., Juan-Cruz, C., Tola-Arribas, M. A., Carreres, A., Cano, M., Hornero, R., 2016. Analysis of spontaneous EEG activity in Alzheimer's disease using cross-sample entropy and graph theory. In: Proceedings of the Annual International Conference of the IEEE Engineering in Medicine and Biology Society, EMBS. Vol. 2016-Octob. pp. 2830–2833.

Gosselin, M. C., Neufeld, E., Moser, H., Huber, E., Farcito, S., Gerber, L., Jedensjo, M., Hilber, I., Gennaro, F. D., Lloyd, B., Cherubini, E., Szczerba, D., Kainz, W., Kuster, N., 2014. Development of a new generation of high-resolution anatomical models for medical device evaluation: The Virtual Population 3.0. Physics in Medicine and Biology 59, 5287–5303.

Guyon, I., Elisseeff, A., 2003. An introduction to variable and feature selection. Journal of Machine Learning Research 3, 1157–1182.

Hatz, F., Hardmeier, M., Benz, N., Ehrensperger, M., Gschwandtner, U., Rüegg, S., Schindler, C., Monsch, A. U., Fuhr, P., dec 2015. Microstate connectivity alterations in patients with early Alzheimer's disease. Alzheimer's Research and Therapy 7 (1), 1–11.

He, Y., Chen, Z., Evans, A., 2008. Structural insights into aberrant topological patterns of large-scale cortical networks in Alzheimer's disease. Journal of Neuroscience 28 (18), 4756–4766.

Herukka, S. K., Helisalmi, S., Hallikainen, M., Tervo, S., Soininen, H., Pirttilä, T., 2007. CSF Aβ42, Tau and phosphorylated Tau, APOE ϵ4 allele and MCI type in progressive MCI. Neurobiology of Aging 28 (4), 507–514.

Heston, T. F., 2011. Standardizing predictive values in diagnostic imaging research. Journal of Magnetic Resonance Imaging 33 (2), 505–507.

Hornero, R., Abasolo, D., Escudero, J., Gomez, C., 2009. Nonlinear analysis of electroencephalogram and magnetoencephalogram recordings in patients with Alzheimer's disease. Philosophical Transactions of the Royal Society A: Mathematical, Physical and Engineering Sciences 367 (1887), 317–336.

Hornik, K., 1991. Approximation capabilities of multilayer feedforward networks. Neural Networks 4 (2), 251–257.

Iqbal, K., del C. Alonso, A., Chen, S., Chohan, M. O., El-Akkad, E., Gong, C.-X., Khatoon, S., Li, B., Liu, F., Rahman, A., Tanimukai, H., Grundke-Iqbal, I., jan 2005. Tau pathology in Alzheimer disease and other tauopathies. Biochimica et Biophysica Acta (BBA) - Molecular Basis of Disease 1739 (2-3), 198–210.

Jack, C. R., Albert, M. S., Knopman, D. S., McKhann, G. M., Sperling, R. A., Carrillo, M. C., Thies, B., Phelps, C. H., 2011. Introduction to the recommendations from the National Institute on Aging-Alzheimer's Association workgroups on diagnostic guidelines for Alzheimer's disease. Alzheimer's and Dementia 7 (3), 257–262.

Jeong, J., jul 2004. EEG dynamics in patients with Alzheimer's disease. Clinical Neurophysiology 115 (7), 1490–1505.

Jeong, J., Gore, J. C., Peterson, B. S., 2001. Mutual information analysis of the EEG in patients with Alzheimer's disease. Clinical Neurophysiology 112 (5), 827–835.

Jicha, G. A., Parisi, J. E., Dickson, D. W., Johnson, K., Cha, R., Ivnik, R. J., Tangalos, E. G., Boeve, B. F., Knopman, D. S., Braak, H., Petersen, R. C., 2006. Neuropathologic outcome of mild cognitive impairment following progression to clinical dementia. Archives of Neurology 63 (5), 674–681.

Kabbara, A., Eid, H., El Falou, W., Khalil, M., Wendling, F., Hassan, M., 2018. Reduced integration and improved segregation of functional brain networks in Alzheimer's disease. Journal of Neural Engineering 15 (2), 026023.

Kang, Y., Escudero, J., Shin, D., Ifeachor, E., Marmarelis, V., mar 2015. Principal Dynamic Mode Analysis of EEG Data for Assisting the Diagnosis of Alzheimer's Disease. IEEE Journal of Translational Engineering in Health and Medicine 3, 1800110.

Karakaya, T., Fußer, F., Schroder, J., Pantel, J., 2013. Pharmacological Treatment of Mild Cognitive Impairment as a Prodromal Syndrome of Alzheimer's Disease. Current Neuropharmacology 11 (1), 102–107.

Karas, G. B., Scheltens, P., Rombouts, S. A. R. B., Visser, P. J., Van Schijndel, R. A., Fox, N. C., Barkhof, F., 2004. Global and local gray matter loss in mild cognitive impairment and Alzheimer's disease. NeuroImage 23 (2), 708–716.

Kelley, B. J., 2015. Treatment of Mild Cognitive Impairment. Current Treatment Options in Neurology 17 (40), 1–11.

Khoury, R., Ghossoub, E., dec 2019. Diagnostic biomarkers of Alzheimer's disease: A state-of-the-art review. Biomarkers in Neuropsychiatry 1, 100005.

Kiss, I. Z., Zhai, Y., Hudson, J. L., 2002. Emerging coherence in a population of chemical oscillators. Science 296, 1676–1678.

Klem, G. H., Lüders, H. O., Jasper, H. H., Elger, C., 1999. The ten-twenty electrode system of the International Federation. The International Federation of Clinical Neurophysiology. Electroencephalography and Clinical Neurophysiology. Supplement 52, 3–6.

Koenig, T., Prichep, L., Dierks, T., Hubl, D., Wahlund, L. O., John, E. R., Jelic, V., 2005. Decreased EEG synchronization in Alzheimer's disease and mild cognitive impairment. Neurobiology of Aging 26 (2), 165–171.

Kumar, A., Singh, A., Ekavali, 2015. A review on Alzheimer's disease pathophysiology and its management: An update. Pharmacological Reports 67 (2), 195–203.

Kuramoto, Y., 1975. Self-entrainment of a population of coupled non-linear oscillators. In: International Symposium on Mathematical Problems in Theoretical Physics. Vol. 39. Berlin, Heidelberg, pp. 420–422.

Lachaux, J. P., Rodriguez, E., Martinerie, J., Varela, F. J., 1999. Measuring phase synchrony in brain signals. Human Brain Mapping 8 (4), 194–208.

Lane, C. A., Hardy, J., Schott, J. M., 2018. Alzheimer's disease. European Journal of Neurology 25 (1), 59–70.

Lempel, A., Ziv, J., 1976. On the Complexity of Finite Sequences. IEEE Transactions on Information Theory 22 (1), 75–81.

Licinio, J., Negrão, a. B., Mantzoros, C., Kaklamani, V., Wong, M. L., Bongiorno, P. B., Mulla, A., Cearnal, L., Veldhuis, J. D., Flier, J. S., McCann, S. M., Gold, P. W., 1998. Synchronicity of frequently sampled, 24-h concentrations of circulating leptin, luteinizing hormone, and estradiol in healthy women. Proceedings of the National Academy of Sciences of the United States of America 95 (5), 2541–2546.

Lin, P. J., Neumann, P. J., 2013. The economics of mild cognitive impairment. Alzheimer's and Dementia 9 (1), 58–62.

Liu, X., Zhang, C., Ji, Z., Ma, Y., Shang, X., Zhang, Q., Zheng, W., Li, X., Gao, J., Wang, R., Wang, J., Yu, H., apr 2016. Multiple characteristics analysis of Alzheimer's electroencephalogram by power spectral density and Lempel–Ziv complexity. Cognitive Neurodynamics 10 (2), 121–133.

Lo, C. Y., Wang, P. N., Chou, K. H., Wang, J., He, Y., Lin, C. P., 2010. Diffusion tensor tractography reveals abnormal topological organization in structural cortical networks in Alzheimer's disease. Journal of Neuroscience 30 (50), 16876–16885.

Makarov, S. N., Noetscher, G. M., Nazarian, A., 2016. Low-Frequency Electromagnetic Modeling for Electrical and Biological Systems Using MATLAB. John Wiley & Sons, Hoboken, New Jersey.

Makeig, S., Jung, T.-P., Bell, A. J., Ghahremani, D., Sejnowski, T. J., 1997. Blind separation of auditory event-related brain responses into independent components. Proceedings of the National Academy of Sciences of the United States of America 94 (20), 10979–10984.

Mammone, N., Bonanno, L., De Salvo, S., Marino, S., Bramanti, P., Bramanti, A., Morabito, F. C., aug 2017. Permutation Disalignment Index as an Indirect, EEG-Based, Measure of Brain Connectivity in MCI and AD Patients. International Journal of Neural Systems 27 (5), 1750020.

Martínez-Zarzuela, M., Gómez, C., Díaz-Pernas, F. J., Fernández, A., Hornero, R., 2013. Cross-Approximate Entropy parallel computation on GPUs for biomedical signal analysis. Application to MEG recordings. Computer Methods and Programs in Biomedicine 112 (1), 189–199.

McBride, J. C., Zhao, X., Munro, N. B., Smith, C. D., Jicha, G. A., Hively, L., Broster, L. S., Schmitt, F. A., Kryscio, R. J., Jiang, Y., 2014. Spectral and complexity analysis of scalp EEG characteristics for mild cognitive impairment and early Alzheimer's disease. Computer Methods and Programs in Biomedicine 114, 153–163.

McKhann, G., Drachman, D., Folstein, M., Katzman, R., Price, D., Stadlan, E. M., 1984. Clinical diagnosis of alzheimer's disease: Report of the NINCDS-ADRDA work group under the auspices of department of health and human services task force on alzheimer's disease. Neurology 34 (7), 939–944.

McKhann, G. M., Knopman, D. S., Chertkow, H., Hyman, B. T., Jack, C. R., Kawas, C. H., Klunk, W. E., Koroshetz, W. J., Manly, J. J., Mayeux, R., Mohs, R. C., Morris, J. C., Rossor, M. N., Scheltens, P., Carrillo, M. C., Thies, B., Weintraub, S., Phelps, C. H., 2011. The diagnosis of dementia due to Alzheimer's disease: Recommendations from the National Institute on Aging-Alzheimer's Association workgroups on diagnostic guidelines for Alzheimer's disease. Alzheimer's and Dementia 7 (3), 263–269.

McShane, R., Westby, M. J., Roberts, E., Minakaran, N., Schneider, L., Farrimond, L. E., Maayan, N., Ware, J., Debarros, J., 2019. Memantine for dementia. Cochrane Database of Systematic Reviews 3 (3), 1–285.

Miraglia, F., Vecchio, F., Bramanti, P., Rossini, P. M., feb 2016. EEG characteristics in "eyes-open" versus "eyes-closed" conditions: Small-world network architecture in healthy aging and age-related brain degeneration. Clinical Neurophysiology 127 (2), 1261–1268.

Moretti, D. V., Babiloni, C., Binetti, G., Cassetta, E., Dal Forno, G., Ferreric, F., Ferri, R., Lanuzza, B., Miniussi, C., Nobili, F., Rodriguez, G., Salinari, S., Rossini, P. M., 2004. Individual analysis of EEG frequency and band power in mild Alzheimer's disease. Clinical Neurophysiology 115, 299–308.

Moretti, D. V., Frisoni, G. B., Pievani, M., Rosini, S., Geroldi, C., Binetti, G., Rossini, P. M., 2008. Cerebrovascular disease and hippocampal atrophy are differently linked to functional coupling of brain areas: An EEG coherence study in MCI subjects. Journal of Alzheimer's Disease 14 (3), 285–299.

Mormann, F., Lehnertz, K., David, P., E. Elger, C., 2000. Mean phase coherence as a measure for phase synchronization and its application to the EEG of epilepsy patients. Physica D: Nonlinear Phenomena 144 (3-4), 358–369.

Musaeus, C. S., Engedal, K., Høgh, P., Jelic, V., Mørup, M., Naik, M., Oeksengaard, A. R., Snaedal, J., Wahlund, L. O., Waldemar, G., Andersen, B. B., jan 2018. EEG Theta Power Is an Early Marker of Cognitive Decline in Dementia due to Alzheimer's Disease. Journal of Alzheimer's Disease 64 (4), 1359–1371.

Narsky, I., Porter, F. C., 2013. Statistical Analysis Techniques in Particle Physics: Fits, Density Estimation and Supervised Learning. John Wiley & Sons.

Noetscher, G. M., Yanamadala, J., Makarov, S. N., Pascual-Leone, A., 2014. Comparison of cephalic and extracephalic montages for transcranial direct current stimulation-a numerical study. IEEE Transactions on Biomedical Engineering 61 (9), 2488–98.

Nolte, G., Bai, O., Wheaton, L., Mari, Z., Vorbach, S., Hallett, M., 2004. Identifying true brain interaction from EEG data using the imaginary part of coherency. Clinical Neurophysiology 115 (10), 2292–2307.

Nunez, P. L., Srinivasan, R., 2009. Electric Fields of the Brain: The neurophysics of EEG. Oxford University Press Inc.

O'Neill, G. C., Tewarie, P., Vidaurre, D., Liuzzi, L., Woolrich, M. W., Brookes, M. J., 2018. Dynamics of large-scale electrophysiological networks: A technical review. NeuroImage 180, 559–576.

Osipova, D., Ahveninen, J., Kaakkola, S., Jääskeläinen, I. P., Huttunen, J., Pekkonen, E., 2003. Effects of scopolamine on MEG spectral power and coherence in elderly subjects. Clinical Neurophysiology 114 (10), 1902–1907.

Palesi, F., Castellazzi, G., Casiraghi, L., Sinforiani, E., Vitali, P., Gandini Wheeler-Kingshott, C. A., D'Angelo, E., 2016. Exploring patterns of Alteration in Alzheimer's disease brain networks: A combined structural and functional connectomics analysis. Frontiers in Neuroscience 10 (380), 1–16.

Pascual-Marqui, R. D., 2002. Standardized low-resolution brain electromagnetic tomography (sLORETA): Technical details. In: Methods and Findings in Experimental and Clinical Pharmacology. pp. 1–12.

Pascual-Marqui, R. D., Lehmann, D., Koukkou, M., Kochi, K., Anderer, P., Saletu, B., Tanaka, H., Hirata, K., John, E. R., Prichep, L., Biscay-Lirio, R., Kinoshita, T., 2011. Assessing interactions in the brain with exact low-resolution electromagnetic tomography. Philosophical Transactions of the Royal Society A: Mathematical, Physical and Engineering Sciences 369 (1952), 3768–3784.

Petersen, R. C., 2016. Mild cognitive impairment. CONTINUUM Lifelong Learning in Neurology 22 (2), 404–418.

Petersen, R. C., Lopez, O., Armstrong, M. J., Getchius, T. S., Ganguli, M., Gloss, D., Gronseth, G. S., Marson, D., Pringsheim, T., Day, G. S., Sager, M., Stevens, J., Rae-Grant, A., 2018. Practice guideline update summary: Mild cognitive impairment. Neurology 90, 126–135.

Pijnenburg, Y. A., Vd Made, Y., Van Cappellen Van Walsum, A. M., Knol, D. L., Scheltens, P., Stam, C. J., jun 2004. EEG synchronization likelihood in mild cognitive impairment and Alzheimer's disease during a working memory task. Clinical Neurophysiology 115 (6), 1332–1339.

Pincus, S. M., 2000. Irregularity and asynchrony in biologic network signals. In: Numerical Computer Methods, Part C, Methods in Enzymology. Vol. 321. Academic Press, pp. 149–182.

Pincus, S. M., Singer, B. H., 1996. Randomness and degrees of irregularity. Proceedings of the National Academy of Sciences of the United States of America 93 (5), 2083–2088.

Poil, S. S., de Haan, W., van der Flier, W. M., Mansvelder, H. D., Scheltens, P., Linkenkaer-Hansen, K., oct 2013. Integrative EEG biomarkers predict progression to Alzheimer's disease at the MCI stage. Frontiers in Aging Neuroscience 5 (58), 1–12.

Powell, G. E., Percival, I. C., 1979. A spectral entropy method for distinguishing regular and irregular motion of Hamiltonian systems. Journal of Physics A: General Physics 12, 2053–2071.

Poza, J., Gómez, C., García, M., Tola-Arribas, M. A., Carreres, A., Cano, M., Hornero, R., 2017. Spatio-Temporal Fluctuations of Neural Dynamics in Mild Cognitive Impairment and Alzheimer's Disease. Current Alzheimer research 14 (9), 924–936.

Richman, J. S., Moorman, J. R., 2000. Physiological time-series analysis using approximate entropy and sample entropy. American Journal of Physiology. Heart and Circulatory Physiology 278 (6), 2039–2049.

Roach, B. J., Mathalon, D. H., 2008. Event-related EEG time-frequency analysis: An overview of measures and an analysis of early gamma band phase locking in schizophrenia. Schizophrenia Bulletin 34 (5), 907–926.

Rodriguez, G., Copello, F., Vitali, P., Perego, G., Nobili, F., 1999. EEG spectral profile to stage Alzheimer's disease. Clinical Neurophysiology 110 (10), 1831–1837.

Roh, J. H., Park, M. H., Ko, D., Park, K. W., Lee, D. H., Han, C., Jo, S. A., Yang, K. S., Jung, K. Y., nov 2011. Region and frequency specific changes of spectral power in Alzheimer's disease and mild cognitive impairment. Clinical Neurophysiology 122 (11), 2169–2176.

Rubinov, M., Sporns, O., 2010. Complex network measures of brain connectivity: Uses and interpretations. NeuroImage 52 (3), 1059–1069.

Ruiz-Gómez, S. J., Gomez, C., Poza, J., Maturana-Candelas, A., Rodriguez-Gonzalez, V., Garcia, M., Tola-Arribas, M. A., Cano, M., Hornero, R., 2019b. Analysis of Volume Conduction Effects on Different Functional Connectivity Metrics: Application to Alzheimer's Disease EEG Signals. In: Proceedings of the Annual International Conference of the IEEE Engineering in Medicine and Biology Society, EMBS. pp. 6434–6437.

Ruiz-Gómez, S. J., Gómez, C., Poza, J., Gutiérrez-Tobal, G. C., Tola-Arribas, M. A., Cano, M., Hornero, R., 2018a. Automated multiclass classification of spontaneous EEG activity in Alzheimer's disease and mild cognitive impairment. Entropy 20 (35), 1–15.

Ruiz-Gómez, S. J., Gómez, C., Poza, J., Martínez-Zarzuela, M., Tola-Arribas, M. A., Cano, M., Hornero, R., 2018b. Measuring alterations of spontaneous EEG neural coupling in alzheimer's disease and mild cognitive impairment by means of cross-entropy metrics. Frontiers in Neuroinformatics 12 (76), 1–11.

Ruiz-Gómez, S. J., Hornero, R., Poza, J., Maturana-Candelas, A., Pinto, N., Gómez, C., 2019b. Computational modeling of the effects of EEG volume conduction on functional connectivity metrics. Application to Alzheimer's disease continuum. Journal of Neural Engineering 16 (6), 066019.

Ruiz-Gómez, S. J., Hornero, R., Poza, J., Santamaría-Vázquez, E., Rodríguez-González, V., Maturana-Candelas, A., Gómez, C., 2021. A new method to build multiplex networks using Canonical Correlation Analysis for the characterization of the Alzheimer's disease continuum. Journal of Neural Engineering 18 (2), 026002.

Sanz-Arigita, E. J., Schoonheim, M. M., Damoiseaux, J. S., Rombouts, S. A., Maris, E., Barkhof, F., Scheltens, P., Stam, C. J., 2010. Loss of 'Small-World' Networks in Alzheimer's Disease: Graph Analysis of fMRI Resting-State Functional Connectivity. PLoS ONE 5 (11), e13788.

Schoffelen, J. M., Gross, J., 2009. Source connectivity analysis with MEG and EEG. Human Brain Mapping 30, 1857–1865.

Simons, S., Espino, P., Abásolo, D., jan 2018. Fuzzy Entropy analysis of the electroencephalogram in patients with Alzheimer's disease: Is the method superior to Sample Entropy? Entropy 20 (21), 1–13.

Stam, C. J., 2014. Modern network science of neurological disorders. Nature Reviews Neuroscience 15 (10), 683–695.

Stam, C. J., De Haan, W., Daffertshofer, A., Jones, B. F., Manshanden, I., Van Cappellen Van Walsum, A. M., Montez, T., Verbunt, J. P., De Munck, J. C., Van Dijk, B. W., Berendse, H. W., Scheltens, P., 2009. Graph theoretical analysis of magnetoencephalographic functional connectivity in Alzheimer's disease. Brain 132 (1), 213–224.

Stam, C. J., Nolte, G., Daffertshofer, A., 2007. Phase lag index: Assessment of functional connectivity from multi channel EEG and MEG with diminished bias from common sources. Human Brain Mapping 28, 1178–1193.

Stam, C. J., Van Dijk, B. W., 2002. Synchronization likelihood: An unbiased measure of generalized synchronization in multivariate data sets. Physica D: Nonlinear Phenomena 163 (3), 236–251.

Stam, C. J., van Straaten, E. C., 2012. The organization of physiological brain networks. Clinical Neurophysiology 123 (6), 1067–1087.

Street, J. S., Clark, W. S., Gannon, K. S., Cummings, J. L., Bymaster, F. P., Tamura, R. N., Mitan, S. J., Kadam, D. L., Sanger, T. M., Feldman, P. D., Tollefson, G. D., Breier, A., 2000. Olanzapine treatment of psychotic and behavioral symptoms in patients with Alzheimer disease in nursing care facilities: A double-blind, randomized, placebo-controlled trial. Archives of General Psychiatry 57 (10), 968–976.

Strogatz, S. H., 2000. From Kuramoto to Crawford: Exploring the onset of synchronization in populations of coupled oscillators. Physica D: Nonlinear Phenomena 143, 1–20.

Tadel, F., Baillet, S., Mosher, J. C., Pantazis, D., Leahy, R. M., 2011. Brainstorm: A user-friendly application for MEG/EEG analysis. Computational Intelligence and Neuroscience 879716, 1–13.

Tatum, W. O., Husain, A. M., Benbadis, S. R., Kaplan, P. W., 2014. Handbook of EEG Interpretation, 2nd Edition. Demos Medical, New York.

Terry, A. V., Buccafusco, J. J., 2003. The cholinergic hypothesis of age and Alzheimer's disease-related cognitive deficits: Recent challenges and their implications for novel drug development. Journal of Pharmacology and Experimental Therapeutics 306 (3), 821–827.

Tijms, B. M., Möller, C., Vrenken, H., Wink, A. M., de Haan, W., van der Flier, W. M., Stam, C. J., Scheltens, P., Barkhof, F., 2013. Single-Subject Grey Matter Graphs in Alzheimer's Disease. PLoS ONE 8 (3), 1–9.

Tóth, B., File, B., Boha, R., Kardos, Z., Hidasi, Z., Gaál, Z. A., Csibri, É., Salacz, P., Stam, C. J., Molnár, M., 2014. EEG network connectivity changes in mild cognitive impairment - Preliminary results. International Journal of Psychophysiology 92 (1), 1–7.

U.S. National Library of Medicine, 2018. Visible Human Project.
URL `https://www.nlm.nih.gov/research/visible/visiblehuman.html`

Vapnik, V. N., 1999. An overview of statistical learning theory. IEEE transactions on neural networks 10 (5), 988–999.

Vecchio, F., Miraglia, F., Piludu, F., Granata, G., Romanello, R., Caulo, M., Onofrj, V., Bramanti, P., Colosimo, C., Rossini, P. M., apr 2017. "Small World" architecture in brain connectivity and hippocampal volume in Alzheimer's disease: a study via graph theory from EEG data. Brain Imaging and Behavior 11 (2), 473–485.

Ward, A., Tardiff, S., Dye, C., Arrighi, H. M., 2013. Rate of Conversion from Prodromal Alzheimer's Disease to Alzheimer's Dementia: A Systematic Review of the Literature. Dementia and Geriatric Cognitive Disorders Extra 3 (1), 320–332.

Webber, K. M., Raina, A. K., Marlatt, M. W., Zhu, X., Prat, M. I., Morelli, L., Casadesus, G., Perry, G., Smith, M. A., oct 2005. The cell cycle in Alzheimer disease: A unique target for neuropharmacology. Mechanisms of Ageing and Development 126 (10), 1019–1025.

Witten, I. H., Frank, E., Hall, M. A., Pal, C. J., 2016. Data Mining: Practical Machine Learning Tools and Techniques, 3rd Edition. Morgan Kaufmann.

Yao, Z., Zhang, Y., Lin, L., Zhou, Y., Xu, C., Jiang, T., 2010. Abnormal cortical networks in mild cognitive impairment and alzheimer's disease. PLoS Computational Biology 6 (11), e1001006.

Yershalmy, J., 1947. Statistical problems in assessing methods of medical diagnosis, with special reference to X-ray techniques. Public Health Reports 62 (2), 1432–1439.

Yu, L., Liu, H., 2004. Efficient feature selection via analysis of relevance and redundancy. Journal of Machine Learning Research 5, 1205–1224.

Yu, M., Engels, M. M., Hillebrand, A., Van Straaten, E. C., Gouw, A. A., Teunissen, C., Van Der Flier, W. M., Scheltens, P., Stam, C. J., 2017. Selective impairment of hippocampus and posterior hub areas in Alzheimer's disease: An MEG-based multiplex network study. Brain 140 (5), 1466–1485.

Yushkevich, P. A., Piven, J., Hazlett, H. C., Smith, R. G., Ho, S., Gee, J. C., Gerig, G., 2006. User-guided 3D active contour segmentation of anatomical structures: Significantly improved efficiency and reliability. NeuroImage 31, 1116–1128.

Zhao, X., Liu, Y., Wang, X., Liu, B., Xi, Q., Guo, Q., Jiang, H., Jiang, T., Wang, P., 2012. Disrupted small-world brain networks in moderate Alzheimer's disease: A resting-state fMRI study. PLoS ONE 7 (3), e33540.

Zucchella, C., Sinforiani, E., Tamburin, S., Federico, A., Mantovani, E., Bernini, S., Casale, R., Bartolo, M., 2018. The Multidisciplinary Approach to Alzheimer's Disease and Dementia. A Narrative Review of Non-Pharmacological Treatment. Frontiers in Neurology 9 (1058), 1–22.

Index

The human brain has billions of neurons with long and branching extensions that enable them to form connections and communicate with each other. The changes in these networks throughout the life span are responsible for physiological brain aging. However, normal brain aging can be altered by some physiopathological processes, like those associated with dementia due to Alzheimer's disease (AD) and mild cognitive impairment (MCI). AD is a progressive neurodegenerative disorder that causes cognitive, behavioral and functional alterations interfering with the patients' ability to carry out the activities of daily living. MCI is usually considered a prodromal stage of AD in which individuals show evidences of AD brain changes and exhibit a memory impairment beyond what would be expected for their age, but do not fully accomplish the criteria for dementia diagnosis. Despite the high prevalence of these neurodegenerative processes, the current knowledge about them is still limited. In this context, the present Doctoral Thesis is focused on the characterization of the spontaneous EEG activity in the different stages of AD and MCI with the aim of gaining further insights into the neural substrates underlying their pathophysiology. Particularly, they have been investigated from three different levels of analysis depending on the way interactions are taken into account: local activation, interaction between pair-wise electrodes, and network organization.

UVa

Doctoral Thesis

Compendium of publications

International Mention